CHARLES UNIVERSITY

Faculty of Science

Study programme:

Molecular and Cell Biology, Genetics and Virology

Mgr. Tomáš Liďák

Novel substrates of cullin-RING ubiquitin ligases: identification and functional characterisation

Identifikace a funkční charakterizace nových substrátů cullin-RING ubiquitin ligáz

Doctoral thesis

Supervisor: Mgr. Lukáš Čermák, Ph.D.

Prague, 2021

Prohlášení autora:

Prohlašuji, že jsem závěrečnou práci zpracoval samostatně a že jsem uvedl všechny použité informační zdroje a literaturu. Tato práce ani její podstatná část nebyla předložena k získání jiného nebo stejného akademického titulu.

V Praze, 18. 11. 2021

.....

Mgr. Tomáš Liďák

Abstract

Selective protein degradation by the ubiquitin-proteasome system is essential for cellular homeostasis and the regulation of diverse biological processes. The selectivity of this system is imparted by hundreds of ubiquitin ligases that specifically recognise substrates and catalyse their ubiquitination, thereby targeting them for degradation. Among ubiquitin ligases, multisubunit cullin-RING ubiquitin ligases constitute the largest group. However, despite significant advances in understanding their assembly, regulation, and molecular architecture, the substrates and functions of most of them remain unknown. This thesis focuses on two ubiquitin ligases from the cullin-RING ubiquitin ligase 4 (CRL4) subfamily: $CRL4^{DCAF4}$ and $CRL4^{DCAF12}$. To identify their candidate substrates and to address their biological roles, several different approaches have been employed. First, proteomic screening revealed a wide range of candidate substrates. Next, detailed characterisation of the identified interactions and exploration of the condition under which candidate substrates undergo degradation was performed. Finally, knockout human cell lines and mice with a targeted disruption of genes encoding DCAF4 and DCAF12 were generated to explore the physiological roles of $CRL4^{DCAF4}$ and $CRL4^{DCAF12}$. In summary, the herein presented identification and validation of novel substrates of $CRL4^{DCAF4}$ and $CRL4^{DCAF12}$ followed by the exploration of their biological roles provides an important insight into the function of these two understudied ubiquitin ligases.

Keywords: cullin-RING ubiquitin ligases, DCAF4, DCAF12, protein degradation

Abstrakt

Selektivní degradace proteinů ubikvitin-proteazomovým systémem je nezbytná pro udržování buněčné homeostázy a regulaci celé řady biologických procesů. Selektivita tohoto systému je dána stovkami ubikvitin ligáz, které specificky rozeznávají proteiny určené k degradaci (tzv. substráty) a katalyzují jejich ubikvitinaci, čímž je označují pro následnou degradaci. Největší skupinu ubikvitin ligáz tvoří vícepodjednotkové cullin-RING ubikvitin ligázy. Navzdory významnému pokroku v pochopení jejich molekulární architektury, sestavení a regulace zůstávají substráty a funkce většiny z nich neznámé. Tato práce se zabývá dvěma ubikvitin ligázami z podrodiny cullin-RING ubikvitin ligáz 4 (CRL4) - $CRL4^{DCAF4}$ a $CRL4^{DCAF12}$. Za účelem identifikace jejich potenciálních substrátů a určení jejich biologických rolí bylo použito několik odlišných přístupů. S využitím proteomického přístupu jsme identifikovali širokou škálu potenciálních substrátů. Následně byla provedena podrobná charakterizace identifikovaných interakcí a testování podmínek, za kterých potenciální substráty podléhají degradaci. Nakonec byly za účelem odhalení fyziologické role $CRL4^{DCAF4}$ a $CRL4^{DCAF12}$ připraveny lidské buněčné linie a myší modely s vyřazeným genem pro DCAF4 a DCAF12. Zde prezentovaná identifikace a validace nových substrátů $CRL4^{DCAF4}$ a $CRL4^{DCAF12}$ a navazující ověření jejich biologických rolí poskytuje důležitý vhled do fungování těchto dvou nedostatečně prostudovaných ubiquitin ligáz.

Klíčová slova: cullin-RING ubikvitin ligázy, DCAF4, DCAF12, degradace proteinů

Acknowledgements

I would like to thank all the Institute of Molecular Genetics staff members who participated in the projects. Without their kind help and support, this work would not have been possible. In particular, I would like to express gratitude to the teams involved in mouse models generation and their phenotyping at the Czech Centre for Phenogenomics. I would also like to thank the Proteomics facility at the Biotechnology and Biomedicine Centre of the Academy of Sciences and Charles University for proteomic analysis. Furthermore, my gratitude extends to the Faculty of Science, Charles University, and the Grant Agency of Charles University (project # 6119) for funding opportunities to undertake my studies. Finally, my appreciation also goes to my loved ones for their encouragement and unwavering support during my painful and nerve-wracking PhD journey.

List of abbreviations

Abbreviation	Explanation
6-4PPs	(6-4) pyrimidine-pyrimidine photoproducts
ACK	ammonium-chloride-potassium
AGO2	argonaute2
anti-CD3/CD28	anti-CD3 and anti-CD28
AP	affinity purification
APAF1	apoptotic protease-activating factor 1
APC/C	anaphase-promoting complex/cyclosome
ARTS	apoptosis-related protein in the TGF-beta signalling pathway
ATCC	American Type Culture Collection
ATF3	activating transcription factor 3
BIO box	biogenesis-promoting box
BIR	baculoviral IAP repeat
BMDCs	bone marrow-derived dendritic cells
BMDMs	bone marrow-derived macrophages
BPA	beta-propeller A
BPB	beta-propeller B
BPC	beta-propeller C
BSA	bovine serum albumin
CAB box	Cajal body box
CAND1	cullin-associated NEDD8-dissociated protein 1
CAND2	cullin-associated NEDD8-dissociated protein 2
CARD	caspase activation and recruitment domain
CCCP	carbonyl cyanide 3-chlorophenylhydrazone
cDC	conventional dendritic cells
CDT2	Cdc10-dependent transcript 2
cFLIP	cellular FLICE-like inhibitory protein
CHX	cycloheximide
cIAP1	cellular IAP1
cIAP2	cellular IAP2
CP110	centrosomal protein of 110 kDa
CPDs	cyclobutane pyrimidine dimers
CPT	camptothecin
CRL(s)	cullin-RING ubiquitin ligase(s)
CRL1	cullin-RING ubiquitin ligase 1
CRL4	cullin-RING ubiquitin ligase 4
cryo-EM	cryogenic electron microscopy
CS	Cockayne syndrome
CSA	Cockayne-syndrome protein A
CSB	Cockayne-syndrome protein B
CSN	COP9 signalosome
CTE	C-terminal extension
CTRL	control

Abbreviation	Explanation
CUL4A	cullin-4A
CUL4B	cullin-4B
DAMPs	danger/damage-associated molecular patterns
DAPI	4’,6-diamidino-2-phenylindole
DCAF12	DDB1- and CUL4-associated factor 12
DCAF12L1	DDB1- and CUL4-associated factor 12-like protein 1
DCAF12L2	DDB1- and CUL4-associated factor 12-like protein 2
DCAF4	DDB1- and CUL4-associated factor 4
DCAF4L1	DDB1- and CUL4-associated factor 4-like protein 1
DCAF4L2	DDB1- and CUL4-associated factor 4-like protein 2
DCAFs	DDB1- and CUL4-associated factors
DDB1	DNA damage-binding protein 1
DDB2	DNA damage-binding protein 2
DED	death-effector domain
DIABLO	direct IAP-binding protein with low pI
DIAP1	Death-associated inhibitor of apoptosis 1
DIAP2	Death-associated inhibitor of apoptosis 2
DISC	death-inducing signalling complex
DKC1	dyskerin
DKCLD	dyskeratosis congenita-like domain
DMEM	Dulbecco’s Modified Eagle’s Medium
DOX	doxycycline
DOXO	doxorubicin
DUBs	deubiquitinating enzymes
E1	ubiquitin-activating enzyme
E2	ubiquitin-conjugating enzyme
E2~Ub	E2 linked to ubiquitin via a thioester bond
E3	ubiquitin ligase
EBV	Epstein-Barr virus
ETO	etoposide
EV	empty vector
FADD	FAS-associated death domain protein
FBS	fetal bovine serum
FBXO1	F-box only protein 1
FC	fold change
FMRP	fragile X mental retardation protein
GAR	glycine- and arginine-rich
GG-NER	global-genome NER
γH2AX	histone H2AX phosphorylated on serine 139
GM-CSF	granulocyte-macrophage colony-stimulating factor
HA tag	hemagglutinin tag
HBSS	Hanks' balanced salt solution
HBV	hepatitis B virus
HCV	hepatitis C virus

Abbreviation	Explanation
HDV	hepatitis delta virus
HECT	homologous to E6-AP carboxyl terminus
HIV-1	human immunodeficiency virus type-1
HLH	hemophagocytic lymphohistiocytosis
IAP	inhibitors of apoptosis protein
IBD	inflammatory bowel disease
IBM	IAP-binding motif
IFNγ	interferon gamma
IKK	Inhibitor of nuclear factor kappa-B kinase
IL-18	interleukin-18
IL-1β	interleukin-1 beta
IL-6	Interleukin-6
Imd	immune deficiency
IP	immunoprecipitation
IRES	internal ribosome entry site
ISG	interferon-stimulated gene
IκBα	I-kappa-B-alpha
KO	knockout
K-turn	kink-turn
LC-MS/MS	liquid chromatography-tandem mass spectrometry
LFQ	label-free quantification
LPS	lipopolysaccharides
LUBAC	linear-chain ubiquitin assembly complex
MAGE(s)	melanoma antigen gene(s)
MAPK	mitogen-activated protein kinase
MDP	muramyl dipeptide
MEFs	mouse embryonic fibroblasts
miRNA	microRNA
MOMP	mitochondrial outer membrane permeabilisation
MOV10	Moloney leukemia virus 10 protein
MOV10L1	MOV10-like protein 1
MPP	mitochondrial processing peptidase
MRE	miRNA recognition element
mRNA(s)	messenger RNA(s)
NAE	NEDD8 activating enzyme
NER	nucleotide excision repair
NF-κB	nuclear factor-kappa B
NIK	NF-kappa-B-inducing kinase
NK	natural killer
NKT	natural killer T
NLRP3	NACHT, LRR and PYD domains-containing protein 3
NLS(s)	nuclear localisation signal(s)
NOD2	nucleotide-binding oligomerization domain 2
ns	not significant

Abbreviation	Explanation
nt	nucleotide
NT	non-treated
NTE	N-terminal extension
PAM	protospacer adjacent motif
PAMPs	pathogen-associated molecular patterns
PARP	poly(ADP-ribose) polymerase
P-bodies	processing bodies
PBS	phosphate-buffered saline
PBS-T	PBS supplemented with 0.1% Tween 20
PCNA	proliferating cell nuclear antigen
PCR	polymerase chain reaction
pDC	plasmacytoid dendritic cells
piRNA(s)	Piwi-interacting RNA(s)
PITX2	pituitary homeobox 2
PLZF	promyelocytic leukemia zinc finger
PNA	peanut agglutinin
pre-mRNA	precursor messenger RNA
PRRs	pattern recognition receptors
PUA	RNA-binding pseudouridine synthase and archaeosine transglycosylase
qPCR	quantitative real-time PCR
RBR	RING-in-between-RING
RBX1	RING-box protein 1
RBX2	RING-box protein 2
RCR	RING-Cys-relay
RING	really interesting new gene
RIPK1	receptor-interacting serine/threonine-protein kinase 1
RIPK2	receptor-interacting serine/threonine-protein kinase 2
RIPK3	receptor-interacting serine/threonine-protein kinase 3
RISC	RNA–induced silencing complex
RNAi	RNA interference
RNAPII	RNA polymerase II
RNA-seq	RNA sequencing
RNP(s)	ribonucleoprotein(s)
rRNAs	ribosomal RNAs
scaRNA(s)	small Cajal body-specific RNA(s)
SCP3	synaptonemal complex protein 3
SF tag	Twin-Strep-FLAG tag
sgRNA(s)	single guide RNA(s)
siRNA(s)	small interfering RNA(s)
SKP1	S-phase kinase-associated protein 1
SMAC	second mitochondria-derived activator of caspase
snoRNA(s)	small nucleolar RNA(s)
snRNA(s)	spliceosomal small nuclear RNA(s)
SPCs	spermatogonial progenitor cells

Abbreviation	Explanation
ST7	suppression of tumorigenicity 7
TAK1	TGF-beta-activated kinase 1
TCAB1	telomerase Cajal body protein 1
TC-NER	transcription-coupled NER
TCR	T cell receptor
TERC	telomerase RNA component
TERT	telomerase reverse transcriptase
TFIIH	transcription factor IIH
THA	thapsigargin
TLR	Toll-like receptor
TLR2	Toll-like receptor 2
TNF	tumour necrosis factor
TNFR	tumour necrosis factor receptor
TNFR1	tumour necrosis factor receptor 1
TNF-α	tumour necrosis factor-alpha
TRAIL	TNF-related apoptosis-inducing ligand
Tregs	regulatory T cells
tRNA	transfer RNA
t-SNE	t-distributed stochastic neighbour embedding
UBA	ubiquitin-associated
UBDs	ubiquitin-binding domains
UPS	ubiquitin-proteasome system
UV	ultraviolet light
UVSSA	UV-stimulated protein A
VSV	vesicular stomatitis virus
WCL	whole-cell lysates
WDR79	WD repeat-containing protein 79
WT	wild type
XIAP	X-linked inhibitor of apoptosis protein
XLP-2	X-linked lymphoproliferative syndrome type-2
XPC	xeroderma pigmentosum group C
XPE	xeroderma pigmentosum group E

Table of contents

1. Introduction

Selective protein degradation by the ubiquitin-proteasome system (UPS) has essential functions in diverse biological processes. Selectivity of the UPS is determined by ubiquitin ligases, which specifically recognise substrates and catalyse their ubiquitination, thus marking them for degradation by the 26S proteasome. Among ubiquitin ligases, cullin-RING ubiquitin ligases (CRLs) constitute the largest group. Because their substrates and functions are largely understudied or unknown, they represent a large reservoir for novel biological discoveries. Here, we focused on two ubiquitin ligases from the cullin-RING ubiquitin ligase 4 (CRL4) subfamily: $CRL4^{DCAF4}$ and $CRL4^{DCAF12}$. The main objective of this thesis was to identify and validate their candidate substrates and address the biological functions of the interactions between the ligase-substrate pairs. The first theoretical part reviews the relevant literature on $CRL4^{DCAF4}$ and $CRL4^{DCAF12}$ and their candidate substrates. Then, the experimental part describes the original results dealing with the identification and validation of the candidate substrates of $CRL4^{DCAF4}$ and $CRL4^{DCAF12}$ and the exploration of their biological roles. Finally, the biological relevance of the herein presented ligase-substrate pairs is discussed, and the main discoveries are summarised in the conclusion.

1.1. Ubiquitin-proteasome system

The UPS is the principal intracellular protein degradation pathway responsible for cellular homeostasis and regulation of diverse cellular processes. In this system, proteins are selectively targeted for proteasomal degradation by a covalent attachment of ubiquitin, a highly conserved small protein consisting of 76 amino acid residues. This posttranslational modification is termed ubiquitination (Figure 1a) and typically serves as a signal for protein degradation by the 26S proteasome (Figure 1b). Dysregulation of this system has been implicated in the pathogenesis of many human disorders, particularly neurodegenerative disorders and cancer, highlighting the relevance of the UPS in health and diseases [1].

Ubiquitination is carried out by a sequential action of three enzymes [2]. In the first step, ubiquitin is activated by a ubiquitin-activating enzyme (E1). This ATP-dependent step involves adenylation of the ubiquitin C-terminal Gly residue followed by thioester bond formation between the ubiquitin C-terminal Gly residue and the E1 active site Cys residue. Next, activated ubiquitin is transferred in a transesterification reaction to an active site Cys residue of a ubiquitin-conjugating enzyme (E2). In the last step, a ubiquitin ligase (E3) mediates ubiquitin transfer from the E2 to a substrate protein. The attachment of ubiquitin to the substrate protein typically occurs through an isopeptide bond, which is formed between the C-terminus of ubiquitin and the ε-amino group of a substrate Lys residue [2]. The isopeptide bond can be cleaved by deubiquitinating enzymes (DUBs). Their enzymatic action reverses

protein ubiquitination, which significantly contributes to the regulation of protein degradation [3]. An enormous number of genes dedicated to ubiquitination and deubiquitination underscores the importance of the UPS for cellular functions. For example, the human genome encodes 2 E1s, ~40 E2s, >600 E3s, and ~90 DUBs, representing ~4% of protein-coding genes [4–6].

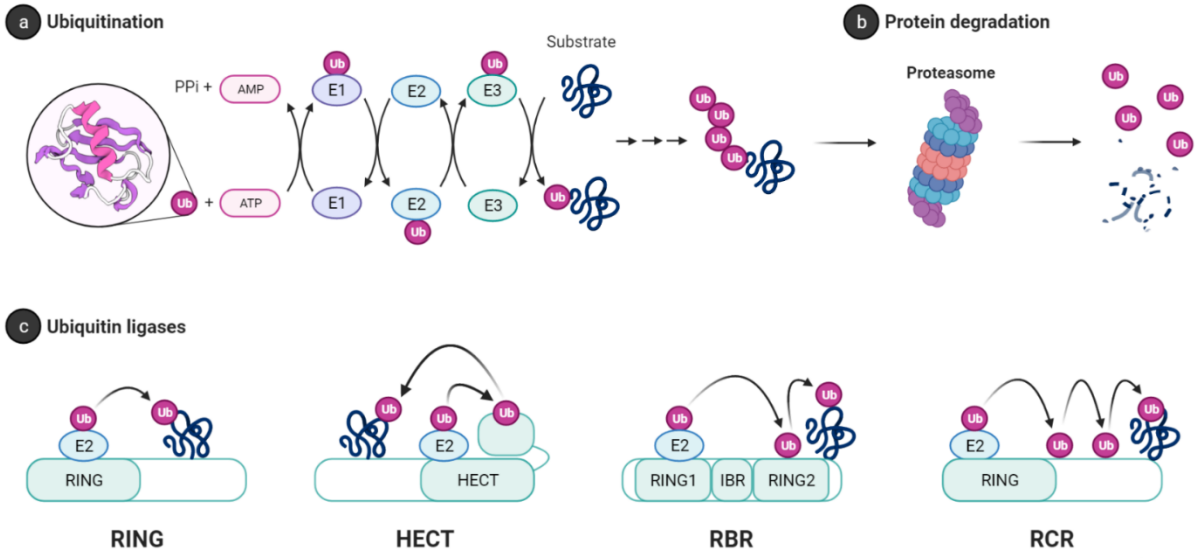

Figure 1. Ubiquitin-proteasome system. Ubiquitination-dependent protein degradation constitutes a principal mechanism of protein degradation in cells. Ubiquitination (a) is carried out by a sequential action of three enzymes: ubiquitin-activating enzyme (E1), ubiquitin-conjugating enzyme (E2), and ubiquitin ligase (E3). Through this enzymatic cascade, substrate proteins are modified by ubiquitin molecules (Ub) and targeted for degradation (b) by the 26S proteasome. The selectivity of this system is provided by ubiquitin ligases (c). They are classified into four families based on the presence of the conserved catalytic domain and the mechanism of ubiquitin transfer. Really interesting new gene (RING) ubiquitin ligases catalyse direct ubiquitin transfer from E2 to a substrate. Homologous to E6-AP carboxyl terminus (HECT), RING-in-between-RING (RBR), and RING-Cys-relay (RCR) ubiquitin ligases first accept ubiquitin from E2 and then transfer it to a substrate. Adapted from "Ubiquitin Proteasome System", by BioRender.com (2021). Retrieved from https://app.biorender.com/biorender-templates.

Ubiquitin ligases (E3) are critical components of the UPS that specifically recognise substrates and thus impart selectivity to the protein ubiquitination and degradation. In addition to the substrate binding, they simultaneously associate with the E2 linked to ubiquitin via a thioester bond (E2~Ub) and mediate ubiquitin transfer to a substrate. Not surprisingly, the activity of ubiquitin ligases and substrate recruitment are thoroughly regulated through various mechanisms, including posttranslational modifications or protein-protein interactions [7,8]. Based on the presence of the conserved catalytic domain and the mechanism of ubiquitin transfer to the substrate, ubiquitin ligases are classified into four families (Figure 1c): really interesting new gene (RING), homologous to E6-AP carboxyl terminus (HECT), RING-in-between-RING (RBR), and RING-Cys-relay (RCR) [7–9].

Most ubiquitin ligases belong to the RING family characterised by the catalytic RING finger or the structurally related U-box domain [7,8]. The RING finger coordinates two zinc atoms, whereas the U-box adopts a similar structure without coordinating any metal ions. The function of the RING and U-box domain is to recruit the E2~Ub and to configure the E2~Ub for ubiquitin transfer. RING ubiquitin ligases catalyse the direct ubiquitin transfer from the E2~Ub to a substrate. Substrates are recruited to the binding site that resides either in the same polypeptide as the catalytic domain or in a separate subunit in the case of multicomponent E3 complexes such as CRLs or the related anaphase-promoting complex/cyclosome (APC/C) [7,8].

The remaining three E3 families catalyse ubiquitin transfer through a reaction in which ubiquitin is first transferred from E2 to an active-site Cys residue of E3 and then from E3 to a substrate. HECT ubiquitin ligases (~28 members in the human genome) are characterised by the C-terminal catalytic HECT domain composed of two lobes. The N-terminal lobe interacts with E2~Ub, whereas the C-terminal lobe harbours an active-site Cys residue [7,10]. RBR ubiquitin ligases (~14 members in the human genome) contain two RING finger domains (RING1 and RING2) separated by an in-between-RING domain. RING1 recruits E2~Ub and transfers ubiquitin to an active-site Cys in the RING2 domain before attaching it to a substrate Lys residue [7,11]. The emerging RCR ubiquitin ligases contain the RING finger domain that recruits E2~Ub but employs a unique 'ubiquitin relay' catalytic step. Ubiquitin is first transferred from E2~Ub to an upstream active-site Cys and subsequently transferred to a downstream active-site Cys in an intramolecular transesterification reaction, termed ubiquitin relay, before it is attached to a substrate Thr residue [9].

Proteins can be modified by either a single ubiquitin attached to one/multiple sites (monoubiquitination/multimonoubiquitination, respectively) or a chain of ubiquitin molecules (polyubiquitination) [12]. Polyubiquitin chains are primarily built on substrates by sequential transfers of single ubiquitin molecules [13]. Ubiquitin contains seven Lys residues and an N-terminus, all of which can be linked to the C-terminus of another ubiquitin monomer through an isopeptide or peptide bond, respectively. By using eight different linkages (Lys6, Lys11, Lys27, Lys29, Lys33, Lys48, Lys63, and Met1), ubiquitin can form structurally distinct types of polyubiquitin chains [12,14]. The polyubiquitin chains are homotypic if the ubiquitin molecules are linked uniformly through the same Lys or Met residues. Alternatively, different types of linkages alternate, which results in heterotypic polyubiquitin chains. Heterotypic chains are further categorised as either mixed or branched, depending on whether they contain ubiquitin molecules modified on only a single or multiple Lys or Met residues [12,14].

The ubiquitin code is interpreted by proteins bearing ubiquitin-binding domains (UBDs), which are specific for different types of ubiquitin modifications and determine the functional outcome of protein ubiquitination [12]. Thus, ubiquitination can have various possible functions. In addition to targeting protein for degradation, ubiquitination can alter protein interactions, localisation, and

activity. A well-known example of the nondegradative function of ubiquitination is the role of Met1- and Lys63-linked homotypic polyubiquitin chains in inflammation [15,16]. On the contrary, Lys48-linked homotypic polyubiquitin chains, which are the most abundant, are the pivotal signals for proteasomal degradation. Several other ubiquitin modifications might target protein for degradation as well, including monoubiquitination, multimonoubiquitination, multiple short ubiquitin chains (Lys11, Lys48, and Lys68), and branched ubiquitin chains (Lys11/Lys48, and Lys48/Lys68) [17].

The 26S proteasome typically executes the selective degradation of the ubiquitinated proteins. The 26S proteasome is a large (~2.5 MDa), ATP-dependent proteolytic machinery consisting of a 20S core particle capped by one or two 19S regulatory particles [18,19]. The core particle comprises four stacked heptameric rings (two outer α- and two inner β-rings) that create a barrel-shaped structure with an interior proteolytic chamber. The two outer α-rings function as a gate, whereas the inner β-rings contain proteolytic sites with multiple specificities. The regulatory particle can be divided into two subcomplexes, the base and the lid. The base comprises ATPase subunits and ubiquitin-binding sites, while the lid harbours primarily structural subunits except for one with deubiquitinating activity [18,19]. Ubiquitinated proteins are recognised either directly by the 19S regulatory particle or by multiple shuttle factors associated with the proteasome. Following recognition, the substrate is unfolded, deubiquitinated, and translocated to the proteolytic chamber. While the substrate is degraded inside the proteolytic chamber into short peptides, ubiquitin molecules are released for another cycle of ubiquitination [18,19].

1.2. Cullin-RING ubiquitin ligases

Multisubunit CRLs constitute the largest family of ubiquitin ligases. They employ different cullins as molecular scaffolds, which organise other CRL subunits to bring E2 and substrate together. CRLs share a common molecular architecture consisting of two modules—the catalytic core and the interchangeable substrate-targeting module (Figure 2). The catalytic core comprises RING protein (RING-box protein 1 (RBX1) or RING-box protein 2 (RBX2)) and cullin. In humans, eight members of the cullin protein family (CUL1, 2, 3, 4A, 4B, 5, 7, and CUL9) assemble distinct CRL subfamilies [20]. While the C-terminal domain of cullin binds RING protein that recruits E2, the N-terminal part binds various substrate receptor subunits, typically linked to the catalytic core through an adaptor protein. Each substrate receptor recognises specific substrate(s), thereby conferring selectivity to ubiquitination. This modular architecture enables the assembly of over 200 distinct CRLs by combining different substrate targeting modules with the same catalytic core [20]. Since the thesis concerns cullin 4-based ubiquitin ligases, the ensuing description of the CRL molecular architecture and biological roles mainly focuses on the CRL4 subfamily.

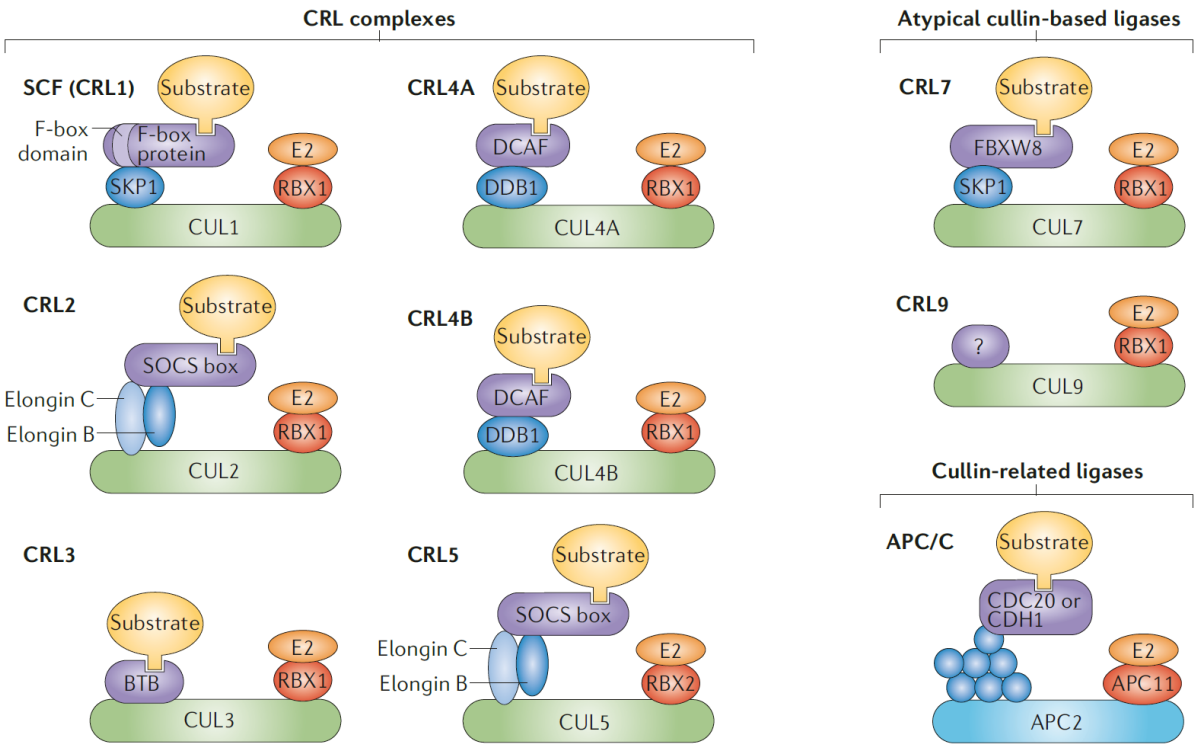

Figure 2. Cullin-RING ubiquitin ligases. Multisubunit cullin-RING ubiquitin ligase (CRL) complexes are composed of the catalytic core and the interchangeable substrate-targeting module. The catalytic core is composed of a RING protein (RBX1 or RBX2) and a cullin protein. In humans, eight members of the cullin protein family (CUL1, 2, 3, 4A, 4B, 5, 7, and CUL9) assemble distinct CRL subfamilies that employ distinct substrate-targeting modules to recognise substrates and bring them to the catalytic core. Anaphase-promoting complex/cyclosome (APC/C) is distantly related to CRL complexes. Reprinted from ref. [21], copyright 2013, with permission from Springer Nature.

1.2.1. Molecular architecture

CRL4s are composed of the catalytic core containing either cullin-4A (CUL4A) or cullin-4B (CUL4B) bound to RING protein RBX1 and an interchangeable adaptor-substrate receptor module. CUL4A and CUL4B are closely related paralogs exhibiting extensive sequence homology (over 80% sequence identity) and substantial functional redundancy [22]. The main difference between these two cullins lies in their spatiotemporal expression patterns and subcellular localisation. CUL4B contains a unique N-terminal extension harbouring nuclear localisation signal (NLS) and localises predominantly to the cell nucleus, whereas CUL4A exhibits nucleocytoplasmic localisation [22,23]. CUL4A and CUL4B are structurally indistinguishable, both of them adopting an elongated shape with a long helical N-terminal domain and a globular C-terminal domain [24,25]. The C-terminal domain of CUL4A/B binds to RBX1, while the N-terminal domain tethers an interchangeable adaptor-substrate receptor module to the catalytic core.

CUL4A/B utilises DNA damage-binding protein 1 (DDB1) as an adaptor to engage multiple DDB1- and CUL4-associated factors (DCAFs) that act as substrate receptors [24,26–28]. DDB1 is a large

protein containing three seven-bladed beta-propellers: beta-propeller A (BPA), beta-propeller B (BPB), and beta-propeller C (BPC) [29]. DDB1 devotes the entire BPB for CUL4A/B binding and use its two other beta-propellers (BPA and BPC) to accommodate distinct DCAFs into the CRL4 complex [24,25]. DCAFs typically consist of a WD-repeat domain responsible for substrate recognition and docking to the DDB1 [24,26–28]. Additionally, several DCAFs, including DCAF4 and DCAF12, also use an α-helical H-box motif outside the WD-repeat domain for docking to the DDB1 [30].

1.2.2. Assembly and regulation

The activity and assembly of CRLs are dynamically regulated by cycles of cullin neddylation and substrate receptor exchange mediated by cullin-associated NEDD8-dissociated protein 1/2 (CAND1/2). Neddylation is a protein post-translation modification by the ubiquitin-like protein NEDD8. It is catalysed by a sequential action of three enzymes, in a similar way to ubiquitination. First, NEDD8 is activated by a NEDD8 activating enzyme (NAE), then transferred to a NEDD8-conjugating enzyme, and finally attached to a target substrate by a NEDD8 ligase. The best-characterised substrates of neddylation are cullin family members [31]. NEDD8 is covalently attached to a single conserved lysine residue on the cullin C-terminal domain, inducing conformational rearrangement in the catalytic core and activating CRL [32,33]. NEDD8-induced rearrangement positions the E2~Ub in proximity to the substrate and prevents the substrate receptor exchange factors CAND1/2 from accessing the cullin [32,33]. Of note, neddylation can be inhibited by a potent, selective NAE inhibitor MLN4924, which represents a valuable research tool as it renders CRLs inactive [34,35]. Proteolytic removal of NEDD8 from cullin (cullin deneddylation), and thus CRL deactivation, is catalysed by an eight-subunit COP9 signalosome (CSN) complex. Substrate binding to the CRL inhibits cullin deneddylation as the bound substrate sterically hinders the access of CSN to the CRL, thereby preventing cullin deneddylation and CRL deactivation [36,37]. On the contrary, NEDD8 is rapidly cleaved from cullin when a substrate is not present, paving the way for CAND1/2-mediated substrate receptor exchange.

CAND1/2 acts as an exchange factor, which binds to deneddylated cullins and dislodges adaptor-substrate receptor modules from the CRL catalytic cores [38–40]. There are limited amounts of the CRL catalytic cores in cells, and the great majority of adaptor-substrate receptor modules are not assembled into CRLs. For example, 90% of cellular DDB1-DCAF modules are not bound to CUL4A/B at a given time. CAND1/2 activity continuously remodels the cellular CRL repertoire by facilitating CRL assembly and disassembly [41–44]. The exchange cycle is temporarily stopped by substrate binding, which inhibits CSN-mediated deneddylation and thus CAND1/2-mediated substrate receptor exchange. In this way, adaptive disequilibrium is created, favouring CRL complexes with available substrates [41–44]. The cycles of cullin neddylation and CAND1/2-mediated substrate receptor exchange maintain the plasticity of the cellular CRL repertoire, thereby ensuring the accumulation of specific CRL complexes for which cognate substrates become available.

1.2.3. Substrate recognition

The mechanisms of substrate recognition by CRLs are incredibly diverse and reflect a wide range of functions performed by the UPS [45]. Substrate receptor subunits of the CRLs specifically recognise their cognate substrate through degradation signals termed degrons. The canonical degron is a minimal element within a substrate sufficient for recognition and degradation by a proteolytic apparatus. Degrons are often short linear motives, either recognised in their native form or modified by posttranslational modifications, such as phosphorylation. However, structural motives (e.g., globular domains, specific conformational and assembly states) and binding to small molecules (e.g., secondary metabolites, hormones) also frequently mediate the interaction and degradation. While aberrant proteins (e.g., the product of erroneous protein synthesis or misfolded proteins) tend to be constitutively recognised once they emerge, regulatory proteins are only recognised in response to (or absence of) specific stimuli. Therefore, the interaction between the CRL substrate receptor subunit and its cognate substrate is often subjected to tight regulation to achieve spatially and temporally specific degradation [45].

Canonical degrons might reside anywhere within a protein sequence but are particularly enriched at the extreme N-termini (N-degrons) and C-termini (C-degrons) [46,47]. Apart from being constitutively present in full-length proteins, they can be exposed following proteolytic cleavage, generated by a posttranslational modification of terminal residues, or present in truncated proteins. Proteins bearing these degrons are degraded by multiple N-degron (formerly N-end rule) and C-degron pathways, which regulate amber biological processes and are often involved in monitoring various aspects of protein quality control [46,47]. While N-degrons were the first degrons to be discovered in short-lived proteins, the diversity of C-degrons has only recently emerged. C-degron motives are broadly underrepresented in eukaryotic proteomes and are often recognised by tandem repeat domains of the CRL substrate receptor subunits [46,48]. Among the C-degron pathways, those targeting proteins ending in the C-terminal glycine residues (C-terminal Gly degron) are best-characterised [48–52]. C-terminal Gly degrons are recognised by the Kelch domain-containing proteins, which are substrate receptor subunits of the cullin 2-based ubiquitin ligases. These C-terminal glycine degron pathways regulate the stability of multiple full-length proteins. Additionally, they eliminate mislocalised proteins, cleavage products of deubiquitinating enzymes, and truncated selenoproteins generated by failed UGA to Sec decoding [48–52]. C-terminal degrons are also known to be targeted by two CRL4 complexes: $CRL4^{TRPC4AP}$ recognising proteins bearing an arginine residue at -3 position (C-terminal -Rxx degron) and $CRL4^{DCAF12}$ regulating the stability of proteins ending in a twin-glutamic acid degron (C-terminal -EE degron) [48]. The physiological roles of these pathways are yet to be determined.

1.2.4. Physiological functions and clinical relevance

CRL4s orchestrate and regulate various cellular processes, including cell cycle progression and maintenance of genomic integrity. However, despite massive progress in uncovering the diversity of CRL4s, the substrates and functions of most of them remain unknown or insufficiently characterised. Arguably, the most extensively studied CRL4s are those that utilise the Cdc10-dependent transcript 2 (CDT2), the DNA damage-binding protein 2 (DDB2) and the Cockayne-syndrome protein A (CSA) as a substrate receptor. The following sections thus focus on these three well-known examples. Finally, the phenotypic abnormalities in CRL4-deficient mice and CRL4 clinical relevance are discussed.

$CRL4^{CDT2}$ has emerged as a master regulator of cell cycle progression and genome stability that targets numerous proteins for degradation during the S phase and after DNA damage [53]. $CRL4^{CDT2}$ recognises its substrates only when bound to the proliferating cell nuclear antigen (PCNA) loaded on DNA. Many substrates of $CRL4^{CDT2}$ are key cell cycle regulators, such as DNA replication factor CDT1, histone methyltransferase SETD8, and cell cycle inhibitor p21. Their timely degradation prevents re-replication, genomic instability, ensures timely cell cycle progression and accurate DNA repair [53].

$CRL4^{DDB2}$ and $CRL4^{CSA}$ function in the nucleotide excision repair (NER) pathway that eliminates a wide range of helix-distorting DNA lesions, including ultraviolet light (UV)-induced pyrimidine dimers and bulky adducts caused by various chemicals [54]. Two distinct NER subpathways differing in the mode of DNA lesion recognition exist: the global-genome NER (GG-NER) surveying the whole genome and the transcription-coupled NER (TC-NER; also referred to as transcription-coupled repair) operating on the transcribed strand of active genes. Both sub-pathways ultimately converge at the point of transcription factor IIH (TFIIH) recruitment followed by the excision of DNA lesion containing oligonucleotides, gap-filling DNA repair synthesis and nick ligation [54].

The GG-NER employs DNA damage sensor XPC (xeroderma pigmentosum group C) to recognise helix-distorting DNA lesions and recruit TFIIH [55]. DNA damage recognition by XPC is facilitated by the DDB1-DDB2 complex (also known as the UV-DDB complex), which directly recognises UV-induced cyclobutane pyrimidine dimers (CPDs) and (6-4) pyrimidine-pyrimidine photoproducts (6-4PPs) [25,56]. In addition to being required for efficient recruitment of XPC to UV-induced lesions, DDB1-DDB2 assembles into active $CRL4^{DDB2}$ on UV-damaged chromatin [57] and mediates ubiquitination of nearby histones [58,59], XPC [60], and DDB2 itself [61,62]. Of these, ubiquitination of DDB2 is particularly critical. It leads to eviction of DDB2 from chromatin and its degradation in the proteasome, which is essential for timely DNA damage handover from DDB2 to XPC and efficient repair [63,64]. The importance of $CRL4^{DDB2}$ in the repair of UV-induced DNA damage is highlighted by mutations in the *DDB2* gene, which give rise to xeroderma pigmentosum group E (XPE) disorder characterised by cutaneous sensitivity to sunlight exposure and predisposition to skin cancer [65].

The TC-NER is initiated when elongating RNA polymerase II (RNAPII) stalls at a DNA lesion. DNA damage-stalled RNAPII associates with Cockayne-syndrome protein B (CSB), which in turn sequentially recruits DDB1-CSA, UV-stimulated protein A (UVSSA), and TFIIH to initiate DNA repair [66]. $CRL4^{CSA}$ complex assembled on stalled RNAPII contributes to UV-induced ubiquitination of K1268 in the largest subunit of RNAPII (RPB1). This ubiquitination has emerged as the most critical regulatory event in TC-NER, promoting TFIIH recruitment and DNA repair but leading to RNAPII degradation when repair fails [67–70]. Additionally, $CRL4^{CSA}$ targets CSB and activating transcription factor 3 (ATF3) for proteasomal degradation in response to UV irradiation, which is also supposed to facilitate transcription recovery after DNA repair [70–72]. Supporting the essential role of $CRL4^{CSA}$ in transcription-coupled repair, mutations in the *CSA* gene abrogate this repair pathway and cause Cockayne syndrome (CS), a developmental and neurological disorder characterised by developmental delay, progressive growth failure and progressive microcephaly [73].

The importance of CRL4 function is underscored by complex phenotypic abnormalities observed in *Ddb1, Cul4a*, *Cul4b* knockout (KO) mice and the clinical presentation of CRL4-deficiency in humans. The germ-line deletion of *Ddb1*, the sole CRL4 adaptor, causes early embryonic lethality [74]. Conditional inactivation of this gene in the epidermis or the brain and lens leads to genomic instability and apoptosis of the proliferating cell. As a result, nearly complete loss of epidermis or neuronal and lens degeneration, respectively, is observed along with neonatal death [74,75]. The genetic ablation of *Ddb1* in other tissues also causes severe defects, including abrogation of haematopoiesis [76], skeleton development [77] or oocyte meiosis [78–80]. CUL4A and CUL4B, the CRL4 scaffold proteins, overlap substantially in their functions and largely compensate for each other. Despite this, they have distinct roles in some biological processes, supposedly due to the difference in their expression and localisation [22]. While *Cul4a* is dispensable for embryonic development [81], germline deletion of *Cul4b* causes embryonic lethality resulting from attenuated growth and increased apoptosis in extra-embryonic tissue [82–84]. Germline deletion of *Cul4a* and epiblast specific deletion of *Cul4b*, which prevents embryonic lethality, generate viable mice with no gross abnormalities except for male infertility [81,82,84–88]. Both *Cul4a* and *Cul4b* are essential for male reproduction due to their distinct roles during spermatogenesis [85–88]. Additionally, *Cul4b*-deficient mice exhibit many phenotypic abnormalities, such as cognitive impairment [83] or a defect in the inflammatory response [89]. In human patients, multiple mutations in the *CUL4B* gene are causal for X-linked mental retardation [90–92]. *CUL4B*-deficient patients display numerous clinical symptoms, such as mental retardation, aggressive outbursts, tremor, macrocephaly, obesity, small testes, gynecomastia, high arch, and abnormal toes [90–92]. No specific syndromes associated with mutations in *CUL4A* or *DDB1* genes have been reported. Nevertheless, aberrant expression of numerous CRL4 components (CUL4A/B, DDB1, and various DCAFs) has been associated with tumorigenesis, highlighting the clinical significance of CRL4s in cancer [93].

1.3. $CRL4^{DCAF4}$ and its potential substrates

1.3.1. DCAF4

DDB1- and CUL4-associated factor 4 (DCAF4) is a CRL4 substrate receptor subunit. *DCAF4* was initially identified as a gene associated with leucocyte telomere length [94]. A single-nucleotide polymorphism rs2535913 lying within the *DCAF4* gene is associated with a decline in *DCAF4* expression and shortened leukocyte telomere length [94]. Recently, DCAF4 was suggested to target suppression of tumorigenicity 7 (ST7) for degradation [95] and to mediate the ubiquitination of optineurin [96]. However, the conclusions drawn in these recent studies are insufficiently supported by experimental evidence. The *bona fide* substrates and function of DCAF4 thus remain elusive. In addition to DCAF4, the human genome encodes its two paralogs with unknown function—DDB1- and CUL4-associated factor 4-like protein 1 (DCAF4L1) and DDB1- and CUL4-associated factor 4-like protein 2 (DCAF4L2).

1.3.2. Box H/ACA ribonucleoproteins

Box H/ACA ribonucleoproteins (RNPs) consist of box H/ACA RNAs and four core box H/ACA proteins. The core proteins are dyskerin (DKC1; CBF5 in yeast and archaea), NHP2 (L7Ae in archaea), NOP10, and GAR1. Box H/ACA RNPs serve several vital functions in cells. Most importantly, they catalyse site-specific isomerisation of uridine to pseudouridine—RNA pseudouridylation. Box H/ACA RNPs utilise the base-pairing between box H/ACA RNAs and substrate RNAs to specify the target uridines and the box H/ACA proteins to catalyse the modification itself. The most abundant substrates of box H/ACA RNPs are ribosomal RNAs (rRNAs) and spliceosomal small nuclear RNAs (snRNAs), which are integral components of the ribosome and spliceosome, respectively [97]. Apart from pseudouridylation, box H/ACA RNPs are essential for the stability of box H/ACA RNAs, including vertebrate telomerase RNA component (TERC) [98]. Box H/ACA RNPs are thus crucial for the correct function of the ribosome and spliceosome and telomere maintenance. In addition to these well-described roles, box H/ACA RNPs act as OCT4/SOX2 coactivators, regulating the expression of essential pluripotency genes critical for self-renewal in embryonic stem cells [99]. Underscoring the importance of box H/ACA RNPs for cellular functions, the central box H/ACA protein CBF5 is essential for viability in yeasts and disruption of the gene encoding its ortholog DKC1 in mice causes embryonic lethality [100,101]. In humans, germline mutations impairing DKC1 function give rise to dyskeratosis congenita, a rare telomere biology disorder [102].

1.3.2.1. Composition, structure, and biogenesis of box H/ACA RNPs

Box H/CA RNPs, composed of one box H/ACA RNA and four core proteins, are evolutionarily conserved across archaeans and eukaryotes. Box H/ACA RNAs are characterised by common sequence

motives and secondary structures (Figure 3a). Most eukaryotic H/ACA RNAs consist of two hairpins connected by a single-stranded hinge region containing consensus AnAnnA sequence (the H box) and followed by a short 3' tail possessing an ACA triplet (the ACA box) [103,104]. In contrast, their archaeal counterparts contain one to three hairpins, followed by the ACA box [105]. Each hairpin comprises a lower stem, an internal loop termed the pseudouridylation pocket, an upper stem, and an apical loop. Functional pseudouridylation pockets are complementary to the sequence flanking the unpaired target uridine in substrate RNA (Figure 3b), hence specifying uridines that are to be converted into pseudouridines [106,107].

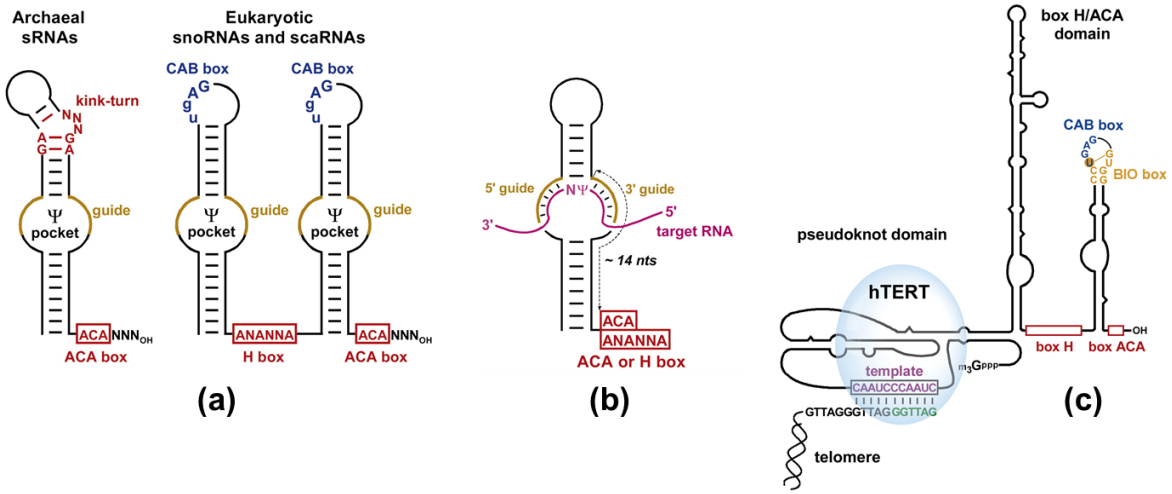

Figure 3. Structure of box H/ACA RNAs. (a) Schematic representation of canonical archaeal and eukaryotic box H/ACA RNAs. The conserved H, ACA, and CAB boxes, kink-turn, and pseudouridylation pocket (Ψ pocket) with guide sequences are depicted. (b) Selection of target uridine by base-pairing between guide sequences in the Ψ pocket and substrate (target) RNA. (c) Schematic representation of human telomerase RNA component (TERC) with the box H/ACA domain at its 3´end. The functionally essential sequence elements and telomerase reverse transcriptase (TERT) are depicted. TERC contains a sequence serving as a template for telomeric repeat synthesis, critical for telomere length maintenance. Adapted from ref. [108], copyright 2010, with permission from Elsevier.

In higher eukaryotes, two important classes of box H/ACA RNAs that function as guide RNAs in site-specific pseudouridylation are small nucleolar RNAs (snoRNAs) and small Cajal body-specific RNAs (scaRNAs) directing rRNA and snRNA pseudouridylation, respectively [103,104,106,107,109,110]. While snoRNAs accumulate and operate in the nucleolus, scaRNAs are confined to the Cajal bodies [109]. The Cajal body-specific accumulation of box H/ACA scaRNAs requires an additional sequence motif (consensus UGAG) called the Cajal body box (CAB box), which is located in each apical loop of their hairpins [111]. The trans-acting factor that recognises the CAB box and is responsible for the Cajal body-specific accumulation of box H/ACA scaRNAs is the WD repeat-containing protein 79 (WDR79; also referred to as telomerase Cajal body protein 1 (TCAB1)) [112,113]. Another prominent member

of box H/ACA RNAs is vertebrate TERC (Figure 3c) that contains a box H/ACA domain required for its accumulation and telomerase enzymatic activity [98,114]. Within the box H/ACA domain of TERC, the conserved terminal stem-loop region (called CR7) of the 3´ hairpin contains a biogenesis-promoting box (BIO box) and a CAB box, the latter being responsible for TERC targeting to Cajal bodies [115–119]. In addition to these box H/ACA RNAs with well-described roles, human cells also express hundreds of low-abundant AluACA snRNAs derived from intronic Alu elements with unknown functions [120,121].

The common core proteins associated with H/ACA RNAs are DKC1 (CBF5 in yeast and archaea), NHP2 (L7Ae in Archaea), NOP10, and GAR1 [122–125]. The catalytic subunit of box H/ACA RNPs is DKC1/CBF5 that belongs to the TruB family of pseudouridine synthases characterised by a central catalytic TruB domain followed by an RNA-binding pseudouridine synthase and archaeosine transglycosylase (PUA) domain [126,127]. Although CBF5 provides the actual catalytic activity, the remaining three core proteins and the guide RNA are also necessary for efficient substrate RNA pseudouridylation catalysed by box H/ACA RNPs [128–131].

Most of our understanding of molecular architecture and catalytic mechanism of box H/ACA RNPs is derived from studies on archaeal H/ACA RNP complexes (Figure 4a) [132–137]. A single hairpin archaeal H/ACA RNA is draped over the CBF5-NOP10-L7Ae core trimer and makes no direct contact with GAR1. The upper stem of the hairpin contains a conserved kink-turn (K-turn) motif bound by L7Ae and interacts with NOP10 and CBF5 as well. The pseudouridylation pocket is located in the vicinity of the active site of CBF5, whereas the lower stem of the hairpin and the ACA box is bound to the PUA domain of CBF5 [134–137]. L7Ae binds the K-turn of H/ACA RNA and anchors the upper stem. This anchoring is critical for positioning the pseudouridylation pocket of H/ACA RNA and substrate RNA in the vicinity of the CBF5 active site. CBF5 is composed of the catalytic domain and PUA domain anchoring the lower stem and the ACA box. The N-terminus of CBF5 contributes an additional β strand to the β sheet of the C-terminal PUA domain. The catalytic domain of CBF5 directly and separately binds NOP10 and GAR1. NOP10 adopts an extended structure and tightly associates with the catalytic domain of CBF5 to stabilise the catalytic centre [132–137]. GAR1, which forms a six-stranded β-barrel structure and makes no contact with H/ACA RNA nor substrate RNA, also interacts with the catalytic domain of CBF5 and is critical for substrate turnover by engaging with a thumb loop of CBF5. This RNA-binding loop, located between strands β7 and β10, oscillates between the substrate-free (open) and the substrate-bound (close) conformations. In the open conformation, the thumb loop binds GAR1, allowing loading and release of substrate RNA. The binding of substrate RNA induces a conformation switch of the thumb loop from open to close conformation, in which the thumb loop locks substrate RNA in the active site of CBF5 to enable the catalysis [133–137]. While the pseudouridylation pocket of internal H/ACA RNA mediates the sequence-specific recognition of substrate RNA, the box H/ACA proteins are responsible for placing the target uridine into the active site of CBF5, the pseudouridylation itself, and substrate turnover.

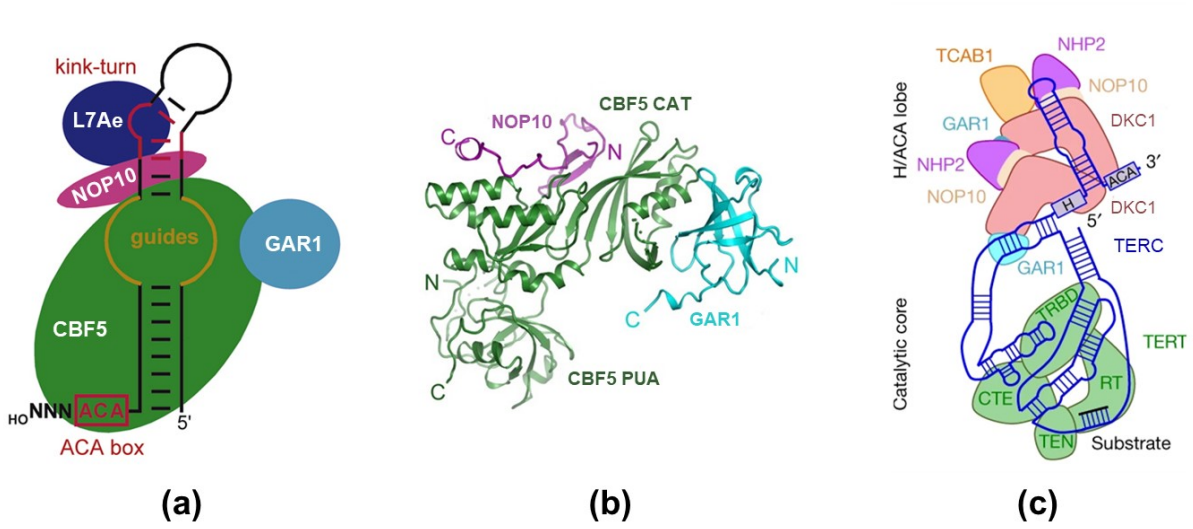

Figure 4. Structure of box H/ACA ribonucleoproteins. (a) Schematic representation of archaeal box H/ACA RNPs. A single hairpin archaeal H/ACA RNA with all core box H/ACA proteins is depicted. Adapted from ref. [108], copyright 2010, with permission from Elsevier. (b) Partial crystal structure of the yeast CBF5-NOP10-GAR1 complex. NOP10, the central catalytic (CAT) and PUA domain of CBF5, and the central core domain of GAR1 were used for crystallisation and structure determination. Adapted from ref. [130], under the CC-BY-NC license. (c) Schematic representation of cryogenic electron microscopy structure of the human telomerase holoenzyme. Adapted from ref. [138], copyright 2018, with permission from Springer Nature.

Eukaryotic H/ACA RNPs display several notable structural differences as revealed by a partial crystal structure of the yeast H/ACA RNP (Figure 4b) [130] and a cryo-electron microscopy structure of the human telomerase holoenzyme (Figure 4c) [138,139]. Firstly, eukaryotic H/ACA RNAs lack the K-turn motif. NHP2, a homolog of archaeal L7Ae, binds RNA non-specifically and is instead more tightly bound to NOP10. Nevertheless, NHP2 occupies a similar position as L7Ae in H/ACA RNPs and performs the same role in anchoring the top region of H/ACA RNA [131]. Secondly, eukaryotic CBF5 possesses an N- and C-terminal extension (NTE and CTE), flanking the central catalytic and PUA domains, and a long C-terminal Lys-rich tail. Notably, the NTE of CBF5 forms an extra structural layer on the PUA domain, whereas the CTE was not observed in the crystal at all [130]. Thirdly, the conserved core domain of eukaryotic GAR1 also possesses an NTE and CTE. The CTE of GAR1 contains a novel eukaryote-specific helix α1 that contacts the base of the CBF5 thumb loop and participates in the regulation of substrate turnover. Moreover, the central core domain of GAR1 is flanked by glycine- and arginine-rich (GAR) domains in eukaryotes [130]. Finally, cryogenic electron microscopy (cryo-EM) structures of human telomerase holoenzyme offered the first glimpse of the overall organisation of eukaryotic box H/ACA RNPs. Box H/ACA domain of TERC adopts the hairpin-hinge-hairpin-tail structure and is bound by two sets of H/ACA core proteins. Furthermore, the CAB box in the 3´hairpin is bound by TCAB1 that also directly interacts with DKC1 and GAR1. Interestingly, the N-terminal region and PUA domain of DKC1, which combine in tertiary structure, mediate the interaction with the box H/ACA RNA and dimerisation of DKC1 molecules [138,139]. Despite

these differences between archaeal and eukaryotic box H/ACA RNPs, their general structure and catalytic mechanism seem to be evolutionary well-conserved.

Biogenesis of eukaryotic box H/ACA RNPs requires several assembly factors, including two box H/ACA RNP-specific factors SHG1 and NAF1 and the general chaperone complex R2TP [140–142]. In lower eukaryotes (e.g., *Saccharomyces cerevisiae*), box H/ACA RNAs are typically found in independent mono- or polycistronic transcription units. In contrast, mammalian box H/ACA RNAs, except for TERC, are processed from introns of precursor messenger RNA (pre-mRNA) transcripts [110,143]. CBF5 initially interacts with assembly factor SHQ1 that protects CBF5 from aggregation and prevents non-specific RNA binding [144–146]. Specifically, SHG1 acts as an RNA mimic, interacting with the PUA domain and CTE of CBF5 similarly to RNA [144,145]. The subsequent replacement of SHQ1 by box H/ACA RNA requires dissociation of SHQ1 from CBF5 catalysed by the R2TP complex containing two closely related AAA+ ATPases, pontin and reptin [147]. The core box H/ACA proteins CBF5, NOP10, and NHP2, are co-transcriptionally recruited along with assembly factor NAF1 to the box H/ACA RNA transcription sites and assembled with box H/ACA RNA to form immature box H/ACA RNPs containing NAF1 instead of GAR1 [148–151]. NAF1 possesses a domain structurally homologous to the core domain of GAR1 and binds to CBF5 in a mutually exclusive manner with GAR1 [130,150,152]. Despite occupying the same sites of CBF5 as GAR1, NAF1 is incapable of substrate turnover, thereby keeping the box H/ACA RNP inactive until NAF1 replace GAR1 during the final steps of the box H/ACA RNP maturation [130,150,152]. Mature box H/ACA RNPs accumulate in the nucleoli and Cajal bodies, the sites of rRNA and snRNAs processing and modification [109].

1.3.2.2. Role of box H/ACA RNPs in RNA pseudouridylation

Pseudouridine (Ψ), a C5-glycoside isomer of uridine, is the most abundant RNA post-transcriptional modification that fine-tunes RNA functions. Its formation involves breakage of the nitrogen-carbon glycosidic bond between uracil and ribose, 180° rotation of detached uracil, and reattachment of uracil to the ribose through a carbon-carbon glycosidic bond. In comparison with uridine, pseudouridine has distinct chemical properties. It possesses the carbon-carbon glycosidic group between uracil and ribose and an imino group in the base acting as an additional hydrogen bond donor [97]. Consequently, the presence of pseudouridine within the RNA sequence stabilises the local RNA structure. Although pseudouridines differ subtly from uridines, they are often clustered in evolutionarily conserved and functionally essential regions of non-coding RNAs and have important biological functions [97]. Pseudouridylation is catalysed by phylogenetically related pseudouridine synthases. They operate either as a stand-alone enzyme (e.g., transfer RNA (tRNA) pseudouridine synthases) or rely on an internal guide RNA to direct site-specific conversion of uridine into pseudouridine [127].

Box H/ACA RNPs, the sole presentative of RNA-guided pseudouridine synthases, mainly catalyse pseudouridylation of rRNAs and snRNAs, the fundamental components of the ribosome and spliceosome, respectively. Additionally, transcriptome-wide approaches identified many CBF5/DKC1-dependent pseudouridylation sites in snoRNAs, TERC, and messenger RNAs (mRNAs), yet the biological relevance of these sites remains unclear [153–155]. In yeasts, strains expressing catalytically inactive CBF5 are viable, but display abolished pseudouridylation of rRNAs and a severe growth defect [156]. Likewise, mouse cells defective in rRNA pseudouridylation due to the expression of catalytically inactive DKC1 display a growth defect and have altered rRNA processing and unstable mature rRNA [157]. Furthermore, in yeasts, it was also demonstrated that the deletion of box H/ACA snoRNAs guiding the pseudouridylation in functionally important regions of rRNA (such as the ribosomal peptidyl transferase centre, the intersubunit bridge, and the decoding centre) impairs the growth and translation [158–161]. In yeast and human cells, the defects in rRNA pseudouridylation lower the affinity of ribosomes for tRNA and internal ribosome entry site (IRES) elements. These defects manifested as decreased translation fidelity and decreased initiation of IRES-dependent translation [162]. In hypomorphic *DKC1* mutant mice and cells derived from patients with mutations in *DKC1*, IRES-mediated translation is particularly impaired, including that of the tumour suppressors p27 and p53 and the anti-apoptotic factors such as Bcl-xL [163–166]. Beyond rRNAs, spliceosomal snRNAs are also extensively pseudouridylated, particularly U2 snRNA. In vertebrates, it was shown that the box H/ACA RNP-catalysed pseudouridylations in and near the U2 branch site recognition region is necessary for snRNP formation and efficient pre-mRNA splicing [167–169]. Collectively, box H/ACA RNPs are crucial for the correct function of the ribosome and spliceosome, thereby fine-tuning translation and splicing.

1.3.2.3. Role of box H/ACA RNPs in telomere maintenance

Telomeres are structures at the ends of eukaryotic chromosomes comprised of telomeric repeat sequences (TTAGGG in vertebrates) and associated proteins. Due to the inherent end-replication problem, telomeres shorten with every round of DNA replication, eventually reaching a critical length and triggering replicative senescence [170]. Telomeric repeats can be extended by telomerase to counteract telomere shortening. Telomerase is a large RNP complex specialised in the synthesis of telomeric DNA repeats at the 3’ ends of linear chromosomes. The catalytic core of telomerase consists of telomerase reverse transcriptase (TERT) and TERC, which serves as a template for the telomeric repeat synthesis. While TERC is broadly expressed, the expression of TERT is usually restricted to highly proliferative cells, thereby providing them with telomerase activity and thus the ability to elongate telomeres. Because telomere length maintenance is the major determinant of replicative lifespan, it is tightly controlled. Not surprisingly, defects in telomerase regulation have dire consequences.

Telomerase reactivation is associated with most cancers, whereas pathological telomere shortening due to defects in the telomerase function is linked to a wide range of disorders, such as dyskeratosis congenita [170].

TERC acquired a box H/ACA domain at its 3´end in vertebrates [98] and thereby hijacked the box H/ACA RNP maturation pathway for its biogenesis and stabilisation. The box H/ACA domain of TERC is bound by two sets of the core box H/ACA proteins and TCAB1; all of them are part of active telomerase holoenzyme [138,139]. A notable difference between conventional box H/ACA RNAs (snoRNAs and scaRNAs) and TERC is the presence of the BIO box in the 3´ hairpin of its box H/ACA domain that enhances box H/ACA RNP assembly [119]. The same 3´ hairpin also contains the CAB box recognised by TCAB1 responsible for TERC concentration in Cajal bodies [111–113,117]. Importantly, the box H/ACA domain of TERC and box H/ACA proteins (except for GAR1) are essential for TERC accumulation, telomerase activity, and telomere length maintenance [98,114,171–174]. Thus, being required for the biogenesis and stabilisation of TERC RNPs, box H/ACA RNPs are essential for telomerase activity and telomere maintenance.

1.3.2.3. Dyskeratosis congenita

Dyskeratosis congenita is a rare heterogeneous disorder characterised by bone marrow failure and the triad of abnormal skin pigmentation, nail dystrophy and mucosal leukoplakia [175]. Additionally, patients suffering from this disorder have a predisposition to cancer. Although sporadic cases frequently occur, dyskeratosis congenita is typically inherited. The pattern of inheritance might be X-linked (often caused by mutations in *DKC1*), autosomal recessive (e.g., caused by mutations in *NHP2*, *NOP10*, or *TCAB1*), or autosomal dominant (e.g., caused by mutations in *TERC* or *TERT*). Collectively, genes found to be mutated in patients with dyskeratosis congenita encode proteins required for telomere maintenance. Accordingly, short telomeres are a hallmark of dyskeratosis congenita, which is therefore considered a telomere biology disorder [176]. The most common X-linked dyskeratosis congenita is caused by mutations in the *DKC1* gene [102]. Most of these mutations are clustered in two regions outside the catalytic domain of DKC1 and are thought to selectively impair the assembly of box H/ACA proteins with TERC [139,177]. As a result, patients with X-linked dyskeratosis congenita have decreased levels of TERC but not conventional box H/ACA RNAs, reduced telomerase activity, and shorter telomeres [171,172]. Although the defect in telomerase maintenance and definitive haematopoiesis is well-established and characterised, the connection between telomere dysfunction and the pathophysiology of dyskeratosis congenita remains poorly understood [172,178].

1.4. CRL4^{DCAF12} and its potential substrates

1.4.1. DCAF12

DDB1- and CUL4-associated factor 12 (DCAF12) is a CRL4 substrate receptor subunit initially identified as a regulator of tissue growth and apoptosis in *Drosophila melanogaster* [179]. DCAF12 is essential for completing Drosophila metamorphosis as its loss is lethal at the pupal stage. During development, DCAF12 limits tissue growth and is required for developmental apoptosis. Notably, misregulation of death-associated inhibitor of apoptosis 1 (DIAP1) during the developmental apoptosis was observed in these flies. Moreover, the DCAF12 role in facilitating apoptosis and limiting abnormal growth seems to be also critical for tissue homeostasis in adults [179]. The same group also discovered that is DCAF12 is involved in innate immunity as its loss caused a strong suppression in antimicrobial peptide expression after infection of larvae with bacteria [180]. At the molecular level, they observed deregulation of death-associated inhibitor of apoptosis 2 (DIAP2) [180]. DIAP2 is an essential component of the immune deficiency (Imd) signalling pathway, which deals with infections with gram-negative bacteria and induces the expression of antimicrobial peptides [181]. Recently, DCAF12 was implicated in regulating the Hippo pathway by targeting Yki/Yap/Taz for ubiquitination and degradation [182]. In the nucleus, Yki/Yap/Taz is phosphorylated and stabilised by CDK7. In the absence of CDK7-mediated phosphorylation, Yki/Yap/Taz was shown to be degraded by DCAF12, which led to downregulation of the Hippo-dependent gene expression (including expression of DIAP1), reduced organ size, and diminished tumour growth [182]. Additionally, DCAF12 is essential for normal synaptic function and plasticity, and its depletion impairs Drosophila larval locomotion [183]. In fly larvae, DCAF12 is expressed in glia, neurons, and muscles. At larval neuromuscular junctions, DCAF12 is primarily found presynaptically in axons, synaptic boutons, and nuclei of motor neurons. Postsynaptically, DCAF12 localises to muscle nuclei. Presynaptic DCAF12 is required for neurotransmitter release and synaptic homeostatic potentiation, while postsynaptic DCAF12 negatively controls the synaptic levels of the glutamate receptor subunits [183].

DCAF12 has two close paralogs (protein sequence similarity ~70%) in placental mammals—DDB1- and CUL4-associated factor 12-like protein 1 (DCAF12L1) and DDB1- and CUL4-associated factor 12-like protein 2 (DCAF12L2) [184]. DCAF12L2 probably emerged by retrotransposition in the placental mammal ancestor. In contrast, the appearance of DCAF12L1 seems to be a result of tandem duplication, and DCAF12L1 is present only in Euarchontoglires (a clade that includes rodents and primates) [185]. The expression pattern of DCAF12 paralogs differs from DCAF12 and whether they assemble into functional CRL4 is unknown. In human cells, DCAF12 regulates the stability of proteins ending in a twin-glutamic acid degron (C-terminal -EE degron) [48]. So far, only the regulation of the melanoma antigen gene (MAGE) family members by DCAF12 was studied [186]. Expression of MAGEs is usually

restricted to male germ cells. However, MAGEs are often aberrantly reactivated in various cancers, in which they drive tumorigenesis. In cancer cells, DCAF12 targets MAGE-A3 and MAGE-A6 for degradation in response to starvation and this degradation was shown to facilitate autophagy induction [186]. However, the physiological function of DCAF12 in vertebrates remains unknown.

1.4.2. XIAP and SMAC

X-linked inhibitor of apoptosis protein (XIAP) belongs to the inhibitors of apoptosis protein (IAP) family characterised by the presence of at least one baculoviral IAP repeat (BIR) domain. This zinc-coordinating domain resembles the classical zinc finger and mediates protein-protein interactions. Members of the IAP family have evolutionarily conserved roles in cell death pathways, inflammation, and innate immunity. Their negative regulators are collectively termed as IAP antagonists, a loosely defined group of proteins binding to the BIR domains of IAPs and thus antagonising their (anti-apoptotic) functions. They typically contain an N-terminal IAP-binding motif (IBM), which they insert into the hydrophobic IBM binding groove on BIR domains. One of these IAP antagonists is the second mitochondria-derived activator of caspase (SMAC; also known as direct IAP-binding protein with low pI—DIABLO), a potent endogenous inhibitor of the XIAP anti-apoptotic activity [187].

The Drosophila genome encodes four IAPs. Of these, DIAP1 prevents apoptosis by binding to and inhibiting apoptotic proteases called caspases, thereby being essential for cell survival [188–190]. Additionally, DIAP1 inhibits the assembly of the death-inducing platform called apoptosome [191]. In contrast, the main function of DIAP2, being an essential component of the Imd pathway, lies in innate immunity. Imd signalling pathway resembles the mammalian tumour necrosis factor receptor (TNFR) signalling, but its role in flies is to sense and combat gram-negative bacterial infections [181,192,193]. The activities of the Drosophila IAPs are antagonised by several IBM-containing proteins such as reaper, hid, grim, sickle, jafrac2, and dOMI, which induce apoptosis in response to different apoptotic stimuli [194–199].

In humans, there are eight members of the IAP family, cellular IAP1 and 2 (cIAP1 and cIAP2) being the two closest XIAP paralogs. XIAP and cIAPs harbour three BIR domains (BIR1 to BIR3), a ubiquitin-associated (UBA) domain and a C-terminal RING domain. BIR domains mediate protein-protein interactions, UBA enables binding to polyubiquitin chains, and the RING domain provides an E3 ubiquitin ligase activity and mediates homodimerisation of IAPs [187]. In addition, cIAPs also possess a caspase activation and recruitment domain (CARD) that mediates autoinhibition of their E3 ubiquitin ligase activity under steady-state conditions [200]. XIAP is the only IAP family member that potently suppresses apoptosis by directly binding to caspases and inhibiting their activity [201]. Additionally, XIAP and cIAPs regulate inflammatory and innate immune responses. They participate in ubiquitin signalling downstream of various pattern recognition receptors (PRRs) and TNFR superfamily members

and mediate activation of nuclear factor-kappa B (NF-κB) and mitogen-activated protein kinase (MAPK) signalling pathways. While XIAP is crucial for signalling downstream of nucleotide-binding oligomerisation domain 2 (NOD2) receptor, cIAPs are involved in Toll-like receptor (TLR) and TNFR pathways [202]. Moreover, XIAP, together with cIAPs, inhibits the assembly of the death-inducing platform called ripoptosome. Besides these well-described roles, XIAP was implicated in a broad range of other cellular activities such as positive regulation of the Wnt signalling pathway [203], a negative regulation of autophagy [204], and regulation of copper homeostasis [205–207].

SMAC is dominantly a mitochondrial protein with a well-described pro-apoptotic role. Upon apoptotic stimuli, it is released from the mitochondrial intermembrane space into the cytosol, where it interacts with IAPs and promotes caspase activation by reliving XIAP-imposed caspases inhibition [208,209]. The SMAC precursor contains the N-terminal pre-sequence responsible for its transport to the mitochondria, where SMAC undergoes two-step processing by mitochondrial processing peptidase (MPP) and inner membrane protease PARL [210]. The cleavage generates the mature form of SMAC with the N-terminal IBM sequence (AVPI), which binds to the BIR2 and BIR3 domains of XIAP [211–214]. Similarly, SMAC also binds to BIR3 domains of cIAPs [215] and the BIR domain of Livin [216]. SMAC binding induces the degradation of cIAP1 and cIAP2 but does not of XIAP and Livin [217]. Of note, there are several SMAC isoforms (β, γ, δ) differing in the N-terminal parts and the subcellular localisation, which might have functions non-related to apoptosis [218]. Importantly, SMAC might also have immunomodulatory functions due to its ability to antagonise various IAPs. It was indeed shown that the mitochondrial release of SMAC dampens the XIAP inflammatory functions [219]. Moreover, the mitochondrial outer membrane permeabilisation (MOMP) followed by the SMAC release is no longer considered a point of no return in apoptosis execution. Indeed, various pro-inflammatory effects of MOMP are now being recognised [220,221]. Therefore, uncovering the potential roles of SMAC in the regulation of innate immune responses might represent a novel, exciting area of research.

1.4.2.1. Role of XIAP and SMAC in apoptosis

Apoptosis is a form of programmed cell death essential in the development and homeostasis of multicellular organisms [222]. Moreover, it constitutes an efficient strategy of host defence against viral infection [223]. Apoptosis is characterised by distinct morphological features, such as cell shrinkage, nucleus condensation and fragmentation, membrane blebbing, and the formation of apoptotic bodies that are rapidly cleared by phagocytic cells [222,223].

The core components of the apoptotic pathway are well-conserved in evolution and centre around a family of cysteine-aspartic proteases called caspases [224,225]. Caspases are synthesised as inactive precursors (procaspases), which are proteolytically activated in response to specific stimuli.

Activation involves the removal of an N-terminal pro-domain and cleavage into a large and a small subunit. Mature caspases are composed of two heterodimers, each formed by the large and small subunits. Upon activation, caspases cleave their substrates after aspartate, glutamate or even phosphoserine residues, thereby orchestrating diverse biological processes [224–226]. Beyond apoptosis, they play crucial roles in inflammation and cell differentiation. Caspases involved in apoptosis are divided based on their function and domain architecture into two groups: initiator and executioner. The initiator caspases contain a long N-terminal pro-domain, which mediates their dimerisation and recruitment into multiprotein complexes essential for their activation. The pro-domains comprise either a CARD domain (caspases-2, -9) or tandem of death-effector domains (DED; caspases-8, -10). On the contrary, the executioner caspases-3, -6 and -7 possess a short N-terminal pro-domain and are activated following their initial cleavage by initiator caspases [224,225].

The initiator caspases are activated in response to external or internal stimuli through extrinsic or intrinsic apoptotic pathways (Figure 5), respectively. Both pathways eventually converge at proteolytic activation of the executioner caspases-3, -6 and -7, which cleave their substrates and execute the cell death [224,225]. The extrinsic (also known as death receptor-mediated) apoptotic pathway is initiated through the engagement of cell surface death receptors of the TNFR superfamily, such as tumour necrosis factor (TNF), TNF-related apoptosis-inducing ligand (TRAIL), and Fas receptors with their cognate ligands [227]. This signalling leads to the assembly of the death-inducing signalling complex (DISC) that recruits and activates caspase-8 and -10. Caspase-8 also cleaves BH3-only protein BID to generate its truncated form (tBID), thereby amplifying the apoptotic response by engaging the intrinsic apoptotic pathway [227]. The amplification is required for apoptosis in so-called “type 1” cells, such as hepatocytes, but not in “type 2” cells, such as thymocytes. XIAP is the crucial discriminator between type 1 and type 2 Fas-induced apoptosis [228]. While the XIAP loss does not affect apoptosis in thymocytes, it renders hepatocytes independent of BID in Fas-induced apoptosis [228].

The intrinsic (also known as mitochondrial or Bcl-2-regulated) apoptotic pathway senses the cellular stress (e.g., DNA damage, growth factor or cytokine deprivation) and activates caspase-9 [229]. The initiation of this pathway is controlled by members of the Bcl-2 protein family that either promote or inhibit apoptosis. The interplay of three subgroups of this family (BH3-only proteins, pro-survival Bcl-2 proteins, and the pro-apoptotic effector proteins BAX and BAK) is crucial for maintaining the balance between pro- and anti-apoptotic signals, thus setting the apoptotic threshold. The stress signal is conveyed by BH3-only proteins that inhibit the pro-survival Bcl-2-like proteins, enabling the activation of the pro-apoptotic effector proteins BAX and BAK [229]. The effector proteins permeabilise the mitochondrial outer membrane, which leads to the release of pro-apoptotic factors such as cytochrome c, SMAC, and serine protease HTRA2/OMI [208,209,230,231]. In the cytoplasm, cytochrome c associates with apoptotic protease-activating factor 1 (APAF1), which triggers the assembly of a multimeric caspase-9-

activating complex called apoptosome [232]. SMAC contributes to the activation of apoptosis by binding to caspase inhibitor XIAP, thereby relieving XIAP-imposed caspase inhibition [187].

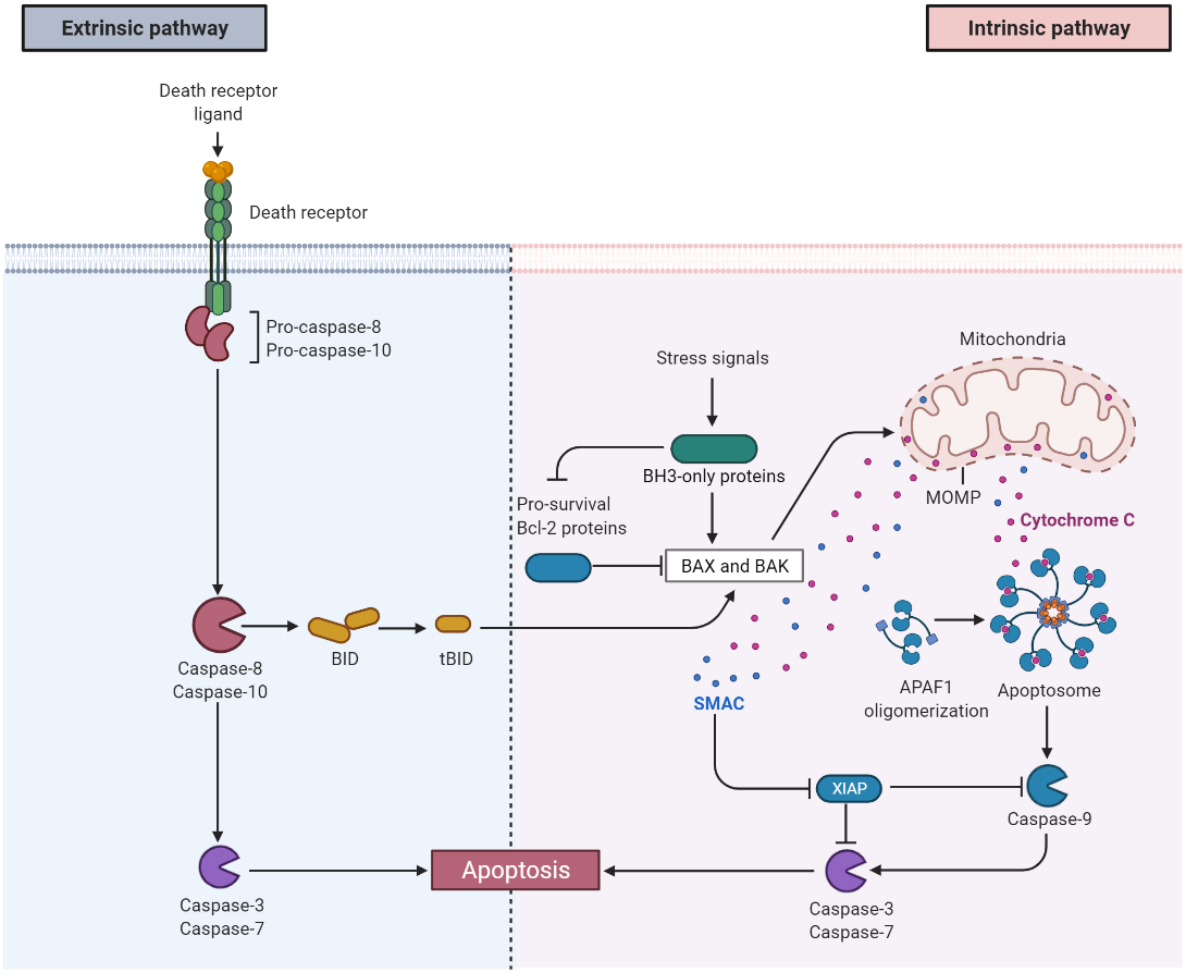

Figure 5. Extrinsic and intrinsic apoptotic pathways. The extrinsic apoptotic pathway is activated by the engagement of death receptors with their cognate ligands, which leads to the activation of the initiator caspase-8 and -10. Activated initiator caspases proteolytically activate executioner caspase-3 and -7, ultimately triggering apoptosis. Caspase-8 also cleaves BH3-only protein BID to generate its truncated form (tBID), amplifying the apoptotic response by engaging the intrinsic apoptotic pathway. Stress signals activate the intrinsic apoptotic pathway. The activation is controlled by the interplay of the Bcl-2 family members (BH3-only proteins, pro-survival Bcl-2 proteins, and the pro-apoptotic effector proteins BAX and BAK). Activated BAX and BAK induce mitochondrial outer membrane permeabilisation (MOMP), releasing mitochondrial pro-apoptotic factors such as cytochrome c and SMAC. In the cytosol, cytochrome c associates with APAF1 and triggers the assembly of the apoptosome, which activates the initiator caspase-9. Activated caspase-9 subsequently proteolytically activates effector caspases, ultimately triggering apoptosis. SMAC contributes to caspase activation by binding to XIAP, thereby relieving the XIAP-mediated inhibition of caspases-3, -7 and -9. Adapted from "Apoptosis Extrinsic and Intrinsic Pathways", by BioRender.com (2021). Retrieved from https://app.biorender.com/biorender-templates.

XIAP inhibits caspases-3, -7 and -9 by distinct mechanisms. Caspases-3 and -7 are directly inhibited by a linker region preceding the BIR2 domain of XIAP in cooperation with the BIR2 domain itself. Specifically, the linker occupies and blocks the active sites of caspases-3 and -7 [233–236]. BIR2 domain contributes to the inhibition by strengthening the XIAP-caspase interaction and is required for relieving caspases-3 and -7 inhibition by SMAC [234–236]. In contrast, caspase-9 is inhibited by the BIR3 domain of XIAP [214,237]. The N-terminus of the small subunit of caspase-9 harbours an IBM, which binds to the BIR3 domain of XIAP [214]. This interaction traps caspase-9 in a monomeric state and thus inhibits its activity [238].

The XIAP-mediated inhibition of caspases-3,-7, and -9 is relieved by SMAC and other IBM-containing proteins during apoptosis. SMAC dimerises and acts as a tetramer, which binds through its four N-terminal IBMs to the BIR2 and BIR3 domains of dimeric XIAP [211–214,239]. Consequently, caspases and SMAC compete for binding to XIAP, which makes their interaction with XIAP mutually exclusive. In addition to SMAC, several other mitochondrial proteins harbouring N-terminal IBM were identified to be released from mitochondria to the cytoplasm during apoptosis and interact with XIAP [240]. Among them, serine protease HTRA2/OMI also potently potentiates caspase activation and apoptosis [230,231,241]. Not only does serine protease HTRA2/OMI directly antagonises the interaction between XIAP and caspases, but it is also able to proteolytically cleave and thus inactivates XIAP to promote apoptosis [242–244].

Apoptosis-related protein in the TGF-beta signalling pathway (ARTS), a splice variant of the *SEPTIN4* gene, also antagonises the anti-apoptotic activities of XIAP. In response to the apoptotic signal, ARTS rapidly translocates from the mitochondrial outer membrane to the cytosol, where it binds XIAP and mediates XIAP degradation [245–247]. Unlike SMAC and serine protease HTRA2/OMI, ARTS does not contain an IBM sequence and binds to the distinct binding pocket in the BIR3 domain of XIAP [248–250]. The XIAP-ARTS interaction triggers the XIAP self-ubiquitination and degradation. Additionally, it bridges XIAP and ARTS-interacting E3 ubiquitin-protein ligase SIAH1, which also targets XIAP for degradation [251]. Moreover, ARTS acts as a scaffold bringing XIAP and Bcl-2 into a ternary complex to promote XIAP-mediated ubiquitination and degradation of Bcl-2 in response to apoptotic stimuli [252]. Importantly, ARTS acts upstream of the MOMP and releases pro-apoptotic factors from mitochondria [245–247]. As an initial burst of caspase activity is required for the MOMP and timely release of cytochrome c and SMAC, it is believed that ARTS promotes apoptosis by this initial derepression of caspases [247].

Degradation of XIAP during apoptosis ultimately overcomes its caspase-inhibitory function. SMAC and XIAP are both degraded after induction of apoptosis, though the exact mechanisms underlying their degradations are still controversial and might be cell-type specific [253–255]. ARTS is responsible for early XIAP degradation preceding MOMP [245,247,251], while serine protease HTRA2/OMI might contribute to XIAP degradation following MOMP [242–244]. The binding of SMAC

to XIAP does not seem to induce XIAP self-ubiquitination and subsequent degradation as it does in the case of cIAPs [217]. Once caspases are activated, caspase-3 cleaves XIAP, leading to subsequent XIAP degradation and sensitising cells to apoptosis [256,257]. Additionally, XIAP E3 ubiquitin ligase activity is itself a determinant of XIAP stability [255]. XIAP ubiquitinates various substrates, including SMAC, serine protease HTRA2/OMI, caspases and itself [258]. Because XIAP-mediated ubiquitination often has a function other than targeting modified protein for degradation, much remains to be learned about the precise roles of these ubiquitination events. Consistently, targeted deletion of the XIAP RING domain revealed stabilisation of truncated XIAP and reduced caspase-3 polyubiquitination accompanied by elevated caspase-3 activity under certain apoptotic condition [255]. The latter indicates that XIAP-mediated non-degradative polyubiquitination of caspases contributes to their inhibition. Importantly, SMAC and XIAP were still degraded following apoptotic induction in cells lacking the XIAP RING domain [255] suggesting that the XIAP and SMAC are degraded during apoptosis independently of the XIAP ubiquitin ligase activity.

Taken together, XIAP is a crucial inhibitor of caspases antagonised by several IAP antagonists upon apoptotic stimuli, including SMAC, and tightly regulated by the UPS. Furthermore, being an E3 ubiquitin ligase itself, XIAP exercises its E3 activity to ubiquitinate its counterparts, thereby adding another layer of complexity to the multilayer crosstalk of various regulatory circuits centred around XIAP and caspase. Consequently, the factors involved in XIAP regulation are critical determinants of the cellular decision between cell death and survival.

1.4.2.2. Targeting XIAP by SMAC and ARTS mimetics

Overexpression of IAPs, including XIAP, frequently occurs in various human cancers, enabling them to evade apoptosis and impeding cancer therapy. Therefore, targeting IAPs by small compounds mimicking the action of endogenous IAP antagonists has become an attractive approach for therapeutic intervention in cancer [259]. Peptides derived from N-terminal IBM of mature SMAC can solely remove the inhibition of caspase-9 and are sufficient to sensitise cells for apoptosis [211–213,260]. Relieving the XIAP-imposed inhibition on caspases-3 and -7 requires a dimeric SMAC N-terminal peptide [261]. These properties of SMAC-derived peptides and the detailed knowledge of the topology of the IBM binding groove on the BIR domains of XIAP paved the way for the development of SMAC mimetics.

SMAC mimetics are small compounds mimicking the SMAC-derived peptides with improved pharmacological properties. There are two types of SMAC mimetics: monovalent and bivalent (dimeric). Monovalent SMAC mimetics (e.g., LCL161) consist of one SMAC-mimicking element, while bivalent SMAC mimetics (e.g., birinapant) utilise two SMAC-mimicking moieties connected with a chemical linker. Bivalent SMAC mimetics concurrently bind both the BIR2 and BIR3 domain of XIAP and

generally display higher binding affinities than monovalent SMAC mimetics [262]. Up to now, five monovalent and three bivalent compounds have completed or are involved in ongoing phases 1 and 2 clinical trials, in which their therapeutic potential in the treatment of various cancers is evaluated. These compounds are generally well-tolerated by patients but have limited clinical benefits as single agents. Therefore, their administration combined with other therapeutic interventions to enhance their clinical potential is now being explored [263,264].

SMAC mimetics were initially designed to have broad specificity and target several IAP proteins containing BIR domains with IBM binding grooves (XIAP, cIAPs, Livin). They usually bind to cIAPS with high affinity and to XIAP with lower affinity. In addition to preventing the interaction between XIAP and caspases, SMAC mimetics induce rapid autoubiquitylation and proteasomal degradation of c-IAPs but not XIAP [265,266]. Autoubiquitylation of cIAPs is caused by conformational rearrangements induced by the SMAC/SMAC mimetics binding to the BIR3 domains of cIAPs, which enables the dimerization of their RING domain and the formation of the active E3 ligase [267]. Consequently, loss of cIAPs promotes tumour necrosis factor-alpha (TNF-α)-induced apoptosis of sensitive cancer cells [265,266]. In more detail, cIAPs meditate constitutive ubiquitylation and proteasomal degradation of NF-kappa-B-inducing kinase (NIK), thereby acting as negative regulators of non-canonical NF-κB signalling. Accordingly, loss of cIAPs results in NIK accumulation and activation of the noncanonical NF-kB pathway [265,266]. The activation of NF-kB signalling induces the expression of numerous pro-inflammatory genes, including TNF-α that engages tumour necrosis factor receptor 1 (TNFR1) in an autocrine or paracrine manner and thus induces apoptosis in responsive cells [265,266]. The binding of TNF-α to TNFR1 triggers the formation of a membrane-associated TNFR1 signalling complex, in which cIAPs mediate non-degradative polyubiquitination of receptor-interacting serine/threonine-protein kinase 1 (RIPK1). This polyubiquitination creates a pro-survival signalling platform for signalling events that eventually activate canonical NF-κB signalling. Accordingly, loss of cIAPs abrogates RIPK1 ubiquitination and enables RIPK1 to form caspase-8-activating complex, thereby switching the pro-survival TNF-α signalling into the cell death-inducing [268,269]. SMAC mimetics thus also inhibits anti-apoptotic functions of cIAPs. In addition to suppressing cell death, IAPs are also crucial regulators of many inflammatory pathways (TNFR, TLR, and NOD2 signalling) and dysregulation of these pathway might also contribute to the clinical effect of SMAC mimetics. Consistently, both the adverse effects caused by inflammation (such as cytokine release syndrome and Bell's palsy) and the suppression of inflammatory signalling were reported [263]. The future direction for SMAC mimetics thus might be in their use as therapeutic for chronic inflammatory diseases.

To selectively target XIAP, a novel small compound mimicking the action of ARTS has recently been developed. ARTS mimetic A4 binds specifically to the unique binding groove on the BIR3 domain of XIAP but not cIAP1. A4 promotes XIAP and Bcl-2 degradation, caspase-9 and -3 activation, leading

subsequently to apoptosis [250]. These unique features of their action make ARTS mimetics a promising candidate for developing a new class of specific XIAP-antagonists used for therapeutic intervention in cancer.

1.4.2.3. Role of XIAP in innate immunity and inflammation

Innate immunity is the first line of defence against invading pathogens. Innate immune responses are initiated upon microbial PAMPs (pathogen-associated molecular patterns) or injured tissue-released DAMPs (danger/damage-associated molecular patterns) recognition by PRRs. These receptors are either intracellular or present on the cell surface. Their ligation usually activates MAPK and NF-κB signalling pathways to induce the expression of inflammatory mediators, such as pro-inflammatory cytokines and chemokines. Some PRRs, instead of triggering transcriptional programs, assemble multiprotein complexes called inflammasomes. Inflammasome activates caspase-1, which proteolytically cleaves inactive precursors of pro-inflammatory interleukin-1 beta (IL-1β) and interleukin-18 (IL-18) as well as the pyroptotic cell death effector gasdermin D to generate their mature active forms [270]. The initial inflammation is essential for controlling infection, eliminating tissue injury, and orchestrating the adaptive immune response. XIAP plays several roles in these innate immunity pathways. In particular, XIAP is critically involved in NOD2 signalling [271–275] and negative regulation of inflammation [276–279].

XIAP is crucial for NOD2-mediated inflammatory signalling. NOD2 is an intracellular PRR that senses a conserved bacterial cell wall peptidoglycan component, muramyl dipeptide (MDP), and triggers pro-inflammatory responses [280]. Upon MDP recognition, NOD2 undergoes oligomerization and recruitment of the receptor-interacting serine/threonine-protein kinase 2 (RIPK2). RIPK2 interacts with XIAP, which builds polyubiquitin chains on RIPK2. These chains are necessary for the recruitment of the linear-chain ubiquitin assembly complex (LUBAC) to the NOD2 signalling complex. LUBAC generates Met1-linked polyubiquitin chains, and the resulting polyubiquitin-based signalling platform recruits and activates the inhibitor of nuclear factor kappa-B kinase (IKK) and TGF-beta-activated kinase 1 (TAK1). These events eventually lead to the activation of MAPK and NF-kB signalling pathways, which activate transcription of pro-inflammatory genes, including cytokines [272–275]. Notably, XIAP binds RIP2 through its BIR2 domain. This interaction can be abolished by the XIAP selective antagonists preferentially binding the BIR2 domain of XIAP, which thereby impairs NOD2-mediated inflammatory signalling [274].

XIAP, in cooperation with cIAPs, has been shown to restrict spontaneous receptor-interacting serine/threonine-protein kinase 3 (RIPK3)- and caspase-8-driven NACHT, LRR and PYD domains-containing protein 3 (NLRP3) inflammasome activation, IL-1β maturation and secretion, and RIPK3-dependent

cell death [276–279]. In myeloid cells, TLR and TNFR1 stimulation (e.g., with lipopolysaccharide (LPS) and TNF, respectively) or IAPs loss (e.g., upon genotoxic stress or induced by SMAC mimetics) leads to the formation of a large complex termed ripoptosome. The core components of this complex are RIPK1, FAS-associated death domain protein (FADD), caspase-8, and additional proteins such as RIPK3 and cellular FLICE-like inhibitory protein (cFLIP) isoforms [281,282]. Ripoptosome determines whether the cell survives, undergoes RIPK3-dependent necroptosis or caspase-8-mediated apoptosis. Additionally, ripoptosome-associated RIPK3 signalling promotes caspase-8 ubiquitination, activation and induces the formation of NLRP3 inflammasome. These events lead to proteolytic processing and maturation of IL-1β, which is mediated by both the active caspases-8 and NLRP3 inflammasome-associated caspase-1 [276–279]. However, how IAPs inhibit ripoptosome formation and how ripoptosome drives the activation of the NLRP3 inflammasome remains an outstanding question in the field.

1.4.2.4. *Xiap* and *Smac* deficiency in mice

Xiap and *Smac* are ubiquitously expressed in mice. The first studies dealing with *Xiap*- and *Smac*-deficient mice focused on their role in apoptosis. Surprisingly, they showed no obvious phenotype, and cells derived from these animals exhibited no defects in apoptosis induced by a variety of stimuli [283,284]. However, the subsequent studies revealed that loss of *Xiap* sensitises certain cell types such as intestinal stem cells and hair follicle stem cells for apoptosis [285,286]. Furthermore, *Xiap*-deficient mice are immunocompromised and fail to clear some pathogens [219,287–289]. *Xiap* deficiency causes a reduction in MAPK and NF-kB activation and early proinflammatory cytokine production following infection with certain pathogens [219,287–289]. Moreover, *Xiap*-deficient mice frequently develop hyperinflammation upon infection, accompanied by excessive secretion of pro-inflammatory cytokines (especially IL-1β) and increased RIPK3-dependent cell death of myeloid cells [279,287,290]. Apart from the innate immune responses, loss of *Xiap* affects the adaptive responses as well. No abnormalities in apoptosis of *Xiap*-deficient thymocytes and splenocytes were observed [283]. However, XIAP and cIAP1 are both required for survival of activated $CD8^+$ T cells and effective anti-viral adaptive immunity [291]. Additionally, *Xiap*-deficient regulatory T cells (Tregs) are impaired in their suppressive function [292]. Altogether, *Xiap*-deficient mice exhibit dysregulation of various immune processes highlighting the crucial role of XIAP and its regulation in the immune system.

1.4.2.5. X-linked lymphoproliferative syndrome type-2

In humans, mutations in the *XIAP* gene are associated with a rare primary immunodeficiency known as X-linked lymphoproliferative syndrome type-2 (XLP-2). A triad of the most frequent clinical manifestations of XLP-2 consists of hemophagocytic lymphohistiocytosis (HLH) frequently triggered by

Epstein-Barr virus (EBV) infection, recurrent splenomegaly, and inflammatory bowel disease (IBD) with the features of Crohn's disease [293–296]. HLH is a condition of severe hyperinflammation caused by uncontrolled proliferation and activation of lymphocytes and macrophages, which produce high amounts of inflammatory cytokines, such as IL-1β, interleukin-6 (IL-6), IL- 18, TNF-α, and interferon gamma (IFNγ). HLH is often triggered by infectious pathogens, particularly viruses, and leads to tissue damage and multiorgan failure [293–296]. Recurrent splenomegaly also frequently occurs in XLP-2 patients without systemic HLH, and it is often associated with cytopenia and fever [295]. Another typical clinical manifestation of XLP-2 is the early-onset IBD with Crohn's disease features, such as focal inflammatory lesions, crypt abscesses, granulomas, and polymorphic cellular infiltrates [293]. Although significant progress in the identification of the molecular mechanisms underlying XLP-2 aetiology has been made (e.g., defects in NOD2 signalling and negative regulation of inflammation, enhanced apoptosis of activated T cells), it is still unclear how they contribute to XLP-2 development and what other XIAP actions are involved.

1.4.3. MOV10

Moloney leukemia virus 10 protein (MOV10) is a highly conserved RNA helicase belonging to the UPF1-like group of the helicase superfamily 1 [297,298]. MOV10 homologs have been found in plants (SDE3 in *Arabidopsis thaliana* [299]), nematodes (ERI-6/7 in *Caenorhabditis elegans* [300,301]), and insects (Armi in *Drosophila melanogaster* [302,303]). The vertebrate genome also encodes MOV10 paralog MOV10-like protein 1 (MOV10L1), which arose by gene duplication [304,305]. MOV10 and its homologs have evolutionary conserved but enigmatic roles in post-transcriptional gene silencing (RNA interference; RNAi) and silencing transposons, viruses, and recently duplicated genes [299,301–308].

Retrotransposons restricting and antiviral activities of MOV10 are a crucial part of the host defence system across diverse species. In human cells, MOV10 binds retrotransposon RNAs and is a potent inhibitor of retrotransposition [309–312]. Specifically, MOV10 was shown to post-transcriptionally reduce levels of retrotransposon transcripts [312] and inhibit reverse transcription [311]. However, the exact mechanism of retrotransposon restriction remains unclear [313,314]. Regarding its antiviral activities, overexpression of MOV10 inhibits replication and reduces infectivity of a wide range of exogenous retroviruses, including human immunodeficiency virus type-1 (HIV-1) [309,315–318]. Contrary, endogenous MOV10 has no effect or is even required as a co-factor for HIV-1 infection [309,315,317,319]. Furthermore, *MOV10* is an interferon-stimulated gene (ISG) [320,321] that exhibits broad antiviral activity against various RNA viruses, such as vesicular stomatitis virus (VSV) [322], hepatitis C virus (HCV) [320,323], influenza A virus [324,325], and bunyavirus [326]. Interestingly, this function of MOV10 is independent of its helicase activity [322,323,325,326]. As with HIV-1, HCV replication is inhibited by the excess of MOV10 but promoted by endogenous MOV10. Similarly, MOV10 facilitates

replication of the hepatitis delta virus (HDV) [327]. In addition, MOV10 restricts hepatitis B virus (HBV) replication [328,329]. Although HBV is a DNA virus, it uses reverse transcription to replicate, which is the stage of the HBV life cycle blocked by MOV10 [328,329].

MOV10 has an important role in post-transcriptional gene regulation, especially in the microRNA (miRNA) pathway [330–333]). Human MOV10 localises to cytoplasmic processing bodies (P-bodies) when overexpressed, associates with RNA-induced silencing complex (RISC), and participates in its functions [330,331,334]. MOV10 predominantly binds to G-rich secondary structures (RNA G-quadruplexes) in the close proximity to miRNA recognition element (MRE) in the 3' UTR and has an ATP-dependent 5' to 3' RNA unwinding activity [333,335]. Such MOV10 unwinding activity is supposed to expose formerly inaccessible MRE for subsequent association with argonaute2 (AGO2), resulting in miRNA-mediated translational suppression. Additionally, a subset of MOV10-bound mRNAs is regulated by the functional association of MOV10 with the fragile X mental retardation protein (FMRP), which has a dual function in regulating translation. FMRP facilitates miRNA-mediated translational suppression by recruiting MOV10 and AGO2 to some mRNAs. However, the proximal binding of FMRP and MOV10 blocks AGO2 association with MRE in other mRNAs and enables their translation [333]. MOV10 also directly interacts with UPF1 and is believed to facilitate nonsense-mediated mRNA decay [335]. Furthermore, MOV10 was also implicated in polycomb-mediated transcriptional silencing of the INK4a locus [336].

The physiological function of MOV10 has been explored in the murine brain and testes [337,338]. *Mov10* is expressed ubiquitously across all tissues. However, its protein level is particularly elevated in the postnatal murine brain, where MOV10 localises to the cell nucleus and cytoplasm. Two-thirds of MOV10-bound RNA in the postnatal murine brain represent retrotransposon RNAs, while the remaining one-third are mRNAs encoding proteins involved predominantly in neuronal projection and cytoskeleton [337]. A subset of MOV10-bound mRNAs in the murine brain is also bound to FMRP and AGO2. This subset is enriched for neuronal genes and likely regulated by the miRNA pathway in the same manner as in human cells [333,337]. Since the loss of both *Mov10* alleles is embryonic lethal, heterozygous *Mov10* KO mice were used to study the MOV10 function in the murine brain. These animals have reduced protein levels of MOV10 and exhibit neuronal and behavioural alterations. Specifically, this reduction of MOV10 in the murine brain results in increased retrotransposition, defects in neuronal morphology, and behavioural changes [337]. Interestingly, MOV10 in mice and its homolog Armi in *Drosophila melanogaster* localise to synapses, where they are degraded in response to neuronal stimuli [339,340]. This degradation releases a set of mRNAs, including *CaMKII*, from translational suppression, thereby regulating localised protein synthesis during synaptic plasticity [339,340].

In murine testes, *Mov10* is mainly expressed in spermatogonia and exhibits nucleocytoplasmic localisation [338]. Most MOV10-bound RNAs in testes mapped to genic regions and were significantly

enriched in GC-rich repeat sequences. Knockdown of *Mov10* in spermatogonial progenitor cells (SPCs) cultured *in vitro* caused profound changes in their transcriptome and negatively impacted their proliferation and *in vivo* repopulation capacity. Importantly, MOV10 was shown to regulate the miRNA biogenesis and implicated in the splicing control [338]. Testes also express a germ-cell-specific paralog of *Mov10*—*Mov10l1*. Contrary to *Mov10*, expression of *Mov10l1* is restricted to germ cells and peaks with the rise of pachytene spermatocytes [304,305]. MOV10L1 associates with Piwi proteins and is essential for biogenesis of the pre-pachytene and pachytene Piwi-interacting RNAs (piRNAs) [304,305,341]. The piRNA pathway protects the germline genome from transposable elements and is necessary for fertility. Consistently with the crucial role of MOV10L1 in the piRNA pathway, loss of *Mov10l1* leads to depletion of piRNA, de-repression of retrotransposons, early meiotic arrest and sterility [304,305]. These findings suggest the divergent evolution of MOV10 and MOV10L1 after gene duplication—MOV10 specialized in the miRNA pathway, whereas MOV10L1 in the piRNA pathway.

2. Objectives

Ubiquitin ligases play essential roles in multiple biological processes. However, the substrates and functions of most of them remain unknown. Therefore, our prime objective was to identify and validate novel substrates of pre-selected ubiquitin ligases from the CRL4 subfamily and address the biological roles of the ligase-substrate interactions. As ubiquitin ligases typically execute their functions through substrate ubiquitination (and degradation), substrate identification is a crucial step in uncovering the biological roles of ubiquitin ligases. Subsequently, the impact of substate ubiquitination and degradation can be investigated, which often broadens our understanding of already described cellular pathways or even uncovers entirely novel biological processes.

Here, we employed the "bottom-up" approach to reveal the biological functions of $CRL4^{DCAF4}$ and $CRL4^{DCAF12}$. After identifying and validating their candidate substrates, we proceeded with the prediction and experimental investigation of their biological roles. The specific aims were:

- to identify proteins recognised by $CRL4^{DCAF4}$ and $CRL4^{DCAF12}$,
- to select and validate candidate substrates of $CRL4^{DCAF4}$ and $CRL4^{DCAF12}$ by examining their proteasome-dependent degradation and characterising the ligase-substrate interaction,
- to explore conditions and molecular mechanisms triggering the degradations,
- to uncover the outcome of such degradations to reveal the biological function of $CRL4^{DCAF4}$ and $CRL4^{DCAF12}$.

3. Materials and methods

3.1. DNA constructs

DNA sequences for human DKC1, GAR1, XIAP, MOV10, GART, CUL4A were amplified by polymerase chain reaction (PCR) from a cancer cell line-derived cDNA library and inserted into modified pcDNA3.1 expression vectors containing N-terminal hemagglutinin (HA) tag sequence (pcDNA3.1-HA). Similarly obtained sequence for human SMAC was inserted into empty pcDNA3.1, and sequences for substrate receptor subunits of CRLs, including DCAF4, DCAF4L1, DCAF4L2, DCAF12, DCAF12L1, and DCAF12L2, were inserted into modified pcDNA3.1 expression vectors containing the previously described [342] N-terminal Twin-Strep-FLAG (SF) tag sequence (pcDNA3.1-SF). Truncation mutants were prepared likewise using corresponding pcDNA3.1 constructs as templates. Desired substitutions of amino-acid residues were created by Phusion site-directed mutagenesis. Ubiquitin-SMAC was prepared by in-frame fusion of the sequences encoding ubiquitin and the mature form of SMAC. Dominant-negative CUL4A was prepared by inserting the N-terminal part (aa 1–337) of CUL4A into the pcDNA3.1-FLAG-HA backbone.

Lentiviral pTRIPZ-SF-DCAF4 and pTRIPZ-SF-DCAF12 vectors were constructed by PCR amplification of cDNA from the corresponding pcDNA3-SF-DCAF4 and pcDNA3-SF-DCAF12 plasmids and cloning it into the pTRIPZ backbone (Dharmacon, Lafayette, CO, USA) using AgeI-XhoI/SalI restriction sites. Retroviral pBABE-SMAC vectors were prepared similarly by PCR amplification of the SMAC sequence and its insertion into pBABE-puro (Addgene plasmid #1764) using PdeI-XhoI/SalI restriction sites. For the Sleeping Beauty system, pSBtet-Pur-SF-DCAF12 and pSBtet-Pur-HA-MOV10 vectors were constructed by subcloning the SF-DCAF12 or HA-MOV10 sequence into pSBtet-Pur (Addgene plasmid # 60507) using SfiI sites. Single guide RNAs (sgRNAs) targeting sequences were designed and cloned into lentiCRISPR plasmid pXPR001 (Addgene plasmid #49535) as described previously [343]. For stable cell lines generation or primary cell immortalization, the following plasmids were used: pCMV-VSV-G (Addgene plasmid #8454), pCMV-dR8.2 (Addgene plasmid #8455), pUMVC-gag-pol (Addgene plasmid #8449), pSB100X (Addgene plasmid #34879), and pLenti CMV/TO SV40 Small and Large T antigen (w612-1) (Addgene plasmid #22298).

All plasmids were verified by sequencing. Primers are outlined in Table 1, and the restricting enzymes used for DNA cloning are indicated in the primer names.

Table 1. List of primers used for DNA cloning.

Application	Primer name	Sequence (5' to 3')
Cloning of DKC1 into pcDNA3.1-HA	DKC1_BglII_f	GGGAGATCTGCGGATGCGGAAGTAAT
	DKC1_XhoI_r	GGGCTCGAGCTACTCAGAAACCAATTCTACC

Application	Primer name	Sequence (5′ to 3′)
	DKC1_22_BglII_f	GGGAGATCTTTGCCAGAAGAAGATGTAGC
	DCK1_48_BglII_f	GGGAGATCTGACACGTCTCAGTGGCCCCT
	DCK1_81_BglII_f	GGGAGATCTAGAGAGATTGGGGACTATAT
	DCK1_377_XhoI_r	GGGCTCGAGCTAAGGGTAAGTGTCTCTCTCCAT
	DCK1_426_XhoI_r	GGGCTCGAGCTACTCTTTTTTGGCAGACTCACT
Site-directed mutagenesis of DKC1	DKC1_R183A_P184A_P185A_f	CTGACAGGTGCCTTATTCCAGGCGGCCGCACTTATTGCTGCAGTAAAGA
	DKC1_R183A_P184A_P185A_r	TCTTTACTGCAGCAATAAGTGCGGCCGCCTGGAATAAGGCACCTGTCAG
	DKC1_R183A_f	TGACAGGTGCCTTATTCCAGGCACCCCCACTTATTGCTG
	DKC1_R183A_r	CAGCAATAAGTGGGGGTGCCTGGAATAAGGCACCTGTCA
	DKC1_R183D_f	CTGACAGGTGCCTTATTCCAGGATCCCCCACTTATTGCTGCAG
	DKC1_R183D_r	CTGCAGCAATAAGTGGGGGATCCTGGAATAAGGCACCTGTCAG
	DKC1_T224A_Y225A_f	TGGGTGAGTTGTGAGGCTGGCGCCGCCATTCGGACATTATGTGTGCA
	DKC1_T224A_Y225A_r	TGCACACATAATGTCCGAATGGCGGCGCCAGCCTCACAACTCACCCA
	DKC1_T224E_Y225D_f	TTTGGGTGAGTTGTGAGGCTGGCGAGGACATTCGGACATTATGTGTGCAC
	DKC1_T224E_Y225D_r	GTGCACACATAATGTCCGAATGTCCTCGCCAGCCTCACAACTCACCCAAA
	DKC1_T224A_f	GTGAGTTGTGAGGCTGGCGCCTACATTCGGACATTAT
	DKC1_T224A_r	ATAATGTCCGAATGTAGGCGCCAGCCTCACAACTCAC
	DKC1_T224E_f	TTGGGTGAGTTGTGAGGCTGGCGAGTACATTCGGACATTATGTGTGC
	DKC1_T224E_r	GCACACATAATGTCCGAATGTACTCGCCAGCCTCACAACTCACCCAA
	DKC1_Y225F_f	AGTTGTGAGGCTGGCACCTTCATTCGGACATTATGTGTG
	DKC1_Y225F_r	CACACATAATGTCCGAATGAAGGTGCCAGCCTCACAACT
	DKC1_Y225D_f	GAGTTGTGAGGCTGGCACCGACATTCGGACATTATGTGT
	DKC1_Y225D_r	ACACATAATGTCCGAATGTCGGTGCCAGCCTCACAACTC
Cloning of GAR1 into pcDNA3.1-HA	GAR1_BamHI_f	GGGGGATCCTCTTTTCGAGGCGGAGGTC
	GAR1_XhoI_r	GGGCTCGAGTTAATGTCCTCTCCCTCTGA
Site-directed mutagenesis of GAR1	GAR1_E115A_I116A_F117A_f	ACTTAGAAAACAAAGAACAAATTGGAAAAGTGGATGCGGCCGCTGGACAACTCAGAGA-TTTTTATTTTTCAGTTAAGTTG
	GAR1_E115A_I116A_F117A_r	CAACTTAACTGAAAAATAAAAATCTCTGAGTTGTCCAGCGGCCGCAT-CCACTTTTCCAATTTGTTCTTTGTTTTCTAAGT
	GAR1_E115A_f	AAAGAACAAATTGGAAAAGTGGATGCAATATTTGGACAACTCAGAGATTTT
	GAR1_E115A_r	AAAATCTCTGAGTTGTCCAAATATTGCATCCACTTTTCCAATTTGTTCTTT
	GAR1_E115K_f	AACAAAGAACAAATTGGAAAAGTGGATAAAATATTTGGACAACTCAGAGATTTTT
	GAR1_E115K_r	AAAAATCTCTGAGTTGTCCAAATATTTTATCCACTTTTCCAATTTGTTCTTTGTT
Cloning of SMAC into pcDNA3.1	SMAC_HindIII_f	GGAAGCTTACCATGGCGGCTCTGAAGAGTTGG
	SMAC_XhoI_r	GGGCTCGAGTCAATCCTCACGCAGGTAGGCCTC
	SMAC_E238X_XhoI_r	GGCTCGAGCTAACGCAGGTAGGCCTCCTGCTCC
	Ubiquitin_HindIII_f	GGGAAGCTTACCATGCAGATCTTCGTGAAGACTCT
	Ubiquitin_KasI_r	GCACGGCGCCACCTCTGAGACGGAGCAC
	SMAC_KasI_f	GGACGGCGCCGTTCCTATTGCACAGAAATC
Cloning of XIAP into pcDNA3.1-HA	XIAP_BamHI_f	GGGGATCCACTTTTAACAGTTTTGAAGGAT
	XIAP_XhoI_r	GGCTCGAGTTAAGACATAAAAATTTTTTGCT
	XIAP_103_BamHI_f	GGGGGATCCACGCAGTCTACAAATTCTGG
	XIAP_243_BamHI_f	GGGGGATCCGCTGTGAGTTCTGATAGGAA
	XIAP_254_BamHI_f	GGGGGATCCAGAACTACTGAGAAAACACC
	XIAP_438_BamHI_f	GGGGGATCCGAAGAGCAGCTAAGGCGCCT

Application	Primer name	Sequence (5' to 3')
	XIAP_102_XhoI_r	GGGCTCGAGTTAGGCACTATTTTCAAGATAAA
	XIAP_242_XhoI_r	GGGCTCGAGTTAATCAGATTCACTTCGAATAT
	XIAP_353_XhoI_r	GGGCTCGAGTTATACCAGACACTCCTCAAGTG
	XIAP_437_XhoI_r	GGGCTCGAGTTAAGTACTAATCTCTTTCTGTA
	XIAP_E219R_H223V_f	CAAAGAAGCAATTAGGAAAGACTCGCCTGTGTCTTGACCAGGCACGATCACAAG
	XIAP_E219R_H223V_r	CTTGTGATCGTGCCTGGTCAAGACACAGGCGAGTCTTTCCTAATTGCTTCTTTG
	XIAP_E314A_f	TTGTTCCCAAGGGTCTGCACTGGGCTTCCAATC
	XIAP_E314A_r	GATTGGGAAGCCCAGTGCAGACCCTTGGGAACAA
Cloning of MOV10 into pcDNA3.1-HA	MOV10_BamHI_f	GGGGGATCCCCCAGTAAGTTCAGCTGCCG
	MOV10_XhoI_r	GGGCTCGAGTCAGAGCTCATTCCTCCACTCT
	MOV10_E1002X_XhoI_r	GGCTCGAGTCAATTCCTCCACTCTGGCTCCACTTG
Cloning of GART into pcDNA3.1-HA	GART_BclI_f	GGGTGATCAGCAGCCCGAGTACTTATAATTGG
	GART_XhoI_r	GGGCTCGAGTCATTCCTCTTTAACCCAACAGATCT
	GART_E1009X_XhoI_r	GGGCTCGAGTCATTTAACCCAACAGATCTTGCCATT
Cloning of CUL4A into pcDNA3.1-HA	CUL4A_BamHI_f	GGGGGATCCGCGGACGAGGCCCCGCGGAAGGGCAGCTTCT
	CUL4A_NotI_r	GGGGCGGCCGCTCAGGCCACGTAGTGGTACTGA
Cloning of DCAFs into pcDNA3.1-SF	DCAF4_NheI_f	CGAGAAAGGAGCTAGCAATAAAAGTCGCTGGCAGAGTAGA
	DCAF4_NheI_r	AATCCTCTCCGCTAGCTTAGCTGTAGGAGTAACAGTAAAG
	DCAF4L1_NheI_f	GGGGCTAGCGAGGCTGAAAGGCTGCGACTC
	DCAF4L1_SalI_r	GGGGTCGACCCACCTGCAGAATTAGCTGA
	DCAF4L2_NHEI_f	GGGGCTAGCGAGAGCAAAAGACCGCGACTG
	DCAF4L2_SalI_r	GGGGTCGACCATCCTGAAGAATTAACCGT
	DCAF12_XbaI_f	GGGTCTAGAGCCCGGAAAGTAGTTAGCAGGAA
	DCAF12_SalI_r	GGGGTCGACTTAACTCCAGAGCCCAGCATAG
	DCAF12L_NheI_f	GGGGCTAGCGCCCAGCAGCAAACAGGTAG
	DCAF12L1_SalI_r	GGGGTCGACTTAGCTCCAGAGGCCTGCAT
	DCAF12L2_SalI_r	GGGGTCGACTTAACTCCAGAGGCCTGCGT
	DCAF12L2new_SalI_r	GGGGTCGACACAAATGCAGCATGAAGAAGGAA
	DCAF12_Δ1-11_SpeI_f	GGGACTAGTGCGCCCGCCTCGCCGGGAGC
	DCAF12_Δ1-38_SpeI_f	GGGACTAGTCTTCCTCCTGTGAAGAGATC
Subcloning into pTRIPZ	NSF_AgeI_f	GGGACCGGTGCCACCATGGATTATAAAGAT
	NSF_XhoI_SalI_r	GGGTCGACTCGAGAGGTGACACTATAGAATAGGGCCC
Subcloning into pSBtet-Pur	NSF_SfiI_f	AAAGGCCTCTGAGGCCACCATGGATTATAAAGATGATGATGATAAAG
	NSF_SfiI_r	CTTGGCCTGACAGGCCATAGGGCCCTCTAGATGCATGCTCG
	HA_SfiI_f	AAAGGCCTCTGAGGCCACCATGGCGTACCCCTACGACGTGCCCGACTA
Oligos encoding the sgRNA targeting sequences cloned into pXPR001	DCAF4_target 1_f	CACCGGGAAGGCTGAGACCCGTTCC
	DCAF4_target 1_r	AAACGGAACGGGTCTCAGCCTTCCC
	DCAF4_target 2_f	CACCGCAGGATTCCCACCCCGCAAG
	DCAF4_target 2_r	AAACCTTGCGGGGTGGGAATCCTGC
	DCAF4_target 3_f	CACCGGTGTCGCAGGGGCATCTAAT
	DCAF4_target 3_r	AAACATTAGATGCCCCTGCGACACC
	DCAF4_target 4_f	CACCGGTGCCTCTGCTAAGTGTCGC
	DCAF4_target 4_r	AAACGCGACACTTAGCAGAGGCACC
	DCAF12_target 1_f	CACCGAAGCCCTCTTTGGCGTCTGT

Application	Primer name	Sequence (5' to 3')
	DCAF12_target 1_r	AAACACAGACGCCAAAGAGGGCTTC
	DCAF12_target 2_f	CACCGAAATCCCACAGACGCCAAAG
	DCAF12_target 2_r	AAACCTTTGGCGTCTGTGGGATTTC
	DCAF12_target 3_f	CACCGAAGCAAGAGGAATACACGTC
	DCAF12_target 3_r	AAACGACGTGTATTCCTCTTGCTTC
	DCAF12_target 4_f	CACCGTACTGCAGACACCAATTGAA
	DCAF12_target 4_r	AAACTTCAATTGGTGTCTGCAGTAC
Verification of oligo insertions into pXPR001	pXPR001-ver_f	TTGCATATACGATACAAGGCTGTT
	pXPR001-ver_r	CGGTGCCACTTTTTCAAGTT
Verification of the deletion of *DCAF4* exon 4	hDCAF4_del-ver_f	GAGTCTCCGTCAACCTCGTC
	hDCAF4_del_ver_r	CTGTCAGGGAAAAGCTAGGG
Verification of the deletion of *DCAF12* exon 5	hDCAF12_del_ver_f	GAGGATGATGCACAAACAGC
	hDCAF12_del_ver_r	CCAGAATACAGCACCTGCAA
Verification of the deletion of *Dcaf12* exon 4	mDcaf12_del_ver_f	ACTGCCAGGCGTATTGTACC
	mDcaf12_del_ver_r	GCACAGGCAGGTGGATCTAT

3.2 Mice

Dcaf12 KO mice (Δexon 4) were generated in a C57BL/6N background using the CRISPR/Cas9 genome-editing system by the Czech Center for Phenogenomics in Vestec, Institute of Molecular Genetics of the Czech Academy of Sciences, Czech Republic. For this purpose, the Cas9 protein and gene-specific sgRNAs (Integrated DNA Technologies, Coralville, IA, USA) were used for zygote electroporation as described previously [344]. Single guide RNA sequences with the protospacer adjacent motif (PAM) in bold (at 3'end) were as follows:

sgRNA target 1: ATAGGGCATGCATACGCTGA**CGG**

sgRNA target 2: GAGGCCGAGGATGCAAGTTC**TGG**

The genome editing was confirmed by PCR amplification in the founder mouse with the primers listed in Table 1. The mutant allele was backcrossed for two generations to C57BL/6N mice. Animals were maintained in a controlled, specific pathogen-free environment.

3.3. Cell lines and primary cells

All cell lines and primary cells were cultured at 37 °C in a humidified atmosphere containing 5% CO_2. HEK293T, HCT116, U2OS, HeLa, RAW 264.7 (all obtained from American Type Culture Collection (ATCC), Manassas, VA, USA), mouse embryonic fibroblasts (MEFs), and mouse peritoneal macrophages were grown in Dulbecco's Modified Eagle's Medium (DMEM; Sigma-Aldrich, St. Louis, MO, USA) supplemented with 10% fetal bovine serum (FBS; Biosera, Nuaille, France), 100 IU/ml penicillin, 100 µg/ml streptomycin, and 40 µg/ml gentamicin. BJAB (ATCC, Manassas, VA, USA), mouse bone marrow-derived macrophages (BMDMs)/bone marrow-derived dendritic cells (BMDCs), and mouse primary

splenocytes were grown in RPMI-1640 (Sigma-Aldrich, St. Louis, MO, USA) supplemented with FBS and antibiotics as described above.

DCAF4 KO and *DCAF12* KO cell lines were generated using the CRISPR/Cas9 genome editing system as described previously [343]. Briefly, sgRNAs were designed to target introns flanking the exon 4 of the *DCAF4* gene and the exon 5 of the *DCAF12* gene. A mixture of lentiCRISPR plasmids (pXPR001) encoding these sgRNAs and Cas9 was transfected into cells. After a short selection with puromycin (1 μg/ml), single-cell clones were generated, and the exon deletions were confirmed by PCR. *XIAP* KO and *SMAC* KO HCT116 cells were kindly provided by Dr Bert Vogelstein (Johns Hopkins University, Baltimore, MA, USA).

Stable cell lines expressing SF-DCAF4 and SF-DCAF12 under the control of doxycycline (DOX)-inducible promoter were generated using the lentiviral system as described previously [345]. Briefly, lentiviral particles were produced in HEK293T cells by co-transfecting one of the pTRIPZ vectors encoding DOX-inducible SF-DCAF4, SF-DCAF12, SF-DCAF12$^{\Delta 1-11}$, or SF-DCAF12$^{\Delta 1-38}$ (Tet-On system) with the pCMV-VSV-G envelope vector and the pCMV-dR8.2 packaging vector. Forty-eight hours after transfection, the viral supernatant was collected, filtered, and added to target cells at a 1:1 ratio in the presence of 10 μg/ml Polybrene (Sigma-Aldrich, St. Louis, MO, USA). The following day, the cell media was changed, and cells were subjected to puromycin (1 μg/ml) selection. Stable HCT116 cell lines expressing SMAC and SMAC^{E238X} were generated likewise using the retroviral system. To generate retrovirus particles, one of the pBABE-puro vectors (pBABE-empty, pBABE-SMAC, or pBABE-SMAC^{E238X}) was co-transfected into HEK293T cells with the pUMVC-gag-pol packaging vector and the pCMV-VSV-G envelope vector. Forty-eight hours after transfection, retrovirus-containing supernatant was processed as described above and added to *SMAC* KO HCT116 cells, which were subsequently subjected to puromycin (1 μg/ml) selection. Stable HEK293 and HCT116 cell lines expressing HA-tagged MOV10 or its E1002X mutant were prepared using the Sleeping Beauty transposable system as described previously [346]. Briefly, cells were co-transfected with pSB100X and pSBtet-Pur-MOV10^{WT} or pSBtet-Pur-MOV10^{E1002X} vectors. Twenty-four hours after transfection, cells were subjected to puromycin selection (1 μg/ml).

MEFs were derived from embryonic day 13.5 *Dcaf12* KO and WT mouse embryos using the previously described protocol [347] and immortalized by two different approaches. Primary MEFs were transduced as described above with pLenti CMV/TO SV40 Small and Large T antigen (w612-1). Alternatively, primary MEFs were immortalized by the loss of p19ARF [348]. To inactivate p19ARF, the CRISPR-Cas9 genome-editing technology and px330-Cas9-p19Arf sgRNA vectors (kindly provided by Prof. Tomas Stopka) were used. Immortalized MEFs were co-transfected with pSB100X and pSBtet-Pur-DCAF12 as described above to generate stable cell lines expressing SF-DCAF12 under the control of DOX-inducible promoter. Puromycin used for selection was at a concentration of 5 μg/ml.

Mouse peritoneal macrophages and BMDMs/BMDCs were derived from 6- to 8-week-old *Dcaf12* KO and WT mice using the previously described protocol [349]. Briefly, peritoneal exudate cells obtained from peritoneal lavage were cultured for 2 h to allow macrophages to adhere to tissue culture plastic. After culturing for 2 h, non-adherent cells were removed by gently washing three times with warm phosphate-buffered saline (PBS; pH 7.4), and the remaining cells (mainly macrophages) were treated as indicated. Bone-marrow cells were flushed from the tibia and femur and cultured in a medium supplemented with granulocyte-macrophage colony-stimulating factor (GM-CSF; 5 ng/ml). The culture medium was replenished on cultivation days 3 and 5. After seven days, BMDMs/BMDCs were seeded and treated as indicated.

Single-cell splenocyte suspensions were prepared by mechanical dissociation of spleen tissue and filtered through 70 µm cell strainers. Red blood cells were depleted by ammonium-chloride-potassium (ACK) lysis buffer (150 mM NH_4Cl, 10 mM $KHCO_3$, 0.1 mM Na_2EDTA; pH 7.2–7.4).

3.4. Cell treatments and transfections

Cells were treated with the following compounds: 1 µM MLN4924 (Santa Cruz Biotechnology, Dallas, TX, USA), 10 µM MG132 (MedChem Express, Monmouth Junction, NJ, USA), 1 µg/ml doxycycline (Sigma-Aldrich, St. Louis, MO, USA), 100 µg/ml cycloheximide (Sigma-Aldrich, St. Louis, MO, USA), 1 µM AZD5582 (MedChem Express, Monmouth Junction, NJ, USA), 10 µM birinapant (MedChem Express, Monmouth Junction, NJ, USA), 10 µM embelin (MedChem Express, Monmouth Junction, NJ, USA), 10 µM LCL161 (MedChem Express, Monmouth Junction, NJ, USA), 0.1–1 µM staurosporine (Santa Cruz Biotechnology, Dallas, TX, USA), 10–100 ng/ml TRAIL (Apronex, Vestec, Czech Republic), 10 µM Z-VAD-FMK (Santa Cruz Biotechnology, Dallas, TX, USA), 10 µM etoposide (MedChem Express, Monmouth Junction, NJ, USA), 2 µM doxorubicin (Sigma-Aldrich, St. Louis, MO, USA), 1 µM camptothecin (MedChem Express, Monmouth Junction, NJ, USA), 0.5 µM thapsigargin (MedChem Express, Monmouth Junction, NJ, USA), 10 µM carbonyl cyanide 3-chlorophenylhydrazone (Sigma-Aldrich, St. Louis, MO, USA), 10 µg/ml poly(I:C) (Invivogen, San Diego, CA, USA), 10 µg/ml MDP (Invivogen, San Diego, CA, USA), and 50 ng/ml to 5 µg/ml LPS (Sigma-Aldrich, St. Louis, MO, USA).

Plasmid transient transfections were carried out using the polyethylenimine (Linear, MW 25000, Transfection Grade) transfection reagent (Polysciences, Valley Road, Warrington, PA, USA) as described previously [350]. To deliver small interfering RNAs (siRNAs) into cells, Lipofectamine RNAiMAX Transfection Reagent (Thermo Fisher Scientific, Waltham, MA, USA) was used according to the manufacturer's instructions. siRNA duplexes were designed using the siDESIGN Center tool (Dharmacon, Lafayette, CO, USA). Sequences of siRNA duplexes are listed in Table 2.

Table 2. List of siRNAs used in this study.

Name	Target	siRNA sequences: Sense strand (5' to 3')	Antisense strand (5' to 3')
siDCAF4	*DCAF4*	AGGUGUUCAUGCACGAAAAUU	UUUUCGUGCAUGAACACCU
siDCAF12 #1	*DCAF12*	GCUGUUCUAUGACAUCCGAUU	UCGGAUGUCAUAGAACAGC
siDCAF12 #2	*DCAF12*	AGAAAUUACCACUGGGAAAUU	UUUCCCAGUGGUAAUUUCUUU
siDCAF12 (m)	*Dcaf12*	CAGGAAAACCCUUGAGUUAUU	UAACUCAAGGGUUUUCCUGUU
siDKC1	*DKC1*	GGAUAUGGGUGGUGAAAGAUU	UCUUUCACCACCCAUAUCCUU
siNHP2	*NHP2*	AGGAGUACCAGGAGGCUUAUU	UAAGCCUCCUGGUACUCCUUU
siNOP10	*NOP10*	CCAUAAAGGGAACACAUUUUU	AAAUGUGUUCCCUUUAUGGUU
siGAR1	*GAR1*	GCAACGGAAUAGUGAAUUUUU	AAAUUCACUAUUCCGUUGCUU
siSHQ1	*SHQ1*	GGAAGUAGUUGACGAUGAAUU	UUCAUCGUCAACUACUUCCUU
siSMAC	*SMAC*	GAAGCGGUGUUUCUCAGAAUU	UUCUGAGAAACACCGCUUCUU
siCTRL #1	non-targeting	AUGAACGUGAAUUGCUCAA[dT][dT]	UUGAGCAAUUCACGUUCAU[dT][dT]
siCTRL #2	non-targeting	UAAGGCUAUGAAGAGAUAC[dT][dT]	GUAUCUCUUCAUAGCCUUA[dT][dT]
siCTRL #3	non-targeting	AUGUAUUGGCCUGUAUUAGUU	CUAAUACAGGCCAAUACAUUU

3.5. Cell lysis, immunoprecipitation, and affinity purification

Cells were lysed in lysis buffer (150 mM NaCl, 50 mM Tris pH 7.5, 1 mM EDTA, 0.4% Triton-X, 2 mM $CaCl_2$, 2 mM $MgCl_2$, 5 mM NaF) supplemented with 1 mM Na_3VO_4, protease inhibitors (10 µM TLCK, 10 µM TPCK, 0.8 mM PMSF), and 1 mM DTT (except for the lysates intended for immunoprecipitation). To digest nucleic acids, benzonase (Santa Cruz Biotechnology, Dallas, TX, USA) was added at a concentration of 125 U/ml. Where indicated, RNase A (Thermo Fisher Scientific, Waltham, MA, USA) was added to digest only RNA. For testes lysis, tunica was first mechanically removed, and the rest of the tissue was mixed with the lysis buffer and disrupted by TissueLyser (Qiagen, Hilden, Germany). After incubation on ice, native lysates were either processed for immunoblotting or cleared by centrifugation and used for immunoprecipitation (IP) or affinity purification (AP). In addition to such prepared whole-cell lysates (WCL), the soluble and insoluble fractions were obtained by lysing cells without benzonase, spinning down the lysates, and using only the supernatant (the soluble fraction) or the pellet (the insoluble fraction) for further analysis.

For immunoblotting, lysates were mixed 1:1 with SDS (2%) in 50 mM Tris-HCl (pH 8), incubated at 95 °C for 5 min, and cleared by centrifugation. The protein concentration was determined using Pierce BCA Protein Assay Kit (Thermo Fisher Scientific, Waltham, MA, USA) and Multiskan EX (Thermo Fisher Scientific, Waltham, MA, USA) according to the manufacturer's instructions. Before immunoblotting, lysates were diluted to the same concentration, mixed with Bolt LDS Sample Buffer (Thermo Fisher Scientific, Waltham, MA, USA) supplemented with 2.5% β-mercaptoethanol, and incubated at 95 °C for 5 min.

HA-tagged proteins were immunoprecipitated using anti-HA magnetic beads (Thermo Fisher Scientific, Waltham, MA, USA), whereas Twin-Strep-tag recombinant proteins were purified using Strep-TactinXT Superflow resin (IBA Lifesciences, Göttingen, Germany). Both isolations were performed according to the manufacturer's instructions. Immunoprecipitated proteins were eluted by Bolt LDS Sample Buffer (Thermo Fisher Scientific, Waltham, MA, USA). Purified proteins were eluted by BXT Buffer (IBA Lifesciences, Göttingen, Germany) and eluates mixed afterwards with Bolt LDS Sample Buffer (Thermo Fisher Scientific, Waltham, MA, USA). Finally, 2.5% β-mercaptoethanol was added to elutes, and they were subsequently incubated at 95 °C for 5 min.

3.6. Immunoblotting

Proteins were separated by SDS-PAGE using NuPAGE 4–12% Bis-Tris gels and NuPAGE MES SDS Running Buffer (Thermo Fisher Scientific, Waltham, MA, USA). Typically, 15-30 µg of total protein or 1-2% of WCL used for IP/AP were loaded per well. After separation, proteins were transferred to Amersham Hybond P 0.45 µm PVDF membrane (GE Healthcare, Chicago, IL, USA). Membranes were blocked with 5% milk (Santa Cruz Biotechnology, Dallas, TX, USA) in PBS supplemented with 0.1% Tween 20 (PBS-T) for 20 min and incubated with indicated primary antibodies diluted in 3% bovine serum albumin (BSA; Applichem, Darmstadt, Germany) in PBS-T at 4 °C overnight. The next day, membranes were incubated with appropriate HRP-conjugated secondary antibodies (Cell Signaling Technology, Danvers, MA, USA) diluted in 5% milk in PBS-T for 30 min and developed with either WesternBright ECL HRP substrate (Advansta, San Jose, CA, USA) or SuperSignal West Femto Maximum Sensitivity Substrate (Thermo Fisher Scientific, Waltham, MA, USA). Primary antibodies are listed in Table 3.

Table 3. List of primary antibodies used for immunodetection.

Primary antibodies	Source/clonality	Supplier	Cat. No.
ADAR1	rabbit/poly	Antibodies-online	ABIN2855100
Cleaved caspase-3 (Asp175)	rabbit/poly	Cell Signaling	9661
Cleaved caspase-8	rabbit/mono	Cell Signaling	9496
Cleaved caspase-9 (Asp330)	rabbit/poly	Cell Signaling	9501
Cleaved PARP (Asp214)	rabbit/poly	Cell Signaling	9544
CLUH	rabbit/poly	Novus Biologicals	NB100-93306
CP110	rabbit/poly	Bethyl	A301-343A
CUL-4	mouse/mono	Santa Cruz	sc-377188
CUL-4A	rabbit/poly	Abcam	ab72548
DCAF4	rabbit/poly	Atlas Antibodies	HPA047276
DCAF7	rabbit/poly	Novus Biologicals	NBP1-92589
DCAF12	rabbit/poly	Novus Biologicals	NBP1-56584
DCAF12	rabbit/poly	MyBiosource	MBS9140890
DCAF12	rabbit/poly	Atlas Antibodies	HPA062279

DCAF12	rabbit/poly	Proteintech	20478-1-AP
DCAF12	rabbit	Toronto RS	AN09473
DDB1	rabbit/poly	Invitrogen	34-2300
DDB1	mouse/mono	Santa Cruz	sc-376860
DKC1	mouse/mono	Santa Cruz	sc-373956
DKC1	rabbit/mono	Cell Signaling	53234
FBXO28	rabbit/poly	Bethyl	A302-377A
FLAG	rabbit/mono	Cell Signaling	14793
FLAG® M2	mouse/mono	Sigma	F1804
GAR1	rabbit/poly	Proteintech	11711-1-AP
GART	mouse/mono	Santa Cruz	sc-73408
HA	rabbit/mono	Cell Signaling	3724
Histone γH2AX	mouse/mono	Millipore	05-636
IKK-β	mouse/mono	Cell Signaling	8943
IκBα	mouse/mono	Cell Signaling	4814
MOV10	mouse/mono	Santa Cruz	sc-515722
MOV10	rabbit/poly	Bethyl	A301-571A-T
NHP2	mouse/mono	Santa Cruz	sc-398430
NHP2	rabbit/poly	Proteintech	15128-1-AP
NOP10	mouse/mono	Santa Cruz	sc-517170
p21	rabbit/poly	Santa Cruz	sc-397
p27	mouse/mono	BD Transduction L.	610242
p53	rabbit/mono	Cell Signaling	2527
Phospho-IκBα (Ser32)	rabbit/mono	Cell Signaling	2859
Phospho-β-catenin (Ser33/37)	rabbit/poly	Cell Signaling	2009
PITX2	mouse/mono	Santa Cruz	sc-390457
PLZF (ZBTB16)	rabbit/poly	Atlas Antibodies	HPA001499
RIP2	rabbit/mono	Cell Signaling	4142
SALL4	mouse/mono	Santa Cruz	sc-101147
SCP3	mouse/mono	Santa Cruz	sc-74569
SKP1	rabbit/poly	Cell Signaling	2156
SMAC	rabbit/mono	Cell Signaling	15108
SMAC	mouse/mono	Santa Cruz	sc-393118
SMAC	mouse/mono	BD Transduction L.	612246
Strep II Tag	mouse/mono	Novus Biologicals	NBP2-43735
Vimentin	rabbit/mono	Cell Signaling	5741
Vinculin	mouse/mono	Millipore	MAB3574
WDR33	mouse/mono	Santa Cruz	sc-374466
WDR5	mouse/mono	Santa Cruz	sc-393080
WDR74	mouse/mono	Santa Cruz	sc-393822
XIAP	mouse/mono	Santa Cruz	sc-55551
XIAP	mouse/mono	BD Transduction L.	610762
α-tubulin	mouse/mono	Proteintech	66031
β-actin	mouse/mono	Santa Cruz	sc-69879
β-catenin	mouse/mono	Cell Signaling	2698

3.7. Tandem affinity purification and mass spectrometry

A tandem affinity purification protocol was adapted to isolate multisubunit CRLs and identify their interacting partners (substrate candidates) by mass spectrometry. HEK293T cells were co-transfected with Twin-Strep-FLAG-tagged substrate receptor and respective HA-tagged cullin, grown for 48 h, treated with MLN4924, harvested and lysed as described above. In the first step, SF-tagged substrate receptors were affinity purified using Strep-TactinXT Superflow resin (IBA Lifesciences, Göttingen, Germany) and eluted by 1× BXT Buffer (IBA Lifesciences, Göttingen, Germany). In the second step, HA-tagged cullins were immunoprecipitated using anti-HA magnetic beads (Thermo Fisher Scientific, Waltham, MA, USA) and eluted by 3M NaSCN. Eluates from both steps were analysed by liquid chromatography-tandem mass spectrometry (LC-MS/MS) at the Proteomics facility of Biotechnology and Biomedicine Center of the Academy of Sciences and Charles University (BIOCEV) in Vestec, the Czech Republic, according to their standardized pipeline. Label-free quantification (LFQ) was applied to compare the samples and determine specific interacting partners for each isolated CRL.

3.8. Immunofluorescence microscopy

Cells were grown on glass coverslips, fixed with 4% paraformaldehyde in PBS for 20 min, permeabilised with 0.2% Triton-X-100 in PBS for 10 min, and blocked in 3% BSA in PBS with 0.1% Triton-X-100 for 1 h. Coverslips were incubated with indicated primary antibodies for 2 h and corresponding anti-mouse or anti-rabbit Alexa Fluor488-, Fluor555-, Fluor647-conjugated secondary antibodies (Abcam, Cambridge, UK) for 1 h. Phalloidin-iFluor 488 Reagent (Abcam, Cambridge, UK) was used to stain F-actin. Nuclei were visualised by 4',6-diamidino-2-phenylindole (DAPI). Slides were mounted with ProLong Gold Antifade Mountant (Thermo Fisher Scientific, Waltham, MA, USA). Image acquisition was performed using a Zeiss Axio Imager.Z2 microscope equipped with ZEN software (Zeiss, Oberkochen, Germany) or confocal microscope Leica TCS SP8 equipped with LAS X software (Leica, Wetzlar, Germany).

3.9. RNA quantification

Total RNA was extracted from cells using the RNeasy Mini Kit (Qiagen, Hilden, Germany), and 1000 ng of total RNA was reverse-transcribed using Maxima H Minus cDNA SynthesisMaster Mix (Thermo Fisher Scientific, Waltham, MA, USA) according to the manufacturer's instructions. Obtained cDNA was used as a template for quantitative real-time PCR (qPCR), performed using the LightCycler 480 SYBR Green I Master Mix and the LightCycler 480 instrument (Roche, Basel, Switzerland). *RPS13/Rps13* genes were used for normalisation. Primers were designed using Primer-BLAST (NCBI, Bethesda, MD, USA). Their sequences are listed in Table 4.

Table 4. List of primers used for qPCR.

Gene	Forward (5' to 3')	Reverse (5' to 3')
18S rRNA	ATGTCTAAGTACGCACGGCC	CAAGTGGGAGAGGAGCGAG
28S rRNA	CGACTTAGAACTGGTGCGGA	GGCAGAAATCACATCGCGTC
Aurka	CAGAGAACAGCTACTTACATC	GTCTGCAATCTTCAACTCTC
Ccnd1	AACACTTCCTCTCCAAAATG	GAACTTCACATCTGTGGC
DCAF4	AGTTTGCTCTCATGGCTCCT	CAAAGATTTCCCCAGAGCGG
DCAF12	TGCAAAGTGATCCAGCCCTA	GTGACACCAACTTCCCACAC
Dcaf12	CTCCAAACTGTCCAGGCCTA	GGTCGGGAGTGGAAGTAACA
DCAF12 (ind.)	CCCCAATGCTGTTTACACCC	AATCCTCTCCGCTAGCTTAACTCCAGAGCCCAGCATAG
DKC1	GAGCCTGGAGATGGGGAC	GGCCTTCACTACTCAGAAACC
Il1b	GCCACCTTTTGACAGTGATGAG	GACAGCCCAGGTCAAAGGTT
Il2	GAAACTCCCCAGGATGCTCA	CGCAGAGGTCCAAGTTCATCT
Il6	CTGCAAGAGACTTCCATCCAGTT	GAAGTAGGGAAGGCCGTGG
Il18	GTTTACAAGCATCCAGGCACA	GAACCACAGAGAACCCCCAC
MOV10	CTGCAAGGTCTGAGCAAGC	GAGGTAGTCATGGCTGTGGG
Mov10	GTCCTCCGGGCTGTTTAGG	CGCGGAAATGAAACCCGAG
RPL19	TGGCAAGAAGAAGGTCTGGT	TGATGAGCTTCCGGATCTGC
RPS13	CAGTCGGCTTTACCCTATCG	CCCTTCTTGGCCAGTTTGTA
Rps13	ACTCCCTCCCAGATAGGTGTAA	AGTCACAAAACGGACCTGGG
SNORA24 (ACA24)	ATCTTTGGGACCTGTCAGCC	ATGCTCTTCCATGGCTAGGA
SNORA36B (ACA36b)	GTTCAGTTCAGGGTAGCTTCC	CCCTAGCCAGTTTCAATGTTCC
SNORA52 (ACA52)	GTTCAGTTCAGGGTAGCTTCC	CCCTAGCCAGTTTCAATGTTCC
SNORA66 (U66)	CTCGATCACTAGCTCTGCGT	TTGCAAACCTGGTTCCCTTC
SNORD3A (U3)	GCGTGATGATTGGGTGTTCA	CCCACGTCGTAACAAGGTTC
TERC	CCTAACTGAGAAGGGCGTAGG	CTTTTCCGCCCGCTGAAA
Tnf	CATCTTCTCAAAATTCGAGTGACAA	TGGGAGTAGACAAGGTACAACCC
U5 snRNA	CTGGTTTCTCTTCAGATCGCA	GGGTTAAGACTCAGAGTTGTTCC

3.10. Cytokine detection, immunophenotyping, T cell enrichment and activation

Mouse TNF and IL-1β in cell culture supernatants were measured using commercial ELISA kits (R&D Systems, Minneapolis, MN, USA) according to the manufacturer's instructions.

Phenotypic immunological characterisation of immune cell populations in the spleen was performed by the Immunology unit of the Czech Center for Phenogenomics in Vestec, Institute of Molecular Genetics of the Czech Academy of Sciences, Czech Republic, according to the standard IMPC immunophenotyping protocol [351].

T cells were enriched by negative selection using biotinylated anti-CD45R (B220) antibody (BioLegend, San Diego, CA, USA). In more detail, freshly isolated splenocytes were incubated for 1 h in a cell culture plate coated with the CD45R (B220) antibody. The medium with unattached cells (further referred to as a T cell-enriched population) was then removed and transferred to the second plate. The cells remaining in the first plate were considered a B cell-enriched population. B cell depletion was

confirmed using flow cytometry analysis. Where indicated, T cells were stimulated for indicated times with Dynabeads Mouse T-Activator CD3/CD28 (Thermo Fisher Scientific, Waltham, MA, USA) according to the manufacturer's instructions.

3.11. Sperm count and testis section staining

To determine mouse sperm counts, both caudal epididymides of 16-week-old Dcaf12 WT and KO animals were collected into 1 ml of PBS and minced with forceps. After 10 min incubation, sperms were counted using the Bürker chamber.

To prepare the testis section for staining, mouse testes were fixed in modified Davidson's fluid and processed as described previously [352] before being embedded in paraffin and cut into 4-6 µm thick testis sections. After deparaffinization and rehydration, testis sections were stained with standard hematoxylin-eosin using automated Ventana Symphony H&E slide stainer (Roche, Basel, Switzerland) and scanned using automated Axio Scan.Z1 slide scanner (Zeiss, Oberkochen, Germany). Alternatively, testis sections were processed for immunohistochemistry. They were subjected to antigen retrieval in 0.01 M citrate buffer (pH 6) and a steam bath for 18 min, permeabilised with 0.2% Triton X-100 in PBS for 10 min, blocked with 5% goat and 5% horse serum for 1 h, and incubated with primary antibodies at 4 ° C overnight. The following antibodies and concentrations were used: anti-vimentin (Cell Signaling; 5741; dilution 1:400), anti-MOV10 (Santa Cruz; sc-515722; dilution 1:100), anti-PLZF (Atlas Antibodies; HPA001499; dilution 1:200), anti-SCP3 (Santa Cruz; sc-74569; dilution 1:400), anti-γH2AX (Millipore; 05-636; dilution 1:1000). Alexa Fluor 555- and 647-conjugated anti-rabbit or mouse IgGs were used as secondary antibodies. Alexa Fluor 594-conjugated peanut agglutinin (PNA) was used to visualise acrosomes of spermatids, and nuclei were counterstained with DAPI. Slides were mounted with ProLong Gold Antifade Mountant (Thermo Fisher Scientific, Waltham, MA, USA). Image acquisition was performed using a Zeiss Axio Imager.Z2 microscope equipped with ZEN software (Zeiss, Oberkochen, Germany).

3.12. Statistical analysis and data visualization

Statistical analyses were performed using GraphPad Prism 9.0 (GraphPad Software, San Diego, CA, USA). An unpaired two-tailed t-test was applied to evaluate differences between two groups, such as *Dcaf12* WT and KO mice. A chi-square test was applied to assess the mouse offspring ratios. *p*-value < 0.05 was considered significant. Figures show individual data points and means. Illustrations were created with BioRender.com.

4. Results

4.1. Novel substrates of $CRL4^{DCAF4}$

4.1.1. DCAF4 interacts with box H/ACA ribonucleoproteins

To identify interaction partners of $CRL4^{DCAF4}$, we performed sequential AP of SF-DCAF4 followed by IP of HA-CUL4A and analysed the co-isolated proteins by LC-MS/MS (Figure 6a). The sequential isolation protocol reduced non-specific background and led to efficient isolation of $CRL4^{DCAF4}$ complexes. The analysis of co-isolated proteins revealed that DCAF4 interacted with the box H/ACA RNPs. Specifically, all protein components (DKC1, GAR1, NOP10, NHP2) of the box H/ACA RNP particles were detected.

To examine whether the interaction between DCAF4 and the box H/ACA RNPs is specific, we expressed a panel of substrate receptor subunits of CRLs in HEK293T cells and performed a small-scale AP (Figure 6b). As anticipated, F-box proteins, substrate receptors of the cullin-RING ubiquitin ligase 1 (CRL1) subfamily, interacted with the CRL1 adaptor S-phase kinase-associated protein 1 (SKP1), while DCAF proteins, substrate receptors of the CRL4 subfamily, interacted with the CRL4 adaptor DDB1. Interaction between F-box only protein 1 (FBXO1; also known as cyclin-F) and its canonical substrate centrosomal protein of 110 kDa (CP110) was used as a positive control. DCAF4 was the only substrate receptor that interacted with endogenous DKC1 and NHP2. The interaction of DCAF4 with GAR1 and NOP10 was confirmed in subsequent experiments. Next, we performed a similar experiment with human paralogs of DCAF4 (Figure 6c). DCAF4L1 and DCAF4L2 interacted with the CRL4 adaptor DDB1 and cullin 4, showing that they assemble into CRL4. However, no interaction with the box H/ACA RNPs was detected, suggesting that the interaction with the box H/ACA RNPs is specific for DCAF4 and that the paralogs of DCAF4 perform different functions.

Finally, we investigated whether DCAF4 interacts with the box H/ACA RNPs in different cell types (Figure 6d). To avoid cell transfection, we prepared several stable cell lines expressing SF-DCAF4 under the control of the DOX-inducible promoter. NAE inhibitor MLN4924 was used to inhibit the enzymatic activity of CRLs. We found that DCAF4 specifically interacted with the box H/ACA RNPs in all tested cells (BJAB, HCT116, HEK293T, HeLa, and U2OS) and that the interaction was significantly increased after CRL inhibition by MLN4924. Moreover, DCAF4 was elevated in cells treated with MLN4924, indicating that its protein level is tightly controlled in a CRL-dependent manner.

Altogether, we identified the interaction between DCAF4 and box H/ACA RNPs and confirmed its specificity in several AP experiments. Based on these results, we considered the box H/ACA RNPs candidate substrates of DCAF4 and proceeded with further experimental validation.

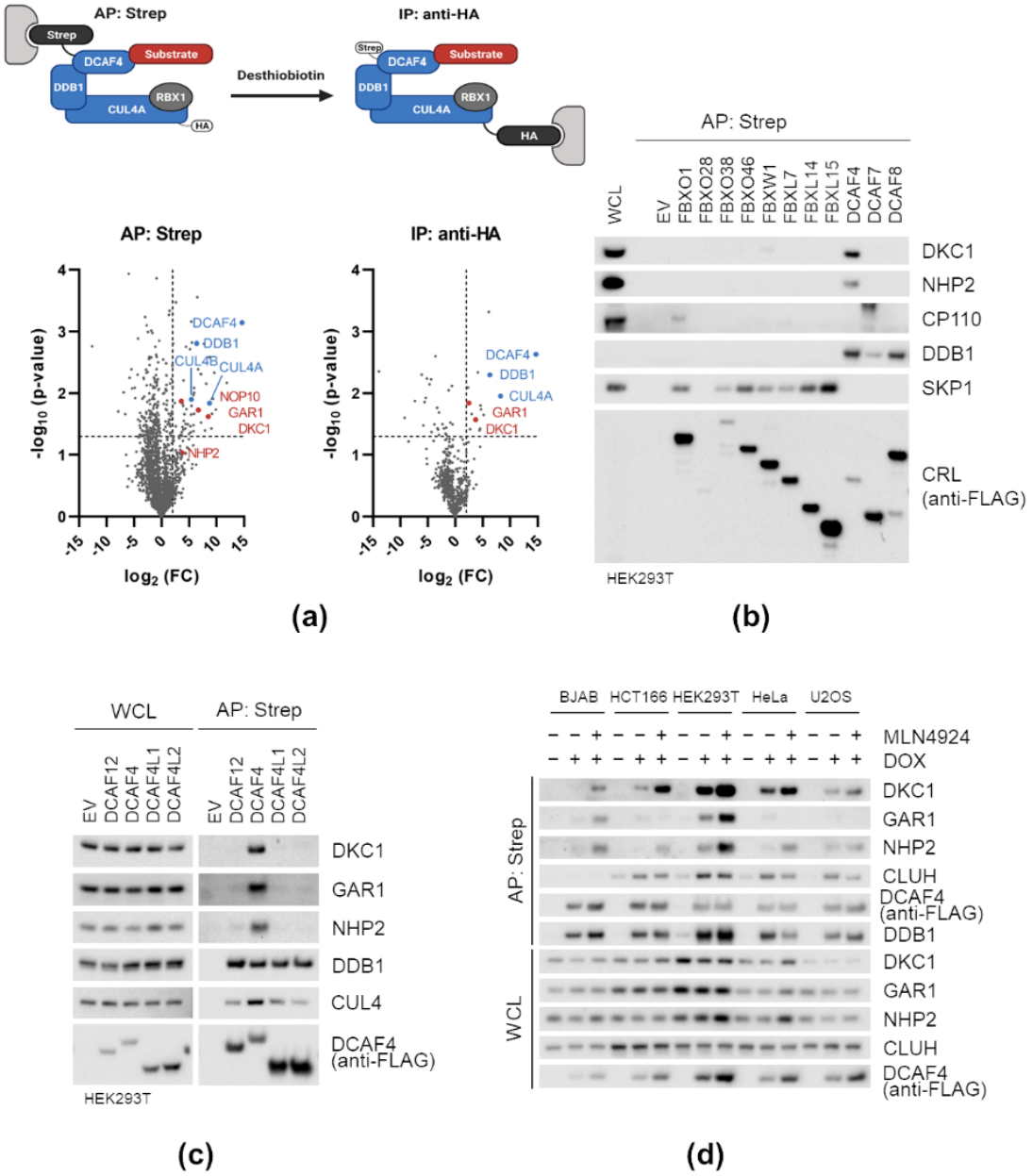

Figure 6. DCAF4 interacts with box H/ACA ribonucleoproteins. (a) Twin-Strep-FLAG-tagged DCAF4 and HA-tagged CUL4A were co-expressed in HEK293T cells and subjected to affinity purification (AP) using Strep-TactinXT resin followed by immunoprecipitation (IP) using anti-HA magnetic beads. The composition of purified complexes from both steps was analysed by liquid chromatography-tandem mass spectrometry and compared to non-related ubiquitin ligase SCF^{FBXL6}. Proteins associated specifically with $CRL4^{DCAF4}$ are in the upper right quadrant. (b, c) HEK293T cells were transfected with an empty vector (EV) or the indicated Twin-Strep-FLAG-tagged substrate receptor subunits of the cullin-RING ubiquitin ligase (CRL). MLN4924 was added to cells 6 h before their collection. Forty-eight hours after transfection, cells were collected and lysed. Whole-cell lysates (WCL) were subjected to AP with Strep-TactinXT resin. Both WCL and eluates were immunoblotted. (d) BJAB, HCT116, HEK293T, HeLa, and U2OS stable cell lines expressing Twin-Strep-FLAG-tagged DCAF4 under the control of the doxycycline (DOX)-inducible promote were treated with DOX (200 ng/ml) for 24 h and MLN4924 for 6 h where indicated. Cells were collected, lysed, and WCL were subjected to AP with Strep-TactinXT resin. Both WCL and eluates were immunoblotted.

4.1.2. DKC1 and GAR1 are required for box H/ACA RNPs interaction with DCAF4

Box H/ACA RNPs are particles, each consisting of a box H/ACA RNA and four core proteins. To reveal the mechanism of the box H/ACA RNPs recognition by DCAF4, we initially examined the requirements of RNA and the core protein subunits for the interaction. To test the dependence on RNA, we overexpressed DCAF4 in HEK193T cells and lysed them in lysis buffer supplemented or not with benzonase or RNase A (Figure 7a). While RNase A cleaves single-stranded RNA, benzonase digests both RNA and DNA. In our AP/IP experiments, we routinely used benzonase for cell lysis to obtain chromatin-bound proteins and reduce nonspecific binding. The interaction between DCAF4 and the box H/ACA proteins was increased when cells were lysed in buffer containing benzonase or RNase A, especially in the latter case. Notably, Box H/ACA proteins were better solubilized when lysis buffer contained RNase A, as evidenced by their increased amount in lysates. Therefore, we sought to compare the effect of benzonase or RNase A on the interaction between DCAF4 and box H/ACA proteins after the removal of the insoluble pellet (Figure 7b). Post-lysis treatment with benzonase and especially RNase A increased the interaction, suggesting that RNA has an inhibitory effect on the ability of DCAF4 to recognise box H/ACA RNPs.

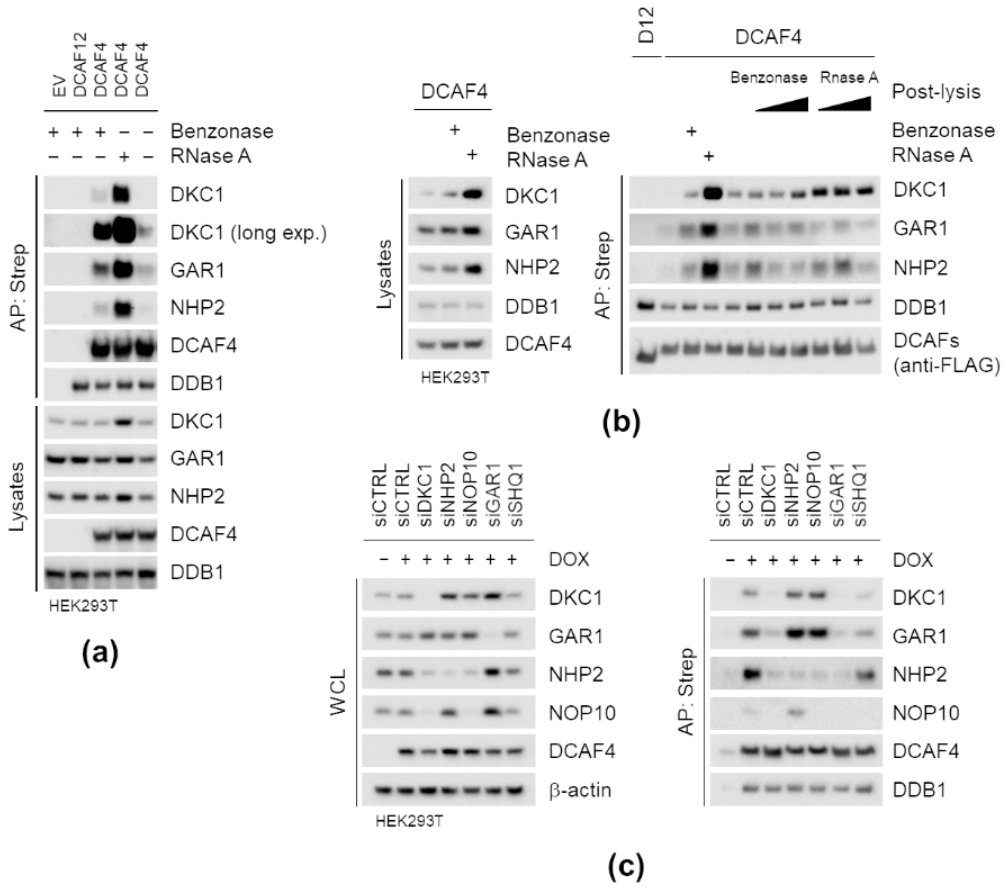

Figure 7. DKC1 and GAR1 are required for box H/ACA RNPs interaction with DCAF4. (a, b) HEK293T cells were transfected with an empty vector (EV), Twin-Strep-FLAG-tagged DCAF12 (abbreviated as D12 in (b)) or Twin-Strep-FLAG-tagged DCAF4. MLN4924 was added to cells 6 h before their collection. Twenty-four hours after transfection, cells were collected and lysed in the lysis buffer supplemented or

not with benzonase (250 U/ml) or RNase A (10 µg/ml) as indicated. In (b), increasing concentration of benzonase (12.5 U/ml, 25 U/ml, 250 U/ml) or RNase A (0.5 µg/ml, 1 µg/ml, 10 µg/ml) was added to cell lysates post-lysis, after the insoluble pellet was discarded. Lysates prepared in this way were subjected to affinity purification (AP) with Strep-TactinXT resin, and both lysates and eluates were immunoblotted. (c) HEK293T stable cell line expressing Twin-Strep-FLAG-tagged DCAF4 under the control of a doxycycline (DOX)-inducible promoter were transfected with control siRNA (siCTRL) or indicated specific siRNAs and treated with DOX (200 ng/ml) for 24 h. Cells were collected, lysed, and whole-cell lysates (WCL) were subjected to AP with Strep-TactinXT resin. Both WCL and eluates were immunoblotted.

To test the differential requirements of the protein subunits for the interaction, we depleted individual core proteins of the box H/ACA RNPs and their assembly factor SHQ1 by siRNA in stable HEK293T cells expressing DCAF4 under the control of DOX-inducible promoter (Figure 7c). Consistently with the previously published results from U2OS cells [353], siRNA-mediated depletion of DKC1 resulted in concurrent depletion of NOP2 and NHP2 but not GAR1. Depletion of GAR1 led to an increase in the protein level of DKC1, NHP2, and NOP10. Depletion of SHQ1 did not affect the protein level of individual core proteins, but decreased their association with DCAF4, probably reflecting the impaired assembly. Upon NHP2 depletion, DCAF4 still interacted with other core proteins of the box H/ACA RNP. Depletion of NOP2 abolished the interaction between DCAF4 and NHP2, reflecting the necessity of NOP10 for the association of NHP2 with the box H/ACA RNPs [354]. Depleting either DKC1 or GAR1 diminished the interaction of box H/ACA RNPs with DCAF4 completely, indicating that DKC1 and GAR1 but not NHP2 and NOP10 are essential for the interaction.

Next, we mapped the DCAF4 binding region in DKC1 and GAR1 to delineate the DCAF4 degron. Human DKC1 contains a highly conserved central part consisting of the catalytic TruB domain, the dyskeratosis congenita-like domain (DKCLD), and the PUA domain. Of them, the last two function together as a box H/ACA RNA interacting and DKC1 dimerization interface [130,138,139]. Outside the central part of DKC1, N-and C-terminal low-complexity and disordered regions have critical regulatory functions, such as regulating its nuclear and subnuclear (e.g., nucleolar) localisation. To narrow the DCAF4 binding region in DKC1, we prepared multiple DKC1 deletion mutants and tested their interaction with DCAF4 (Figure 8a,b). The deletion of the N-terminal 1-47 amino acid residues slightly reduced the interaction. The removal of more N-terminal amino acid residues abolished the interaction entirely. However, it also caused the box H/ACA RNPs complex disintegration, as evidenced by DKC1 failure to co-immunoprecipitate other subunits of the complex. Similarly, deletion of the last 88 C-terminal amino acid residues did not affect the interaction with DCAF4 (not shown), whereas removing the last 133 C-terminal amino acid residues abolished the interaction of DKC1 with DCAF4 but also with other subunits of the complex. These experiments indicated that the integrity of the entire central region of DKC1 must be preserved. We thus had to employ a different, hypothesis-driven approach to delineate the DCAF4 degron.

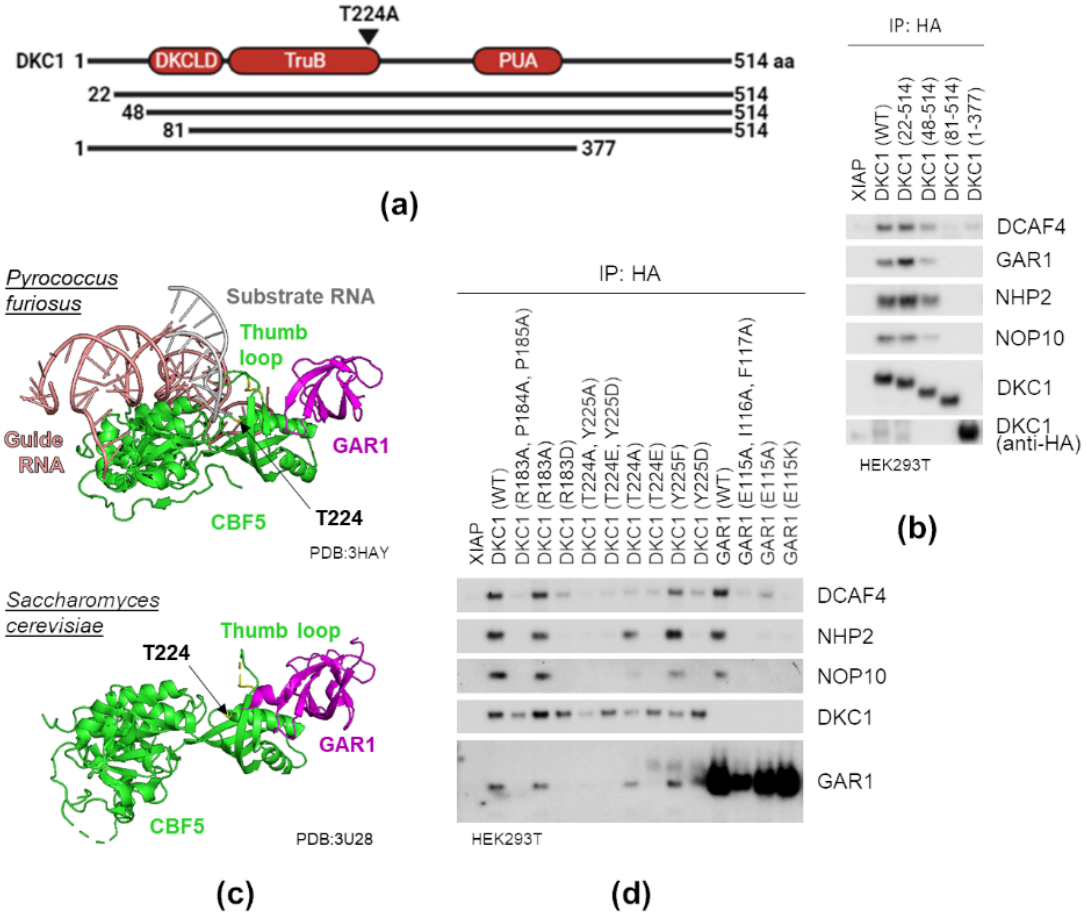

Figure 8. Threonine 224 in DKC1 is required for interaction with DCAF4. (a) Schematic representation of DKC1 and its N- and C-terminally truncated mutants. (b) HEK293T cells were transfected with HA-tagged XIAP, DKC1 and its N- and C-terminally truncated mutants. MLN4924 was added to cells 6 h before their collection. Twenty-four hours after transfection, cells were collected and lysed. Whole-cell lysates (WCL) were subjected to immunoprecipitation (IP) using anti-HA magnetic beads and immunoblotted. (c) Crystal structures of the box H/ACA RNP from *Pyrococcus furiosus* (PDB: 3HAY) and *Saccharomyces cerevisiae* (PDB: 3U28). Only CBF5 (DKC1 ortholog) and GAR1 subunits are depicted. RPP motif in the movable thumb loop and nearby threonine 224 (T224) are highlighted in yellow. Adapted from [130,137]. (d) HEK293T cells were transfected with HA-tagged XIAP, DKC1, GAR1, and their indicated mutants. MLN4924 was added to cells 6 h before their collection. Twenty-four hours after transfection, cells were collected and lysed. WCL were subjected to IP using anti-HA magnetic beads and immunoblotted.

To predict the candidate regions involved in the interaction with DCAF4, we carefully examined the already published crystal structures of the box H/ACA RNP complex from *Pyrococcus furiosus* and *Saccharomyces cerevisiae* [130,137] (Figure 8c). The complex structures are highly conserved, and we assumed that we could extrapolate the findings from these structures to human DKC1 and GAR1. GAR1 regulates substrate turnover by controlling the conformation of the thumb loop of DKC1. The thump loop adopts a closed conformation in the presence of substrate RNA, while GAR1 induces an open

conformation to enable the release and loading of substrate RNA [130,137]. As both DKC1 and GAR1 are required for the interaction with DCAF4, we hypothesized that DCAF4 could interact with the thumb loop or the nearby region. To test this hypothesis, we prepared a set of DKC1 and GAR1 mutants in which selected residues were mutated to alanines (Figure 8d). Mutational analysis of these regions revealed that Thr224 in DKC1 is essential for the interaction with DCAF4. The DKC1 mutant containing alanine substitution at Thr224 failed to co-immunoprecipitate DCAF4 while it retained the ability to interact with other protein subunits of the box H/ACA RNPs. This residue lies in the region close to the thumb and seems somewhat more accessible in the open conformation. No other contributing residues in the thumb loop and nearby regions of DKC1 (exemplified here by the RPP motif and TY motif) or in GAR1 were found to selectively lose the interaction with DCAF4 while not with other subunits of the box H/ACA RNPs. The identification of other residues contributing to the interaction was presumably prevented by the sensitivity of these vital regions to amino acid substitutions, which often led to the disintegration of the entire complex.

To summarise, we found that RNA has an inhibitory effect on the interaction between DCAF4 and box H/ACA RNPs and that the interaction depends on DKC1 and GAR1. Moreover, we demonstrated that Thr224 in DKC1, a residue lying in close proximity to the DKC1 thump loop, is selectively required for the interaction with DCAF4 but not for the interaction with other protein subunits of box H/ACA RNPs.

4.1.3. DCAF4 controls abundance of box H/ACA RNPs

To test whether DCAF4 controls the abundance of the box H/ACA RNPs, we prepared several cell lines in which we deleted the exon 4 of the *DCAF4* gene using the CRISPR/Cas9 genome-editing system. The deletion was confirmed by PCR amplification of the region encompassing the exon 4 and DNA sequencing (not shown). Additionally, the loss of DCAF4 protein expression in these cells was confirmed by immunoblotting (Figure 9a). Finally, the specificity of the DCAF4 antibody was validated by the siRNA-mediated depletion of DCAF4 in parental cells.

Having established *DCAF4* KO cells, we initially used them to explore the effect of the DCAF4 loss on the abundance of the protein subunits of the box H/ACA RNPs. DKC1 and other protein subunits of the box H/ACA complex were up-regulated in *DCAF*4 KO HeLa, U2OS, and HCT116 cells (Figure 9b). Subsequently, we re-introduced DOX-inducible DCAF4 into the genome of these cells (Figure 9c,d). Induction of DCAF4 restored or even down-regulated the abundance of the protein subunits of the box H/ACA RNPs. These experiments demonstrated that DCAF4 regulates the protein subunits of the box H/ACA RNP complex.

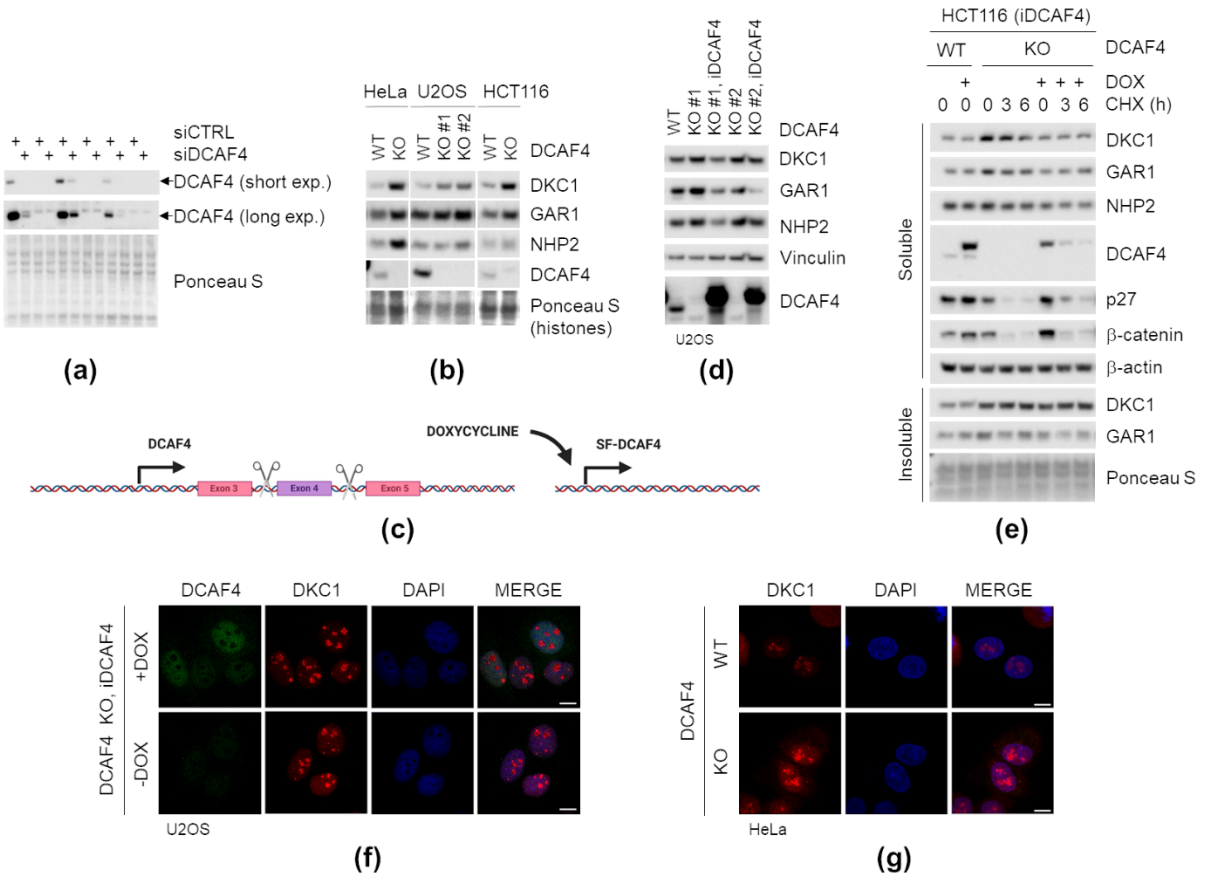

Figure 9. DCAF4 controls the abundance of protein subunits of box H/ACA RNPs. (a) The exon 4 of the *DCAF4* gene was deleted using the CRISPR/Cas9 genome-editing system in U2OS, HCT116, HeLa cell lines. Parental and *DCAF4* knockout (KO) single-cell clones were transfected with control siRNA (siCTRL) or siRNA targeting *DCAF4* (siDCAF4) to validate the specificity of the DCAF4 antibody. Seventy-two hours later, cells were collected, lysed, and whole-cell lysates (WCL) were immunoblotted. (b) *DCAF4* wild type (WT) and KO HeLa, U2OS, and HCT116 cells were collected, lysed, and WCL immunoblotted. (c) Illustration of the strategy used to generate *DCAF4* KO cells with doxycycline (DOX)-inducible expression of Twin-Strep-FLAG-tagged DCAF14 (SF-DCAF4). *DCAF4* KO cells, in which the deletion of the exon 4 disrupted the *DCAF4* gene, were transduced with a lentiviral vector expressing SF-DCAF4 under the control of DOX-inducible promotor, and stably transduced cells were selected. (d) *DCAF4* WT and two different clones of *DCAF4* KO U2OS cells with DOX-inducible expression of SF-DCAF4 were treated with DOX, lysed, and WCL were immunoblotted. (e) *DCAF4* WT and *DCAF4* KO HCT116 cells with DOX-inducible expression of SF-DCAF4 were treated with DOX (200 ng/ml) for 24 h where indicated. Cells were then treated with cycloheximide (CHX), collected at the indicated times and lysed. The soluble and insoluble fractions of the cell lysates were immunoblotted. (f,g) *DCAF4* KO U2OS cells with DOX-inducible expression of SF-DCAF4 were treated with DOX (200 ng/ml) and fixed 24 h later (f), while *DCAF4* WT and *DCAF4* KO HeLa cells were fixed untreated (g). DCAF4 and DKC1 were detected by immunofluorescence. Nuclei were visualized by 4',6-diamidino-2-phenylindole (DAPI). Scale bar, 10 µm.

Next, we tested the stability of DKC1, the main protein subunit of the box H/ACA RNPs, in DCAF4 KO cells harbouring the DCAF4 expression construct under the control of DOX-inducible promotor. Consistently with the previous results, DKC1 was up-regulated in DCAF4 KO HCT116 cells, and induction of

DCAF4 restored its protein level in the soluble fraction but not in the insoluble one (Figure 9e). To test the stability of DKC1, we employed the cycloheximide (CHX) chase assays. Administration of CHX inhibited protein synthesis (the pulse phase). Reduction in the levels of studied proteins at specific time points (the chase phase) could then be examined by immunoblotting. As a control of the CHX treatment, we stained the canonical targets of CRL-dependent protein degradation—p27 and β-catenin. The CHX experiments revealed that DCAF4 is an unstable protein as its abundance declined following the inhibition of protein synthesis by CHX. Counterintuitively, the excessive soluble DKC1 in DCAF4 KO cells was unstable, suggesting the existence of an alternative pathway targeting this DKC1 for degradation. No effect on the DKC1 protein level in cells expressing inducible DCAF4 was observed, either due to the instability of DCAF4 itself or the absence of permissive conditions for DKC1 degradation.

The observation that DCAF4 controls the DKC1 protein level only in the soluble fraction prompted us to investigate the subcellar localisation of DCAF4 (Figure 9f). DCAF4 was localised to the cell nucleus but was absent from the nucleoli, where the bulk of DKC1 was present. The localisation experiments suggested that DCAF4 controls DKC1 in the nucleoplasm. Consistently, DKC1 was increased in the nucleoplasm of *DCAF4* KO cells. In *DCAF4* KO HeLa cells, DKC1 was also present in the cytoplasm and concentrated in distinct cytoplasmic foci (Figure 9g).

Finally, we explore the effect of the DCAF4 loss on the abundance of the box H/ACA RNAs. The abundance of the box H/ACA RNAs was previously shown to depend on the availability of the protein subunits of the box H/ACA RNPs [353]. Consistently, the box H/ACA RNAs were down-regulated upon DKC1 depletion by siRNA (Figure 10). In *DCAF4* KO cells, the box H/ACA RNAs were up-regulated, and this effect was rescued by DKC1 down-regulation. Notably, the relative RNA level of the box H/ACA-containing TERC was also increased, indicating that DCAF4 could impact the telomere homeostasis by controlling the abundance of the TERC RNP. To obtain a broader picture of the changes in RNA expression in *DCAF4* KO cells, we also prepared samples for RNA sequencing (RNA-seq). No statistically significant differences in RNA expression were found in *DCAF4* KO cancer cells (not shown). As the changes in gene expression and the telomere lengths are better addressed in mouse models than in immortal cancer cells, we established *Dcaf4* KO mice to investigate the function of the DCAF4-mediated control of the box H/ACA RNPs *in vivo*. *Dcaf4* KO mice were viable, fertile, and displayed no gross physical abnormalities. Further investigation of the biological function of $CRL4^{DCAF4}$ (e.g., changes in telomere lengths and gene expression) are to be continued and taken over by another student.

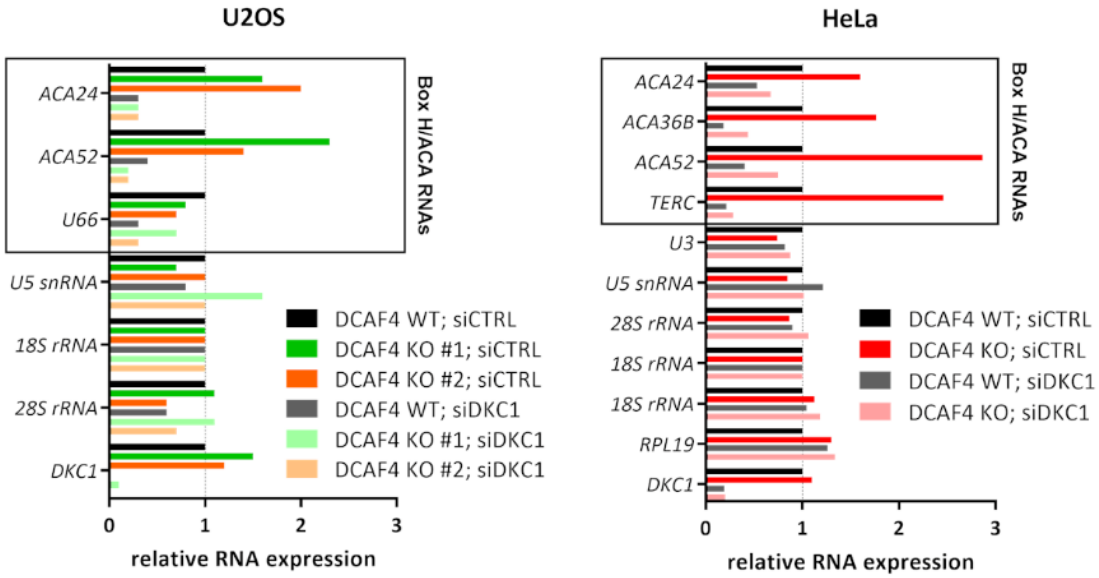

Figure 10. DCAF4 controls the abundance of box H/ACA RNAs. U2OS and HeLa *DCAF4* wild type (WT) and knockout (KO) cells were transfected with control siRNA (siCTRL) or siRNA targeting *DKC1* (siDKC1). Cells were collected 72 hours later, and cDNA was synthesized from isolated RNA. Relative RNA levels of indicated RNAs were determined by qPCR.

In summary, we discovered that DCAF4 controls the abundance of the box H/ACA RNPs, suggesting a role of DCAF4 in RNA biology and potentially in telomere homeostasis. Still, the biological relevance of the DCAF4-mediated regulation of the box H/ACA RNPs remains to be addressed.

4.2. Novel substrates of CRL4^{DCAF12}

4.2.1. DCAF12 interacts with proteins containing C-terminal acidic motif

To identify candidate substrates of multisubunit CRL4^{DCAF12}, we performed a sequential AP of SF-DCAF12 followed by IP of HA-CUL4A (Figure 11a) and identified co-isolated proteins by LC-MS/MS, the same procedure applied for CRL4^{DCAF4} (chapter 4.1.1.). In general, we obtained identical hits from both isolation steps (Figure 11b,c), indicating that these DCAF12-interacting proteins were associated with fully assembled CRL4^{DCAF12}. Functional classification of the DCAF12-associated proteins showed a substantial enrichment of proteins involved in immune and especially antiviral responses, such as MOV10, GART, ADAR, and XIAP [294,322,355,356]. As DCAF12 has been recently reported to recognise the C-terminal -EE degron [48,186], we also analysed the C-terminal amino acid sequences of DCAF12-associated proteins (Figure 11d). Consistently with previous reports, C-terminal twin glutamic acid residues (-EE) were overrepresented. However, we also noticed a remarkable overrepresentation of proteins with glutamic acid residue at penultimate (-2) position but different than glutamic acid residue at terminal (-1) position. Specifically, C-terminal glutamic acid-leucine residues (-EL) were particularly enriched, indicating a certain degree of flexibility regarding the specific residue at the C-terminal position.

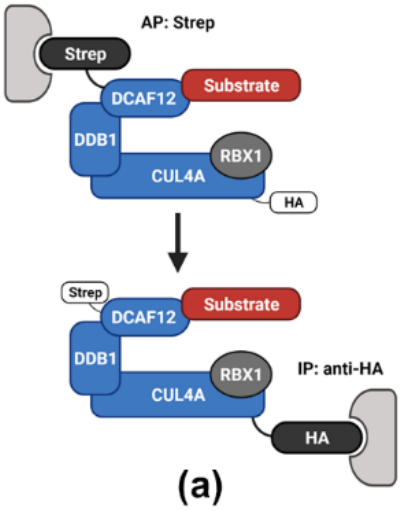

(a)

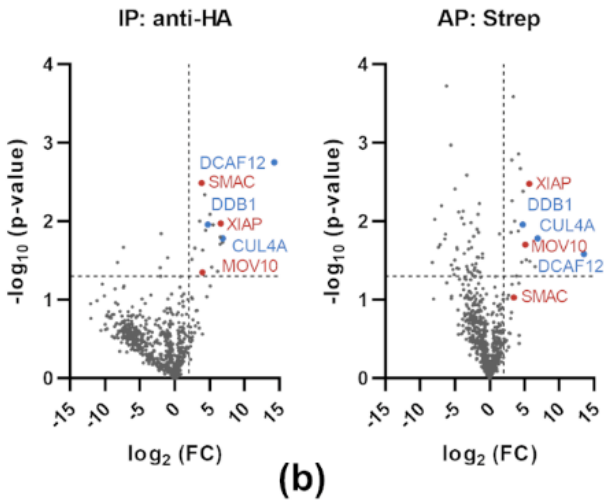

(b)

Protein	Mean log_2 (LFQ intensity) AP: Strep	IP: anti-HA	C-term.
DCAF12	33.7	31.1	-WS
CUL4A	33.3	28.8	-VA
DDB1	35.9	28.9	-IH
KPNA3	32.1	23.9	-NF
KPNA4	31.1	22.9	-QF
ADAR	31.7	24.3	-PV
XIAP	30.7	23.6	-MS
FAM120A	29.2	24.0	-EE
LONP1	32.4	23.8	-ER
ACOT9	30.3	23.7	-EP
USP30	29.0	22.8	-EE
GART	32.2	22.0	-EE
MOV10	30.6	22.0	-EL
MTO1	29.6	21.9	-EL
SDF2	27.1	21.8	-EL
SMAC	30.9	21.7	-ED
MCMBP	29.6	21.1	-EL

(c)

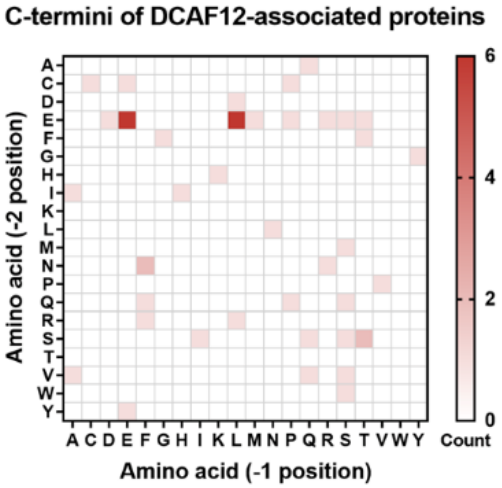

(d)

Figure 11. Proteomic analysis of proteins interacting with CRL4^{DCAF12}. (a) Schematic representation of the tandem affinity purification strategy. Twin-Strep-FLAG-tagged DCAF12 and HA-tagged CUL4A were co-expressed in HEK293T cells and subjected to affinity purification (AP) using Strep-TactinXT resin followed by immunoprecipitation (IP) using anti-HA magnetic beads. (b) Proteins interacting with CRL4^{DCAF12} were identified by liquid chromatography-tandem mass spectrometry (LC-MS/MS). The composition of purified complexes from both steps was analysed by LC-MS/MS and compared to a non-related ubiquitin ligase SCF^{FBXL6}. Proteins that specifically interacted with CRL4^{DCAF12} are in the upper right quadrant. (c) The top hits obtained from LC-MS/MS analysis of proteins interacting with CRL4^{DCAF12}. Log_2 (label-free quantitation (LFQ) intensities) from both purification steps and the last two C-terminal amino acids are shown. Components of CRL4^{DCAF12} are depicted in blue, putative substrates in red, other associated proteins in black. (d) Analysis of C-termini of DCAF12-associated proteins. The top 50 hits were included in the analysis. The heat map shows the count of specific amino acid combinations at −2 (penultimate) and −1 (terminal) positions.

To investigate whether the interactions between DCAF12 and its potential substrates are specific, we expressed a panel of substrate receptor subunits of CRLs in HEK293T cells and performed a small-scale AP (Figure 12a). As anticipated, F-box proteins interacted with CRL adaptor SKP1, while DCAF proteins interacted with CRL adaptor DDB1. Interaction between $CRL1^{\beta\text{-}TrCP1}$ and its canonical substrate phospho-β-catenin was used as a positive control. DCAF12 specifically interacted with multiple proteins containing the C-terminal acidic motif, such as SMAC, MOV10, and GART. We also confirmed the interaction with other proteins identified by LC-MS/MS, including XIAP and ADAR1. Next, we performed a similar experiment with mammalian paralogs of DCAF12 (Figure 12b,c). DCAF12L1 and DCAF12L2 were associated weakly with CUL4, and no interaction with potential substrates of DCAF12 was detected, indicating that DCAF12 and its paralogs are not functionally redundant.

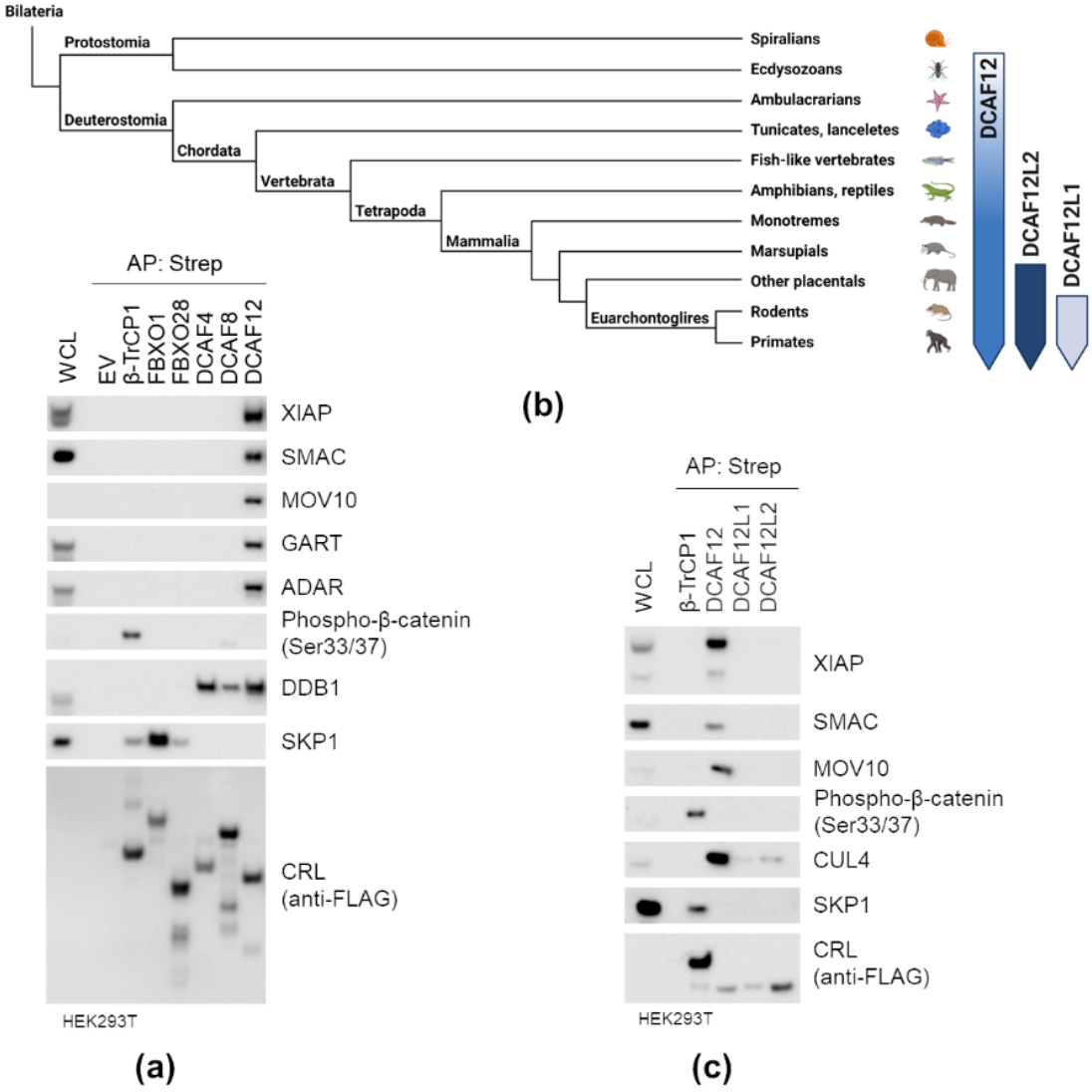

Figure 12. DCAF12 specifically interacts with proteins containing C-terminal acidic motif. (a,c) HEK293T cells were transfected with an empty vector (EV) or the indicated Twin-Strep-FLAG-tagged substrate receptor subunits of the cullin-RING ubiquitin ligase (CRL). MLN4924 was added to cells 6 h before their collection. Forty-eight hours after transfection, cells were collected and lysed. Whole-cell

lysates (WCL) were subjected to affinity purification (AP) with Strep-TactinXT resin, and eluates were immunoblotted. (b) A simplified evolutionary scheme illustrating the emergence of DCAF12 and its paralogs in bilaterians. DCAF12 is present in vertebrates and insects, DCAF12L2 in all placental mammals, and DCAF12L1 only in Euarchontoglires.

Taken together, we identified multiple interaction partners of DCAF12 and confirmed the specificity of the interactions in our AP experiments. Based on the presence of glutamic acid residue at penultimate position (-2) in DCAF12-associated proteins, we compiled a list of the $CRL4^{DCAF12}$ candidate substrates, including XIAP-SMAC, MOV10, and GART, and proceeded with further experimental validation.

4.2.2. Subcellular localisation of DCAF12

The candidate substrates of DCAF12 localise to distinct subcellular compartments, e.g., to the mitochondrial intermembrane space (SMAC), the mitochondrial outer membrane (USP30), and the cytosol (MOV10 and GART). On the contrary, DCAF12 possesses two putative nuclear localisation signals (NLSs), suggesting nuclear localisation. Hence, we employed immunofluorescence microscopy to detect DCAF12 and its mutants lacking the putative NLSs to address the question of the DCAF12 subcellular localisation.

To detect endogenous DCAF12, we tested several commercially available anti-DCAF12 antibodies. Unfortunately, none of them was reliable, and therefore we had to switch to systems in which DCAF12 was artificially overexpressed. In addition to $DCAF12^{WT}$, we explored the localisation of DCAF12 mutants lacking the putative NLSs. As both NLSs are located near the N-terminus of DCAF12, we prepared N-terminal truncations of DCAF12 (Figure 13a), lacking either the very N-terminal NLS ($DCAF12^{\Delta 1-11}$) or both NLSs ($DCAF12^{\Delta 1-38}$). Removing the N-terminal sequence, which precedes the H-box motif and WD-repeats responsible for DDB1 and substrate binding, was not supposed to influence the assembly of DCAF12 into CRL and substrate recognition [30]. Indeed, these N-terminally truncated mutants of DCAF12 interacted with CRL adaptor DDB1 and potential substrates of DCAF12 (Figure 13b). Interestingly, their interaction with XIAP and SMAC was even increased. Finally, we examined their subcellular localisation (Figure 13c, the upper panel). $DCAF12^{WT}$ was localised to the nucleus, whereas $DCAF12^{\Delta 1-11}$ and $DCAF12^{\Delta 1-38}$ to the cytoplasm, confirming the functionality of the first NLS.

The nuclear localisation of $DCAF12^{WT}$ was seemingly counterintuitive as DCAF12 predominantly interacted with cytoplasmic proteins. We thus hypothesised that the cytoplasmic localisation of DCAF12 might be transient and sensitive to the degradation of its yet unknown cytoplasmic adaptor. To test this hypothesis, we treated cells with a proteasome inhibitor MG132 (Figure 13c, the lower panel). This treatment caused a cytoplasmic accumulation of $DCAF12^{WT}$, indicating that the localisation of DCAF12 could be subjected to regulation by the UPS. Taken together, DCAF12 predominantly localises to the nucleus in human cancer cell lines, and its nuclear localisation depends on the N-terminal NLSs. Additionally, an unstable factor seems to affect the localisation of DCAF12 to the cytoplasm.

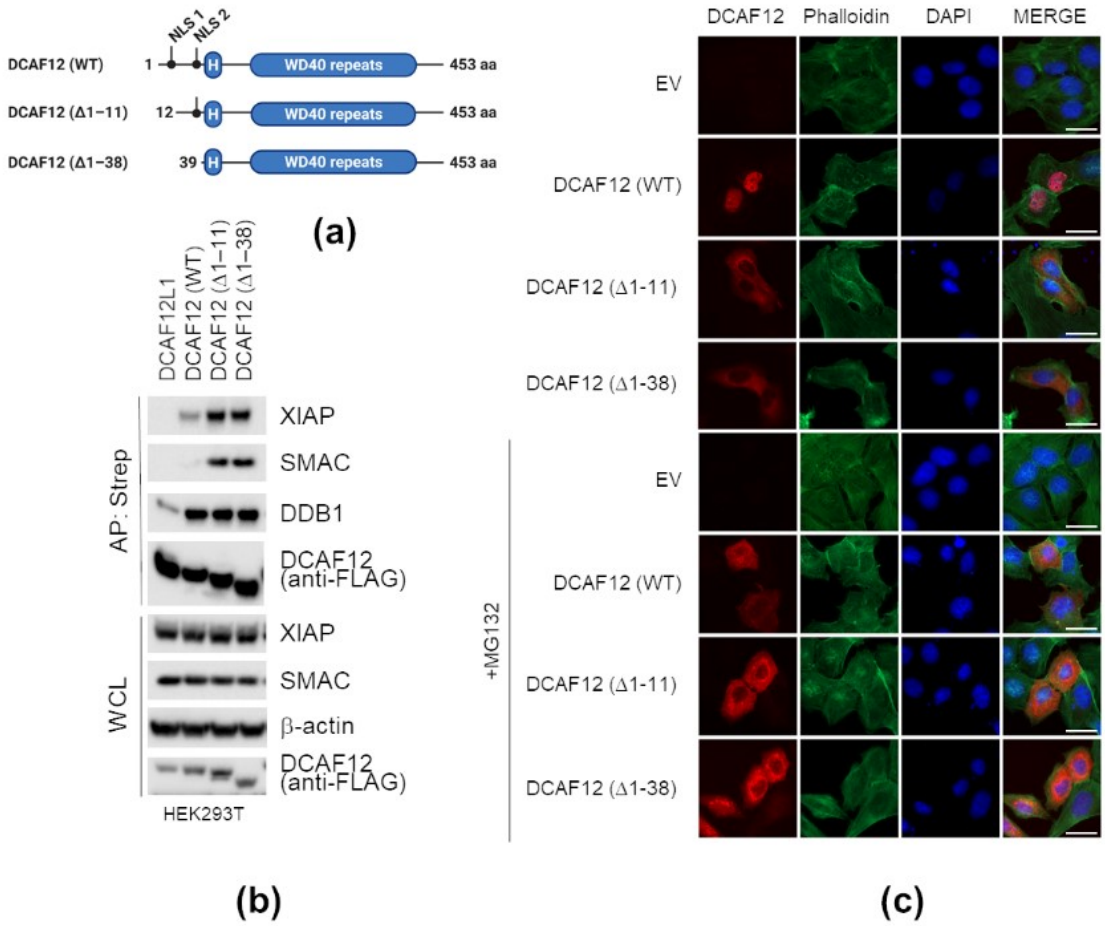

Figure 13. Subcellular localisation of DCAF12. (a) Schematic representation of DCAF12 and its N-terminally truncated mutants. Two predicted nuclear localisation signals (NLS) and H-box are highlighted. (b) HEK293T cells were transfected with the indicated Twin-Strep-FLAG-tagged DCAF12 constructs or Twin-Strep-FLAG-tagged DCAF12L1 as a control and treated with MLN4924 for 6 h before harvesting. Forty-eight hours after transfection, cells were harvested, lysed, and whole-cell lysates (WCL) were subjected to affinity purification (AP) with Strep-TactinXT resin. WCL and eluates were immunoblotted with indicated antibodies. (c) U2OS cells were transfected with an empty vector (EV) or the indicated Twin-Strep-FLAG-tagged DCAF12 constructs and fixed 36 h later. DCAF12 was detected with the anti-Strep antibody. Phalloidin-iFluor 488 and 4',6-diamidino-2-phenylindole (DAPI) were used to counterstain actin filaments and nuclei, respectively. Where indicated, cells were pre-treated for 6 h with MG132 before fixation. Scale bar, 30 μm.

4.2.3. Cytoplasmic DCAF12 down-regulates MOV10 but not XIAP and SMAC

Having established the subcellular localisation of DCAF12 and its interactions with several potential substrates, we asked whether DCAF12 regulates their protein level under steady-state conditions in cancer cell lines. To investigate the effects of the DCAF12 nuclear and cytoplasmic expression on its potential substrates, we prepared stable cell lines with DOX-inducible expression of predominantly nuclear DCAF12^{WT} or cytoplasmic DCAF12$^{\Delta 1\text{-}11}$ and DCAF12$^{\Delta 1\text{-}38}$. In these HEK293T and HCT116 cells, we first confirmed the interaction between inducible DCAF12 and its potential substrates (Figure

14a,b). Consistently with the results obtained from the overexpression system, the interaction between XIAP-SMAC and cytoplasmic mutants of DCAF12 was increased compared to DCAF12^{WT}. At the same time, the interaction between cytoplasmic mutants of DCAF12 and MOV10 was decreased, which probably reflected down-regulation of MOV10 upon induction of cytoplasmic DCAF12. The abundance of XIAP and SMAC seemed to be unaffected by either nuclear or cytoplasmic expression of DCAF12.

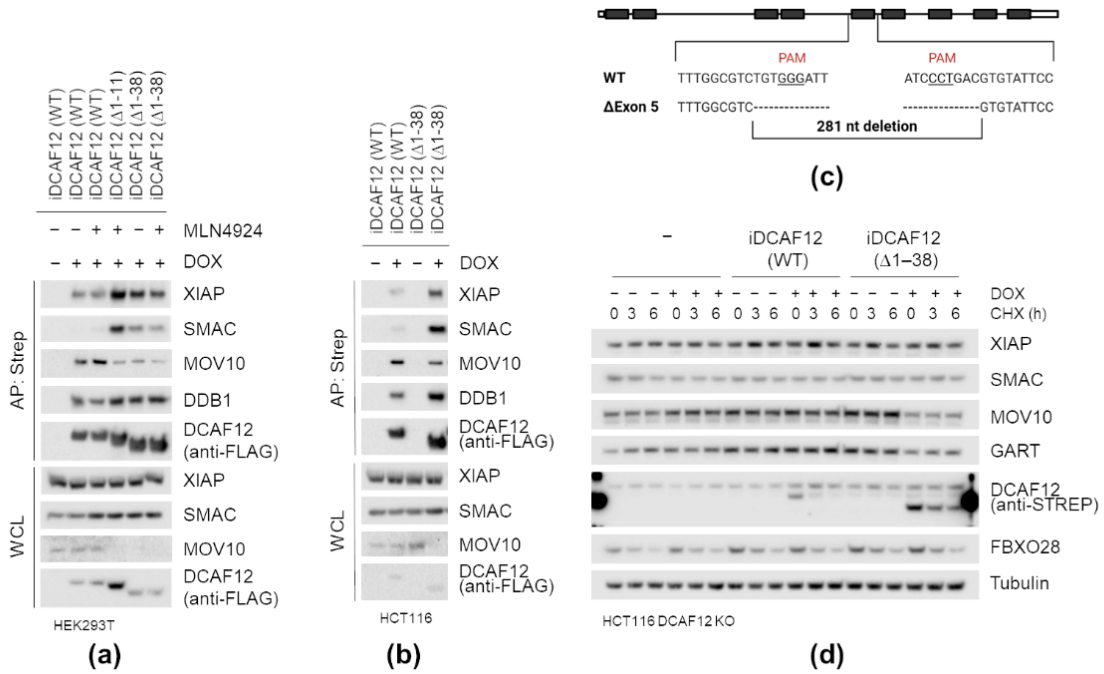

Figure 14. Cytoplasmic DCAF12 down-regulates MOV10 but not XIAP and SMAC. (a,b) HEK293T (a) and HCT116 (b) stable cell lines expressing doxycycline (DOX)-inducible Twin-Strep-FLAG-tagged DCAF12 constructs (iDCAF12^{wt}, iDCAF12$^{\Delta1–11}$, or iDCAF12$^{\Delta1–38}$) were treated with DOX for 48 h where indicated. MLN4924 was added to cells 6 h before their collection. Cells were lysed and whole-cell lysates (WCL) subjected to affinity purification (AP) using Strep-TactinXT resin. Both WCL and eluates were immunoblotted. (c) Schematic diagram of targeted disruption of the *DCAF12* gene using the CRISPR/Cas9 genome-editing system. Two single guide RNAs were designed to target introns flanking the exon 5 of the *DCAF12* gene. Protospacer adjacent motif (PAM) is underlined. The clone used in (d) had a 281-nucleotide (nt) deletion encompassing the exon 5. (d) *DCAF12* KO HCT116 cells with DOX-inducible expression of Twin-Strep-FLAG-tagged DCAF12 constructs (iDCAF12^{wt}, iDCAF12$^{\Delta1–38}$) were treated with DOX for 48 h and cycloheximide (CHX) for the indicated times, collected, lysed, and WCL were immunoblotted.

Next, we investigated the effect of the DCAF12 loss on its potential substrates using RNAi or the CRISPR/Cas9 genome-editing system. Although the *DCAF12* mRNA level was effectively down-regulated in both systems, the tested potential substrates of DCAF12 (XIAP, SMAC, MOV10, and GART) were not up-regulated in our assays (not shown). Considering the previous localisation experiments, this could be possibly caused by the spatial-temporal separation of DCAF12 and its substrates in cancer cell lines under

steady-state conditions. However, as we could not detect endogenous DCAF12 by anti-DCAF12 antibodies, an alternative explanation might be the absence of DCAF12 in cancer cell lines owing to its instability.

Finally, we tested the stability of DCAF12 potential substrates in the CHX chase assays. We used several cancer cell lines, including HCT116 *DCAF12* KO cells in which the exon 5 of the DCAF12 gene was deleted and DOX-inducible DCAF12 expression constructs reintroduced into the genome (Figure 14c,d). As a control of the CHX treatment, we stained an unstable ubiquitin ligase FBXO28, the abundance of which declines rapidly following the inhibition of protein synthesis by CHX [357]. Induction of cytoplasmic DCAF12 decreased the protein level of MOV10 (and GART). Nevertheless, this was not further influenced by the CHX administration. No apparent differences in protein stability of the DCAF12 potential substrates (XIAP, SMAC, MOV10, and GART) were noticed in the CHX experiments under steady-state conditions in HCT116 cells expressing either the nuclear $DCAF12^{WT}$ or its cytoplasmic mutants. DCAF12 itself proved unstable, especially the nuclear $DCAF12^{WT}$, which disappeared rapidly after inhibiting protein synthesis. Similar conclusions were drawn from different cancer cell lines (not shown).

In short, the expression of cytoplasmic DCAF12 in cancer cell lines leads to a decrease in the protein levels of MOV10 and GART but not in the protein levels of XIAP and SMAC. To gain more insight into the DCAF12-dependent recognition of these candidate substrates, we next more closely examined the interactions between 1) DCAF12 and XIAP-SMAC, and 2) DCAF12 and MOV10 (and GART).

4.2.4. SMAC C-terminal -ED motif and XIAP BIR2-BIR3 domains are required for XIAP-SMAC interaction with DCAF12

XIAP and SMAC have been previously shown to interact directly with each other. Specifically, the N-terminal IBM motif of SMAC inserts into the IBM binding groove on the BIR2 and BIR3 domains of XIAP. As DCAF12 recognise proteins bearing negatively charged residues at their C-termini and SMAC poses such residues while XIAP does not, we hypothesised that DCAF12-XIAP interaction is SMAC-dependent. To test this hypothesis, we examined the interaction between DCAF12 and XIAP upon the loss of SMAC. Firstly, we down-regulated SMAC by siRNA in HEK293T cells. siRNA-mediated down-regulation of SMAC did not affect XIAP expression and resulted in a concurrent decrease in the interaction of DCAF12 with SMAC and XIAP, not affecting the interaction between DCAF12 and MOV10 (Figure 15a). Next, we tested these interactions in HCT116 *XIAP* and *SMAC* KO cells. DCAF12 did not interact with XIAP in *SMAC* KO cells (Figure 15b). Surprisingly, the interaction between DCAF12 and SMAC was also lost in the absence of XIAP in *XIAP* KO cells and rescued by the induction of XIAP (Figure 15b,c). Finally, we prepared a mutant form of SMAC (E228X) lacking the C-terminal negatively charged -ED residues (Figure 15d). The overexpressed SMAC was not sufficiently processed into mature SMAC, and the unprocessed full-length SMAC interacted non-specifically with DCAF12 (not shown). Therefore, we employed a previously-

described ubiquitin-SMAC expression system to express mature, biologically active SMAC in the cytosol [358]. Expression of $SMAC^{WT}$ in HCT116 *SMAC* KO cells rescued the interaction between DCAF12 and XIAP, while $SMAC^{E228X}$ did not interact with DCAF12 nor rescued the interaction between DCAF12 and XIAP (Figure 15e). Taken together, the interaction between DCAF12 and XIAP depends on the C-terminal -ED motif of SMAC. Intriguingly, the DCAF12-SMAC interaction also requires XIAP.

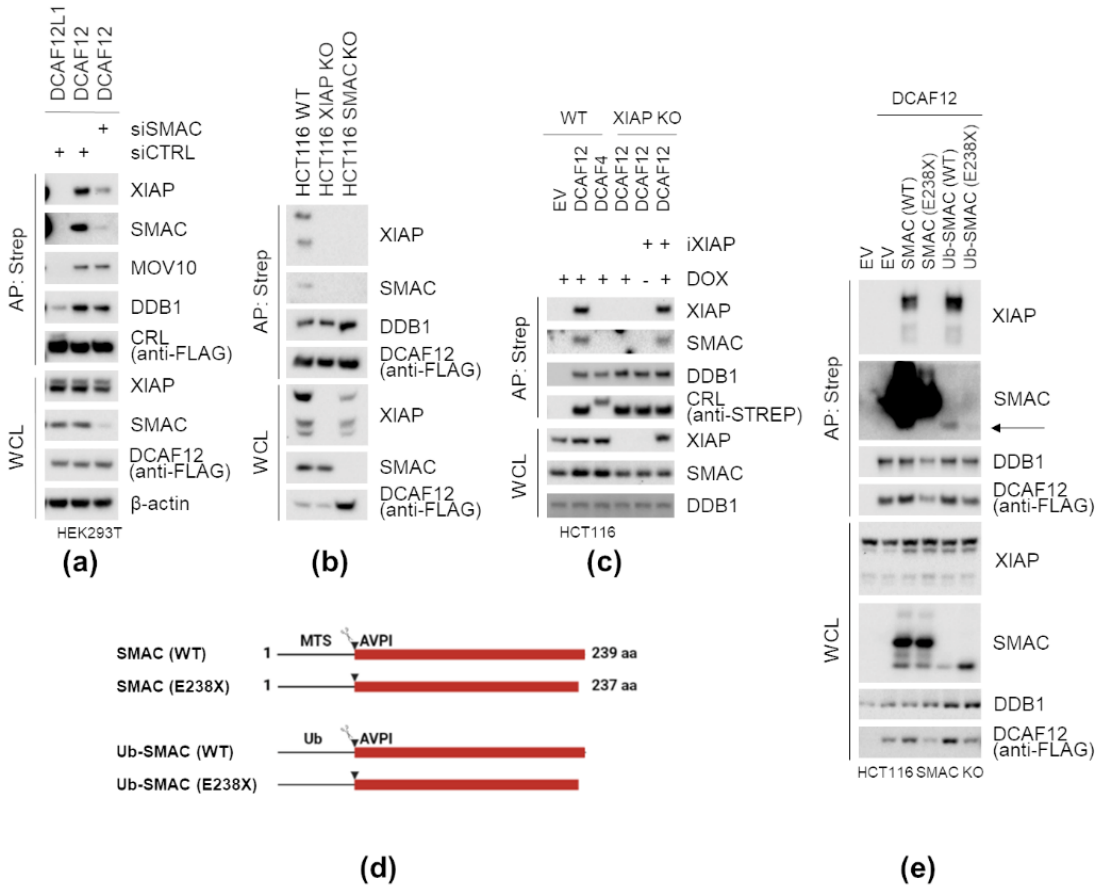

Figure 15. SMAC C-terminal -ED motif is required for XIAP-SMAC interaction with DCAF12. (a) HEK293T cells were transfected with control siRNA (siCTRL) or siRNA targeting *SMAC* (siSMAC) and subsequently (24 h later) with Twin-Strep-FLAG-tagged substrate receptor subunits of cullin-RING ubiquitin ligase (CRL)—DCAF12 or DCAF12L1. Twenty-four hours after transfection, cells were collected, lysed, and whole-cell lysates (WCL) were subjected to affinity purification (AP) using Strep-TactinXT resin. Both WCL and eluates were immunoblotted. (b) HCT116 wild type (WT), HCT116 *XIAP* knockout (*XIAP* KO), and HCT116 *SMAC* knockout (*SMAC* KO) cells were transfected with Twin-Strep-FLAG-tagged DCAF12 and treated with MLN4924 for 6 h. Forty-eight hours after transfection, cells were collected, lysed, and WCL were subjected to AP using Strep-TactinXT resin. Both WCL and eluates were immunoblotted. (c) HCT116 WT, HCT116 *XIAP* KO, and HCT116 *XIAP* KO with doxycycline (DOX)-inducible expression of XIAP were transfected with an empty vector (EV), Twin-Strep-FLAG-tagged substrate receptor subunits of cullin-RING ubiquitin ligase (CRL)—DCAF12 or DCAF4. Cells were treated with DOX for 24 h as indicated and with MLN4924 for 6 h. Forty-eight hours after transfection, cells were collected, lysed, and WCL were subjected to AP using Strep-TactinXT resin. Both WCL and eluates were immunoblotted. (d) Schematic representation of SMAC, SMAC mutant lacking the C-terminal -ED

motif (E238X), ubiquitin-SMAC, and ubiquitin-SMAC lacking the C-terminal -ED motif. (e) *SMAC* KO HCT116 cells were co-transfected with Twin-Strep-FLAG-tagged DCAF12 and an EV or indicated SMAC constructs, treated with MLN4924 for 6 h, and collected 48 h after transfection. WCL were subjected to AP using Strep-TactinXT resin. Both WCL and eluates were immunoblotted.

Our observations that XIAP and SMAC are both needed for the interaction with DCAF12 suggested that DCAF12 only recognises SMAC associated with XIAP. The requirement of XIAP prompted us to investigate which domains of XIAP are required for the interaction with DCAF12. Firstly, we prepared a series of truncation mutants of XIAP and tested their interactions with DCAF12 (Figure 16a,b). Deletion of the BIR1 domain did not affect the interaction between XIAP and DCAF12, while concurrent deletion of the BIR1 and BIR2 domains abolished the interaction. C-terminal truncation mutants of XIAP were less expressed. Nevertheless, mutants of XIAP lacking RING and UBA domains still interacted with DCAF12. Only the concurrent deletion of the RING, UBA, and BIR3 domains abolished the interaction. The BIR2 and BIR3 domains of XIAP are thus both necessary for the interaction with DCAF12. A truncated mutant of XIAP consisting only of the BIR2 and BIR3 domains was sufficient for the interaction yet interacted less effectively than full-length XIAP.

Next, we mutated residues in the BIR2 and BIR3 domains of XIAP, which were previously described as critical for the interaction with SMAC [261,359]. The E314A mutation in the BIR3 domain of XIAP completely abolished the interaction of XIAP with SMAC and DCAF12, demonstrating that the BIR3 domain of XIAP is essential for the interaction (Figure 16c,d). Interestingly, the E219R, H223V double mutation in the BIR2 domain of XIAP had a minimal effect on the interaction of XIAP with SMAC while effectively reducing the interaction of XIAP with DCAF12, suggesting that the BIR2 domain of XIAP contributes uniquely to the interaction. Finally, we prepared another series of N-terminal truncation mutants more closely covering the linker region preceding the BIR2 domain and performed alanine scanning mutagenesis of the BIR2 domain (not shown) to narrow further the minimal region of XIAP required for the interaction and to find essential residues. Interaction studies with these mutants revealed that the linker is not needed for the interaction with DCAF12 and that mutating the critical residues of the BIR2 domain reduces but not completely abolishes the interaction with DCAF12 in a way analogous to the E219R, H223V double mutation in the BIR2 domain of XIAP. Taken together, the BIR2 and BIR3 domains of XIAP are necessary for the interaction of XIAP and SMAC with DCAF12. This observation suggests that SMAC must be bound to the BIR2-BIR3 domains of XIAP to be recognised by DCAF12.

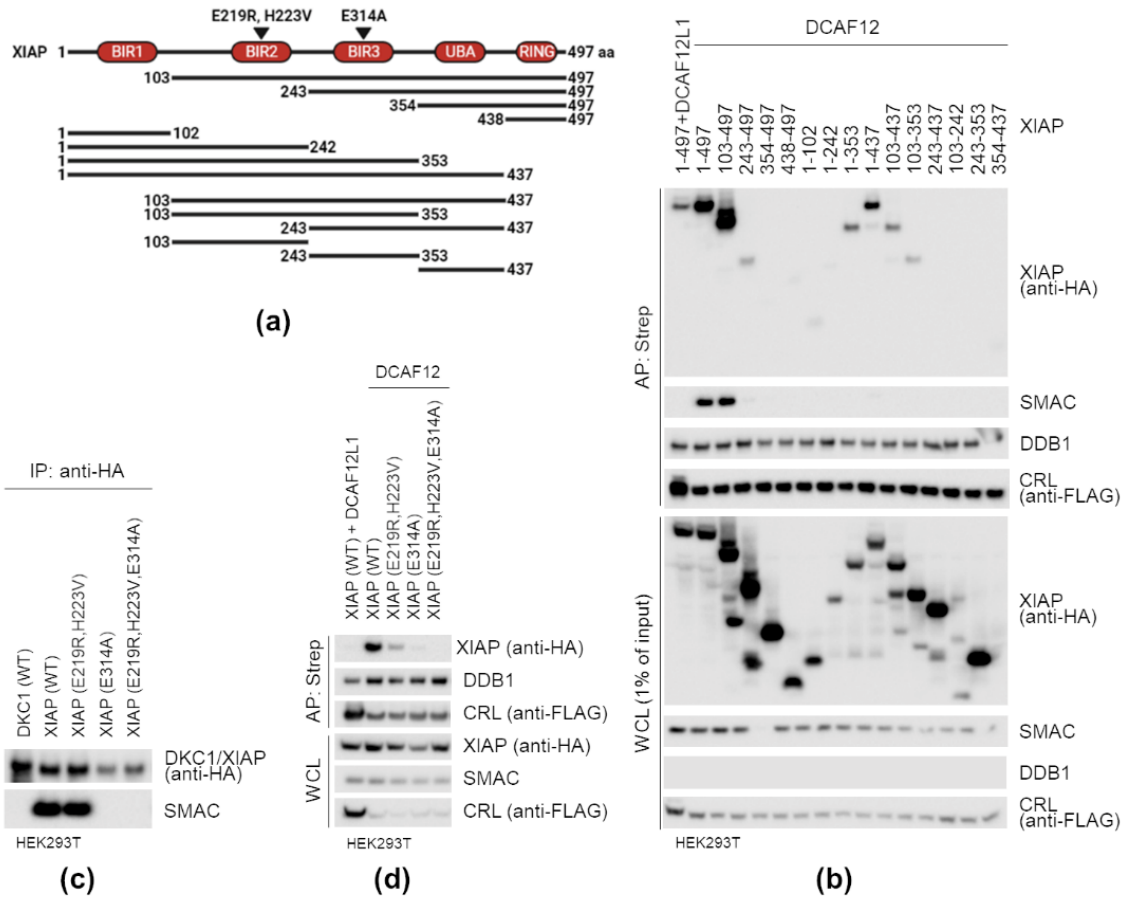

Figure 16. XIAP BIR2-BIR3 domains are required for XIAP-SMAC interaction with DCAF12. (a) Schematic representation of XIAP and its N- and C-terminally truncated mutants. The positions of the E219R, H223V, and E314A mutations in the BIR2 and BIR3 domains are shown. (b) HEK293T cells were co-transfected with HA-tagged XIAP or its indicated truncation mutants and Twin-Strep-FLAG-tagged substrate receptor subunits of the cullin-RING ubiquitin ligase (CRL)—DCAF12 or DCAF12L1. MLN4924 was added to cells 6 h before cell collection. Forty-eight hours after transfection, cells were collected and lysed. Whole-cell lysates (WCL) were subjected to affinity purification (AP) using Strep-TactinXT resin. Both WCL and eluates were immunoblotted. (c) HEK293T cells were transfected with the indicated HA-tagged XIAP mutants and treated with MLN4924 for 6 h before cell collection. Forty-eight hours after transfection, cells were collected and lysed. Whole-cell lysates (WCL) were subjected to immunoprecipitation (IP) using anti-HA magnetic beads and immunoblotted. (d) HEK293T cells were co-transfected with the indicated HA-tagged XIAP mutants and Twin-Strep-FLAG-tagged substrate receptor subunits of the CRL—DCAF12 or DCAF12L1. MLN4924 was added to cells 6 h before cell collection. Forty-eight hours after transfection, cells were collected and lysed. Whole-cell lysates (WCL) were subjected to affinity purification (AP) using Strep-TactinXT resin. Both WCL and eluates were immunoblotted.

The BIR2 and BIR3 domains of XIAP can be targeted by SMAC mimetics, which binds to the IBM-containing BIR domains of IAPs, including the XIAP BIR2 and BIR3 domains, and mimic the inhibitory activity of endogenous SMAC. Since the interaction between DCAF12 and SMAC seemed to require SMAC binding to the BIR2-BIR3 domains of XIAP, we hypothesised that SMAC mimetics could disrupt it. To test this hypothesis, we firstly incubated purified DCAF12 complexes with SMAC mimetics for a short time *in*

vitro (Figure 17a). Indeed, the SMAC mimetics AZD5582 and LCL161, which have a high affinity to XIAP, completely disrupted the interaction between DCAF12 and the XIAP-SMAC complex. On the other hand, the SMAC mimetics birinapant and embelin, which have a lower affinity for XIAP, were consistently less effective in dissociating XIAP and SMAC from DCAF12. Next, we added these compounds to cells and tested the interaction between DCAF12 and the XIAP-SMAC complex (Figure 17b). All tested SMAC inhibitors (AZD5582 and birinapant are shown here) efficiently prevented XIAP and SMAC to interact with DCAF12. In addition to SMAC mimetics, we treated cells with staurosporine and TRAIL to induce apoptosis and release endogenous SMAC from mitochondria into the cytosol, which is where and when they are supposed to interact with each other. Surprisingly, induction of apoptosis correlated with the loss of the interaction between DCAF12 and the XIAP-SMAC complex, which was caspase-dependent as caspase inhibitor Z-VAD could have prevented it. In summary, SMAC mimetics disrupt the interaction between DCAF12 and the XIAP-SMAC complex. Additionally, apoptosis also ultimately disrupts this interaction, which probably reflects the degradation of XIAP during apoptosis.

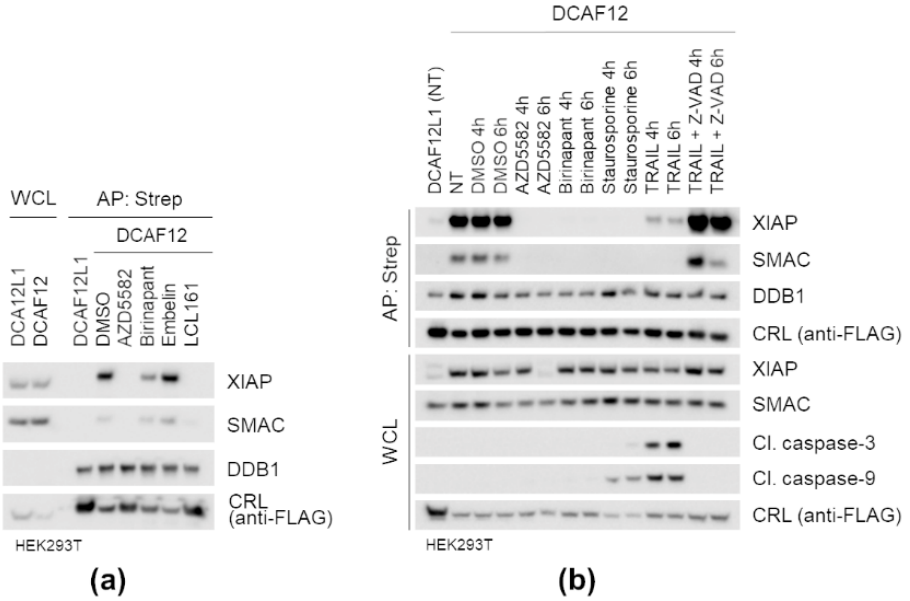

Figure 17. SMAC mimetics disrupt XIAP-SMAC interaction with DCAF12. (a) HEK293T cells were transfected with Twin-Strep-FLAG-tagged substrate receptor subunits of the cullin-RING ubiquitin ligase (CRL), DCAF12 or DCAF12L1, and treated with MLN4924 for 6 h before cell collection. Forty-eight hours after transfection, cells were collected and lysed. Whole-cell lysates (WCL) were subjected to affinity purification (AP) using Strep-TactinXT resin. Purified DCAF12 complexes were incubated for 20 min with indicated SMAC mimetics (100 µM each) and subsequently washed, eluted, and immunoblotted. (b) HEK293T cells were transfected with Twin-Strep-FLAG-tagged substrate receptor subunits of the CRL), DCAF12 or DCAF12L1, and treated as indicated (not-treated (NT), 1 µM AZD558, 10 µM birinapant, 1 µM staurosporine, 100 ng/ml TRAIL, 10 µM Z-VAD-FMK). Forty-eight hours after transfection, cells were collected and lysed. Whole-cell lysates (WCL) were subjected to affinity purification (AP) using Strep-TactinXT resin. Both WCL and eluates were immunoblotted.

4.2.5. Regulation of XIAP and SMAC by DCAF12 during apoptosis

DCAF12 recognises SMAC bound to the BIR2 and BIR3 domains of XIAP. In cells, this interaction typically occurs during apoptosis following the MOMP and the subsequent release of SMAC from mitochondria to cytosol, where SMAC binds XIAP. To investigate whether DCAF12 targets XIAP and SMAC for degradation during apoptosis, we established several experimental systems. We initially down-regulated DCAF12 in human cancer cell lines using RNAi and treated these cells with various apoptosis-inducing stimuli (Figure 18a). DCAF12 siRNA #2 was more toxic to cells than DCAF12 siRNA #1 and therefore could not have been used to draw valid conclusions. In cells treated with DCAF12 siRNA #1, XIAP was elevated during TRAIL-induced apoptosis, which correlated with decreased apoptosis as detected by several apoptotic markers, such as cleaved caspases and cleaved PARP.

We further mainly focused on TRAIL-induced apoptosis as a model system as TRAIL-induced apoptosis requires mitochondrial release of SMAC to antagonise the anti-apoptotic activity of XIAP, and TRAIL receptors are expressed in epithelial cancer cells [360,361]. To monitor more precisely the effect of DCAF12 on apoptosis and the protein level of XIAP and SMAC, we established several DCAF12-inducible or *DCAF12* KO cancer cell lines (Figure 18b,c). As SMAC binds to XIAP in the cytoplasm during apoptosis, we also evaluated the effect of DCAF12 localisation on apoptosis and the protein levels of XIAP and SMAC. As anticipated, the cytoplasmic DCAF12$^{\Delta 1-38}$ (and the nuclear DCAF12^{WT}) led to down-regulation of MOV10 but not of XIAP and SMAC. During apoptosis, degradation of XIAP ultimately occurred but was not enhanced by cytoplasmic DCAF12$^{\Delta 1-38}$. No degradation of SMAC was observed in our experimental systems. The sensitivity of different single-cell clones (*DCAF12* WT and KO) to apoptosis varied significantly, and these differences seemed to be independent of DCAF12. As these systems could not distinguish the effect of all DCAF12-mediated actions from those mediated specifically by the interaction between DCAF12 and the XIAP-SMAC complex, we reintroduced SMAC^{WT} and SMAC^{E238X} into the *SMAC* KO HCT116 cell lines (Figure 18d). Unexpectedly, the reintroduction of SMAC^{WT} increased the XAIP protein level. However, no significant TRAIL dose-dependent differences in XIAP and SMAC protein levels were observed between cells expressing SMAC^{WT} and SMAC^{E238X}. As the protein level and localisation of endogenous DCAF12 could not be determined, the exogenous expression of DCAF12 and its cytoplasmic mutant in these cells will be vital to evaluate the effect of the interaction between DCAF12 and XIAP-SMAC on apoptosis. Taken together, DCAF12 seemed to promote apoptosis. Still, we could not gather sufficient evidence to answer whether DCAF12 targets XIAP and SMAC for degradation during apoptosis using the cell lines mentioned above.

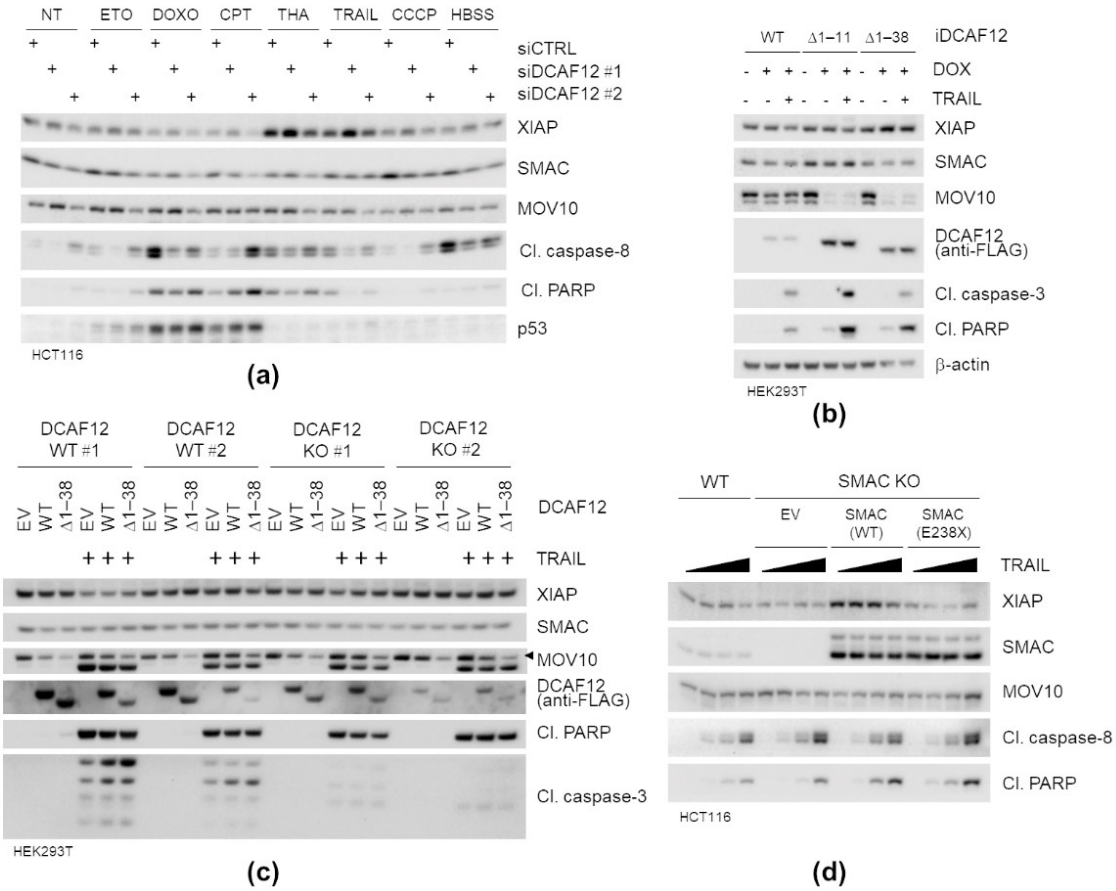

Figure 18. Regulation of XIAP and SMAC by DCAF12 during apoptosis. (a) HCT116 cells were transfected with control siRNA (siCTRL) or siRNAs targeting *DCAF12* (siDCAF12). After 48 hours, cells were starved by culturing in Hanks' Balanced Salt Solution (HBSS) or treated overnight as indicated: non-treated (NT), etoposide (ETO; 10 µM), doxorubicin (DOXO; 2 µM), camptothecin (CPT; 1 µM), thapsigargin (THA; 0.5 µM), TRAIL (10ng/ml), carbonyl cyanide 3-chlorophenylhydrazone (CCCP; 10 µM). Cells were collected, lysed, and whole-cell lysates (WCL) immunoblotted. (b) HEK293T stable cell lines expressing doxycycline (DOX)-inducible Twin-Strep-FLAG-tagged DCAF12 constructs (iDCAF12^{WT}, DCAF12$^{\Delta1–11}$, or DCAF12$^{\Delta1–38}$) were treated with DOX for 48 h and TRAIL (100 ng/ml) for 6 h where indicated. Cells were collected, lysed, and WCL were immunoblotted. (c) *DCAF12* wild type (WT) and knockout (KO) HEK293T single-cell clones were transfected with an empty vector (EV), Twin-Strep-FLAG-tagged DCAF12^{WT} or DCAF12$^{\Delta1–38}$. Forty-eight hours after transfection, cells were treated overnight with TRAIL (50 ng/ml), collected, lysed, and WCL were immunoblotted. (d) *SMAC* WT and *SMAC* KO HCT116 cells stably expressing SMAC^{WT} or SMAC^{E238X} were treated overnight with increasing concentrations of TRAIL (10, 25, 50 ng/ml), collected, lysed, and WCL were immunoblotted.

4.2.6. MOV10 C-terminal -EL motif is required for interaction with DCAF12

MOV10 poses the C-terminal -EL motif. This motif, especially the glutamic acid residue at the penultimate position (-2), is evolutionary conserved and can be found in animals as divergent as oysters, termites, and lampreys (Figure 19a). To examine whether this motif is necessary for the interaction of MOV10 with DCAF12, we prepared a mutant form of MOV10 (E1002X) lacking the C-terminal -EL amino acid residues (Figure 19b) and tested its ability to interact with DCAF12. Firstly, we co-

expressed HA-tagged MOV10^{WT} or MOV10^{E1002X} with SF-DCAF12 in HEK293T cells and found that HA-MOV10^{WT} but not the MOV10^{E1002X} mutant co-immunoprecipitated SF-DCAF12, endogenous CUL4A and DDB1. Moreover, none of the four additional WD-repeat domain proteins tested co-immunoprecipitated with HA-MOV10 (Figure 19c). Then, we prepared HEK293T and HCT116 cell lines expressing HA-MOV10 or its E1002X mutant under the control of the DOX-inducible promoter. DOX-inducible HA-MOV10^{WT} and HA-MOV10^{E1002X} localised to the cytoplasm in human cancer cell lines (Figure 19d). SF-DCAF12^{WT} and SF-DCAF12$^{\Delta 1-38}$ interacted only with inducible HA-MOV10^{WT} but not with HA-MOV10^{E1002X} (Figure 19e). Finally, we tested whether the C-terminal -EE motif of GART is required for its interaction with DCAF12. Deleting the last two amino acid residues of GART prevented its interaction with SF-DCAF12, endogenous CUL4A and DDB1 (Figure 19f). Our findings thus provided substantial evidence that DCAF12 directly recognises various C-terminal acidic motives with glutamic acid residue at the penultimate position. For example, the C-terminal -EE motif (e.g., in GART), the C-terminal -ED motif (e.g., in SMAC), or C-terminal -EL motif (e.g., in MOV10).

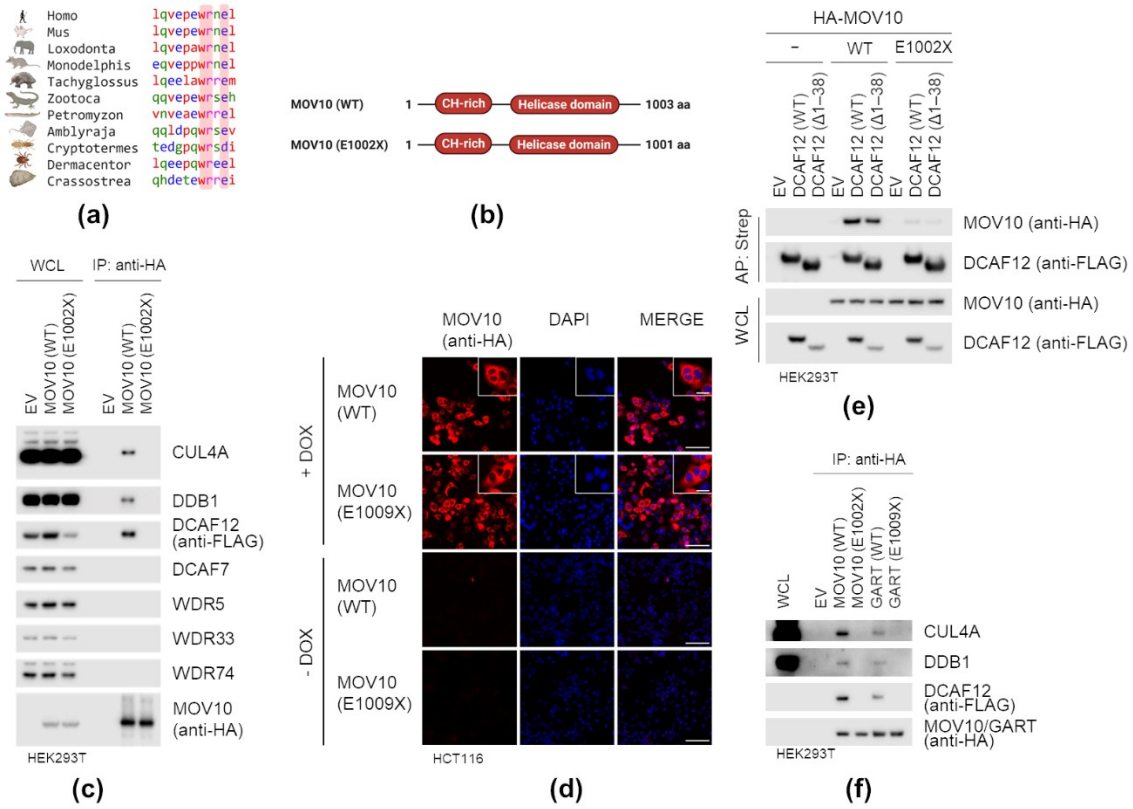

Figure 19. MOV10 C-terminal -EL motif is necessary for interaction with DCAF12. (a) Multiple sequence alignment of the C-termini of MOV10 from indicated species genera. Sequences were aligned using Kalign [66]. (b) Schematic representation of MOV10 and its E1002X mutant lacking the C-terminal -EL motif. (c) HEK293T cells were co-transfected with Twin-Strep-FLAG-tagged DCAF12 and either an empty vector (EV), HA-tagged MOV10^{WT}, or HA-tagged MOV10^{E1002X}. MLN4924 was added for the last 6 h before harvesting. After lysis, whole-cell lysates (WCL) were subjected to anti-HA Immunoprecipi-

tation (IP) and immunoblotted as indicated. (d) HCT116 stable cell lines expressing HA-tagged MOV10^{WT} and MOV10^{E1002X} under the control of doxycycline (DOX)-inducible promoter were treated with DOX for 24 h, fixed, and stained with anti-HA antibody to detect MOV10. To counterstain nuclei, 4',6-diamidino-2-phenylindole (DAPI) was used. Scale bar, 100 µm. (e) Parental and stably transduced HEK293T cells with DOX-inducible HA-tagged MOV10^{WT} and MOV10^{E1002X} constructs were transfected with an EV, Twin-Strep-FLAG-tagged DCAF12^{WT} or DCAF12$^{\Delta1–38}$. Twenty-four hours after transfection, cells were treated with DOX (100 ng/ml) for another 24 h. MLN4924 was added for the last 6 h before harvesting. After cell lysis, WCL were subjected to affinity purification (AP) and immunoblotted as indicated. (f) HEK293T cells were co-transfected with Twin-Strep-FLAG-tagged DCAF12 and either an EV or HA-tagged MOV10^{W}, MOV10^{E1002X}, GART^{WT}, and GART^{E1009X}. MLN4924 was added for the last 6 h before harvesting. After lysis, WCL were subjected to anti-HA IP and immunoblotted as indicated.

4.2.7. DCAF12 controls MOV10 protein level via its C-terminal degron

We established that DCAF12 recognises the C-terminal -EL motif of MOV10 (chapter 4.2.6.). To answer whether this motif represents a DCAF12 degron, we next investigated whether it is necessary for the MOV10 degradation. In cancer cells harbouring DOX-inducible DCAF12 expression constructs, induction of DCAF12^{WT} and especially its cytoplasmic mutants down-regulated MOV10 under the steady-state condition (chapter 4.2.3.). Firstly, we confirmed that no changes in the *MOV10* mRNA level occurred in these cells upon induction of DCAF12 (Figure 20a). Next, we tested whether the decrease in MOV10 protein level is CRL-dependent by treating cells with neddylation inhibitor MLN4924 (Figure 20b,c). This treatment rescued the reduction in MOV10 protein level upon induction of SF-DCAF12$^{\Delta1–38}$ (and SF-DCAF12^{WT} in HEK293T cells). GART responded similarly to the induction of DCAF12 and MLN4924 treatment, suggesting that both proteins are targeted by cytoplasmic DCAF12 for degradation in cancer cells. As controls for MLN4924 treatment, cullin-dependent substrates FBXO28, p27, p21 were stained. Interestingly, DCAF12 was also stabilised by MLN4924 treatment, indicating that it also underwent CRL-dependent degradation. Finally, we expressed HA-MOV10^{WT} and HA-MOV10^{E1002X} in *DCAF12* KO HCT116 cell lines with inducible expression of SF-DCAF12 to test whether the deletion of C-terminal-EL amino acid residues was sufficient to prevent MOV10 degradation (Figure 20d). The induction of SF-DCAF12$^{\Delta1–38}$ eliminated endogenous GART and HA-MOV10^{WT}, but not HA-MOV10^{E1002X}. This elimination of HA-MOV10^{WT} was abolished by MLN4924 (CRL inhibitor), MG132 (proteasome inhibitor), and co-expression of a dominant-negative form (amino acids 1–337) of CUL4, providing further evidence that the CRL4-dependent pathway mediated HA-MOV10 degradation (Figure 20e). Altogether, our biochemical studies demonstrated that DCAF12 mediates the CRL- and proteasome-dependent degradation of MOV10 and that this degradation depends on the C-terminal residues of MOV10, which thus represent the DCAF12 degron.

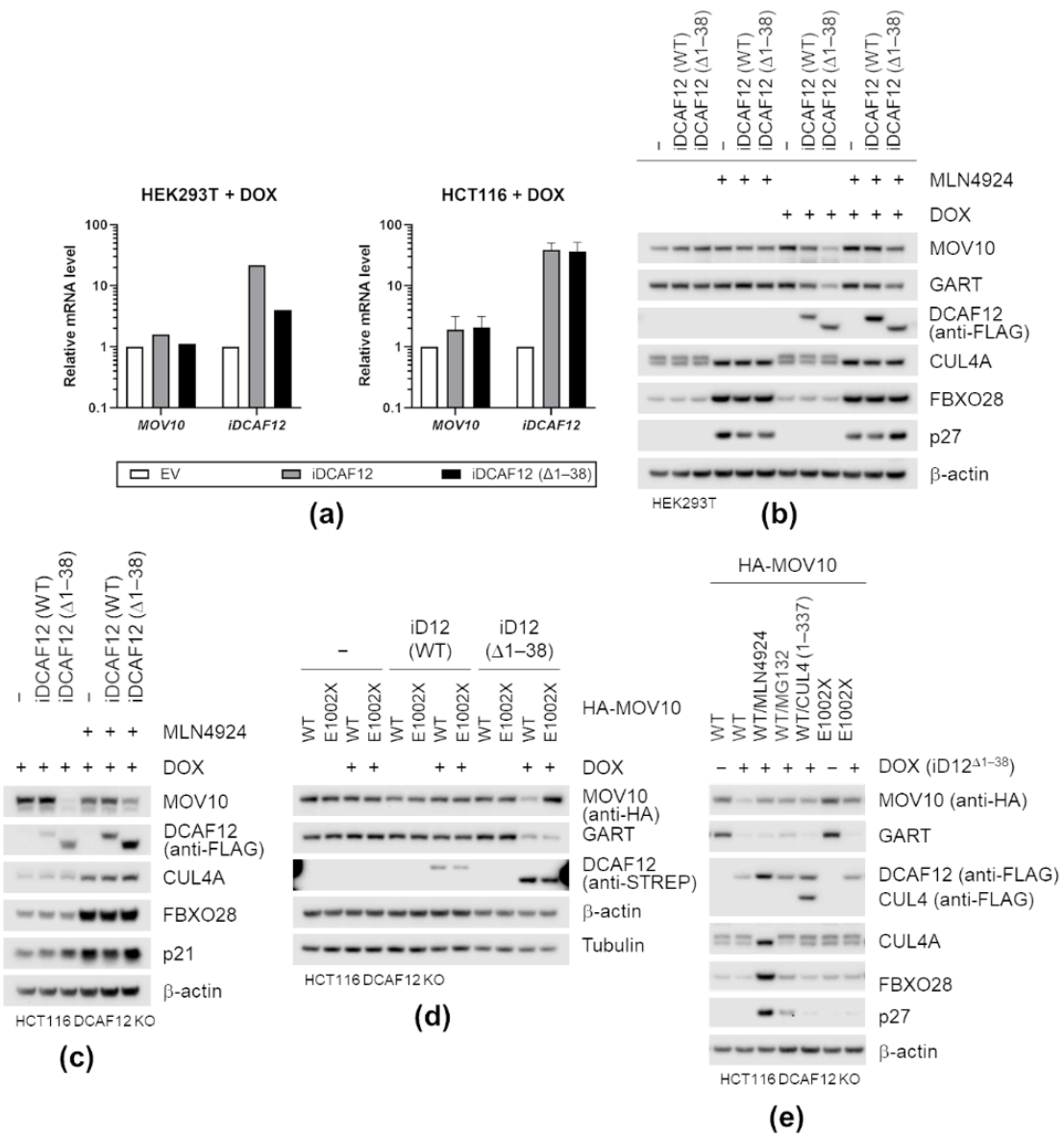

Figure 20. DCAF12 controls MOV10 protein level via its C-terminal degron. (a) Relative expression levels of *MOV10* mRNA in HEK293T and HCT116 DCAF12 knockout (KO) stable cell lines expressing Twin-Strep-FLAG-tagged DCAF12 constructs under the control of doxycycline (DOX)-inducible promoter (iDCAF12^{WT} and DCAF12$^{\Delta1–38}$). Cells were treated with DOX for 48 h, and relative mRNA levels of *MOV10* and *iDCAF12* were determined by qPCR. Values are presented as means ± standard deviations. (b,c) HEK293T (b) and HCT116 *DCAF12* knockout (KO) (c) stable cell lines expressing Twin-Strep-FLAG-tagged DCAF12 constructs under the control of DOX-inducible promoter (iDCAF12^{WT} and DCAF12$^{\Delta1–38}$) were treated with DOX for 48 h and MLN4924 overnight, as indicated. Whole-cell lysates (WCL) were subjected to immunoblotting with indicated antibodies. (d,e) HCT116 *DCAF12* KO stable cell lines expressing Twin-Strep-FLAG-tagged DCAF12 constructs controlled by DOX-inducible promoter (iD12^{WT} and iD12$^{\Delta1–38}$) were treated with DOX for 48 h and transiently transfected with either HA-tagged MOV10^{WT} or MOV10^{E1002X} 16 h before harvesting. Where indicated (e), cells were incubated with MLN4924 (overnight), MG132 (8 h), or co-transfected with a dominant-negative FLAG-tagged CUL4A construct. WCL were subjected to immunoblotting with indicated antibodies.

4.2.8. DCAF12 controls MOV10 protein level in mice

To investigate the function of DCAF12 under physiological conditions, we generated mice with deletion of the *Dcaf12* exon 4 (Figure 21a) and asked whether DCAF12 controls the protein level of MOV10 and other potential substrates *in vivo*. Available expression data indicated that the *Dcaf12* exon 4 is constitutively used, and its deletion inactivates *Dcaf12* by creating a frameshift. Moreover, we observed a significant decrease in the *Dcaf12* transcript abundance in *Dcaf12* KO mice, presumably due to the nonsense-mediated decay pathway. *Dcaf12* KO mice were born at expected Mendelian ratios and manifested no apparent physical abnormalities (Figure 21b,c). Next, we isolated *Dcaf12* WT and KO MEFs and tested whether the potential substrates of DCAF12 accumulate in these mouse cells. MOV10 was elevated in *Dcaf12* KO MEFs, and its physiological amount was restored upon reintroducing SF-DCAF12 (Figures 21d). DCAF12-dependent changes in the protein levels of XIAP and SMAC were observed neither under steady-state conditions nor during apoptosis (Figures 21e). We concluded that DCAF12 controlled the protein level of MOV10 in mouse cells and embarked on a search of specific physiological processes in which this regulation of MOV10 occurs *in vivo*.

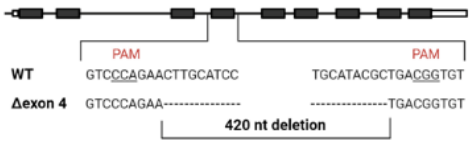

(a)

	Males		Females	
	Observed	Expected	Observed	Expected
Dcaf12$^{+/+}$	22	27	22	27.5
Dcaf12$^{+/-}$	59	54	62	55
Dcaf12$^{-/-}$	27	27	26	27.5
Chi-square		1.389		2.073
P-value		0.499		0.355

(b)

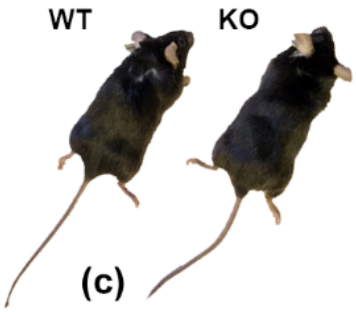

(c)

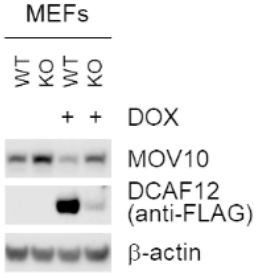

(d)

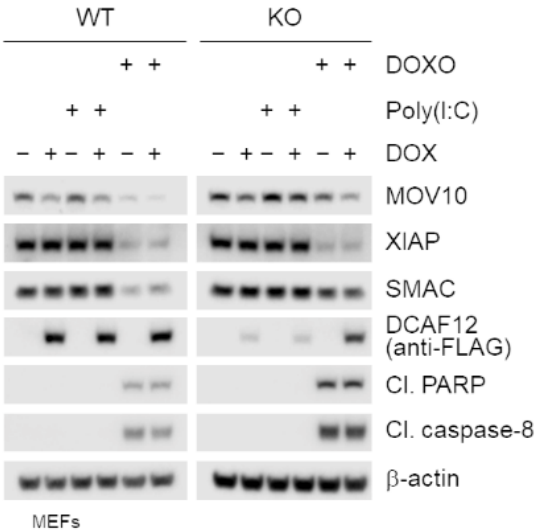

(e)

Figure 21. DCAF12 controls MOV10 protein level in mice. (a) Schematic diagram of targeted disruption of the *Dcaf12* gene using the CRISPR/Cas9 genome-editing system in mice. Two single guide RNAs were

designed to target introns flanking the exon 4 of the *Dcaf12* gene. The resulting deletion of the exon 4 was 420-nucleotide (nt) long. Protospacer adjacent motif (PAM) motives are underlined; dashes indicate deleted nucleotides. (b) Mice of all genotypes were born at expected Mendelian and gender ratios. The ratios were analysed by chi-square test, p-value > 0.05. (c) Representative images of male mice of the indicated genotype. Mice did not display any apparent physical abnormalities. (d,e) *Dcaf12* wild type (WT) and *Dcaf12* knockout (KO) mouse embryonic fibroblasts (MEFs) were immortalized either by the CRISPR/Cas9-mediated inactivation of p19ARF (d) or by SV40 large T antigen (e). Subsequently, stable cell lines expressing Twin-Strep-FLAG-tagged DCAF12 under the doxycycline (DOX)-inducible promoter were established. Where indicated, cells were treated with DOX for 48 h, poly(I:C) for 24 h, and doxorubicin (DOXO) for 24 h. Whole-cell lysates were immunoblotted.

Dcaf12 is a ubiquitously expressed gene, the expression of which is not limited to any tissue or biological process. However, publicly available data and our measurements indicated especially strong expression in the male reproductive system and haematopoietic system. We noticed no significant changes in the fetal liver and postnatal bone marrow erythropoiesis (not shown) and therefore further directed our attention to spermatogenesis and immune cells.

4.2.9. DCAF12 controls MOV10 protein level during spermatogenesis

Analysis of publicly available data indicated that *Dcaf12* is strongly expressed in the male reproductive system (Figure 22a). In testes, *Dcaf12* is highly expressed during late spermatogenesis from pachytene spermatocytes (Figure 22b). Contrary, *Mov10* was mainly expressed in spermatogonia and certain subpopulations of pachytene spermatocytes. Consistently with the expression data, MOV10 was previously shown to be abundant in spermatogonia but nearly absent in spermatocytes [338]. To determine whether DCAF12 targets MOV10 for degradation during spermatogenesis, we initially analysed the lysates from *Dcaf12* WT and KO testes. We found that MOV10 was reproducibly increased in the testes of *Dcaf12* KO animals (Figure 22c,d). Additionally, meiotic marker SCP3 (synaptonemal complex protein 3) was slightly decreased while γH2AX (histone H2AX phosphorylated on serine 139) increased, suggesting a slight defect during meiosis. At the same time, we detected no changes in spermatogonial marker PLZF (promyelocytic leukemia zinc finger) and spermatocyte marker PITX2 (pituitary homeobox 2). Next, we asked whether loss of *Dcaf12* affects sperm production or fertility. No differences in the testes weight were found, yet a moderate decline in sperm count was observed (Figure 22e,f). Still, *Dcaf12* KO animals were fertile. To address at which stage of spermatogenesis the defect occurred, we examined the histological sections of *Dcaf12* WT and KO testes (Figure 23a,b,c). Neither morphological abnormalities nor arrest of spermatogenesis was detected. We thus concluded that *Dcaf12* deficiency causes only a subtle disruption of spermatogenesis. Altogether, DCAF12 controls MOV10 protein level during spermatogenesis, which is slightly impaired by the loss of *Dcaf12*.

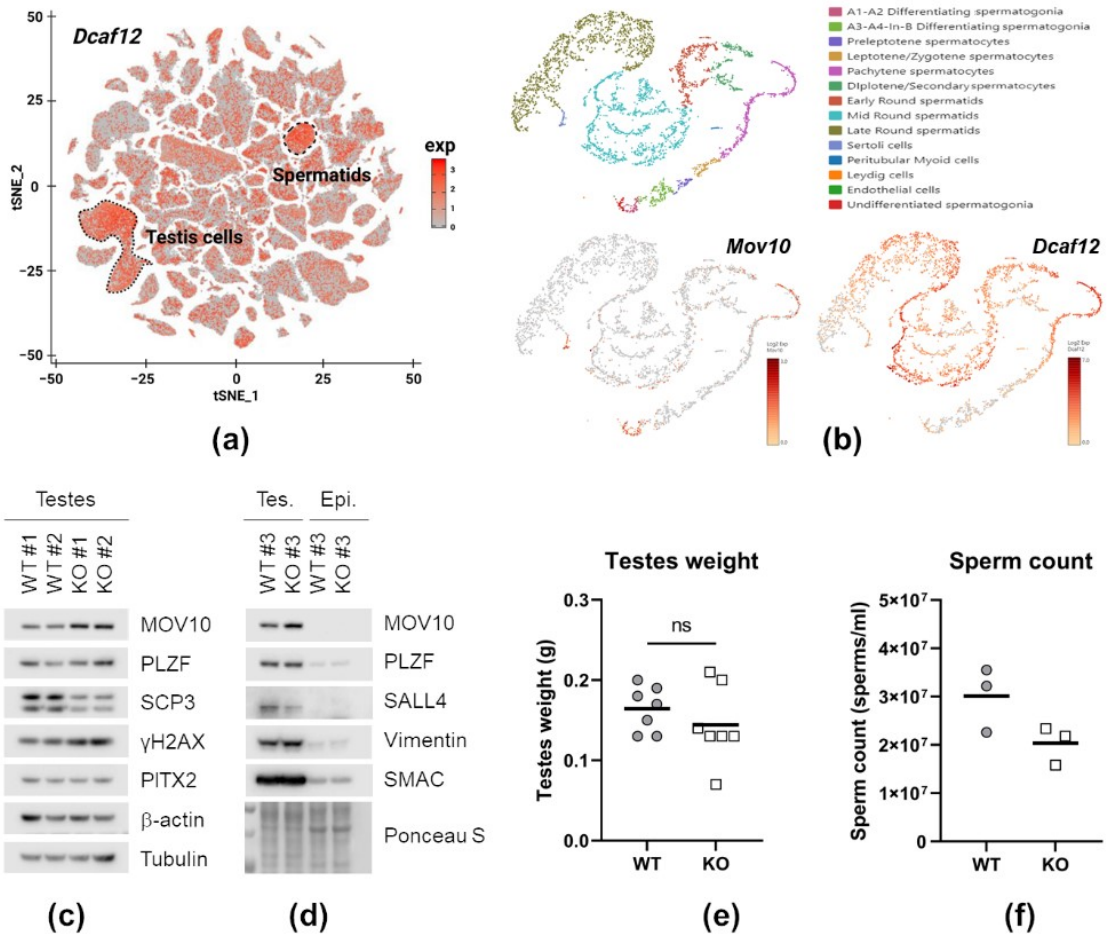

Figure 22. DCAF12 controls MOV10 protein level during spermatogenesis. (a) *Dcaf12* expression projected on the t-distributed stochastic neighbour embedding (t-SNE) plot of single cells from publicly available mouse cell atlas (available at bis.zju.edu.cn/MCA; GEO accession number GSE108097) [362]. Testis cell and spermatid clusters are encircled. (b) Expression of *Dcaf12* and *Mov10* projected on t-SNE plots of spermatogenic cells from publicly available spermatogenesis single-cell transcriptome datasets [363]. Colours distinguish unbiased cell clusters according to the key. (c) Testis whole tissue lysates from 16-week-old *Dcaf12* WT and KO mice (littermates, four animals). Testes without the tunica albuginea were lysed and subjected to immunoblotting with indicated antibodies. (d) Testis (Tes.) and epididymis (Epi.) whole tissue lysates from 16-week-old *Dcaf12* WT and KO mice. Testes without the tunica albuginea or epididymis were lysed and subjected to immunoblotting with indicated antibodies. (e) Testes weight of 16-week-old *Dcaf12* WT and KO animals. Individual data points and means are shown (n = 7 per group). Statistical significance was assessed by an unpaired two-tailed t-test. p-value < 0.05 was considered significant; ns = not significant. (f) Sperm count of 16-week-old *Dcaf12* WT and KO animals. Individual data points and means are shown (n = 3 per group).

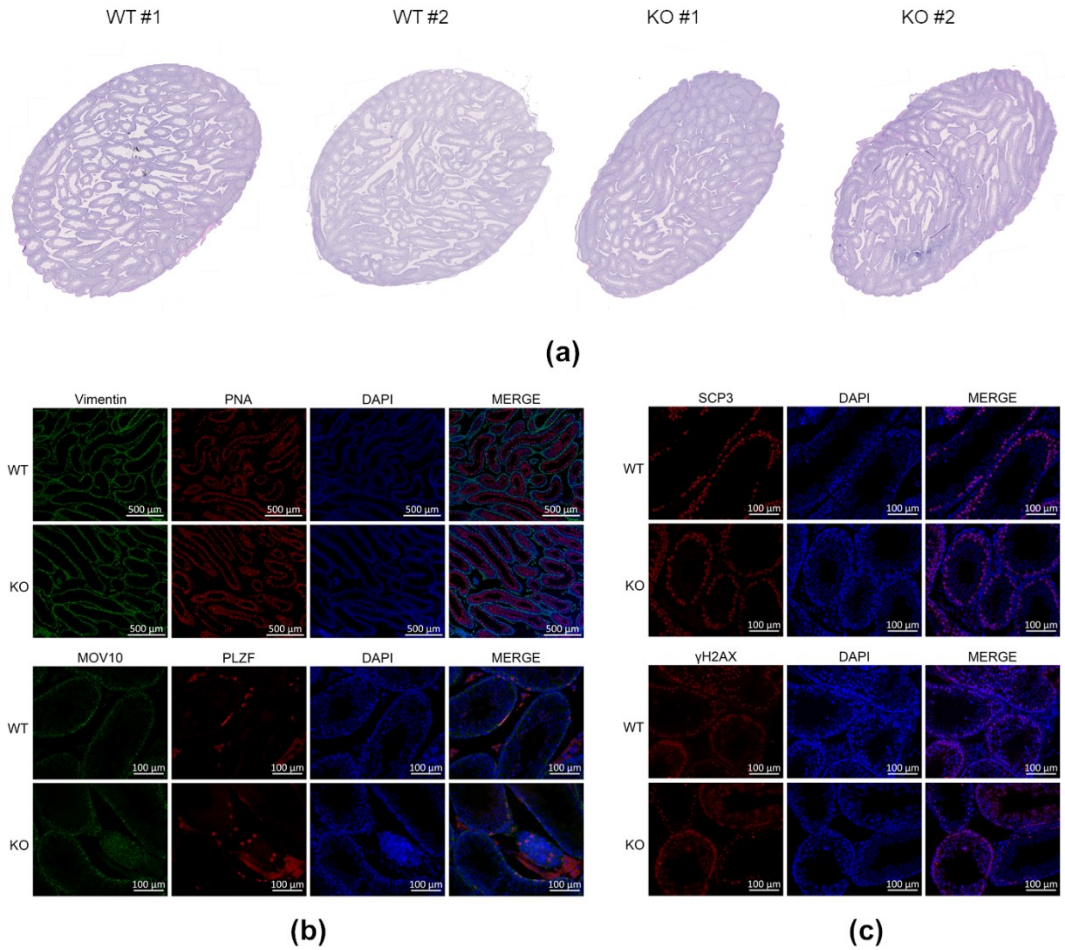

Figure 23. No apparent morphological abnormalities in *Dcaf12* KO testes. (a) A preview of high-resolution cross-sections of *Dcaf12* WT and KO testes. Testes from 5- to 7-week-old mice were sectioned and stained with haematoxylin and eosin. Raw data are available at the Mendeley data repository (http://dx.doi.org/10.17632/h4g7ctf2wc.1). (b) Immunohistological analysis of *Dcaf12* WT and KO testes. Testes from 5- to 7-week-old animals were sectioned and stained with indicated antibodies or Alexa Fluor 594-conjugated peanut agglutinin (PNA). To counterstain nuclei, 4',6-diamidino-2-phenylindole (DAPI) was used. Scale bars are as indicated.

4.2.10. Uncovering roles of DCAF12 in the immune system

DCAF12 interacts with many proteins, which have well-established roles in the immune system. Specifically, XIAP promotes NOD2 signalling [271–275] and restricts inflammation [276–279], while MOV10 manifest broad antiviral and retrotransposon restriction activities [307–327]. Moreover, Drosophila DCAF12 was implicated in the innate immune response to bacteria [180]. We thus hypothesised that DCAF12 could target the XIAP-SMAC complex or MOV10 during innate immune responses and thus regulate their outcome. To test whether *Dcaf12* deficiency causes a defect in the immune system, we employed several approaches.

Initially, we focused on the responses to bacteria-derived PAMPs such as MDP and LPS. To reveal whether DCAF12 targets XIAP for degradation during the response to MDP, we treated murine

macrophage-like RAW 264.7 cells with MDP and examined the protein levels of XIAP, SMAC and MOV10. MDP treatment effectively activated the NF-κB pathway (Figure 24a) as determined by phosphorylation and degradation of NF-kappa-B inhibitor alpha (frequently referred to as I-kappa-B-alpha; IκBα). In addition, RIPK2, a component of the NOD2 signalling complex, was degraded, suggesting that at least some elements of the NOD2 signalling complex undergo degradation after stimulation with MDP, probably to attenuate the signalling. However, only limited degradation of XIAP was observed, and it seemed to be DCAF12-independent as it also occurred in cells in which DCAF12 was depleted by siRNA (Figure 24b). Up-regulation of MOV10 upon DCAF12 depletion suggested that the siRNA was effective and showed that DCAF12 controls the protein level of MOV10 in RAW 264.7 cells.

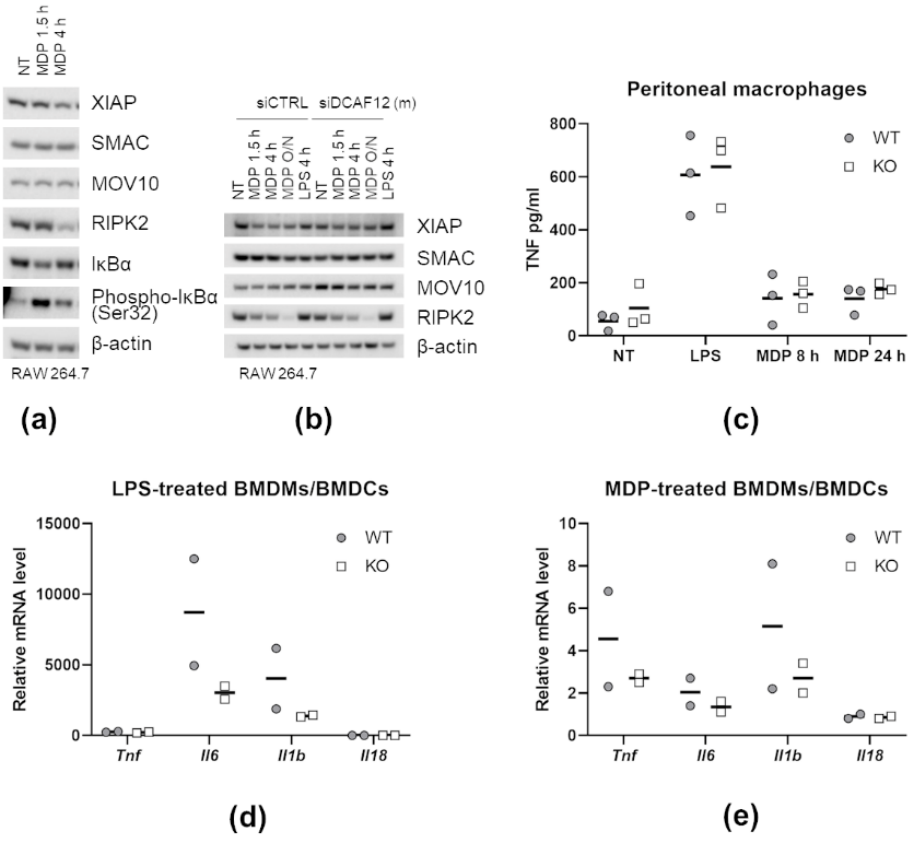

Figure 24. Response of *Dcaf12*-deficient cells to MDP and LPS. (a, b) RAW 264.7 cells were transfected with control siRNA (siCTRL) or *Dcaf12*-targeting siRNA (siDCAF12 (m)), grown for 48 h, and treated with MDP (10 µg/ml) or LPS (5 µg/ml) for indicated times. Whole-cell lysates (WCL) were immunoblotted. (c) Peritoneal macrophages isolated from *Dcaf12* wild type (WT) or *Dcaf12* knockout (KO) mice were treated with LPS (50 ng/ml) or MDP (10 µg/ml) for indicated times. The concentration of released TNF in collected supernatants was analysed by ELISA. (d,e) Bone-marrow-derived macrophages (BMDMs)/Bone marrow-derived dendritic cells (BMDCs) were treated with LPS (50 ng/ml) or MDP (10 µg/mL) for 4 h. Relative mRNA levels of indicated RNAs were determined by qPCR.

Next, we isolated murine peritoneal macrophages from *Dcaf12* WT and KO mice and treated them *ex vivo* with MDP and LPS. We observed neither defect in the induction of the pro-inflammatory

cytokine in response to stimulation as determined by qPCR or ELISA (Figure 24c) nor the spontaneous release of IL-1β following the LPS-treatment (not shown). As a limited number of peritoneal macrophages made this experimental system unsuitable for precise western blot analysis of changes in the protein abundance, we prepared *Dcaf12*-deficient BMDMs/BMDCs to obtain more cells. Afterwards, we treated them with different stimuli (such as LPS, MDP, poly(I:C), TNF) and measured inflammatory response by qPCR (Figure 24d,e) and ELISA. Nevertheless, this initial screening did not reveal any remarkable differences between cells derived from *Dcaf12* WT and KO mice.

As an alternative approach to disclose a potential defect in the immune system, we performed immunophenotyping of immune cell populations in the spleen of *Dcaf12* KO animals. This analysis revealed alternations in the T cell populations (Figure 25). The percentage of $CD4^+$ T cells was slightly but significantly reduced, and the proportion of Tregs was elevated within the $CD4^+$ T cell population. Additionally, *Dcaf12* KO mice displayed a higher percentage of splenic natural killer T (NKT) cells. No significant changes were observed in the percentages of B cells or cells of the myeloid lineage. These alternations in splenic immune cell populations collectively indicated that DCAF12 is required for the development or homeostasis of T cells.

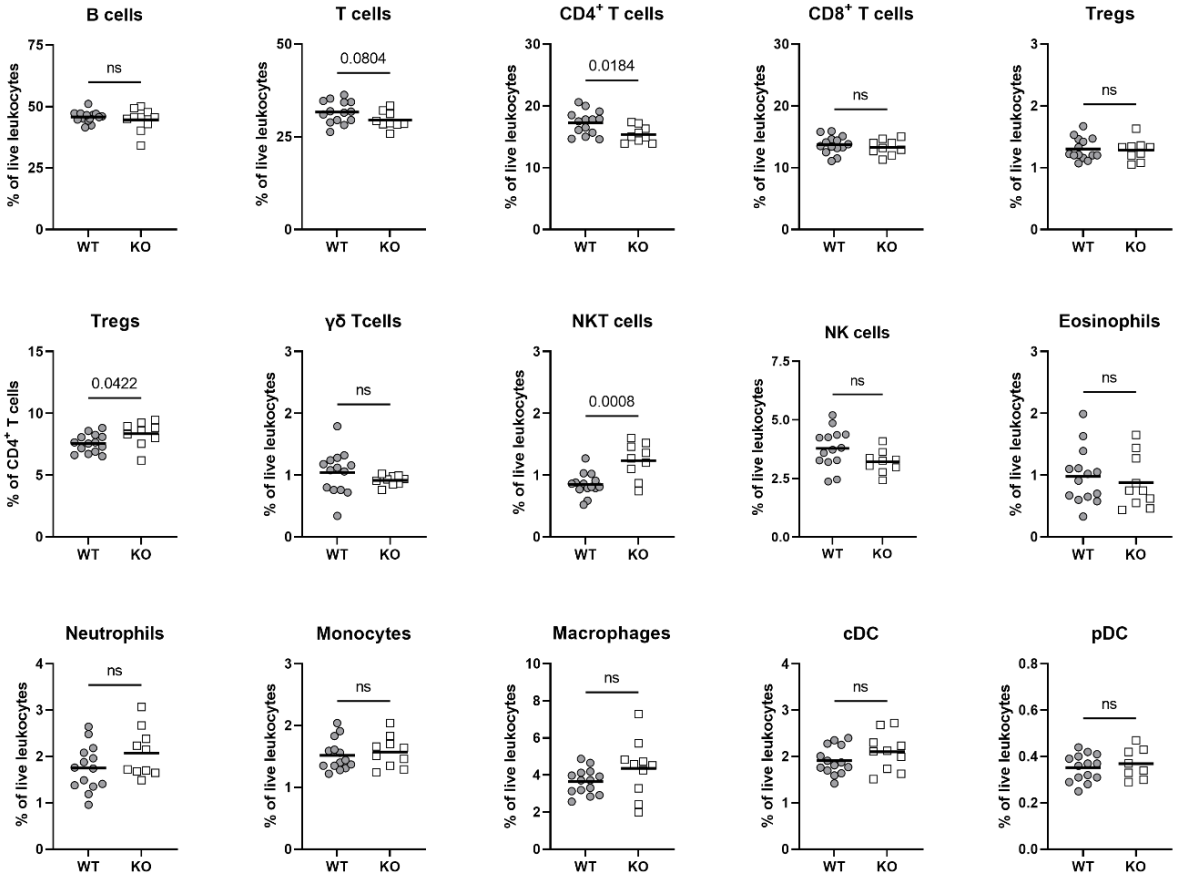

Figure 25. *Dcaf12* deficiency leads to dysregulation of splenic immune cell populations. Quantification of immune cell populations in the spleen of 16–20-week-old *Dcaf12* wild type (WT) or knockout

(KO) female mice. The populations were analysed by flow cytometry, individual data points and group means are shown (n = 10–14 per group). Statistical significance was assessed by an unpaired two-tailed t-test. p-value < 0.05 was considered significant; ns = not significant. NK, natural killer; NKT, natural killer T; cDC, conventional dendritic cells; pDC, plasmacytoid dendritic cells.

4.2.11. DCAF12 controls MOV10 protein level during T cell activation

Dysregulation of T cell populations in *Dcaf12*-deficient mice prompted us to explore the role of DCAF12 in T cells. A thorough analysis of publicly available RNA-seq data showed that the expression of *DCAF12/Dcaf12* is up-regulated during T cell activation in both human and mouse T cells (Figure 26a). Specifically, this up-regulation was observed in T cells activated by either CD3/CD28 receptor crosslinking or T cell receptor (TCR)-specific peptide. In contrast, the expression of *MOV10/Mov10* was either not changed or down-regulated.

To examine whether DCAF12 targets MOV10 for degradation during T cell activation, we stimulated mouse splenocytes with anti-CD3 and anti-CD28 (anti-CD3/CD28) antibody-coupled beads (Figure 26b). The protein level of MOV10 was slightly but reproducibly increased in *Dcaf12* KO splenocytes even without stimulation. However, the accumulation of MOV10 in *Dcaf12* KO splenocytes became especially pronounced after stimulation with anti-CD3/CD28 beads. Concurrently, the stimulated *Dcaf12* KO splenocytes displayed increased apoptosis as determined by cleaved poly(ADP-ribose) polymerase (PARP) and cleaved caspase-3. No increase in the protein level of SMAC or XIAP was observed. On the contrary, XIAP was strongly down-regulated in both *Dcaf12* WT and KO splenocytes during their activation, which appeared to be independent of DCAF12. In our experimental setting, the *Mov10* mRNA levels were up-regulated (Figure 26c), which presumably reflected the transcriptional activation of other than T cell populations. Notably, the *Mov10* mRNA up-regulation occurred similarly in both *Dcaf12* KO and WT splenocytes. The differences in the protein level of MOV10 thus could be wholly attributed to post-transcriptional regulation.

Next, we examined the MOV10 protein level in splenocytes treated with different stimuli. We observed a comparable up-regulation of MOV10 in both *Dcaf12* KO and WT splenocytes stimulated with poly(I:C) or LPS (Figure 26d). Therefore, T cell activation with anti-CD3/CD28 beads might represent a specific condition in splenocytes under which DCAF12 targets MOV10 for degradation. Finally, we asked in which splenic cell populations was MOV10 up-regulated. We found a pronounced increase of MOV10 in lysates enriched in T cells but not B cells (Figure 26e). Taken together, DCAF12 controls the MOV10 protein level and prevents apoptosis during T cell activation.

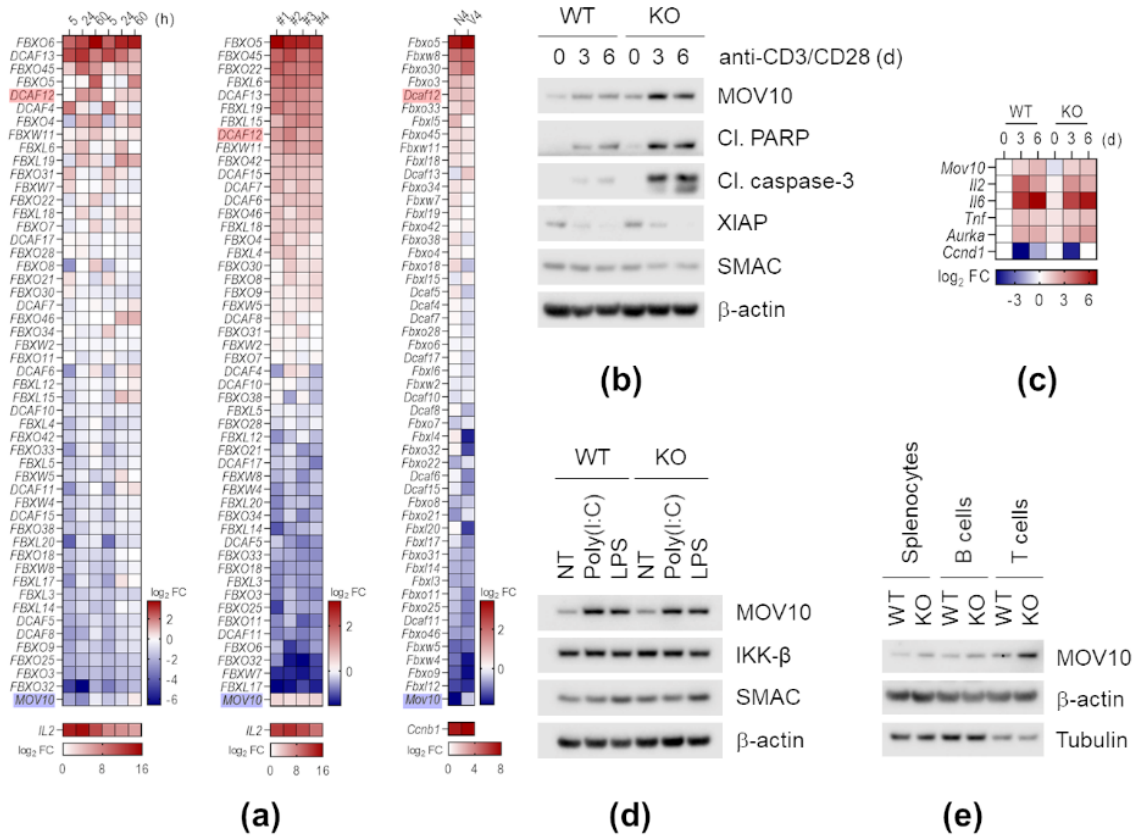

Figure 26. DCAF12 controls MOV10 protein level during T cell activation. (a) Expression of substrate receptors of the cullin-RING ubiquitin ligase 1 and 4 after T cell activation. Data from publicly available RNA sequencing datasets were analysed and visualized as a heat map showing mean log_2 fold change (FC) of gene expression relative to the non-activated state. Left panel: Human naïve $CD4^+$ T cells were activated with anti-CD3 and anti-CD28 (anti-CD3/CD28; the first three columns) or only anti-CD3 beads (the last three columns) for the indicated time (GEO accession number GSE116697) [364]. Middle panel: Human naïve $CD4^+$ T cells obtained from four donors were activated with anti-CD3/CD28 beads for two days (GEO accession number GSE81810) [365]. Right panel: Mouse antigen-specific $CD8^+$ T cells were activated for 48 h in the presence of high-affinity peptide N4 or low-affinity peptide V4 (right panel; GEO accession number GSE49929) [366]. Only substrate receptors appearing in all datasets are presented. Additionally, *MOV10/Mov10*, *IL2*, and *Ccnb1* as controls are shown. *DCAF12/Dcaf12* is highlighted in red, *MOV10/Mov10* in blue. (b) Soluble fractions of lysates obtained from CD3/CD28-activated splenocytes. *Dcaf12* WT and KO splenocytes were stimulated with anti-CD3/CD28 Dynabeads for indicated times, lysed, and the soluble fractions were immunoblotted with indicated antibodies. (c) Relative mRNA expression levels of indicated genes in CD3/CD28-activated splenocytes from (b) as determined by qPCR. The heat map shows log_2 fold change (FC) of gene expression relative to the non-activated state of *Dcaf12* WT splenocytes. (d) Splenocyte whole-cell lysates obtained from poly(I:C)- and LPS-stimulated splenocytes. Freshly isolated splenocytes from *Dcaf12* WT and KO mice were stimulated with poly(I:C) and LPS (5µg/ml) for 24 h, lysed and immunoblotted with indicated antibodies. (e) Soluble fractions of *Dcaf12* WT and KO splenocyte lysates. B and T cell-enriched populations were separated from freshly isolated splenocytes by negative selection using anti-CD45R (B220) antibody, lysed, and the soluble fractions were immunoblotted with indicated antibodies; Cl. PARP, cleaved form of poly (ADP-ribose) polymerase (PARP); Cl. Caspase-3, cleaved form of caspase-3.

5. Discussion

5.1. $CRL4^{DCAF4}$

$CRL4^{DCAF4}$ is a ubiquitin ligase with elusive substrates and functions. We demonstrated that DCAF4 directly recognises and regulates the abundance of box H/ACA RNPs, ribonucleoprotein particles consisting of box H/ACA RNAs and four core proteins. As all core box H/ACA proteins but not the box H/ACA RNP-specific assembly factors co-purified with DCAF4, we assume that DCAF4 recognises fully assembled mature particles containing internal box H/ACA RNA. Alternatively, DCAF4 could recognise core box H/ACA proteins-only complexes. However, the existence of such complexes in cells is questionable given that DKC1 interacts with a high affinity and in a mutually exclusive manner with RNA and RNA mimicking assembly factor SHQ1 [131,144,145,367]. Moreover, biogenesis of mature box H/ACA RNPs is a highly organised and stepwise process during which the presence of GAR1 is believed to signify that box H/ACA RNA had been loaded into the particle [150]. Once assembled, box H/ACA proteins bind box H/ACA RNA with extremely high affinity and no exchanges of RNA components among the box H/ACA RNP particles were detected, suggesting that the formation of new particles requires *de novo* synthesis [131,354]. Therefore, based on the literature and our experimental findings, we propose that DCAF4 recognises mature box H/ACA RNP particles containing internal box H/ACA RNAs, a hypothesis that needs to be further experimentally validated.

DCAF4 interacts with all four core box H/ACA proteins, and the interaction depends on protein subunits DKC1 and GAR1 but not on RNA. Crystal and cryo-EM structures of the box H/ACA RNPs show that GAR1 associates with the catalytic domain of DKC1 and seems to enable the loading and release of substrate RNA by stabilising the open state of the DKC1 thumb loop [130,137–139]. Our mutational analysis of the DKC1 thumb loop and the nearby region revealed that Thr224 is selectively required for the interaction of DKC1 with DCAF4 but not for the association of DKC1 with other core box H/ACA proteins. This result strongly suggests that DCAF4 interacts directly with DKC1. As DCAF4-DKC1 interaction also depended on GAR1, we speculate that DCAF4 might recognise either the structural degron composed of both DKC1 and GAR1 or the conformational state of DKC1 induced by GAR1. In the first case, DCAF4 could associate with box H/ACA RNPs in a similar way as another WD40 repeat protein—TCAB1, which makes direct contact with both DKC1 and GAR1 [138]. This model predicts competition between TCAB1 and DCAF4 for binding to box H/ACA RNP. Alternatively, DCAF4 could directly recognise only DKC1 in the open conformation of its thumb loop induced by GAR1. Because this is the conformation of substrate RNA-free box H/ACA RNPs, this model predicts the competition between substrate RNA and DCAF4. In support of the latter model, RNA has an inhibitory effect on the interaction and Thr224 in DKC1 seems to be particularly accessible in an RNA-free conformational state. In our experiments, the inhibitory effect of RNA seemed to be dual. Firstly, the treatment with RNase A is

known to help solubilise certain insoluble nucleolar components [368]. Indeed, the addition of RNase A to the cell lysis buffer improved the solubility of the box H/ACA proteins, which led to a marked increase in their co-purification with DCAF4. Secondly, the amount of box H/ACA proteins co-purified with DCAF4 was also increased when digestion of RNA was carried out during AP (after removing the insoluble pellet). The latter suggested that the inhibitory effect of RNA might also result from steric clashes of substrate RNA with DCAF4 or from the substrate RNA-induced closed conformation of the DKC1 thumb loop [130,137], which might be incompatible with the interaction with DCAF4. Based on these findings, we propose that DCAF4 recognises mature box H/ACA RNPs in the absence of substrate RNA, presumably in the open conformation of the DKC1 thumb loop.

Our biochemical and microscopy experiments provided an important insight into the regulation of box H/ACA RNPs recognition by DCAF4 and their subsequent degradation. We observed markedly increased co-purification of box H/ACA RNPs with DCAF4 after the RNase A treatment, indicating a ready-to-be-recognised cellular pool of box H/ACA RNPs secluded from DCAF4 by RNA, presumably in nucleoli and Cajal bodies. We also showed that GAR1 is necessary for the interaction between box H/ACA RNPs and DCAF4. Moreover, it was already noted that depletion of GAR1 increases the protein levels of DKC1, NOP10, NHP2 [353], suggesting that the stability of box H/ACA RNPs could be regulated by the association-dissociation of the DKC1-NOP10-NHP2 trimer and GAR1. Based on these observations, we speculated that all mature box H/ACA RNPs are potentially recognisable by DCAF4 as they contain GAR1 and that the recognition could be regulated through the control of subcellular localisation. Mature box H/ACA snoRNA and scaRNA RNPs concentrate in the nucleoli and Cajal bodies. In contrast, DCAF4 was excluded from these subnuclear compartments under normal conditions. This finding implied that DCAF4 could recognise mature box H/ACA RNPs in the nucleoplasm or on chromatin. Consistently, in *DCAF4* KO cells, the protein level of DKC1 was elevated in the nucleus (and even in the cytoplasm) but not in the subnuclear compartments. We hypothesise that mature box H/ACA snoRNA and scaRNA RNPs could be targeted by DCAF4 once they are excluded from nucleoli (or Cajal bodies). Such exclusion could be a part of the quality control mechanism that ensures that defective box H/ACA RNPs are removed from nucleoli and Cajal bodies and subsequently degraded by the UPS. Intriguingly, the nucleolus and Cajal bodies dissolve and reassemble during each passage through the mitosis, which could create a window of opportunity for DCAF4 to target box H/ACA snoRNA and scaRNA RNPs. However, only minor fluctuations in the DKC1 protein level were observed during the cell cycle progression despite the DKC1 redistribution from the nucleoli in mitosis [369], arguing against the cell-cycle dependent degradation of box H/ACA RNPs. In addition to snoRNA and scaRNA RNPs, numerous GAR1-containing box H/ACA RNPs, including those functioning as OCT4/SOX2 coactivators on chromatin [99] or AluACA snRNA RNPs with unknown functions [120], are not present in the subnuclear compartments, and it remains to be addressed how they are protected from DCAF4-mediated

degradation. Therefore, despite the vital clues provided by our observations that GAR1 is necessary for the interaction and that the box H/ACA RNPs concentrated in subnuclear compartments are spatially separated from DCAF4, how exactly the recognition of box H/ACA RNPs by DCAF4 is regulated remains to be elucidated.

We demonstrated that DCAF4 controls the abundance of the box H/ACA RNPs. Specifically, we observed up-regulation of both the box H/ACA proteins and RNAs in *DCAF4* KO cells. As discussed above, DCAF4 could target either the protein-only box H/ACA complexes or the mature box H/ACA RNP particles containing box H/ACA RNA. Either of these two scenarios could increase the box H/ACA proteins and RNAs in *DCAF4* KO cells as it was already shown that the abundance of box H/ACA RNAs depends on the availability of the box H/ACA proteins [353]. By controlling the abundance of box H/ACA RNPs, DCAF4 might regulate multiple fundamental cellular processes, including ribosome biogenesis and telomere maintenance. Both the perturbation of ribosome biogenesis and the telomere shortening in the absence of fully active DKC1 (either because of its depletion or dyskeratosis congenita mutations) activate the p53 pathway and trigger senescence [172,178,370–374]. Conversely, the up-regulation of DKC1 renders ribosomes more efficient, increases TERC levels, and promotes tumorigenesis [375]. Consistently, DKC1 is up-regulated in numerous cancers, and its high levels are associated with poor disease prognosis [376–379]. Therefore, the levels of DKC1 (and the entire box H/ACA RNP particles) must be tightly regulated, and we speculate that DCAF4 could target the box H/ACA RNPs for degradation to cease proliferation. Beyond that, box H/ACA RNPs are necessary for the self-renewal of stem cells [99,172]. In embryonic stem cells, they also function as OCT4/SOX2 coactivators and regulate the expression of key pluripotency genes critical for self-renewal [99]. As the levels of box H/ACA proteins rapidly decline during embryonic stem cell differentiation [99], it is tempting to speculate that DCAF4 could mediate their degradation to restrain the self-renewal capacity of embryonic and potentially other stem and progenitor cells. Taken together, we propose that DCAF4 could control the abundance of box H/ACA RNPs to cease proliferation under various conditions and to limit stem cell self-renewal, thereby preventing tumorigenesis.

Among box H/ACA RNAs up-regulated in *DCAF4* KO cells, increased TERC levels are of particular interest. Both TERT and TERC are limiting factors for telomerase activity, and an increase in the TERC level augments the telomerase activity, which leads to telomere elongation [380–383]. Consistently, the up-regulation of DKC1 increases TERC levels and is in itself sufficient to boost the telomerase activity and promote telomere lengthening in certain cell types [366]. In *DCAF4* KO cells, we observed the up-regulation of TERC and therefore speculated that it could lead to telomere elongation and hyper-long telomeres. However, lower expression of DCAF4 and shorter leukocyte telomere length were associated with the rs2535913 polymorphism in the *DCAF4* gene [94]. These contradictory observations require further experimental investigation. While progressive telomere shortening leads to severe defects in

highly proliferative tissues in later generations of *Terc*-deficient mice [384,385], mice with hyper-long telomeres manifest delayed metabolic ageing, longer lifespan, and surprisingly lower incidence of cancer [386]. Therefore, unravelling how DCAF4 affects telomere length in *DCAF4* KO human cells and especially in *Dcaf4* KO mice is of paramount importance as it could significantly impact our understanding of telomere maintenance mechanisms and the consequences of their dysregulation.

5.2. CRL4^{DCAF12}

CRL4^{DCAF12} is a ubiquitin ligase that targets proteins bearing the C-terminal acidic degron for degradation, yet the physiological function of this pathway remains elusive. It has been recently established that DCAF12 regulates the stability of proteins ending in the C-terminal -EE degron [48,186]. Here, we demonstrated that DCAF12 recognises a wide range of proteins containing glutamic acid at the penultimate position (-2) and that there is some degree of flexibility regarding the amino acid residue at the terminal (-1) position. Specifically, we found that DCAF12 also mediates the degradation of proteins ending in the C-terminal -EL degron, such as MOV10. Among the potential substrates of DCAF12, proteins directed to mitochondria or the secretory pathway were significantly enriched. Therefore, we speculate that DCAF12 could contribute to the elimination of mislocalised proteins, the function that was already attributed to other ubiquitin ligases recognising C-terminal degrons [52]. Additionally, functional classification of DCAF12-associated proteins revealed that DCAF12 interacts with numerous proteins operating in the antiviral response, such as MOV10, GART, ADAR, or XIAP [294,322,355,356]. Their overrepresentation raises an intriguing possibility that DCAF12 could regulate immune responses, especially those against viruses. As DCAF12 might target a broad range of proteins and thus control diverse biological processes, a crucial question is how it is regulated.

Our biochemical and microscopic experiments suggested that the regulation of the substrate recognition by DCAF12 is at least partly achieved through the control of DCAF12 subcellular localisation. DCAF12 recognises degrons constitutively present in proteins. Therefore, we speculate that DCAF12 might either target its substrates constitutively or be regulated through its expression or localisation. Under steady-state conditions in cancer cells, *DCAF12* is ubiquitously expressed. However, neither overexpression nor depletion of DCAF12 affected the protein levels of its potential substrates. Under steady-state conditions in cancer cells, DCAF12 localised mainly to the nucleus, whereas the tested candidate substrates exhibited cytoplasmic localisation (MOV10, GAR1, XIAP) or mitochondrial localisation (SMAC). The nuclear localisation of DCAF12 depended on its N-terminal NLS and the expression of its cytoplasmic (NLS-lacking) mutants effectively down-regulated MOV10 and GAR1. Based on these findings, we hypothesise that DCAF12 might be sequestered to the nucleus and might only transiently localise to the cytoplasm, where it gains access to its cytoplasmic substrates. Our

observation of the DCAF12 accumulation in the cytoplasm after proteasome inhibition suggested that an unstable and yet unknown cytoplasmic factor might be responsible for the cytoplasmic retention of DCAF12 under certain conditions. Alternatively, the localisation of DCAF12 could be regulated by a posttranslational modification. Such candidate modification is phosphorylation of serine residues located in the vicinity of the first NLS. Phosphorylation of serine 15 has been frequently reported, even in immune cells or after viral infection [387–389]. Adjacent serine 13 has been identified to be phosphorylated upon stimulation of serum-starved cells with insulin [390]. Interestingly, insulin stimulation was shown to rescue the DCAF12-dependent degradation of MAGE-A3/6 in serum-starved cells [186]. Therefore, it is tempting to speculate that immune signalling pathways or those operating downstream of the insulin receptor (e.g., the Akt signalling pathway) regulate the subcellular localisation of DCAF12 and thus its function. In addition to the subcellular localisation, the DCAF12 pathway might be controlled by the stability of DCAF12 itself. We repeatedly observed a rapid degradation of DCAF12 after inhibition of protein synthesis (cycloheximide treatment) and an increase in its protein level after inhibition of CRL neddylation (MLN4924 treatment) or proteasome (MG132 treatment). The unavailability of DCAF12 substrates might cause the instability of DCAF12 under normal conditions, as the absence of CRL substrates often leads to CRL self-ubiquitination and degradation [357,391]. Alternatively, other E3 ubiquitin ligases might control the DCAF12 pathway, another common CRL regulation mechanism [392]. The substrate recognition by DCAF12 thus seems to be controlled by the subcellular localisation and stability of DCAF12 itself.

DCAF12 interacts with XIAP and SMAC, the candidate substrates on which we initially focused. Specifically, we found that the interaction requires both the C-terminal -ED motif of SMAC and the BIR2-BIR3 domains of XIAP. SMAC is synthesised as a precursor. It is only after two-step processing in mitochondria that SMAC contains the N-terminal IBM sequence (AVPI), which binds to the BIR2 and BIR3 domains of XIAP [210–214]. The overall topology of the XIAP-SMAC complex is unknown, but the current model assumes that SMAC acts as a tetramer bound to the BIR2-BIR3 domains of dimeric XIAP [239]. We hypothesise that XIAP could be an accessory factor that either makes direct contact with DCAF12 to enhance the interaction with SMAC or is needed to position the C-terminus of SMAC so that it is accessible for DCAF12. Although we described the interaction in substantial detail, it remains to be answered whether XIAP, SMAC, or both are ubiquitinated by $CRL4^{DCAF12}$, under which condition the ubiquitination occurs, and what are its consequences. As XIAP and SMAC are spatially separated under normal conditions, we speculate that the interaction between DCAF12 and SMAC-bound to XIAP naturally occurs only following MOMP and a release of SMAC from mitochondria. This typically happens during apoptosis. Unexpectedly, the interaction was disrupted when apoptosis was induced. This counterintuitive observation needs to be further evaluated as it implies that the interaction might occur only transiently during the decision-making process before cells commit apoptosis or could be relevant

under conditions other than apoptosis. Therefore, we explored several biologically relevant conditions to determine whether DCAF12 regulates the XIAP-SMAC complex and what function this regulation may have.

To assess the effect of DCAF12 on apoptosis, we set up several experimental systems. Unfortunately, neither of them was sufficient to answer whether DCAF12 targets XIAP and SMAC for degradation during apoptosis. During cellular commitment to apoptosis, XIAP is extensively regulated and targeted for degradation by several distinct mechanisms and pathways [233–236,238,242,244–248]. In our experiments, it was difficult to distinguish the effects of DCAF12 on the protein level of XIAP (and SMAC) and apoptosis from those caused by other factors that regulate XIAP concurrently during apoptosis or promote apoptosis independently of XIAP. Although DCAF12 seemed to promote apoptosis, this effect might have been independent of the interaction with the XIAP-SMAC complex as any cellular stress ultimately indirectly promoted XIAP degradation and apoptosis. Therefore, it is vital to establish a proper experimental system to evaluate the specific effect of the interaction between DCAF12 and the XIAP-SMAC complex on apoptosis. We propose that reintroduction of $SMAC^{WT}$ or $SMACE^{238X}$ into *Smac* KO cells together with $DCAF12^{WT}$ or $DCAF12^{\Delta 1\text{-}38}$ might be such a system. In this setup, the question of whether and how the DCAF12-XIAP-SMAC interaction affects XIAP/SMAC degradation and apoptosis might be elegantly addressed.

The interaction between DCAF12 and the XIAP-SMAC complex might also be relevant in other biological processes as MOMP has several functions beyond apoptosis, including induction of pro-inflammatory signalling [220,221]. For instance, MOMP leads to proteasomal degradation of IAPs, including XIAP, which ultimately activates NIK and non-canonical NF-κB signalling [221]. In macrophages, MOMP-dependent depletion of IAPs triggers activation of caspase-8 and NLRP3 inflammasome, both of which promote the maturation and release of pro-inflammatory cytokine IL- 1β [393,394]. We thus hypothesise that DCAF12 could target the XIAP-SMAC complex during certain inflammatory responses following MOMP to promote inflammation and cell death, which are often inextricably linked. As XIAP has well-described roles in promoting MDP-activated NOD2 signalling and restricting LPS-induced inflammation [271–279], we focused on the cellular response to these two bacteria-derived PAMPs in *Dcaf12*-deficient immune cells. In our experiments, no significant changes in the inflammatory response or XIAP and SMAC protein levels were observed. We speculate that MOMP was not triggered under our experimental conditions, and thus the interaction between DCAF12 and the XIAP-SMAC complex could not have occurred. Nevertheless, DCAF12 might target XIAP and SMAC under the harsher conditions of MDP- and LPS-induced cell death. Intriguingly, the loss of DCAF12 in *Drosophila melanogaster* leads to a deregulation of DIAP1/2 and causes a defect in apoptosis and the Imd pathway [179,180], an immune response to gram-negative bacterial infections [181]. Therefore, it is tempting to speculate that the regulation of cell death pathways, inflammation, and innate immunity might be

the evolutionarily conserved role of DCAF12. MOMP and the associated release of SMAC is a late addition to the ancestral repertoire of mechanisms regulating cell death pathways and inflammation. Therefore, an adequate vertebrate model system of the inflammatory response associated with the release of $SMAC^{WT}$ and $SMAC^{238X}$ from mitochondria needs to be established to study the role of DCAF12 in regulating the XIAP-SMAC complex and inflammation.

MOV10 was another candidate substrate of DCAF12. We demonstrated that DCAF12 controls the MOV10 protein level via its C-terminal -EL degron. In human cancer cells, MOV10 is predominantly cytoplasmic protein, whereas DCAF12 is localised to the nucleus. Nevertheless, the nuclear localisation of MOV10 was also reported in human primary fibroblasts [336]. We speculate that the different subcellular localisation of DCAF12 and MOV10 in human cancer cells could explain why we could not reliably observe an increase in the MOV10 protein level and stability after DCAF12 depletion using RNAi and the CRISPR/Cas9 genome-editing system. However, when DCAF12 and MOV10 were localised to the same compartment, MOV10 was effectively degraded in a CRL- and proteasome-dependent manner. Likewise, cytoplasmic $DCAF12^{\Delta 1–38}$ controlled the protein level of GAR1, a cytoplasmic protein ending in the C-terminal -EE degron. MOV10 localises to the cytosol and the nucleus in mice, depending on the cell type and developmental stage [337,338]. In *Dcaf12* KO MEFS, MOV10 was up-regulated, which could be rescued by reintroduction of DCAF12. Moreover, *Dcaf12* deficiency led to up-regulation of MOV10 in several mice tissues, demonstrating that MOV10 is a *bona fide* substrate of DCAF12 and that the degradation is biologically relevant.

One of the biological processes in which DCAF12 controls the MOV10 protein level is spermatogenesis. In murine testes, *Mov10* is mainly expressed in spermatogonia, and its protein level sharply declines in pachytene spermatocytes [338]. In stark contrast, *Dcaf12* is highly expressed from pachytene spermatocytes onwards. These data suggest that DCAF12 could target MOV10 for degradation during late spermatogenesis. Intriguingly, spermatogenesis in *Dcaf12*-deficient mice was abnormal. Specifically, we observed a slight decline in the sperm count. Moreover, we detected a decrease in meiotic marker SCP3 and an increase in DNA damage marker γH2AX. This observation might indicate meiotic disturbances, which often reduce the number of mature sperms [395,396]. However, our histological examination of tubular sections did not reveal apparent morphological abnormalities or arrest in spermatogenesis. Therefore, further investigation is required to elucidate at which stage of spermatogenesis the defect occurred and whether it is caused solely by the up-regulation of MOV10. We speculate that up-regulation of MOV10 in the testes of *Dcaf12*-deficient mice could impact the miRNA pathway, which is essential for spermatogenesis [338,397–399] and somewhat regulated by MOV10 [338]. Additionally, up-regulation of MOV10 could affect the restriction of retrotransposons, an evolutionarily conserved function of MOV10 [299–308]. In the germline, retrotransposons are silenced by the piRNA pathway, the essential biogenesis factor of which is MOV10L1 [304,305].

However, the contribution of MOV10 to the restriction of retrotransposons during spermatogenesis is largely unknown. Notably, a specific subset of endogenous retroviruses is required to drive the transcription of germline genes in late spermatogenesis [400]. As MOV10 was also implicated in transcriptional silencing [336], excessive retrotransposon silencing by elevated MOV10 could be detrimental. Altogether, we propose that DCAF12-mediated degradation of MOV10 and possibly other substrates fine-tunes spermatogenesis, yet the underlying mechanism remains to be elucidated.

We further discovered that DCAF12 controls the MOV10 protein level in T cells, especially after their activation. The reduced percentage of T cells in the spleen and their increased apoptosis upon stimulation were both reminiscent of the miRNA pathway-deficient T cells [401–403]. The miRNA pathway, somewhat affected by MOV10, has a central role in regulating the development, homeostasis, and function of immune cells [404,405]. Intriguingly, MOV10- and miRNA pathway-associated protein AGO2 is degraded following T cell activation [406]. Moreover, T cell activation induces dramatic changes in the miRNA repertoire, which causes global post-transcriptional reprogramming and enables precise immune responses [406–408]. We thus speculate that DCAF12-mediated degradation of MOV10 could contribute to the changes in the miRNA repertoire in T cells.

Beyond its role in the miRNA pathway, MOV10 restricts retrotransposons, including endogenous retroviruses [301–313,329]. Most retrotransposons are silenced, but some are transcriptionally active and contribute to the normal regulation of gene expression in immune cells [409,410]. Additionally, it was already demonstrated that exposure of immune cells to microbial products, e.g., LPS or poly(I:C), triggers the expression of distinct retrotransposons and endogenous retroviruses [411]. Analysing publicly available data, we noticed that this is often accompanied by increased expression of *Mov10* and down-regulation of *Dcaf12* mRNA. For example, this occurs after the stimulation of the immune cells with Toll-like receptor 2 (TLR2) agonists or LPS. Consistently, we observed the up-regulation of MOV10 in the splenocytes treated with various TLR agonists, such as LPS or poly(I:C). This up-regulation of MOV10 could protect cells from increased expression of retrotransposons and endogenous retroviruses. Here, we showed that *Dcaf12* is up-regulated and controls the MOV10 protein level when splenocytes are activated with anti-CD3/CD28 antibody-coupled beads. Therefore, we speculate that MOV10 could be dynamically regulated after exposure to different stimuli in immune cells. Interestingly, CD3/CD28 receptor crosslinking, but not LPS stimulation, leads to reactivation of latent HIV-1 in resting $CD4^+$ T cells [412,413]. Based on these observations, we speculate that the down-regulation of the MOV10 protein level by DCAF12 in activated T cells could create a window of opportunity for HIV-1 to evade the host retrovirus surveillance pathways. Similarly, endogenous retroviruses and retrotransposons could be left unrestricted after TCR stimulation, thereby potentially pre-activating antiviral innate immunity pathways in T cells, which could represent a novel cellular self-defence mechanism against viruses. *Dcaf12* KO mice thus represent an elegant model to test this intriguing

hypothesis experimentally. Moreover, retrotransposons are immunogenic, and defects in their restriction trigger autoimmune diseases, such as Aicardi-Goutières syndrome [414,415]. Increased levels of MOV10 were shown to restrict retrotransposons more efficiently and thus reduce the expression of proinflammatory genes related to rheumatoid arthritis progression [313]. DCAF12 itself was associated with intestinal Behçet's disease, chronic inflammatory disorder [416]. Based on these observations, it is tempting to speculate that dysregulation of the DCAF12-mediated control of MOV10 could lead to autoimmune diseases. Taken together, DCAF12 could fine-tune the regulation of retrotransposons and retroviruses through the control of the MOV10 protein level, which might be particularly important in immune cells.

DCAF12 was previously implicated in several immunological processes. For example, the decreased expression of *DCAF12* (also known as WDR40A in clinical articles) precedes the onset of post-transplantation organ rejection in the human peripheral blood [417,418]. Additionally, *DCAF12* was associated with the development of intestinal Behçet's disease [416]. Our data suggest that *Dcaf12* KO animals might be immunocompromised as they display dysregulation of various splenic T cell populations, and their T cells exhibit increased apoptosis upon activation. Considering the sheer number of immune processes in which distinct T cell subpopulations are involved, further examination of the immune responses in the *Dcaf12* KO animals might offer a fertile ground for unexpected discoveries, especially in the field of transplantation immunology and research of inflammatory disorders. Although the specific mechanisms by which DCAF12 affects immune responses remain unknown, the herein presented description of the DCAF12-mediated control of MOV10 and the DCAF12 association with the XIAP-SMAC complex might provide important clues for their unravelling.

6. Conclusions

Selective protein degradation by the UPS is essential for cellular homeostasis and regulation of diverse biological processes. This system centres around ubiquitin ligases that recognise substrates and mark them with ubiquitin(s) for degradation. The human genome encodes hundreds of ubiquitin ligases, most of which have not yet been matched with their respective substrates and their function remained unknown. Herein, we presented a comprehensive identification and validation of candidate substrates of two ubiquitin ligases from the CRL4 subfamily, followed by an exploration of their biological roles.

Regarding $CRL4^{DCAF4}$, we demonstrated that DCAF4 specifically interacts with the box H/ACA RNPs and regulates their abundance. Characterisation of the interaction revealed that it depends on DKC1 and GAR1 but not on RNA. Biochemical and microscopic experiments indicated that DCAF4 recognises and regulates the box H/ACA RNPs in the nucleoplasm (and the cytosol). Box H/ACA RNPs catalyse RNA pseudouridylation and stabilise the box H/ACA RNAs, including TERC. Therefore, fundamental cellular processes, such as ribosome biogenesis and telomere maintenance, could be impaired without DCAF4-mediated degradation of the box H/ACA RNPs. Furthermore, by controlling the abundance of box H/ACA RNPs, DCAF4 might cease proliferation under various conditions and limit stem cell self-renewal, thereby preventing tumorigenesis.

As for $CRL4^{DCAF12}$, we demonstrated that DCAF12 specifically interacts with numerous proteins containing the C-terminal acidic motif. Initially, we focused on the XIAP-SMAC complex and showed that its interaction with DCAF12 depends on the C-terminal -ED motif of SMAC and the BIR2-BIR3 domains of XIAP. As no DCAF12-mediated degradation of the XIAP-SMAC complex during apoptosis and inflammation was observed under our experimental conditions, we moved our attention to other candidate substrates. Characterisation of the interaction with MOV10 revealed that DCAF12 mediates the degradation of MOV10 via its C-terminal -EL degron. Exploration of biological processes affected by the loss of *Dcaf12* in mice uncovered that DCAF12 controls the MOV10 protein level during spermatogenesis and after T cell activation. MOV10 is crucial for retrotransposon restriction and miRNA-mediated post-transcriptional regulation of gene expression. Therefore, DCAF12 could regulate MOV10 to balance the control of retrotransposons and viruses on the one hand and the miRNA-regulated transitions (e.g., from spermatogonia to pachytene spermatocytes and from resting to activated T cells) on the other. Finally, dysregulation of immune cell populations in *Dcaf12* KO mice and increased apoptosis of activated T cells derived from *Dcaf12* KO mice provided compelling evidence on the role of DCAF12 in the immune system, highlighting the clinical relevance of the DCAF12 pathway.

7. List of publications

Author's publications related to the topic of the doctoral thesis:

- **Lidak**, **T**.; Baloghova, N.; Korinek, V.; Sedlacek, R.; Balounova, J.; Kasparek, P.; Cermak, L. CRL4-DCAF12 ubiquitin ligase controls MOV10 RNA helicase during spermatogenesis and T cell activation. *Int*. *J*. *Mol*. *Sci*. **2021**, 22, 5394, doi:10.3390/ijms22105394.
- Baloghova, N.; **Lidak**, **T**.; Cermak, L. Ubiquitin ligases involved in the regulation of Wnt, TGF-β, and Notch signaling pathways and their roles in mouse development and homeostasis. *Genes*. **2019**, 10, 815, doi:10.3390/genes10100815.

Other author's publications:

- von Morgen, P.; **Lidak**, **T**.; Horejsi, Z.; Macurek, L. Nuclear localisation of 53BP1 is regulated by phosphorylation of the nuclear localisation signal. *Biol*. *Cell* **2018**, 110, 137–146, doi:10.1111/boc.201700067.
- Benada, J.; Burdová, K.; **Lidak**, **T**.; von Morgen, P.; Macurek, L. Polo-like kinase 1 inhibits DNA damage response during mitosis. *Cell Cycle* **2015**, 14, 219–31, doi:10.4161/15384101.2014.977067.

8. References

1. Ciechanover, A. The ubiquitin proteolytic system and pathogenesis of human diseases: a novel platform for mechanism-based drug targeting. *Biochem. Soc. Trans.* **2003**, *31*, 474–481, doi:10.1042/bst0310474.

2. Hershko, A.; Ciechanover, A. The ubiquitin system. *Annu. Rev. Biochem.* **1998**, *67*, 425–479, doi:10.1146/annurev.biochem.67.1.425.

3. Reyes-Turcu, F.E.; Ventii, K.H.; Wilkinson, K.D. Regulation and cellular roles of ubiquitin-specific deubiquitinating enzymes. *Annu. Rev. Biochem.* **2009**, *78*, 363–397, doi:10.1146/annurev.biochem.78.082307.091526.

4. Nijman, S.M.B.; Luna-Vargas, M.P.A.; Velds, A.; Brummelkamp, T.R.; Dirac, A.M.G.; Sixma, T.K.; Bernards, R. A genomic and functional inventory of deubiquitinating enzymes. *Cell* **2005**, *123*, 773–786, doi:10.1016/j.cell.2005.11.007.

5. Wijk, S.J.L.; Timmers, H.T.M. The family of ubiquitin-conjugating enzymes (E2s): deciding between life and death of proteins. *FASEB J.* **2010**, *24*, 981–993, doi:10.1096/fj.09-136259.

6. Li, W.; Bengtson, M.H.; Ulbrich, A.; Matsuda, A.; Reddy, V.A.; Orth, A.; Chanda, S.K.; Batalov, S.; Joazeiro, C.A.P. Genome-wide and functional annotation of human E3 ubiquitin ligases identifies MULAN, a mitochondrial E3 that regulates the organelle's dynamics and signaling. *PLoS One* **2008**, *3*, e1487, doi:10.1371/journal.pone.0001487.

7. Zheng, N.; Shabek, N. Ubiquitin ligases: structure, function, and regulation. *Annu. Rev. Biochem.* **2017**, *86*, 129–157, doi:10.1146/annurev-biochem-060815-014922.

8. Deshaies, R.J.; Joazeiro, C.A.P. RING domain E3 ubiquitin ligases. *Annu. Rev. Biochem.* **2009**, *78*, 399–434, doi:10.1146/annurev.biochem.78.101807.093809.

9. Mabbitt, P.D.; Loreto, A.; Déry, M.A.; Fletcher, A.J.; Stanley, M.; Pao, K.C.; Wood, N.T.; Coleman, M.P.; Virdee, S. Structural basis for RING-Cys-Relay E3 ligase activity and its role in axon integrity. *Nat. Chem. Biol.* **2020**, *16*, 1227–1236, doi:10.1038/s41589-020-0598-6.

10. Weber, J.; Polo, S.; Maspero, E. HECT E3 ligases: a tale with multiple facets. *Front. Physiol.* **2019**, *10*, 370, doi:10.3389/fphys.2019.00370.

11. Dove, K.K.; Klevit, R.E. RING-Between-RING E3 ligases: emerging themes amid the variations. *J. Mol. Biol.* **2017**, *429*, 3363–3375, doi:10.1016/j.jmb.2017.08.008.

12. Komander, D.; Rape, M. The ubiquitin code. *Annu. Rev. Biochem.* **2012**, *81*, 203–229, doi:10.1146/annurev-biochem-060310-170328.

13. Pierce, N.W.; Kleiger, G.; Shan, S.; Deshaies, R.J. Detection of sequential polyubiquitylation on a millisecond timescale. *Nature* **2009**, *462*, 615–619, doi:10.1038/nature08595.

14. Swatek, K.N.; Komander, D. Ubiquitin modifications. *Cell Res.* **2016**, *26*, 399–422, doi:10.1038/cr.2016.39.

15. Fiil, B.K.; Gyrd-Hansen, M. The Met1-linked ubiquitin machinery in inflammation and infection. *Cell Death Differ.* **2021**, *28*, 557–569, doi:10.1038/s41418-020-00702-x.

16. Corn, J.E.; Vucic, D. Ubiquitin in inflammation: The right linkage makes all the difference. *Nat. Struct. Mol. Biol.* **2014**, *21*, 297–300, doi:10.1038/nsmb.2808.

17. Saeki, Y. Ubiquitin recognition by the proteasome. *J. Biochem.* **2017**, *161*, 113–124, doi:10.1093/jb/mvw091.

18. Rousseau, A.; Bertolotti, A. Regulation of proteasome assembly and activity in health and disease. *Nat. Rev. Mol. Cell Biol.* **2018**, *19*, 697–712, doi:10.1038/s41580-018-0040-z.

19. Bard, J.A.M.; Goodall, E.A.; Greene, E.R.; Jonsson, E.; Dong, K.C.; Martin, A. Structure and function of the 26S proteasome. *Annu. Rev. Biochem.* **2018**, *87*, 697–724, doi:10.1146/ annurev-biochem-062917-011931.

20. Sarikas, A.; Hartmann, T.; Pan, Z.Q. The cullin protein family. *Genome Biol.* **2011**, *12*, 220, doi:10.1186/gb-2011-12-4-220.

21. Skaar, J.R.; Pagan, J.K.; Pagano, M. Mechanisms and function of substrate recruitment by F-box proteins. *Nat. Rev. Mol. Cell Biol.* **2013**, *14*, 369–381, doi:10.1038/nrm3582.

22. Hannah, J.; Zhou, P. Distinct and overlapping functions of the cullin E3 ligase scaffolding proteins CUL4A and CUL4B. *Gene* **2015**, *573*, 33–45, doi:10.1016/j.gene.2015.08.064.

23. Zou, Y.; Mi, J.; Cui, J.; Lu, D.; Zhang, X.; Guo, C.; Gao, G.; Liu, Q.; Chen, B.; Shao, C.; et al. Characterization of nuclear localization signal in the N terminus of CUL4B and its essential role in cyclin E degradation and cell cycle progression. *J. Biol. Chem.* **2009**, *284*, 33320–33332, doi:10.1074/jbc.M109.050427.

24. Angers, S.; Li, T.; Yi, X.; MacCoss, M.J.; Moon, R.T.; Zheng, N. Molecular architecture and assembly of the DDB1-CUL4A ubiquitin ligase machinery. *Nature* **2006**, *443*, 590–593, doi:10.1038/nature05175.

25. Fischer, E.S.; Scrima, A.; Böhm, K.; Matsumoto, S.; Lingaraju, G.M.; Faty, M.; Yasuda, T.; Cavadini, S.; Wakasugi, M.; Hanaoka, F.; et al. The molecular basis of CRL4DDB2/CSA ubiquitin ligase architecture, targeting, and activation. *Cell* **2011**, *147*, 1024–1039, doi:10.1016/ j.cell.2011. 10.035.

26. He, Y.J.; McCall, C.M.; Hu, J.; Zeng, Y.; Xiong, Y. DDB1 functions as a linker to recruit receptor WD40 proteins to CUL4-ROC1 ubiquitin ligases. *Genes Dev.* **2006**, *20*, 2949–2954, doi:10.1101/ gad.1483206.

27. Higa, L.A.; Wu, M.; Ye, T.; Kobayashi, R.; Sun, H.; Zhang, H. CUL4-DDB1 ubiquitin ligase interacts with multiple WD40-repeat proteins and regulates histone methylation. *Nat. Cell Biol.* **2006**, *8*, 1277–1283, doi:10.1038/ncb1490.

28. Jin, J.; Arias, E.E.; Chen, J.; Harper, J.W.; Walter, J.C. A family of diverse Cul4-Ddb1-interacting proteins includes Cdt2, which is required for S phase destruction of the replication factor Cdt1. *Mol. Cell* **2006**, *23*, 709–721, doi:10.1016/j.molcel.2006.08.010.

29. Li, T.; Chen, X.; Garbutt, K.C.; Zhou, P.; Zheng, N. Structure of DDB1 in complex with a paramyxovirus V protein: viral hijack of a propeller cluster in ubiquitin ligase. *Cell* **2006**, *124*, 105–117, doi:10.1016/j.cell.2005.10.033.

30. Li, T.; Robert, E.I.; van Breugel, P.C.; Strubin, M.; Zheng, N. A promiscuous α-helical motif anchors viral hijackers and substrate receptors to the CUL4–DDB1 ubiquitin ligase machinery. *Nat. Struct. Mol. Biol.* **2010**, *17*, 105–112, doi:10.1038/nsmb.1719.

31. Enchev, R.I.; Schulman, B.A.; Peter, M. Protein neddylation: beyond cullin-RING ligases. *Nat. Rev. Mol. Cell Biol.* **2015**, *16*, 30–44, doi:10.1038/nrm3919.

32. Duda, D.M.; Borg, L.A.; Scott, D.C.; Hunt, H.W.; Hammel, M.; Schulman, B.A. Structural insights into NEDD8 activation of cullin-RING ligases: conformational control of conjugation. *Cell* **2008**, *134*, 995–1006, doi:10.1016/j.cell.2008.07.022.

33. Saha, A.; Deshaies, R.J. Multimodal activation of the ubiquitin ligase SCF by Nedd8 conjugation. *Mol. Cell* **2008**, *32*, 21–31, doi:10.1016/j.molcel.2008.08.021.

34. Soucy, T.A.; Smith, P.G.; Milhollen, M.A.; Berger, A.J.; Gavin, J.M.; Adhikari, S.; Brownell, J.E.; Burke, K.E.; Cardin, D.P.; Critchley, S.; et al. An inhibitor of NEDD8-activating enzyme as a new approach to treat cancer. *Nature* **2009**, *458*, 732–736, doi:10.1038/nature07884.

35. Brownell, J.E.; Sintchak, M.D.; Gavin, J.M.; Liao, H.; Bruzzese, F.J.; Bump, N.J.; Soucy, T.A.; Milhollen, M.A.; Yang, X.; Burkhardt, A.L.; et al. Substrate-assisted inhibition of ubiquitin-like protein-activating enzymes: the NEDD8 E1 inhibitor MLN4924 forms a NEDD8-AMP mimetic in situ. *Mol. Cell* **2010**, *37*, 102–111, doi:10.1016/j.molcel.2009.12.024.

36. Mosadeghi, R.; Reichermeier, K.M.; Winkler, M.; Schreiber, A.; Reitsma, J.M.; Zhang, Y.; Stengel, F.; Cao, J.; Kim, M.; Sweredoski, M.J.; et al. Structural and kinetic analysis of the COP9-signalosome activation and the cullin-RING ubiquitin ligase deneddylation cycle. *Elife* **2016**, *5*, e12102, doi:10.7554/eLife.12102.

37. Cavadini, S.; Fischer, E.S.; Bunker, R.D.; Potenza, A.; Lingaraju, G.M.; Goldie, K.N.; Mohamed, W.I.; Faty, M.; Petzold, G.; Beckwith, R.E.J.; et al. Cullin-RING ubiquitin E3 ligase regulation by the COP9 signalosome. *Nature* **2016**, *531*, 598–603, doi:10.1038/nature17416.

38. Pierce, N.W.; Lee, J.E.; Liu, X.; Sweredoski, M.J.; Graham, R.L.J.; Larimore, E.A.; Rome, M.; Zheng, N.; Clurman, B.E.; Hess, S.; et al. Cand1 promotes assembly of new SCF complexes through dynamic exchange of F box proteins. *Cell* **2013**, *153*, 206–215, doi:10.1016/j.cell.2013. 02.024.

39. Zemla, A.; Thomas, Y.; Kedziora, S.; Knebel, A.; Wood, N.T.; Rabut, G.; Kurz, T. CSN- and CAND1-dependent remodelling of the budding yeast SCF complex. *Nat. Commun.* **2013**, *4*, 1641, doi:10.1038/ncomms2628.

40. Wu, S.; Zhu, W.; Nhan, T.; Toth, J.I.; Petroski, M.D.; Wolf, D.A. CAND1 controls in vivo dynamics of the cullin 1-RING ubiquitin ligase repertoire. *Nat. Commun.* **2013**, *4*, 1642, doi:10.1038/ncomms2636.

41. Liu, X.; a protein exchange, J.M.; Mamrosh, J.L.; Zhang, Y.; Straube, R.; Deshaies, R.J. Cand1-mediated adaptive exchange mechanism enables variation in F-box protein expression. *Mol. Cell* **2018**, *69*, 773–786.e6, doi:10.1016/j.molcel.2018.01.038.

42. Reitsma, J.M.; Liu, X.; Reichermeier, K.M.; Moradian, A.; Sweredoski, M.J.; Hess, S.; Deshaies, R.J. Composition and regulation of the cellular repertoire of SCF ubiquitin ligases. *Cell* **2017**, *171*, 1326–1339.e14, doi:10.1016/j.cell.2017.10.016.

43. Reichermeier, K.M.; Straube, R.; Reitsma, J.M.; Sweredoski, M.J.; Rose, C.M.; Moradian, A.; den Besten, W.; Hinkle, T.; Verschueren, E.; Petzold, G.; et al. PIKES analysis reveals response to degraders and key regulatory mechanisms of the CRL4 network. *Mol. Cell* **2020**, *77*, 1092–1106.e9, doi:10.1016/j.molcel.2019.12.013.

44. Mayor-Ruiz, C.; Jaeger, M.G.; Bauer, S.; Brand, M.; Sin, C.; Hanzl, A.; Mueller, A.C.; Menche, J.; Winter, G.E. Plasticity of the cullin-RING ligase repertoire shapes sensitivity to ligand-induced protein degradation. *Mol. Cell* **2019**, *75*, 849–858.e8, doi:10.1016/j.molcel.2019.07.013.

45. Ravid, T.; Hochstrasser, M. Diversity of degradation signals in the ubiquitin-proteasome system. *Nat. Rev. Mol. Cell Biol.* **2008**, *9*, 679–690, doi:10.1038/nrm2468.

46. Timms, R.T.; Koren, I. Tying up loose ends: The N-degron and C-degron pathways of protein degradation. *Biochem. Soc. Trans.* **2020**, *48*, 1557–1567, doi:10.1042/BST20191094.

47. Varshavsky, A. N-degron and C-degron pathways of protein degradation. *Proc. Natl. Acad. Sci. U. S. A.* **2019**, *116*, 358–366, doi:10.1073/pnas.1816596116.

48. Koren, I.; Timms, R.T.; Kula, T.; Xu, Q.; Li, M.Z.; Elledge, S.J. The eukaryotic proteome is shaped by E3 ubiquitin ligases targeting C-terminal degrons. *Cell* **2018**, *173*, 1622–1635.e14, doi: 10.1016/j.cell.2018.04.028.

49. Lin, H.-C.; Ho, S.-C.; Chen, Y.-Y.; Khoo, K.-H.; Hsu, P.-H.; Yen, H.-C.S. CRL2 aids elimination of truncated selenoproteins produced by failed UGA/Sec decoding. *Science* **2015**, *349*, 91–95, doi:10.1126/science.aab0515.

50. Lin, H.C.; Yeh, C.W.; Chen, Y.F.; Lee, T.T.; Hsieh, P.Y.; Rusnac, D. V.; Lin, S.Y.; Elledge, S.J.; Zheng, N.; Yen, H.C.S. C-terminal end-directed protein elimination by CRL2 ubiquitin ligases. *Mol. Cell* **2018**, *70*, 602–613.e3, doi:10.1016/j.molcel.2018.04.006.

51. Rusnac, D.V.; Lin, H.C.; Canzani, D.; Tien, K.X.; Hinds, T.R.; Tsue, A.F.; Bush, M.F.; Yen, H.C.S.; Zheng, N. Recognition of the diglycine C-end degron by CRL2 KLHDC2 ubiquitin ligase. *Mol. Cell* **2018**, *72*, 813–822.e4, doi:10.1016/j.molcel.2018.10.021.

52. Yeh, C.; Huang, W.; Hsu, P.; Yeh, K.; Wang, L.; Hsu, P.W.; Lin, H.; Chen, Y.; Chen, S.; Yeang, C.; et al. The C-degron pathway eliminates mislocalized proteins and products of deubiquitinating enzymes. *EMBO J.* **2021**, *40*, e105846, doi:10.15252/embj.2020105846.

53. Abbas, T.; Mueller, A.C.; Shibata, E.; Keaton, M.; Rossi, M.; Dutta, A. CRL1-FBXO11 promotes Cdt2 ubiquitylation and degradation and regulates Pr-Set7/Set8-mediated cellular migration. *Mol. Cell* **2013**, *49*, 1147–1158, doi:10.1016/j.molcel.2013.02.003.

54. Scrima, A.; Fischer, E.S.; Lingaraju, G.M.; Böhm, K.; Cavadini, S.; Thomä, N.H. Detecting UV-lesions in the genome: the modular CRL4 ubiquitin ligase does it best! *FEBS Lett.* **2011**, *585*, 2818–2825, doi:10.1016/j.febslet.2011.04.064.

55. Sugasawa, K. Molecular mechanisms of DNA damage recognition for mammalian nucleotide excision repair. *DNA Repair* **2016**, *44*, 110–117, doi:10.1016/j.dnarep.2016.05.015.

56. Scrima, A.; Konícková, R.; Czyzewski, B.K.; Kawasaki, Y.; Jeffrey, P.D.; Groisman, R.; Nakatani, Y.; Iwai, S.; Pavletich, N.P.; Thomä, N.H. Structural basis of UV DNA-damage recognition by the DDB1-DDB2 complex. *Cell* **2008**, *135*, 1213–1223, doi:10.1016/j.cell.2008.10.045.

57. Groisman, R.; Polanowska, J.; Kuraoka, I.; Sawada, J.I.; Saijo, M.; Drapkin, R.; Kisselev, A.F.; Tanaka, K.; Nakatani, Y. The ubiquitin ligase activity in the DDB2 and CSA complexes is differentially regulated by the COP9 signalosome in response to DNA damage. *Cell* **2003**, *113*, 357–367, doi:10.1016/S0092-8674(03)00316-7.

58. Wang, H.; Zhai, L.; Xu, J.; Joo, H.Y.; Jackson, S.; Erdjument-Bromage, H.; Tempst, P.; Xiong, Y.; Zhang, Y. Histone H3 and H4 ubiquitylation by the CUL4-DDB-ROC1 ubiquitin ligase facilitates cellular response to DNA damage. *Mol. Cell* **2006**, *22*, 383–394, doi:10.1016/j.molcel.2006. 03.035.

59. Kapetanaki, M.G.; Guerrero-Santoro, J.; Bisi, D.C.; Hsieh, C.L.; Rapić-Otrin, V.; Levine, A.S. The DDB1-CUL4ADDB2 ubiquitin ligase is deficient in xeroderma pigmentosum group E and targets histone H2A at UV-damaged DNA sites. *Proc. Natl. Acad. Sci. U. S. A.* **2006**, *103*, 2588–2593, doi:10.1073/pnas.0511160103.

60. Sugasawa, K.; Okuda, Y.; Saijo, M.; Nishi, R.; Matsuda, N.; Chu, G.; Mori, T.; Iwai, S.; Tanaka, K.; Tanaka, K.; et al. UV-induced ubiquitylation of XPC protein mediated by UV-DDB-ubiquitin ligase complex. *Cell* **2005**, *121*, 387–400, doi:10.1016/j.cell.2005.02.035.

61. Chen, X.; Zhang, Y.; Douglas, L.; Zhou, P. UV-damaged DNA-binding proteins are targets of CUL-4A-mediated ubiquitination and degradation. *J. Biol. Chem.* **2001**, *276*, 48175–48182, doi:10.1074/jbc.M106808200.

62. Nag, A.; Bondar, T.; Shiv, S.; Raychaudhuri, P. The xeroderma pigmentosum group E gene product DDB2 is a specific target of cullin 4A in mammalian cells. *Mol. Cell. Biol.* **2001**, *21*, 6738–6747, doi:10.1128/mcb.21.20.6738-6747.2001.

63. Ribeiro-Silva, C.; Sabatella, M.; Helfricht, A.; Marteijn, J.A.; Theil, A.F.; Vermeulen, W.; Lans, H. Ubiquitin and TFIIH-stimulated DDB2 dissociation drives DNA damage handover in nucleotide excision repair. *Nat. Commun.* **2020**, *11*, 4868, doi:10.1038/s41467-020-18705-0.

64. Puumalainen, M.-R.; Lessel, D.; Rüthemann, P.; Kaczmarek, N.; Bachmann, K.; Ramadan, K.; Naegeli, H. Chromatin retention of DNA damage sensors DDB2 and XPC through loss of p97 segregase causes genotoxicity. *Nat. Commun.* **2014**, *5*, 3695, doi:10.1038/ncomms4695.

65. Moriwaki, S.; Kanda, F.; Hayashi, M.; Yamashita, D.; Sakai, Y.; Nishigori, C. Xeroderma pigmentosum clinical practice guidelines. *J. Dermatol.* **2017**, *44*, 1087–1096, doi:10.1111/1346-8138.13907.

66. van der Weegen, Y.; Golan-Berman, H.; Mevissen, T.E.T.; Apelt, K.; González-Prieto, R.; Goedhart, J.; Heilbrun, E.E.; Vertegaal, A.C.O.; van den Heuvel, D.; Walter, J.C.; et al. The cooperative action of CSB, CSA, and UVSSA target TFIIH to DNA damage-stalled RNA polymerase II. *Nat. Commun.* **2020**, *11*, 2104, doi:10.1038/s41467-020-15903-8.

67. Tufegdžić Vidaković, A.; Mitter, R.; Kelly, G.P.; Neumann, M.; Harreman, M.; Rodríguez-Martínez, M.; Herlihy, A.; Weems, J.C.; Boeing, S.; Encheva, V.; et al. Regulation of the RNAPII pool is integral to the DNA damage response. *Cell* **2020**, *180*, 1245–1261.e21, doi:10.1016/j.cell.2020.02.009.

68. Nakazawa, Y.; Hara, Y.; Oka, Y.; Komine, O.; van den Heuvel, D.; Guo, C.; Daigaku, Y.; Isono, M.; He, Y.; Shimada, M.; et al. Ubiquitination of DNA damage-stalled RNAPII promotes transcription-coupled repair. *Cell* **2020**, *180*, 1228–1244.e24, doi:10.1016/j.cell.2020.02.010.

69. van der Weegen, Y.; de Lint, K.; van den Heuvel, D.; Nakazawa, Y.; Mevissen, T.E.T.; van Schie, J.J.M.; San Martin Alonso, M.; Boer, D.E.C.; González-Prieto, R.; Narayanan, I. V.; et al. ELOF1 is a transcription-coupled DNA repair factor that directs RNA polymerase II ubiquitylation. *Nat. Cell Biol.* **2021**, *23*, 595–607, doi:10.1038/s41556-021-00688-9.

70. Kokic, G.; Wagner, F.R.; Chernev, A.; Urlaub, H.; Cramer, P. Structural basis of human transcription–DNA repair coupling. *Nature* **2021**, *598*, 368–372, doi:10.1038/s41586-021-03906-4.

71. Groisman, R.; Kuraoka, I.; Chevallier, O.; Gaye, N.; Magnaldo, T.; Tanaka, K.; Kisselev, A.F.; Harel-Bellan, A.; Nakatani, Y. CSA-dependent degradation of CSB by the ubiquitin-proteasome pathway establishes a link between complementation factors of the Cockayne syndrome. *Genes Dev.* **2006**, *20*, 1429–1434, doi:10.1101/gad.378206.

72. Epanchintsev, A.; Costanzo, F.; Rauschendorf, M.A.; Caputo, M.; Ye, T.; Donnio, L.M.; Proietti-de-Santis, L.; Coin, F.; Laugel, V.; Egly, J.M. Cockayne's syndrome A and B proteins regulate transcription arrest after genotoxic stress by promoting ATF3 degradation. *Mol. Cell* **2017**, *68*, 1054–1066.e6, doi:10.1016/j.molcel.2017.11.009.

73. Laugel, V. Cockayne syndrome: The expanding clinical and mutational spectrum. *Mech. Ageing Dev.* **2013**, *134*, 161–170, doi:10.1016/j.mad.2013.02.006.

74. Cang, Y.; Zhang, J.; Nicholas, S.A.; Bastien, J.; Li, B.; Zhou, P.; Goff, S.P. Deletion of DDB1 in mouse brain and lens leads to p53-dependent elimination of proliferating cells. *Cell* **2006**, *127*, 929–940, doi:10.1016/j.cell.2006.09.045.

75. Cang, Y.; Zhang, J.; Nicholas, S.A.; Kim, A.L.; Zhou, P.; Goff, S.P. DDB1 is essential for genomic stability in developing epidermis. *Proc. Natl. Acad. Sci. U. S. A.* **2007**, *104*, 2733–2737, doi:10.1073/pnas.0611311104.

76. Gao, J.; Buckley, S.M.; Cimmino, L.; Guillamot, M.; Strikoudis, A.; Cang, Y.; Goff, S.P.; Aifantis, I. The CUL4-DDB1 ubiquitin ligase complex controls adult and embryonic stem cell differentiation and homeostasis. *Elife* **2015**, *4*, e07539, doi:10.7554/eLife.07539.

77. Zhao, L.; Wang, X.; Pomlok, K.; Liao, H.; Yang, G.; Yang, X.; Chen, Y.G. DDB1 promotes the proliferation and hypertrophy of chondrocytes during mouse skeleton development. *Dev. Biol.* **2020**, *465*, 100–107, doi:10.1016/j.ydbio.2020.05.011.

78. Yu, C.; Ji, S.Y.; Sha, Q.Q.; Sun, Q.Y.; Fan, H.Y. CRL4-DCAF1 ubiquitin E3 ligase directs protein phosphatase 2A degradation to control oocyte meiotic maturation. *Nat. Commun.* **2015**, *6*, 8017, doi:10.1038/ncomms9017.

79. Yu, C.; Zhang, Y.L.; Pan, W.W.; Li, X.M.; Wang, Z.W.; Ge, Z.J.; Zhou, J.J.; Cang, Y.; Tong, C.; Sun, Q.Y.; et al. CRL4 complex regulates mammalian oocyte survival and reprogramming by activation of tet proteins. *Science* **2013**, *342*, 1518–1521, doi:10.1126/science.1244587.

80. Yu, C.; Xu, Y.W.; Sha, Q.Q.; Fan, H.Y. CRL4DCAF1 is required in activated oocytes for follicle maintenance and ovulation. *Mol. Hum. Reprod.* **2014**, *21*, 195–205, doi:10.1093/molehr/gau103.

81. Liu, L.; Lee, S.; Zhang, J.; Peters, S.B.; Hannah, J.; Zhang, Y.; Yin, Y.; Koff, A.; Ma, L.; Zhou, P. CUL4A abrogation augments DNA damage response and protection against skin carcinogenesis. *Mol. Cell* **2009**, *34*, 451–460, doi:10.1016/j.molcel.2009.04.020.

82. Liu, L.; Yin, Y.; Li, Y.; Prevedel, L.; Lacy, E.H.; Ma, L.; Zhou, P. Essential role of the CUL4B ubiquitin ligase in extra-embryonic tissue development during mouse embryogenesis. *Cell Res.* **2012**, *22*, 1258–1269, doi:10.1038/cr.2012.48.

83. Chen, C.Y.; Tsai, M.S.; Lin, C.Y.; Yu, I.S.; Chen, Y.T.; Lin, S.R.; Juan, L.W.; Chen, Y.T.; Hsu, H.M.; Lee, L.J.; et al. Rescue of the genetically engineered Cul4b mutant mouse as a potential model for human X-linked mental retardation. *Hum. Mol. Genet.* **2012**, *21*, 4270–4285, doi:10.1093/hmg/dds261.

84. Jiang, B.; Zhao, W.; Yuan, J.; Qian, Y.; Sun, W.; Zou, Y.; Guo, C.; Chen, B.; Shao, C.; Gong, Y. Lack of Cul4b, an E3 ubiquitin ligase component, leads to embryonic lethality and abnormal placental development. *PLoS One* **2012**, *7*, e37070, doi:10.1371/journal.pone.0037070.

85. Kopanja, D.; Roy, N.; Stoyanova, T.; Hess, R.A.; Bagchi, S.; Raychaudhuri, P. Cul4A is essential for spermatogenesis and male fertility. *Dev. Biol.* **2011**, *352*, 278–287, doi:10.1016/j.ydbio.2011.01.028.

86. Yin, Y.; Lin, C.; Kim, S.T.; Roig, I.; Chen, H.; Liu, L.; Veith, G.M.; Jin, R.U.; Keeney, S.; Jasin, M.; et al. The E3 ubiquitin ligase Cullin 4A regulates meiotic progression in mouse spermatogenesis. *Dev. Biol.* **2011**, *356*, 51–62, doi:10.1016/j.ydbio.2011.05.661.

87. Yin, Y.; Liu, L.; Yang, C.; Lin, C.; Veith, G.M.; Wang, C.; Sutovsky, P.; Zhou, P.; Ma, L. Cell autonomous and nonautonomous function of CUL4B in mouse spermatogenesis. *J. Biol. Chem.* **2016**, *291*, 6923–6935, doi:10.1074/jbc.M115.699660.

88. Lin, C.Y.; Chen, C.Y.; Yu, C.H.; Yu, I.S.; Lin, S.R.; Wu, J.T.; Lin, Y.H.; Kuo, P.L.; Wu, J.C.; Lin, S.W. Human X-linked intellectual disability factor CUL4B is required for post-meiotic sperm development and male fertility. *Sci. Rep.* **2016**, *6*, 20227, doi:10.1038/srep20227.

89. Hung, M.H.; Jian, Y.R.; Tsao, C.C.; Lin, S.W.; Chuang, Y.H. Enhanced LPS-induced peritonitis in mice deficiency of cullin 4B in macrophages. *Genes Immun.* **2014**, *15*, 404–412, doi:10.1038/ gene.2014.32.

90. Tarpey, P.S.; Raymond, F.L.; O'Meara, S.; Edkins, S.; Teague, J.; Butler, A.; Dicks, E.; Stevens, C.; Tofts, C.; Avis, T.; et al. Mutations in CUL4B, which encodes a ubiquitin E3 ligase subunit, cause an X-linked mental retardation syndrome associated with aggressive outbursts, seizures, relative macrocephaly, central obesity, hypogonadism, pes cavus, and tremor. *Am. J. Hum. Genet.* **2007**, *80*, 345–352, doi:10.1086/511134.

91. Zou, Y.; Liu, Q.; Chen, B.; Zhang, X.; Guo, C.; Zhou, H.; Li, J.; Gao, G.; Guo, Y.; Yan, C.; et al. Mutation in CUL4B, which encodes a member of cullin-RING ubiquitin ligase complex, causes X-linked mental retardation. *Am. J. Hum. Genet.* **2007**, *80*, 561–566, doi:10.1086/512489.

92. Cabezas, D.A.; Slaugh, R.; Abidi, F.; Arena, J.F.; Stevenson, R.E.; Schwartz, C.E.; Lubs, H.A. A new X linked mental retardation (XLMR) syndrome with short stature, small testes, muscle wasting, and tremor localises to Xq24-q25. *J. Med. Genet.* **2000**, *37*, 663–668, doi:10.1136/jmg.37.9.663.

93. Zhou, Z.; Song, X.; Wavelet, C.M.; Wan, Y. Cullin 4-DCAF proteins in tumorigenesis. *Adv. Exp. Med. Biol.* **2020**, *1217*, 241–259, doi:10.1007/978-981-15-1025-0_15.

94. Mangino, M.; Christiansen, L.; Stone, R.; Hunt, S.C.; Horvath, K.; Eisenberg, D.T.A.; Kimura, M.; Petersen, I.; Kark, J.D.; Herbig, U.; et al. DCAF4, a novel gene associated with leucocyte telomere length. *J. Med. Genet.* **2015**, *52*, 157–162, doi:10.1136/jmedgenet-2014-102681.

95. Liu, H.; Lu, W.; He, H.; Wu, J.; Zhang, C.; Gong, H.; Yang, C. Inflammation-dependent overexpression of c-Myc enhances $CRL4^{DCAF4}$ E3 ligase activity and promotes ubiquitination of ST7 in colitis-associated cancer. *J. Pathol.* **2019**, *248*, 464–475, doi:10.1002/path.5273.

96. Homma, K.; Takahashi, H.; Tsuburaya, N.; Naguro, I.; Fujisawa, T.; Ichijo, H. Genome-wide siRNA screening reveals that DCAF4-mediated ubiquitination of optineurin stimulates autophagic degradation of Cu,Zn-superoxide dismutase. *J. Biol. Chem.* **2020**, *295*, 3148–3158, doi:10.1074/jbc.RA119.010239.

97. Yu, Y.T.; Meier, U.T. RNA-guided isomerization of uridine to pseudouridine — pseudouridylation. *RNA Biol.* **2014**, *11*, 1483–1494, doi:10.4161/15476286.2014.972855.

98. Mitchell, J.R.; Cheng, J.; Collins, K. A Box H/ACA small nucleolar RNA-like domain at the human telomerase RNA 3' end. *Mol. Cell. Biol.* **1999**, *19*, 567–576, doi:10.1128/mcb.19.1.567.

99. Fong, Y.W.; Ho, J.J.; Inouye, C.; Tjian, R. The dyskerin ribonucleoprotein complex as an OCT4/SOX2 coactivator in embryonic stem cells. *Elife* **2014**, *3*, e03573, doi:10.7554/ eLife.03573.

100. Jiang, W.; Middleton, K.; Yoon, H.J.; Fouquet, C.; Carbon, J. An essential yeast protein, CBF5p, binds in vitro to centromeres and microtubules. *Mol. Cell. Biol.* **1993**, *13*, 4884–4893, doi:10.1128/mcb.13.8.4884-4893.1993.

101. He, J.; Navarrete, S.; Jasinski, M.; Vulliamy, T.; Dokal, I.; Bessler, M.; Mason, P.J. Targeted disruption of Dkc1, the gene mutated in X-linked dyskeratosis congenita, causes embryonic lethality in mice. *Oncogene* **2002**, *21*, 7740–7744, doi:10.1038/sj.onc.1205969.

102. Heiss, N.S.; Knight, S.W.; Vulliamy, T.J.; Klauck, S.M.; Wiemann, S.; Mason, P.J.; Poustka, A.; Dokal, I. X-linked dyskeratosis congenita is caused by mutations in a highly conserved gene with putative nucleolar functions. *Nat. Genet.* **1998**, *19*, 32–38, doi:10.1038/ng0598-32.

103. Ganot, P.; Caizergues-Ferrer, M.; Kiss, T. The family of box ACA small nucleolar RNAs is defined by an evolutionarily conserved secondary structure and ubiquitous sequence elements essential for RNA accumulation. *Genes Dev.* **1997**, *11*, 941–956, doi:10.1101/gad.11.7.941.

104. Balakin, A.G.; Smith, L.; Fournier, M.J. The RNA world of the nucleolus: two major families of small RNAs defined by different box elements with related functions. *Cell* **1996**, *86*, 823–834, doi:10.1016/s0092-8674(00)80156-7.

105. Tang, T.H.; Bachellerie, J.P.; Rozhdestvensky, T.; Bortolin, M.L.; Huber, H.; Drungowski, M.; Elge, T.; Brosius, J.; Hüttenhofer, A. Identification of 86 candidates for small non-messenger RNAs from the archaeon *Archaeoglobus fulgidus*. *Proc. Natl. Acad. Sci. U. S. A.* **2002**, *99*, 7536–7541, doi:10.1073/pnas.112047299.

106. Ganot, P.; Bortolin, M.L.; Kiss, T. Site-specific pseudouridine formation in preribosomal RNA is guided by small nucleolar RNAs. *Cell* **1997**, *89*, 799–809, doi:10.1016/S0092-8674(00)80263-9.

107. Wang, P.; Malumbres, M.; Archambault, V. The greatwall-PP2A axis in cell cycle control. *Methods Mol. Biol.* **2014**, *1170*, 99–111, doi:10.1007/978-1-4939-0888-2_6.

108. Kiss, T.; Fayet-Lebaron, E.; Jády, B.E. Box H/ACA small ribonucleoproteins. *Mol. Cell* **2010**, *37*, 597–606, doi:10.1016/j.molcel.2010.01.032.

109. Darzacq, X.; Jády, B.E.; Verheggen, C.; Kiss, A.M.; Bertrand, E.; Kiss, T. Cajal body-specific small nuclear RNAs: a novel class of 2'-O-methylation and pseudouridylation guide RNAs. *EMBO J.* **2002**, *21*, 2746–2756, doi:10.1093/emboj/21.11.2746.

110. Kiss, A.M.; Jády, B.E.; Bertrand, E.; Kiss, T. Human box H/ACA pseudouridylation guide RNA machinery. *Mol. Cell. Biol.* **2004**, *24*, 5797–5807, doi:10.1128/MCB.24.13.5797-5807.2004.

111. Richard, P.; Darzacq, X.; Bertrand, E.; Jády, B.E.; Verheggen, C.; Kiss, T. A common sequence motif determines the Cajal body-specific localization of box H/ACA scaRNAs. *EMBO J.* **2003**, *22*, 4283–4293, doi:10.1093/emboj/cdg394.

112. Venteicher, A.S.; Abreu, E.B.; Meng, Z.; McCann, K.E.; Terns, R.M.; Veenstra, T.D.; Terns, M.P.; Artandi, S.E. A human telomerase holoenzyme protein required for Cajal body localization and telomere synthesis. *Science* **2009**, *323*, 644–648, doi:10.1126/science.1165357.

113. Tycowski, K.T.; Shu, M. Di; Kukoyi, A.; Steitz, J.A. A conserved WD40 protein binds the cajal body localization signal of scaRNP particles. *Mol. Cell* **2009**, *34*, 47–57, doi:10.1016/j.molcel. 2009.02.020.

114. Mitchell, J.R.; Collins, K. Human telomerase activation requires two independent interactions between telomerase RNA and telomerase reverse transcriptase. *Mol. Cell* **2000**, *6*, 361–371, doi:10.1016/S1097-2765(00)00036-8.

115. Martín-Rivera, L.; Blasco, M.A. Identification of functional domains and dominant negative mutations in vertebrate telomerase RNA using an in vivo reconstitution system. *J. Biol. Chem.* **2001**, *276*, 5856–5865, doi:10.1074/jbc.M008419200.

116. Fu, D.; Collins, K. Distinct biogenesis pathways for human telomerase RNA and H/ACA small nucleolar RNAs. *Mol. Cell* **2003**, *11*, 1361–1372, doi:10.1016/S1097-2765(03)00196-5.

117. Jády, B.E.; Bertrand, E.; Kiss, T. Human telomerase RNA and box H/ACA scaRNAs share a common Cajal body-specific localization signal. *J. Cell Biol.* **2004**, *164*, 647–652, doi:10.1083/jcb.200310138.

118. Theimer, C.A.; Jády, B.E.; Chim, N.; Richard, P.; Breece, K.E.; Kiss, T.; Feigon, J. Structural and functional characterization of human telomerase RNA processing and Cajal body localization signals. *Mol. Cell* **2007**, *27*, 869–881, doi:10.1016/j.molcel.2007.07.017.

119. Egan, E.D.; Collins, K. An enhanced H/ACA RNP assembly mechanism for human telomerase RNA. *Mol. Cell. Biol.* **2012**, *32*, 2428–2439, doi:10.1128/mcb.00286-12.

120. Jády, B.E.; Ketele, A.; Kiss, T. Human intron-encoded Alu RNAs are processed and packaged into Wdr79-associated nucleoplasmic box H/ACA RNPs. *Genes Dev.* **2012**, *26*, 1897–1910, doi:10.1101/gad.197467.112.

121. Ketele, A.; Kiss, T.; Jády, B.E. Human intron-encoded AluACA RNAs and telomerase RNA share a common element promoting RNA accumulation. *RNA Biol.* **2016**, *13*, 1274–1285, doi:10.1080/15476286.2016.1239689.

122. Henras, A.; Henry, Y.; Bousquet-Antonelli, C.; Noaillac-Depeyre, J.; Gélugne, J.P.; Caizergues-Ferrer, M. Nhp2p and Nop10p are essential for the function of H/ACA snoRNPs. *EMBO J.* **1998**, *17*, 7078–7090, doi:10.1093/emboj/17.23.7078.

123. Watkins, N.J.; Gottschalk, A.; Neubauer, G.; Kastner, B.; Fabrizio, P.; Mann, M.; Lührmann, R. Cbf5p, a potential pseudouridine synthase, and Nhp2p, a putative RNA-binding protein, are present together with Gar1p in all H BOX/ACA-motif snoRNPs and constitute a common bipartite structure. *RNA* **1998**, *4*, 1549–1568, doi:10.1017/s1355838298980761.

124. Rozhdestvensky, T.S.; Tang, T.H.; Tchirkova, I. V.; Brosius, J.; Bachellerie, J.P.; Hüttenhofer, A. Binding of L7Ae protein to the K-turn of archaeal snoRNAs: a shared RNA binding motif for C/D and H/ACA box snoRNAs in Archaea. *Nucleic Acids Res.* **2003**, *31*, 869–877, doi:10.1093/nar/gkg175.

125. Pogacic, V.; Dragon, F.; Filipowicz, W. Human H/ACA small nucleolar RNPs and telomerase share evolutionarily conserved proteins NHP2 and NOP10. *Mol. Cell. Biol.* **2000**, *20*, 9028–9040, doi:10.1007/978-3-319-24789-2.

126. Lafontaine, D.L.J.; Bousquet-Antonelli, C.; Henry, Y.; Caizergues-Ferrer, M.; Tollervey, D. The box H + ACA snoRNAs carry Cbf5p, the putative rRNA pseudouridine synthase. *Genes Dev.* **1998**, *12*, 527–537, doi:10.1101/gad.12.4.527.

127. Hamma, T.; Ferré-D'Amaré, A.R. Pseudouridine synthases. *Chem. Biol.* **2006**, *13*, 1125–1135, doi:10.1016/j.chembiol.2006.09.009.

128. Baker, D.L.; Youssef, O.A.; Chastkofsky, M.I.R.; Dy, D.A.; Terns, R.M.; Terns, M.P. RNA-guided RNA modification: functional organization of the archaeal H/ACA RNP. *Genes Dev.* **2005**, *19*, 1238–1248, doi:10.1101/gad.1309605.

129. Charpentier, B.; Muller, S.; Branlant, C. Reconstitution of archaeal H/ACA small ribonucleoprotein complexes active in pseudouridylation. *Nucleic Acids Res.* **2005**, *33*, 3133–3144, doi:10.1093/nar/gki630.

130. Li, S.; Duan, J.; Li, D.; Yang, B.; Dong, M.; Ye, K. Reconstitution and structural analysis of the yeast box H/ACA RNA-guided pseudouridine synthase. *Genes Dev.* **2011**, *25*, 2409–2421, doi:10.1101/gad.175299.111.

131. Caton, E.A.; Kelly, E.K.; Kamalampeta, R.; Kothe, U. Efficient RNA pseudouridylation by eukaryotic H/ACA ribonucleoproteins requires high affinity binding and correct positioning of guide RNA. *Nucleic Acids Res.* **2018**, *46*, 905–916, doi:10.1093/nar/gkx1167.

132. Hamma, T.; Reichow, S.L.; Varani, G.; Ferré-D'Amaré, A.R. The Cbf5-Nop10 complex is a molecular bracket that organizes box H/ACA RNPs. *Nat. Struct. Mol. Biol.* **2005**, *12*, 1101–1107, doi:10.1038/nsmb1036.

133. Rashid, R.; Liang, B.; Baker, D.L.; Youssef, O.A.; He, Y.; Phipps, K.; Terns, R.M.; Terns, M.P.; Li, H. Crystal structure of a Cbf5-Nop10-Gar1 complex and implications in RNA-guided pseudouridylation and dyskeratosis congenita. *Mol. Cell* **2006**, *21*, 249–260, doi:10.1016/j.molcel.2005.11.017.

134. Li, L.; Ye, K. Crystal structure of an H/ACA box ribonucleoprotein particle. *Nature* **2006**, *443*, 302–307, doi:10.1038/nature05151.

135. Liang, B.; Xue, S.; Terns, R.M.; Terns, M.P.; Li, H. Substrate RNA positioning in the archaeal H/ACA ribonucleoprotein complex. *Nat. Struct. Mol. Biol.* **2007**, *14*, 1189–1195, doi:10.1038/nsmb1336.

136. Liang, B.; Zhou, J.; Kahen, E.; Terns, R.M.; Terns, M.P.; Li, H. Structure of a functional ribonucleoprotein pseudouridine synthase bound to a substrate RNA. *Nat. Struct. Mol. Biol.* **2009**, *16*, 740–746, doi:10.1038/nsmb.1624.

137. Duan, J.; Li, L.; Lu, J.; Wang, W.; Ye, K. Structural mechanism of substrate RNA recruitment in H/ACA RNA-guided pseudouridine synthase. *Mol. Cell* **2009**, *34*, 427–439, doi:10.1016/j.molcel.2009.05.005.

138. Nguyen, T.H.D.; Tam, J.; Wu, R.A.; Greber, B.J.; Toso, D.; Nogales, E.; Collins, K. Cryo-EM structure of substrate-bound human telomerase holoenzyme. *Nature* **2018**, *557*, 190–195, doi:10.1038/s41586-018-0062-x.

139. Ghanim, G.E.; Fountain, A.J.; van Roon, A.M.M.; Rangan, R.; Das, R.; Collins, K.; Nguyen, T.H.D. Structure of human telomerase holoenzyme with bound telomeric DNA. *Nature* **2021**, *593*, 449–453, doi:10.1038/s41586-021-03415-4.

140. Dez, C.; Noaillac-Depeyre, J.; Caizergues-Ferrer, M.; Henry, Y. Naf1p, an essential nucleoplasmic factor specifically required for accumulation of box H/ACA small nucleolar RNPs. *Mol. Cell. Biol.* **2002**, *22*, 7053–7065, doi:10.1128/mcb.22.20.7053-7065.2002.

141. Fatica, A.; Dlakić, M.; Tollervey, D. Naf1p is a box H/ACA snoRNP assembly factor. *RNA* **2002**, *8*, 1502–1514, doi:10.1017/S1355838202022094.

142. Yang, P.K.; Rotondo, G.; Porras, T.; Legrain, P.; Chanfreau, G. The Shq1p·Naf1p complex is required for box H/ACA small nucleolar ribonucleoprotein particle biogenesis. *J. Biol. Chem.* **2002**, *277*, 45235–45242, doi:10.1074/jbc.M207669200.

143. Schattner, P.; Barberan-Soler, S.; Lowe, T.M. A computational screen for mammalian pseudouridylation guide H/ACA RNAs. *RNA* **2006**, *12*, 15–25, doi:10.1261/rna.2210406.

144. Li, S.; Duan, J.; Li, D.; Ma, S.; Ye, K. Structure of the Shq1-Cbf5-Nop10-Gar1 complex and implications for H/ACA RNP biogenesis and dyskeratosis congenita. *EMBO J.* **2011**, *30*, 5010–5020, doi:10.1038/emboj.2011.427.

145. Walbott, H.; Machado-Pinilla, R.; Liger, D.; Blaud, M.; Réty, S.; Grozdanov, P.N.; Godin, K.; van Tilbeurgh, H.; Varani, G.; Meier, U.T.; et al. The H/ACA RNP assembly factor SHQ1 functions as an RNA mimic. *Genes Dev.* **2011**, *25*, 2398–2408, doi:10.1101/gad.176834.111.

146. Grozdanov, P.N.; Roy, S.; Kittur, N.; Meier, U.T. SHQ1 is required prior to NAF1 for assembly of H/ACA small nucleolar and telomerase RNPs. *RNA* **2009**, *15*, 1188–1197, doi:10.1261/rna.1532109.

147. Machado-Pinilla, R.; Liger, D.; Leulliot, N.; Meier, U.T. Mechanism of the AAA+ ATPases pontin and reptin in the biogenesis of H/ACA RNPs. *RNA* **2012**, *18*, 1833–1845, doi:10.1261/rna.034942.112.

148. Yang, P.K.; Hoareau, C.; Froment, C.; Monsarrat, B.; Henry, Y.; Chanfreau, G. Cotranscriptional recruitment of the pseudouridylsynthetase Cbf5p and of the RNA binding protein Naf1p during H/ACA snoRNP assembly. *Mol. Cell. Biol.* **2005**, *25*, 3295–3304, doi:10.1128/MCB.25.8.3295-3304.2005.

149. Ballarino, M.; Morlando, M.; Pagano, F.; Fatica, A.; Bozzoni, I. The cotranscriptional assembly of snoRNPs controls the biosynthesis of H/ACA snoRNAs in *Saccharomyces cerevisiae*. *Mol. Cell. Biol.* **2005**, *25*, 5396–5403, doi:10.1128/MCB.25.13.5396-5403.2005.

150. Darzacq, X.; Kittur, N.; Roy, S.; Shav-Tal, Y.; Singer, R.H.; Meier, U.T. Stepwise RNP assembly at the site of H/ACA RNA transcription in human cells. *J. Cell Biol.* **2006**, *173*, 207–218, doi:10.1083/jcb.200601105.

151. Richard, P.; Kiss, A.M.; Darzacq, X.; Kiss, T. Cotranscriptional recognition of human intronic box H/ACA snoRNAs occurs in a splicing-independent manner. *Mol. Cell. Biol.* **2006**, *26*, 2540–2549, doi:10.1128/MCB.26.7.2540-2549.2006.

152. Leulliot, N.; Godin, K.S.; Hoareau-Aveilla, C.; Quevillon-Cheruel, S.; Varani, G.; Henry, Y.; Van Tilbeurgh, H. The box H/ACA RNP assembly factor Naf1p contains a domain homologous to Gar1p mediating its interaction with Cbf5p. *J. Mol. Biol.* **2007**, *371*, 1338–1353, doi:10.1016/j.jmb.2007.06.031.

153. Schwartz, S.; Bernstein, D.A.; Mumbach, M.R.; Jovanovic, M.; Herbst, R.H.; León-Ricardo, B.X.; Engreitz, J.M.; Guttman, M.; Satija, R.; Lander, E.S.; et al. Transcriptome-wide mapping reveals widespread dynamic-regulated pseudouridylation of ncRNA and mRNA. *Cell* **2014**, *159*, 148–162, doi:10.1016/j.cell.2014.08.028.

154. Carlile, T.M.; Rojas-Duran, M.F.; Zinshteyn, B.; Shin, H.; Bartoli, K.M.; Gilbert, W. V. Pseudouridine profiling reveals regulated mRNA pseudouridylation in yeast and human cells. *Nature* **2014**, *515*, 143–146, doi:10.1038/nature13802.

155. Lovejoy, A.F.; Riordan, D.P.; Brown, P.O. Transcriptome-wide mapping of pseudouridines: pseudouridine synthases modify specific mRNAs in *S. cerevisiae*. *PLoS One* **2014**, *9*, e110799, doi:10.1371/journal.pone.0110799.

156. Zebarjadian, Y.; King, T.; Fournier, M.J.; Clarke, L.; Carbon, J. Point mutations in yeast *CBF5* can abolish in vivo pseudouridylation of rRNA. *Mol. Cell. Biol.* **1999**, *19*, 7461–7472, doi:10.1128/MCB.19.11.7461.

157. Gu, B.W.; Ge, J.; Fan, J.M.; Bessler, M.; Mason, P.J. Slow growth and unstable ribosomal RNA lacking pseudouridine in mouse embryonic fibroblast cells expressing catalytically inactive dyskerin. *FEBS Lett.* **2013**, *587*, 2112–2117, doi:10.1016/j.febslet.2013.05.028.

158. King, T.H.; Liu, B.; McCully, R.R.; Fournier, M.J. Ribosome structure and activity are altered in cells lacking snoRNPs that form pseudouridines in the peptidyl transferase center. *Mol. Cell* **2003**, *11*, 425–435, doi:10.1016/S1097-2765(03)00040-6.

159. Badis, G.; Fromont-Racine, M.; Jacquier, A. A snoRNA that guides the two most conserved pseudouridine modifications within rRNA confers a growth advantage in yeast. *RNA* **2003**, *9*, 771–779, doi:10.1261/rna.5240503.

160. Liang, X. hai; Liu, Q.; Fournier, M.J. rRNA modifications in an intersubunit bidge of the ribosome strongly affect both ribosome biogenesis and activity. *Mol. Cell* **2007**, *28*, 965–977, doi:10.1016/j.molcel.2007.10.012.

161. Liang, X.-H.; Liu, Q.; Fournier, M.J. Loss of rRNA modifications in the decoding center of the ribosome impairs translation and strongly delays pre-rRNA processing. *RNA* **2009**, *15*, 1716–1728, doi:10.1261/rna.1724409.

162. Jack, K.; Bellodi, C.; Landry, D.M.; Niederer, R.O.; Meskauskas, A.; Musalgaonkar, S.; Kopmar, N.; Krasnykh, O.; Dean, A.M.; Thompson, S.R.; et al. RRNA Pseudouridylation defects affect ribosomal ligand binding and translational fidelity from yeast to human cells. *Mol. Cell* **2011**, *44*, 660–666, doi:10.1016/j.molcel.2011.09.017.

163. Yoon, A.; Peng, G.; Brandenburg, Y.; Zollo, O.; Xu, W.; Rego, E.; Ruggero, D. Impaired control of IRES-mediated translation in X-linked dyskeratosis congenita. *Science* **2006**, *312*, 902–906, doi:10.1126/science.1123835.

164. Bellodi, C.; Kopmar, N.; Ruggero, D. Deregulation of oncogene-induced senescence and p53 translational control in X-linked dyskeratosis congenita. *EMBO J.* **2010**, *29*, 1865–1876, doi:10.1038/emboj.2010.83.

165. Bellodi, C.; Krasnykh, O.; Haynes, N.; Theodoropoulou, M.; Peng, G.; Montanaro, L.; Ruggero, D. Loss of function of the tumor suppressor DKC1 perturbs p27 translation control and contributes to pituitary tumorigenesis. *Cancer Res.* **2010**, *70*, 6026–6035, doi:10.1158/0008-5472.CAN-09-4730.

166. Ruggero, D.; Grisendi, S.; Piazza, F.; Rego, E.; Mari, F.; Rao, P.H.; Cordon-Cardo, C.; Pandolfi, P.P. Dyskeratosis congenita and cancer in mice deficient in ribosomal RNA modification. *Science* **2003**, *299*, 259–262, doi:10.1126/science.1079447.

167. Zhao, X.; Li, Z.-H.; Terns, R.M.; Terns, M.P.; Yu, Y.-T. An H/ACA guide RNA directs U2 pseudouridylation at two different sites in the branchpoint recognition region in *Xenopus* oocytes. *RNA* **2002**, *8*, 1515–1525, doi:10.1017/S1355838202022537.

168. Zhao, X.; Yu, Y.T. Pseudouridines in and near the branch site recognition region of U2 snRNA are required for snRNP biogenesis and pre-mRNA splicing in *Xenopus* oocytes. *RNA* **2004**, *10*, 681–690, doi:10.1261/rna.5159504.

169. Dönmez, G.; Hartmuth, K.; Lührmann, R. Modified nucleotides at the 5′ end of human U2 snRNA are required for spliceosomal E-complex formation. *RNA* **2004**, *10*, 1925–1933, doi:10.1261/rna.7186504.

170. Roake, C.M.; Artandi, S.E. Regulation of human telomerase in homeostasis and disease. *Nat. Rev. Mol. Cell Biol.* **2020**, *21*, 384–397, doi:10.1038/s41580-020-0234-z.

171. Mitchell, J.R.; Wood, E.; Collins, K. A telomerase component is defective in the human disease dyskeratosis congenita. *Nature* **1999**, *402*, 551–555, doi:10.1038/990141.

172. Batista, L.F.Z.; Pech, M.F.; Zhong, F.L.; Nguyen, H.N.; Xie, K.T.; Zaug, A.J.; Crary, S.M.; Choi, J.; Sebastiano, V.; Cherry, A.; et al. Telomere shortening and loss of self-renewal in dyskeratosis congenita induced pluripotent stem cells. *Nature* **2011**, *474*, 399–402, doi:10.1038/nature10084.

173. Vulliamy, T.; Beswick, R.; Kirwan, M.; Marrone, A.; Digweed, M.; Walne, A.; Dokal, I. Mutations in the telomerase component NHP2 cause the premature ageing syndrome dyskeratosis congenita. *Proc. Natl. Acad. Sci. U. S. A.* **2008**, *105*, 8073–8078, doi:10.1073/pnas.0800042105.

174. Vulliamy, T.; Marrone, A.; Goldman, F.; Dearlove, A.; Bessler, M.; Mason, P.J.; Dokal, I. The RNA component of telomerase is mutated in autosomal dominant dyskeratosis congenita. *Nature* **2001**, *413*, 432–435, doi:10.1038/35096585.

175. Dokal, I. Dyskeratosis congenita in all its forms. *Br. J. Haematol.* **2000**, *110*, 768–779, doi: 10.1046/j.1365-2141.2000.02109.x.

176. Sarek, G.; Marzec, P.; Margalef, P.; Boulton, S.J. Molecular basis of telomere dysfunction in human genetic diseases. *Nat. Struct. Mol. Biol.* **2015**, *22*, 867–874, doi:10.1038/nsmb.3093.

177. Egan, E.D.; Collins, K. An enhanced H/ACA RNP assembly mechanism for human telomerase RNA. *Mol. Cell. Biol.* **2012**, *32*, 2428–2439, doi:10.1128/MCB.00286-12.

178. Fok, W.C.; Niero, E.L. de O.; Dege, C.; Brenner, K.A.; Sturgeon, C.M.; Batista, L.F.Z. p53 mediates failure of human definitive hematopoiesis in dyskeratosis congenita. *Stem Cell Reports* **2017**, *9*, 409–418, doi:10.1016/j.stemcr.2017.06.015.

179. Hwangbo, D.S.; Biteau, B.; Rath, S.; Kim, J.; Jasper, H. Control of apoptosis by *Drosophila* DCAF12. *Dev. Biol.* **2016**, *413*, 50–59, doi:10.1016/j.ydbio.2016.03.003.

180. Hwangbo Laboratory. Research. Available online: www.hwangbo-lab.org/ research-2. Accessed on 17.11.2021.

181. Leulier, F.; Lhocine, N.; Lemaitre, B.; Meier, P. The *Drosophila* inhibitor of apoptosis protein DIAP2 functions in innate immunity and is essential to resist gram-negative bacterial infection. *Mol. Cell. Biol.* **2006**, *26*, 7821–7831, doi:10.1128/mcb.00548-06.

182. Cho, Y.S.; Li, S.; Wang, X.; Zhu, J.; Zhuo, S.; Han, Y.; Yue, T.; Yang, Y.; Jiang, J. CDK7 regulates organ size and tumor growth by safeguarding the Hippo pathway effector Yki/Yap/Taz in the nucleus. *Genes Dev.* **2020**, *34*, 53–71, doi:10.1101/gad.333146.119.

183. Patrón, L.A.; Nagatomo, K.; Eves, D.T.; Imad, M.; Young, K.; Torvund, M.; Guo, X.; Rogers, G.C.; Zinsmaier, K.E. Cul4 ubiquitin ligase cofactor DCAF12 promotes neurotransmitter release and homeostatic plasticity. *J. Cell Biol.* **2019**, *218*, 993–1010, doi:10.1083/jcb.201805099.

184. Zou, X.D.; Hu, X.J.; Ma, J.; Li, T.; Ye, Z.Q.; Wu, Y.D. Genome-wide analysis of WD40 protein family in human. *Sci. Rep.* **2016**, *6*, 39262, doi:10.1038/srep39262.

185. Szcześniak, M.W.; Ciomborowska, J.; Nowak, W.; Rogozin, I.B.; Makałowska, I. Primate and rodent specific intron gains and the origin of retrogenes with splice variants. *Mol. Biol. Evol.* **2011**, *28*, 33–37, doi:10.1093/molbev/msq260.

186. Ravichandran, R.; Kodali, K.; Peng, J.; Potts, P.R. Regulation of MAGE-A3/6 by the CRL4-DCAF12 ubiquitin ligase and nutrient availability. *EMBO Rep.* **2019**, *20*, e47352, doi:10.15252/ embr.201847352.

187. Gyrd-Hansen, M.; Meier, P. IAPs: From caspase inhibitors to modulators of NF-κB, inflammation and cancer. *Nat. Rev. Cancer* **2010**, *10*, 561–574, doi:10.1038/nrc2889.

188. Wilson, R.; Goyal, L.; Ditzel, M.; Zachariou, A.; Baker, D.A.; Agapite, J.; Steller, H.; Meier, P. The DIAP1 RING finger mediates ubiquitination of Dronc and is indispensable for regulating apoptosis. *Nat. Cell Biol.* **2002**, *4*, 445–450, doi:10.1038/ncb799.

189. Chai, J.; Yan, N.; Huh, J.R.; Wu, J.W.; Li, W.; Hay, B.A.; Shi, Y. Molecular mechanism of Reaper-Grim-Hid-mediated suppression of DIAP1-dependent Dronc ubiquitination. *Nat. Struct. Biol.* **2003**, *10*, 892–898, doi:10.1038/nsb989.

190. Yan, N.; Wu, J.W.; Chai, J.; Li, W.; Shi, Y. Molecular mechanisms of DrICE inhibition by DIAP1 and removal of inhibition by Reaper, Hid and Grim. *Nat. Struct. Mol. Biol.* **2004**, *11*, 420–428, doi:10.1038/nsmb764.

191. Shapiro, P.J.; Hsu, H.H.; Jung, H.; Robbins, E.S.; Ryoo, H.D. Regulation of the *Drosophila* apoptosome through feedback inhibition. *Nat. Cell Biol.* **2008**, *10*, 1440–1446, doi:10.1038/ncb1803.

192. Paquette, N.; Broemer, M.; Aggarwal, K.; Chen, L.; Husson, M.; Ertürk-Hasdemir, D.; Reichhart, J.-M.; Meier, P.; Silverman, N. Caspase-mediated cleavage, IAP binding, and ubiquitination: linking three mechanisms crucial for *Drosophila* NF-kappaB signaling. *Mol. Cell* **2010**, *37*, 172–182, doi:10.1016/j.molcel.2009.12.036.

193. Huh, J.R.; Foe, I.; Muro, I.; Chen, C.H.; Seol, J.H.; Yoo, S.J.; Guo, M.; Park, J.M.; Hay, B.A. The *Drosophila* inhibitor of apoptosis (IAP) DIAP2 is dispensable for cell survival, required for the innate immune response to gram-negative bacterial infection, and can be negatively regulated by the Reaper/Hid/Grim family of IAP-binding apoptosis inducers. *J. Biol. Chem.* **2007**, *282*, 2056–2068, doi:10.1074/jbc.M608051200.

194. Christich, A.; Kauppila, S.; Chen, P.; Sogame, N.; Ho, S.I.; Abrams, J.M. The damage-responsive *Drosophila* gene sickle encodes a novel IAP binding protein similar to but distinct from Reaper, Grim, and Hid. *Curr. Biol.* **2002**, *12*, 137–140, doi:10.1016/S0960-9822(01)00658-3.

195. Tenev, T.; Zachariou, A.; Wilson, R.; Paul, A.; Meier, P. Jafrac2 is an IAP antagonist that promotes cell death by liberating Dronc from DIAP1. *EMBO J.* **2002**, *21*, 5118–5129, doi:10.1093/emboj/cdf530.

196. Challa, M.; Malladi, S.; Pellock, B.J.; Dresnek, D.; Varadarajan, S.; Yin, Y.W.; White, K.; Bratton, S.B. *Drosophila* Omi, a mitochondrial-localized IAP antagonist and proapoptotic serine protease. *EMBO J.* **2007**, *26*, 3144–3156, doi:10.1038/sj.emboj.7601745.

197. White, K.; Grether, M.E.; Abrams, J.M.; Young, L.; Farrell, K.; Steller, H. Genetic control of programmed cell death in *Drosophila*. *Science* **1994**, *264*, 677–83, doi:10.1126/science.8171319.

198. Chen, P.; Nordstrom, W.; Gish, B.; Abrams, J.M. grim, a novel cell death gene in *Drosophila*. *Genes Dev.* **1996**, *10*, 1773–1782, doi:10.1101/gad.10.14.1773.

199. Grether, M.E.; Abrams, J.M.; Agapite, J.; White, K.; Steller, H. The head involution defective gene of *Drosophila melanogaster* functions in programmed cell death. *Genes Dev.* **1995**, *9*, 1694–1708, doi:10.1101/gad.9.14.1694.

200. Lopez, J.; John, S.W.; Tenev, T.; Rautureau, G.J.P.; Hinds, M.G.; Francalanci, F.; Wilson, R.; Broemer, M.; Santoro, M.M.; Day, C.L.; et al. CARD-mediated autoinhibition of cIAP1's E3 ligase activity suppresses cell proliferation and migration. *Mol. Cell* **2011**, *42*, 569–583, doi:10.1016/j.molcel.2011.04.008.

201. Eckelman, B.P.; Salvesen, G.S.; Scott, F.L. Human inhibitor of apoptosis proteins: why XIAP is the black sheep of the family. *EMBO Rep.* **2006**, *7*, 988–994, doi:10.1038/sj.embor.7400795.

202. Estornes, Y.; Bertrand, M.J.M. IAPs, regulators of innate immunity and inflammation. *Semin. Cell Dev. Biol.* **2015**, *39*, 106–114, doi:10.1016/j.semcdb.2014.03.035.

203. Hanson, A.J.; Wallace, H.A.; Freeman, T.J.; Beauchamp, R.D.; Lee, L.A.; Lee, E. XIAP monoubiquitylates Groucho/TLE to promote canonical Wnt signaling. *Mol. Cell* **2012**, *45*, 619–628, doi:10.1016/j.molcel.2011.12.032.

204. Huang, X.; Wu, Z.; Mei, Y.; Wu, M. XIAP inhibits autophagy via XIAP-Mdm2-p53 signalling. *EMBO J.* **2013**, *32*, 2204–2216, doi:10.1038/emboj.2013.133.

205. Mufti, A.R.; Burstein, E.; Csomos, R.A.; Graf, P.C.F.; Wilkinson, J.C.; Dick, R.D.; Challa, M.; Son, J.K.; Bratton, S.B.; Su, G.L.; et al. XIAP is a copper binding protein deregulated in Wilson's disease and other copper toxicosis disorders. *Mol. Cell* **2006**, *21*, 775–785, doi:10.1016/j.molcel.2006.01.033.

206. Burstein, E.; Ganesh, L.; Dick, R.D.; Van De Sluis, B.; Wilkinson, J.C.; Klomp, L.W.J.; Wijmenga, C.; Brewer, G.J.; Nabel, G.J.; Duckett, C.S. A novel role for XIAP in copper homeostasis through regulation of MURR1. *EMBO J.* **2004**, *23*, 244–254, doi:10.1038/sj.emboj.7600031.

207. Liao, Y.; Zhao, J.; Bulek, K.; Tang, F.; Chen, X.; Cai, G.; Jia, S.; Fox, P.L.; Huang, E.; Pizarro, T.T.; et al. Inflammation mobilizes copper metabolism to promote colon tumorigenesis via an IL-17-STEAP4-XIAP axis. *Nat. Commun.* **2020**, *11*, 900, doi:10.1038/s41467-020-14698-y.

208. Du, C.; Fang, M.; Li, Y.; Li, L.; Wang, X. Smac, a mitochondrial protein that promotes cytochrome c-dependent caspase activation by eliminating IAP inhibition. *Cell* **2000**, *102*, 33–42, doi:10.1016/S0092-8674(00)00008-8.

209. Verhagen, A.M.; Ekert, P.G.; Pakusch, M.; Silke, J.; Connolly, L.M.; Reid, G.E.; Moritz, R.L.; Simpson, R.J.; Vaux, D.L. Identification of DIABLO, a mammalian protein that promotes apoptosis by binding to and antagonizing IAP proteins. *Cell* **2000**, *102*, 43–53, doi:10.1016/S0092-8674(00)00009-X.

210. Saita, S.; Nolte, H.; Fiedler, K.U.; Kashkar, H.; Saskia, A.V.; Zahedi, R.P.; Krüger, M.; Langer, T. PARL mediates Smac proteolytic maturation in mitochondria to promote apoptosis. *Nat. Cell Biol.* **2017**, *19*, 318–328, doi:10.1038/ncb3488.

211. Chai, J.; Du, C.; Wu, J.W.; Kyin, S.; Wang, X.; Shi, Y. Structural and biochemical basis of apoptotic activation by Smac/DIABLO. *Nature* **2000**, *406*, 855–862, doi:10.1038/35022514.

212. Wu, G.; Chai, J.; Suber, T.L.; Wu, J.W.; Du, C.; Wang, X.; Shi, Y. Structural basis of IAP recognition by Smac/DIABLO. *Nature* **2000**, *408*, 1008–1012, doi:10.1038/35050012.

213. Liu, Z.; Sun, C.; Olejniczak, E.T.; Meadows, R.P.; Betz, S.F.; Oost, T.; Herrmann, J.; Wu, J.C.; Fesik, S.W. Structural basis for binding of Smac/DIABLO to the XIAP BIR3 domain. *Nature* **2000**, *408*, 1004–1008, doi:10.1038/35050006.

214. Srinivasula, S.M.; Hegde, R.; Saleh, A.; Datta, P.; Shiozaki, E.; Chai, J.; Lee, R.A.; Robbins, P.D.; Fernandes-Alnemri, T.; Shi, Y.; et al. A conserved XIAP-interaction motif in caspase-9 and Smac/DIABLO regulates caspase activity and apoptosis. *Nature* **2001**, *410*, 112–6, doi:10.1038/35065125.

215. Samuel, T.; Welsh, K.; Lober, T.; Togo, S.H.; Zapata, J.M.; Reed, J.C. Distinct BIR domains of cIAP1 mediate binding to and ubiquitination of tumor necrosis factor receptor-associated factor 2 and second mitochondrial activator of caspases. *J. Biol. Chem.* **2006**, *281*, 1080–1090, doi:10.1074/jbc.M509381200.

216. Vucic, D.; Deshayes, K.; Ackerly, H.; Pisabarro, M.T.; Kadkhodayan, S.; Fairbrother, W.J.; Dixit, V.M. SMAC negatively regulates the anti-apoptotic activity of melanoma inhibitor of apoptosis (ML-IAP). *J. Biol. Chem.* **2002**, *277*, 12275–12279, doi:10.1074/jbc.M112045200.

217. Yang, Q.H.; Du, C. Smac/DIABLO selectively reduces the levels of c-IAP1 and c-IAP2 but not that of XIAP and Livin in HeLa Cells. *J. Biol. Chem.* **2004**, *279*, 16963–16970, doi:10.1074/jbc.M401253200.

218. Roberts, D.L.; Merrison, W.; MacFarlane, M.; Cohen, G.M. The inhibitor of apoptosis protein-binding domain of Smac is not essential for its proapoptotic activity. *J. Cell Biol.* **2001**, *153*, 221–227, doi:10.1083/jcb.153.1.221.

219. Andree, M.; Seeger, J.M.; Schüll, S.; Coutelle, O.; Wagner-Stippich, D.; Wiegmann, K.; Wunderlich, C.M.; Brinkmann, K.; Broxtermann, P.; Witt, A.; et al. BID-dependent release of mitochondrial SMAC dampens XIAP-mediated immunity against *Shigella*. *EMBO J.* **2014**, *33*, 2171–2187, doi:10.15252/embj.201387244.

220. Bock, F.J.; Tait, S.W.G. Mitochondria as multifaceted regulators of cell death. *Nat. Rev. Mol. Cell Biol.* **2020**, *21*, 85–100, doi:10.1038/s41580-019-0173-8.

221. Giampazolias, E.; Zunino, B.; Dhayade, S.; Bock, F.; Cloix, C.; Cao, K.; Roca, A.; Lopez, J.; Ichim, G.; Proïcs, E.; et al. Mitochondrial permeabilization engages NF-κB-dependent anti-tumour activity under caspase deficiency. *Nat. Cell Biol.* **2017**, *19*, 1116–1129, doi:10.1038/ncb3596.

222. Fuchs, Y.; Steller, H. Programmed cell death in animal development and disease. *Cell* **2011**, *147*, 742–758, doi:10.1016/j.cell.2011.10.033.

223. Orzalli, M.H.; Kagan, J.C. Apoptosis and necroptosis as host defense strategies to prevent viral infection. *Trends Cell Biol.* **2017**, *27*, 800–809, doi:10.1016/j.tcb.2017.05.007.

224. Riedl, S.J.; Shi, Y. Molecular mechanisms of caspase regulation during apoptosis. *Nat. Rev. Mol. Cell Biol.* **2004**, *5*, 897–907, doi:10.1038/nrm1496.

225. Van Opdenbosch, N.; Lamkanfi, M. Caspases in cell death, inflammation, and disease. *Immunity* **2019**, *50*, 1352–1364, doi:10.1016/j.immuni.2019.05.020.

226. Seaman, J.E.; Julien, O.; Lee, P.S.; Rettenmaier, T.J.; Thomsen, N.D.; Wells, J.A. Cacidases: Caspases can cleave after aspartate, glutamate and phosphoserine residues. *Cell Death Differ.* **2016**, *23*, 1717–1726, doi:10.1038/cdd.2016.62.

227. Kumar, R.; Herbert, P.E.; Warrens, A.N. An introduction to death receptors in apoptosis. *Int. J. Surg.* **2005**, *3*, 268–277, doi:10.1016/j.ijsu.2005.05.002.

228. Jost, P.J.; Grabow, S.; Gray, D.; McKenzie, M.D.; Nachbur, U.; Huang, D.C.S.; Bouillet, P.; Thomas, H.E.; Borner, C.; Silke, J.; et al. XIAP discriminates between type i and type II FAS-induced apoptosis. *Nature* **2009**, *460*, 1035–1039, doi:10.1038/nature08229.

229. Czabotar, P.E.; Lessene, G.; Strasser, A.; Adams, J.M. Control of apoptosis by the BCL-2 protein family: Implications for physiology and therapy. *Nat. Rev. Mol. Cell Biol.* **2014**, *15*, 49–63, doi:10.1038/nrm3722.

230. Hegde, R.; Srinivasula, S.M.; Zhang, Z.; Wassell, R.; Mukattash, R.; Cilenti, L.; Dubois, G.; Lazebnik, Y.; Zervos, A.S.; Fernandes-Alnemri, T.; et al. Identification of Omi/HtrA2 as a mitochondrial apoptotic serine protease that disrupts inhibitor of apoptosis protein-caspase interaction. *J. Biol. Chem.* **2002**, *277*, 432–438, doi:10.1074/jbc.M109721200.

231. Miguel Martins, L.; Iaccarino, I.; Tenev, T.; Gschmeissner, S.; Totty, N.F.; Lemoine, N.R.; Savopoulos, J.; Gray, C.W.; Creasy, C.L.; Dingwall, C.; et al. The serine protease Omi/HtrA2 regulates apoptosis by binding XIAP through a Reaper-like motif. *J. Biol. Chem.* **2002**, *277*, 439–444, doi:10.1074/jbc.M109784200.

232. Zou, H.; Li, Y.; Liu, X.; Wang, X. An APAF-1·cytochrome c multimeric complex is a functional apoptosome that activates procaspase-9. *J. Biol. Chem.* **1999**, *274*, 11549–11556, doi:10.1074/jbc.274.17.11549.

233. Sun, C.; Cai, M.; Gunasekera, A.H.; Meadows, R.P.; Wang, H.; Chen, J.; Zhang, H.; Wu, W.; Xu, N.; Ng, S.C.; et al. NMR structure and mutagenesis of the inhibitor-of-apoptosis protein XIAP. *Nature* **1999**, *401*, 818–822, doi:10.1038/44617.

234. Riedl, S.J.; Renatus, M.; Schwarzenbacher, R.; Zhou, Q.; Sun, C.; Fesik, S.W.; Liddington, R.C.; Salvesen, G.S. Structural basis for the inhibition of caspase-3 by XIAP. *Cell* **2001**, *104*, 791–800, doi:10.1016/S0092-8674(01)00274-4.

235. Huang, Y.; Park, Y.C.; Rich, R.L.; Segal, D.; Myszka, D.G.; Wu, H. Structural basis of caspase inhibition by XIAP: differential roles of the linker versus the BIR domain. *Cell* **2001**, *104*, 781–790, doi:10.1016/s0092-8674(01)00273-2.

236. Chai, J.; Shiozaki, E.; Srinivasula, S.M.; Wu, Q.; Dataa, P.; Alnemri, E.S.; Shi, Y. Structural basis of caspase-7 inhibition by XIAP. *Cell* **2001**, *104*, 769–780, doi:10.1016/S0092-8674(01)00272-0.

237. Sun, C.; Cai, M.; Meadows, R.P.; Xu, N.; Gunasekera, A.H.; Herrmann, J.; Wu, J.C.; Fesik, S.W. NMR structure and mutagenesis of the third Bir domain of the inhibitor of apoptosis protein XIAP. *J. Biol. Chem.* **2000**, *275*, 33777–33781, doi:10.1074/jbc.M006226200.

238. Shiozaki, E.N.; Chai, J.; Rigotti, D.J.; Riedl, S.J.; Li, P.; Srinivasula, S.M.; Alnemri, E.S.; Fairman, R.; Shi, Y. Mechanism of XIAP-mediated inhibition of caspase-9. *Mol. Cell* **2003**, *11*, 519–527, doi:10.1016/s1097-2765(03)00054-6.

239. Mastrangelo, E.; Vachette, P.; Cossu, F.; Malvezzi, F.; Bolognesi, M.; Milani, M. The activator of apoptosis Smac-DIABLO acts as a tetramer in solution. *Biophys. J.* **2015**, *108*, 714–723, doi:10.1016/j.bpj.2014.11.3471.

240. Verhagen, A.M.; Kratina, T.K.; Hawkins, C.J.; Silke, J.; Ekert, P.G.; Vaux, D.L. Identification of mammalian mitochondrial proteins that interact with IAPs via N-terminal IAP binding motifs. *Cell Death Differ.* **2007**, *14*, 348–357, doi:10.1038/sj.cdd.4402001.

241. Verhagen, A.M.; Silke, J.; Ekert, P.G.; Pakusch, M.; Kaufmann, H.; Connolly, L.M.; Day, C.L.; Tikoo, A.; Burke, R.; Wrobel, C.; et al. HtrA2 promotes cell death through its serine protease activity and its ability to antagonize inhibitor of apoptosis proteins. *J. Biol. Chem.* **2002**, *277*, 445–454, doi:10.1074/jbc.M109891200.

242. Jin, S.; Kalkum, M.; Overholtzer, M.; Stoffel, A.; Chait, B.T.; Levine, A.J. CIAP1 and the serine protease HTRA2 are involved in a novel p53-dependent apoptosis pathway in mammals. *Genes Dev.* **2003**, *17*, 359–367, doi:10.1101/gad.1047003.

243. Yang, Q.H.; Church-Hajduk, R.; Ren, J.; Newton, M.L.; Du, C. Omi/HtrA2 catalytic cleavage of inhibitor of apoptosis (IAP) irreversibly inactivates IAPs and facilitates caspase activity in apoptosis. *Genes Dev.* **2003**, *17*, 1487–1496, doi:10.1101/gad.1097903.

244. Suzuki, Y.; Takahashi-Niki, K.; Akagi, T.; Hashikawa, T.; Takahashi, R. Mitochondrial protease Omi/HtrA2 enhances caspase activation through multiple pathways. *Cell Death Differ.* **2004**, *11*, 208–216, doi:10.1038/sj.cdd.4401343.

245. Gottfried, Y.; Rotem, A.; Lotan, R.; Steller, H.; Larisch, S. The mitochondrial ARTS protein promotes apoptosis through targeting XIAP. *EMBO J.* **2004**, *23*, 1627–1635, doi:10.1038/sj.emboj.7600155.

246. Larisch, S.; Yi, Y.; Lotan, R.; Kerner, H.; Eimerl, S.; Tony Parks, W.; Gottfried, Y.; Birkey Reffey, S.; De Caestecker, M.P.; Danielpour, D.; et al. A novel mitochondrial septin-like protein, ARTS, mediates apoptosis dependent on its P-loop motif. *Nat. Cell Biol.* **2000**, *2*, 915–921, doi:10.1038/35046566.

247. Edison, N.; Zuri, D.; Maniv, I.; Bornstein, B.; Lev, T.; Gottfried, Y.; Kemeny, S.; Garcia-Fernandez, M.; Kagan, J.; Larisch, S. The IAP-antagonist ARTS initiates caspase activation upstream of cytochrome C and SMAC/Diablo. *Cell Death Differ.* **2012**, *19*, 356–368, doi:10.1038/cdd.2011.112.

248. Bornstein, B.; Gottfried, Y.; Edison, N.; Shekhtman, A.; Lev, T.; Glaser, F.; Larisch, S. ARTS binds to a distinct domain in XIAP-BIR3 and promotes apoptosis by a mechanism that is different from other IAP-antagonists. *Apoptosis* **2011**, *16*, 869–881, doi:10.1007/s10495-011-0622-0.

249. Reingewertz, T.H.; Shalev, D.E.; Sukenik, S.; Blatt, O.; Rotem-Bamberger, S.; Lebendiker, M.; Larisch, S.; Friedler, A. Mechanism of the interaction between the intrinsically disordered C-terminus of the pro-apoptotic ARTS protein and the Bir3 domain of XIAP. *PLoS One* **2011**, *6*, e24655, doi:10.1371/journal.pone.0024655.

250. Mamriev, D.; Abbas, R.; Klingler, F.-M.; Kagan, J.; Kfir, N.; Donald, A.; Weidenfeld, K.; Sheppard, D.W.; Barkan, D.; Larisch, S. A small-molecule ARTS mimetic promotes apoptosis through degradation of both XIAP and Bcl-2. *Cell Death Dis.* **2020**, *11*, 483, doi:10.1038/s41419-020-2670-2.

251. Garrison, J.B.; Correa, R.G.; Gerlic, M.; Yip, K.W.; Krieg, A.; Tamble, C.M.; Shi, R.; Welsh, K.; Duggineni, S.; Huang, Z.; et al. ARTS and Siah collaborate in a pathway for XIAP degradation. *Mol. Cell* **2011**, *41*, 107–116, doi:10.1016/j.molcel.2010.12.002.

252. Edison, N.; Curtz, Y.; Paland, N.; Mamriev, D.; Chorubczyk, N.; Haviv-Reingewertz, T.; Kfir, N.; Morgenstern, D.; Kupervaser, M.; Kagan, J.; et al. Degradation of Bcl-2 by XIAP and ARTS promotes apoptosis. *Cell Rep.* **2017**, *21*, 442–454, doi:10.1016/j.celrep.2017.09.052.

253. Yang, Y.; Fang, S.; Jensen, J.P.; Weissman, A.M.; Ashwell, J.D. Ubiquitin protein ligase activity of IAPs and their degradation in proteasomes in response to apoptotic stimuli. *Science* **2000**, *288*, 874–877, doi:10.1126/science.288.5467.874.

254. MacFarlane, M.; Merrison, W.; Bratton, S.B.; Cohen, G.M. Proteasome-mediated degradation of Smac during apoptosis: XIAP promotes Smac ubiquitination in vitro. *J. Biol. Chem.* **2002**, *277*, 36611–36616, doi:10.1074/jbc.M200317200.

255. Schile, A.J.; García-Fernández, M.; Steller, H. Regulation of apoptosis by XIAP ubiquitin-ligase activity. *Genes Dev.* **2008**, *22*, 2256–2266, doi:10.1101/gad.1663108.

256. Deveraux, Q.L.; Leo, E.; Stennicke, H.R.; Welsh, K.; Salvesen, G.S.; Reed, J.C. Cleavage of human inhibitor of apoptosis protein XIAP results in fragments with distinct specificities for caspases. *EMBO J.* **1999**, *18*, 5242–5251, doi:10.1093/emboj/18.19.5242.

257. Hörnle, M.; Peters, N.; Thayaparasingham, B.; Vörsmann, H.; Kashkar, H.; Kulms, D. Caspase-3 cleaves XIAP in a positive feedback loop to sensitize melanoma cells to TRAIL-induced apoptosis. *Oncogene* **2011**, *30*, 575–587, doi:10.1038/onc.2010.434.

258. Zhuang, M.; Guan, S.; Wang, H.; Burlingame, A.L.; Wells, J.A. Substrates of IAP ubiquitin ligases identified with a designed orthogonal E3 ligase, the NEDDylator. *Mol. Cell* **2013**, *49*, 273–282, doi:10.1016/j.molcel.2012.10.022.

259. Fulda, S.; Vucic, D. Targeting IAP proteins for therapeutic intervention in cancer. *Nat. Rev. Drug Discov.* **2012**, *11*, 109–124, doi:10.1038/nrd3627.

260. Fulda, S.; Wick, W.; Weller, M.; Debatin, K.M. Smac agonists sensitize for Apo2L/TRAIL-or anticancer drug-induced apoptosis and induce regression of malignant glioma in vivo. *Nat. Med.* **2002**, *8*, 808–815, doi:10.1038/nm735.

261. Gao, Z.; Tian, Y.; Wang, J.; Yin, Q.; Wu, H.; Li, Y.M.; Jiang, X. A dimeric Smac/Diablo peptide directly relieves caspase-3 inhibition by XIAP: dynamic and cooperative regulation of XIAP by Smac/Diablo. *J. Biol. Chem.* **2007**, *282*, 30718–30727, doi:10.1074/jbc.M705258200.

262. Sun, H.; Nikolovska-Coleska, Z.; Lu, J.; Meagher, J.L.; Yang, C.-Y.; Qiu, S.; Tomita, Y.; Ueda, Y.; Jiang, S.; Krajewski, K.; et al. Design, synthesis, and characterization of a potent, nonpeptide, cell-permeable, bivalent Smac mimetic that concurrently targets both the BIR2 and BIR3 domains in XIAP. *J. Am. Chem. Soc.* **2007**, *129*, 15279–94, doi:10.1021/ja074725f.

263. Jensen, S.; Seidelin, J.B.; LaCasse, E.C.; Nielsen, O.H. SMAC mimetics and RIPK inhibitors as therapeutics for chronic inflammatory diseases. *Sci. Signal.* **2020**, *13*, eaax8295, doi:10.1126/scisignal.aax8295.

264. Morrish, E.; Brumatti, G.; Silke, J. Future therapeutic directions for Smac-mimetics. *Cells* **2020**, *9*, 406, doi:10.3390/cells9020406.

265. Vince, J.E.; Wong, W.W.L.; Khan, N.; Feltham, R.; Chau, D.; Ahmed, A.U.; Benetatos, C.A.; Chunduru, S.K.; Condon, S.M.; McKinlay, M.; et al. IAP antagonists target cIAP1 to induce TNFα-dependent apoptosis. *Cell* **2007**, *131*, 682–693, doi:10.1016/j.cell.2007.10.037.

266. Varfolomeev, E.; Blankenship, J.W.; Wayson, S.M.; Fedorova, A. V.; Kayagaki, N.; Garg, P.; Zobel, K.; Dynek, J.N.; Elliott, L.O.; Wallweber, H.J.A.; et al. IAP antagonists induce autoubiquitination of c-IAPs, NF-κB activation, and TNFα-dependent apoptosis. *Cell* **2007**, *131*, 669–681, doi:10.1016/j.cell.2007.10.030.

267. Dueber, E.C.; Schoeffler, A.J.; Lingel, A.; Elliott, J.M.; Fedorova, A. V.; Giannetti, A.M.; Zobel, K.; Maurer, B.; Varfolomeev, E.; Wu, P.; et al. Antagonists induce a conformational change in cIAP1 that promotes autoubiquitination. *Science* **2011**, *334*, 376–80, doi:10.1126/science. 1207862.

268. Varfolomeev, E.; Goncharov, T.; Fedorova, A. V.; Dynek, J.N.; Zobel, K.; Deshayes, K.; Fairbrother, W.J.; Vucic, D. c-IAP1 and c-IAP2 are critical mediators of tumor necrosis factor α (TNFα)-induced NF-κB activation. *J. Biol. Chem.* **2008**, *283*, 24295–24299, doi:10.1074/jbc. C800128200.

269. Bertrand, M.J.M.; Milutinovic, S.; Dickson, K.M.; Ho, W.C.; Boudreault, A.; Durkin, J.; Gillard, J.W.; Jaquith, J.B.; Morris, S.J.; Barker, P.A. cIAP1 and cIAP2 facilitate cancer cell Survival by functioning as E3 ligases that promote RIP1 ubiquitination. *Mol. Cell* **2008**, *30*, 689–700, doi:10.1016/j.molcel.2008.05.014.

270. Martinon, F.; Burns, K.; Tschopp, J. The inflammasome: a molecular platform triggering activation of inflammatory caspases and processing of proIL-1β. *Mol. Cell* **2002**, *10*, 417–426, doi:10.1016/S1097-2765(02)00599-3.

271. Krieg, A.; Correa, R.G.; Garrison, J.B.; Le Negrate, G.; Welsh, K.; Huang, Z.; Knoefel, W.T.; Reed, J.C. XIAP mediates NOD signaling via interaction with RIP2. *Proc. Natl. Acad. Sci. U. S. A.* **2009**, *106*, 14524–14529, doi:10.1073/pnas.0907131106.

272. Damgaard, R.B.; Nachbur, U.; Yabal, M.; Wong, W.W.L.; Fiil, B.K.; Kastirr, M.; Rieser, E.; Rickard, J.A.; Bankovacki, A.; Peschel, C.; et al. The ubiquitin ligase XIAP recruits LUBAC for NOD2 signaling in inflammation and innate immunity. *Mol. Cell* **2012**, *46*, 746–758, doi:10.1016/j.molcel.2012.04.014.

273. Damgaard, R.B.; Fiil, B.K.; Speckmann, C.; Yabal, M.; Stadt, U. zur; Bekker-Jensen, S.; Jost, P.J.; Ehl, S.; Mailand, N.; Gyrd-Hansen, M. Disease-causing mutations in the XIAP BIR2 domain impair NOD2-dependent immune signalling. *EMBO Mol. Med.* **2013**, *5*, 1278–1295, doi:10.1002/emmm.201303090.

274. Goncharov, T.; Hedayati, S.; Mulvihill, M.M.; Izrael-Tomasevic, A.; Zobel, K.; Jeet, S.; Fedorova, A. V.; Eidenschenk, C.; deVoss, J.; Yu, K.; et al. Disruption of XIAP-RIP2 association blocks NOD2-mediated inflammatory signaling. *Mol. Cell* **2018**, *69*, 551–565.e7, doi:10.1016/j.molcel.2018.01.016.

275. Stafford, C.A.; Lawlor, K.E.; Heim, V.J.; Bankovacki, A.; Bernardini, J.P.; Silke, J.; Nachbur, U. IAPs regulate distinct innate immune pathways to co-ordinate the response to bacterial peptidoglycans. *Cell Rep.* **2018**, *22*, 1496–1508, doi:10.1016/j.celrep.2018.01.024.

276. Vince, J.E.; Wong, W.W.L.; Gentle, I.; Lawlor, K.E.; Allam, R.; O'Reilly, L.; Mason, K.; Gross, O.; Ma, S.; Guarda, G.; et al. Inhibitor of apoptosis proteins limit RIP3 kinase-dependent interleukin-1 activation. *Immunity* **2012**, *36*, 215–227, doi:10.1016/j.immuni.2012.01.012.

277. Lawlor, K.E.; Khan, N.; Mildenhall, A.; Gerlic, M.; Croker, B.A.; D'Cruz, A.A.; Hall, C.; Kaur Spall, S.; Anderton, H.; Masters, S.L.; et al. RIPK3 promotes cell death and NLRP3 inflammasome activation in the absence of MLKL. *Nat. Commun.* **2015**, *6*, 6282, doi:10.1038/ncomms7282.

278. Lawlor, K.E.; Feltham, R.; Yabal, M.; Conos, S.A.; Chen, K.W.; Ziehe, S.; Graß, C.; Zhan, Y.; Nguyen, T.A.; Hall, C.; et al. XIAP loss triggers RIPK3- and caspase-8-driven IL-1β activation and cell death as a consequence of TLR-MyD88-induced cIAP1-TRAF2 degradation. *Cell Rep.* **2017**, *20*, 668–682, doi:10.1016/j.celrep.2017.06.073.

279. Yabal, M.; Müller, N.; Adler, H.; Knies, N.; Groß, C.J.; Damgaard, R.B.; Kanegane, H.; Ringelhan, M.; Kaufmann, T.; Heikenwälder, M.; et al. XIAP restricts TNF- and RIP3-dependent cell death and inflammasome activation. *Cell Rep.* **2014**, *7*, 1796–1808, doi:10.1016/j.celrep.2014.05.008.

280. Philpott, D.J.; Sorbara, M.T.; Robertson, S.J.; Croitoru, K.; Girardin, S.E. NOD proteins: regulators of inflammation in health and disease. *Nat. Rev. Immunol.* **2014**, *14*, 9–23, doi:10. 1038/nri3565.

281. Tenev, T.; Bianchi, K.; Darding, M.; Broemer, M.; Langlais, C.; Wallberg, F.; Zachariou, A.; Lopez, J.; MacFarlane, M.; Cain, K.; et al. The ripoptosome, a signaling platform that assembles in response to genotoxic stress and loss of IAPs. *Mol. Cell* **2011**, *43*, 432–448, doi:10.1016/j.molcel.2011.06.006.

282. Feoktistova, M.; Geserick, P.; Kellert, B.; Dimitrova, D.P.; Langlais, C.; Hupe, M.; Cain, K.; MacFarlane, M.; Häcker, G.; Leverkus, M. CIAPs block ripoptosome formation, a RIP1/caspase-8 containing intracellular cell death complex differentially regulated by cFLIP Isoforms. *Mol. Cell* **2011**, *43*, 449–463, doi:10.1016/j.molcel.2011.06.011.

283. Harlin, H.; Reffey, S.B.; Duckett, C.S.; Lindsten, T.; Thompson, C.B. Characterization of XIAP-deficient mice. *Mol. Cell. Biol.* **2001**, *21*, 3604–3608, doi:10.1128/MCB.21.10.3604-3608.2001.

284. Okada, H.; Suh, W.-K.; Jin, J.; Woo, M.; Du, C.; Elia, A.; Duncan, G.S.; Wakeham, A.; Itie, A.; Lowe, S.W.; et al. Generation and characterization of Smac/DIABLO-deficient mice. *Mol. Cell. Biol.* **2002**, *22*, 3509–3517, doi:10.1128/mcb.22.10.3509-3517.2002.

285. Koren, E.; Yosefzon, Y.; Ankawa, R.; Soteriou, D.; Jacob, A.; Nevelsky, A.; Ben-Yosef, R.; Bar-Sela, G.; Fuchs, Y. ARTS mediates apoptosis and regeneration of the intestinal stem cell niche. *Nat. Commun.* **2018**, *9*, 4582, doi:10.1038/s41467-018-06941-4.

286. Fuchs, Y.; Brown, S.; Gorenc, T.; Rodriguez, J.; Fuchs, E.; Steller, H. Sept4/ARTS regulates stem cell apoptosis and skin regeneration. *Science* **2013**, *341*, 286–9, doi:10.1126/science.1233029.

287. Hsieh, W.-C.; Chuang, Y.-T.; Chiang, I.-H.; Hsu, S.-C.; Miaw, S.-C.; Lai, M.-Z. Inability to resolve specific infection generates innate immunodeficiency syndrome in Xiap-/- mice. *Blood* **2014**, *124*, 2847–2857, doi:10.1182/blood-2014-03-564609.

288. Bauler, L.D.; Duckett, C.S.; O'Riordan, M.X.D. XIAP regulates cytosol-specific innate immunity to *Listeria* infection. *PLoS Pathog.* **2008**, *4*, e1000142, doi:10.1371/journal.ppat.1000142.

289. Prakash, H.; Albrecht, M.; Becker, D.; Kuhlmann, T.; Rudel, T. Deficiency of XIAP leads to sensitization for *Chlamydophila pneumoniae* pulmonary infection and dysregulation of innate immune response in mice. *J. Biol. Chem.* **2010**, *285*, 20291–20302, doi:10.1074/jbc.M109.096297.

290. Wicki, S.; Gurzeler, U.; Wei-Lynn Wong, W.; Jost, P.J.; Bachmann, D.; Kaufmann, T. Loss of XIAP facilitates switch to TNFα-induced necroptosis in mouse neutrophils. *Cell Death Dis.* **2016**, *7*, e2422, doi:10.1038/cddis.2016.311.

291. Gentle, I.E.; Moelter, I.; Lechler, N.; Bambach, S.; Vucikuja, S.; Häcker, G.; Aichele, P. Inhibitors of apoptosis proteins (IAPs) are required for effective T-cell expansion/survival during antiviral immunity in mice. *Blood* **2014**, *123*, 659–668, doi:10.1182/blood-2013-01-479543.

292. Hsieh, W.-C.; Hsu, T.-S.; Chang, Y.-J.; Lai, M.-Z. IL-6 receptor blockade corrects defects of XIAP-deficient regulatory T cells. *Nat. Commun.* **2018**, *9*, 463, doi:10.1038/s41467-018-02862-4.

293. Latour, S.; Aguilar, C. XIAP deficiency syndrome in humans. *Semin. Cell Dev. Biol.* **2015**, *39*, 115–123, doi:10.1016/j.semcdb.2015.01.015.

294. Rigaud, S.; Fondanèche, M.C.; Lambert, N.; Pasquier, B.; Mateo, V.; Soulas, P.; Galicier, L.; Le Deist, F.; Rieux-Laucat, F.; Revy, P.; et al. XIAP deficiency in humans causes an X-linked lymphoproliferative syndrome. *Nature* **2006**, *444*, 110–114, doi:10.1038/nature05257.

295. Schmid, J.P.; Canioni, D.; Moshous, D.; Touzot, F.; Mahlaoui, N.; Hauck, F.; Kanegane, H.; Lopez-Granados, E.; Mejstrikova, E.; Pellier, I.; et al. Clinical similarities and differences of patients with X-linked lymphoproliferative syndrome type 1 (XLP-1/SAP deficiency) versus type 2 (XLP-2/XIAP deficiency). *Blood* **2011**, *117*, 1522–1529, doi:10.1182/blood-2010-07-298372.

296. Marsh, R.A.; Madden, L.; Kitchen, B.J.; Mody, R.; McClimon, B.; Jordan, M.B.; Bleesing, J.J.; Zhang, K.; Filipovich, A.H. XIAP deficiency: a unique primary immunodeficiency best classified as X-linked familial hemophagocytic lymphohistiocytosis and not as X-linked lymphoproliferative disease. *Blood* **2010**, *116*, 1079–1082, doi:10.1182/blood-2010-01-256099.

297. Jankowsky, E. RNA helicases at work: binding and rearranging. *Trends Biochem. Sci.* **2011**, *36*, 19–29, doi:10.1016/j.tibs.2010.07.008.

298. Fairman-Williams, M.E.; Guenther, U.P.; Jankowsky, E. SF1 and SF2 helicases: family matters. *Curr. Opin. Struct. Biol.* 2010, *20*, 313–324, doi: 10.1016/j.sbi.2010.03.011.

299. Dalmay, T.; Horsefield, R.; Braunstein, T.H.; Baulcombe, D.C. SDE3 encodes an RNA helicase required for post-transcriptional gene silencing in *Arabidopsis*. *EMBO J.* **2001**, *20*, 2069–2077, doi:10.1093/emboj/20.8.2069.

300. Fischer, S.E.J.; Butler, M.D.; Pan, Q.; Ruvkun, G. Trans-splicing in *C. elegans* generates the negative RNAi regulator ERI-6/7. *Nature* **2008**, *455*, 491–496, doi:10.1038/nature07274.

301. Fischer, S.E.J.; Montgomery, T.A.; Zhang, C.; Fahlgren, N.; Breen, P.C.; Hwang, A.; Sullivan, C.M.; Carrington, J.C.; Ruvkun, G. The ERI-6/7 helicase acts at the first stage of an siRNA amplification pathway that targets recent gene duplications. *PLoS Genet.* **2011**, *7*, e1002369, doi:10.1371/journal.pgen.1002369.

302. Cook, H.A.; Koppetsch, B.S.; Wu, J.; Theurkauf, W.E. The *Drosophila* SDE3 homolog armitage is required for oskar mRNA silencing and embryonic axis specification. *Cell* **2004**, *116*, 817–829, doi:10.1016/S0092-8674(04)00250-8.

303. Tomari, Y.; Du, T.; Haley, B.; Schwarz, D.S.; Bennett, R.; Cook, H.A.; Koppetsch, B.S.; Theurkauf, W.E.; Zamore, P.D. RISC assembly defects in the *Drosophila* RNAi mutant armitage. *Cell* **2004**, *116*, 831–841, doi:10.1016/S0092-8674(04)00218-1.

304. Zheng, K.; Xiol, J.; Reuter, M.; Eckardt, S.; Leu, N.L.; McLaughlin, K.J.; Stark, A.; Sachidanandam, R.; Pillai, R.S.; Wang, P.J. Mouse MOV10L1 associates with Piwi proteins and is an essential component of the Piwi-interacting RNA (piRNA) pathway. *Proc. Natl. Acad. Sci. U. S. A.* **2010**, *107*, 11841–11846, doi:10.1073/pnas.1003953107.

305. Frost, R.J.A.; Hamra, F.K.; Richardson, J.A.; Qi, X.; Bassel-Duby, R.; Olson, E.N. MOV10L1 is necessary for protection of spermatocytes against retrotransposons by Piwi-interacting RNAs. *Proc. Natl. Acad. Sci. U. S. A.* **2010**, *107*, 11847–11852, doi:10.1073/pnas.1007158107.

306. Garcia, D.; Garcia, S.; Pontier, D.; Marchais, A.; Renou, J.P.; Lagrange, T.; Voinnet, O. Ago Hook and RNA helicase motifs underpin dual roles for SDE3 in antiviral defense and silencing of non-conserved intergenic regions. *Mol. Cell* **2012**, *48*, 109–120, doi:10.1016/j.molcel.2012.07.028.

307. Fischer, S.E.J.; Ruvkun, G. *Caenorhabditis elegans* ADAR editing and the ERI-6/7/ MOV10 RNAi pathway silence endogenous viral elements and LTR retrotransposons. *Proc. Natl. Acad. Sci. U. S. A.* **2020**, *117*, 5987–5996, doi:10.1073/pnas.1919028117.

308. Saito, K.; Ishizu, H.; Komai, M.; Kotani, H.; Kawamura, Y.; Nishida, K.M.; Siomi, H.; Siomi, M.C. Roles for the Yb body components Armitage and Yb in primary piRNA biogenesis in *Drosophila*. *Genes Dev.* **2010**, *24*, 2493–2498, doi:10.1101/gad.1989510.

309. Arjan-Odedra, S.; Swanson, C.M.; Sherer, N.M.; Wolinsky, S.M.; Malim, M.H. Endogenous MOV10 inhibits the retrotransposition of endogenous retroelements but not the replication of exogenous retroviruses. *Retrovirology* **2012**, *9*, 53, doi:10.1186/1742-4690-9-53.

310. Goodier, J.L.; Cheung, L.E.; Kazazian, H.H. MOV10 RNA helicase is a potent inhibitor of retrotransposition in cells. *PLoS Genet.* **2012**, *8*, e1002941, doi:10.1371/journal.pgen.1002941.

311. Lu, C.; Luo, Z.; Jager, S.; Krogan, N.J.; Peterlin, B.M. Moloney leukemia virus type 10 inhibits reverse transcription and retrotransposition of intracisternal a particles. *J. Virol.* **2012**, *86*, 10517–10523, doi:10.1128/jvi.00868-12.

312. Li, X.; Zhang, J.; Jia, R.; Cheng, V.; Xu, X.; Qiao, W.; Guo, F.; Liang, C.; Cen, S. The MOV10 helicase inhibits LINE-1 mobility. *J. Biol. Chem.* **2013**, *288*, 21148–21160, doi:10.1074/jbc.M113.465856.

313. Choi, J.; Hwang, S.Y.; Ahn, K. Interplay between RNASEH2 and MOV10 controls LINE-1 retrotransposition. *Nucleic Acids Res.* **2018**, *46*, 1912–1926, doi:10.1093/nar/gkx1312.

314. Warkocki, Z.; Krawczyk, P.S.; Adamska, D.; Bijata, K.; Garcia-Perez, J.L.; Dziembowski, A. Uridylation by TUT4/7 restricts retrotransposition of human LINE-1s. *Cell* **2018**, *174*, 1537–1548.e29, doi:10.1016/j.cell.2018.07.022.

315. Burdick, R.; Smith, J.L.; Chaipan, C.; Friew, Y.; Chen, J.; Venkatachari, N.J.; Delviks-Frankenberry, K.A.; Hu, W.-S.; Pathak, V.K. P body-associated protein Mov10 inhibits HIV-1 replication at multiple stages. *J. Virol.* **2010**, *84*, 10241–10253, doi:10.1128/jvi.00585-10.

316. Wang, X.; Han, Y.; Dang, Y.; Fu, W.; Zhou, T.; Ptak, R.G.; Zheng, Y.H. Moloney leukemia virus 10 (MOV10) protein inhibits retrovirus replication. *J. Biol. Chem.* **2010**, *285*, 14346–14355, doi:10.1074/jbc.M110.109314.

317. Furtak, V.; Mulky, A.; Rawlings, S.A.; Kozhaya, L.; Lee, K.; Kewalramani, V.N.; Unutmaz, D. Perturbation of the P-body component Mov10 inhibits HIV-1 infectivity. *PLoS One* **2010**, *5*, e9081, doi:10.1371/journal.pone.0009081.

318. Abudu, A.; Wang, X.; Dang, Y.; Zhou, T.; Xiang, S.H.; Zheng, Y.H. Identification of molecular determinants from Moloney leukemia virus 10 homolog (MOV10) protein for virion packaging and anti-HIV-1 activity. *J. Biol. Chem.* **2012**, *287*, 1220–1228, doi:10.1074/jbc.M111.309831.

319. Huang, F.; Zhang, J.; Zhang, Y.; Geng, G.; Liang, J.; Li, Y.; Chen, J.; Liu, C.; Zhang, H. RNA helicase MOV10 functions as a co-factor of HIV-1 Rev to facilitate Rev/RRE-dependent nuclear export of viral mRNAs. *Virology* **2015**, *486*, 15–26, doi:10.1016/j.virol.2015.08.026.

320. Schoggins, J.W.; Wilson, S.J.; Panis, M.; Murphy, M.Y.; Jones, C.T.; Bieniasz, P.; Rice, C.M. A diverse range of gene products are effectors of the type I interferon antiviral response. *Nature* **2011**, *472*, 481–485, doi:10.1038/nature09907.

321. Shaw, A.E.; Hughes, J.; Gu, Q.; Behdenna, A.; Singer, J.B.; Dennis, T.; Orton, R.J.; Varela, M.; Gifford, R.J.; Wilson, S.J.; et al. Fundamental properties of the mammalian innate immune system revealed by multispecies comparison of type I interferon responses. *PLoS Biol.* **2017**, *15*, e2004086, doi:10.1371/journal.pbio.2004086.

322. Cuevas, R.A.; Ghosh, A.; Wallerath, C.; Hornung, V.; Coyne, C.B.; Sarkar, S.N. MOV10 provides antiviral activity against RNA viruses by enhancing RIG-I–MAVS-independent IFN induction. *J. Immunol.* **2016**, *196*, 3877–3886, doi:10.4049/jimmunol.1501359.

323. Liu, D.; Ndongwe, T.P.; Puray-Chavez, M.; Casey, M.C.; Izumi, T.; Pathak, V.K.; Tedbury, P.R.; Sarafianos, S.G. Effect of P-body component Mov10 on HCV virus production and infectivity. *FASEB J.* **2020**, *34*, 9433–9449, doi:10.1096/fj.201800641R.

324. Zhang, J.; Huang, F.; Tan, L.; Bai, C.; Chen, B.; Liu, J.; Liang, J.; Liu, C.; Zhang, S.; Lu, G.; et al. Host protein Moloney leukemia virus 10 (MOV10) acts as a restriction factor of influenza A virus by inhibiting the nuclear import of the viral nucleoprotein. *J. Virol.* **2016**, *90*, 3966–3980, doi:10.1128/jvi.03137-15.

325. Li, J.; Hu, S.; Xu, F.; Mei, S.; Liu, X.; Yin, L.; Zhao, F.; Zhao, X.; Sun, H.; Xiong, Z.; et al. MOV10 sequesters the RNP of influenza A virus in the cytoplasm and is antagonized by viral NS1 protein. *Biochem. J.* **2019**, *476*, 467–481, doi:10.1042/BCJ20180754.

326. Mo, Q.; Xu, Z.; Deng, F.; Wang, H.; Ning, Y.J. Host restriction of emerging high-pathogenic bunyaviruses via MOV10 by targeting viral nucleoprotein and blocking ribonucleoprotein assembly. *PLoS Pathog.* **2020**, *16*, e1009129, doi:10.1371/journal.ppat.1009129.

327. Haussecker, D.; Cao, D.; Huang, Y.; Parameswaran, P.; Fire, A.Z.; Kay, M.A. Capped small RNAs and MOV10 in human hepatitis delta virus replication. *Nat. Struct. Mol. Biol.* **2008**, *15*, 714–721, doi:10.1038/nsmb.1440.

328. Liu, T.; Sun, Q.; Liu, Y.; Cen, S.; Zhang, Q. The MOV10 helicase restricts hepatitis B virus replication by inhibiting viral reverse transcription. *J. Biol. Chem.* **2019**, *294*, 19804–19813, doi:10.1074/jbc.RA119.009435.

329. Puray-Chavez, M.; Farghali, M.; Yapo, V.; Huber, A.; Liu, D.; Ndongwe, T.; Casey, M.; Laughlin, T.; Hannink, M.; Tedbury, P.; et al. Effects of Moloney leukemia virus 10 protein on hepatitis B virus infection and viral replication. *Viruses* **2019**, *11*, 651, doi:10.3390/v11070651.

330. Meister, G.; Landthaler, M.; Peters, L.; Chen, P.Y.; Urlaub, H.; Lührmann, R.; Tuschl, T. Identification of novel argonaute-associated proteins. *Curr. Biol.* **2005**, *15*, 2149–2155, doi:10.1016/j.cub.2005.10.048.

331. Chendrimada, T.P.; Finn, K.J.; Ji, X.; Baillat, D.; Gregory, R.I.; Liebhaber, S.A.; Pasquinelli, A.E.; Shiekhattar, R. MicroRNA silencing through RISC recruitment of eIF6. *Nature* **2007**, *447*, 823–828, doi:10.1038/nature05841.

332. Liu, C.; Zhang, X.; Huang, F.; Yang, B.; Li, J.; Liu, B.; Luo, H.; Zhang, P.; Zhang, H. APOBEC3G inhibits microRNA-mediated repression of translation by interfering with the interaction between Argonaute-2 and MOV10. *J. Biol. Chem.* **2012**, *287*, 29373–29383, doi:10.1074/jbc.M112.354001.

333. Kenny, P.J.; Zhou, H.; Kim, M.; Skariah, G.; Khetani, R.S.; Drnevich, J.; Arcila, M.L.; Kosik, K.S.; Ceman, S. MOV10 and FMRP regulate AGO2 association with microRNA recognition elements. *Cell Rep.* **2014**, *9*, 1729–1741, doi:10.1016/j.celrep.2014.10.054.

334. Liang, X. hai; Crooke, S.T. RNA helicase A is not required for RISC activity. *Biochim. Biophys. Acta - Gene Regul. Mech.* **2013**, *1829*, 1092–1101, doi:10.1016/j.bbagrm.2013.07.008.

335. Gregersen, L.H.; Schueler, M.; Munschauer, M.; Mastrobuoni, G.; Chen, W.; Kempa, S.; Dieterich, C.; Landthaler, M. MOV10 is a 5' to 3' RNA helicase contributing to UPF1 mRNA target degradation by translocation along 3' UTRs. *Mol. Cell* **2014**, *54*, 573–585, doi:10.1016/j.molcel.2014.03.017.

336. Messaoudi-Aubert, S.E.L.; Nicholls, J.; Maertens, G.N.; Brookes, S.; Bernstein, E.; Peters, G. Role for the MOV10 RNA helicase in Polycomb-mediated repression of the INK4a tumor suppressor. *Nat. Struct. Mol. Biol.* **2010**, *17*, 862–868, doi:10.1038/nsmb.1824.

337. Skariah, G.; Seimetz, J.; Norsworthy, M.; Lannom, M.C.; Kenny, P.J.; Elrakhawy, M.; Forsthoefel, C.; Drnevich, J.; Kalsotra, A.; Ceman, S. Mov10 suppresses retroelements and regulates neuronal development and function in the developing brain. *BMC Biol.* **2017**, *15*, 54, doi:10.1186/s12915-017-0387-1.

338. Fu, K.; Tian, S.; Tan, H.; Wang, C.; Wang, H.; Wang, M.; Wang, Y.; Chen, Z.; Wang, Y.; Yue, Q.; et al. Biological and RNA regulatory function of MOV10 in mammalian germ cells. *BMC Biol.* **2019**, *17*, 39, doi:10.1186/s12915-019-0659-z.

339. Banerjee, S.; Neveu, P.; Kosik, K.S. A coordinated local translational control point at the synapse involving relief from silencing and MOV10 degradation. *Neuron* **2009**, *64*, 871–884, doi:10.1016/j.neuron.2009.11.023.

340. Ashraf, S.I.; McLoon, A.L.; Sclarsic, S.M.; Kunes, S. Synaptic protein synthesis associated with memory is regulated by the RISC pathway in *Drosophila*. *Cell* **2006**, *124*, 191–205, doi:10.1016/j.cell.2005.12.017.

341. Zheng, K.; Wang, P.J. Blockade of pachytene piRNA biogenesis reveals a novel requirement for maintaining post-meiotic germline genome integrity. *PLoS Genet.* **2012**, *8*, 13–16, doi:10.1371/journal.pgen.1003038.

342. Gloeckner, C.J.; Boldt, K.; Schumacher, A.; Ueffing, M. Tandem affinity purification of protein complexes from mammalian cells by the Strep/FLAG (SF)-TAP tag. *Methods Mol. Biol.* **2009**, *564*, 359–372, doi:10.1007/978-1-60761-157-8_21.

343. Shalem, O.; Sanjana, N.E.; Hartenian, E.; Shi, X.; Scott, D.A.; Mikkelsen, T.S.; Heckl, D.; Ebert, B.L.; Root, D.E.; Doench, J.G.; et al. Genome-scale CRISPR-Cas9 knockout screening in human cells. *Science* **2014**, *343*, 84–87, doi:10.1126/science.1247005.

344. Chen, S.; Lee, B.; Lee, A.Y.F.; Modzelewski, A.J.; He, L. Highly efficient mouse genome editing by CRISPR ribonucleoprotein electroporation of zygotes. *J. Biol. Chem.* **2016**, *291*, 14457–14467, doi:10.1074/jbc.M116.733154.

345. Tandon, N.; Thakkar, K.; LaGory, E.; Liu, Y.; Giaccia, A. Generation of stable expression mammalian cell lines using lentivirus. *Bio-Protocol* **2018**, *8*, e3073, doi:10.21769/bioprotoc.3073.

346. Kowarz, E.; Löscher, D.; Marschalek, R. Optimized Sleeping Beauty transposons rapidly generate stable transgenic cell lines. *Biotechnol. J.* **2015**, *10*, 647–653, doi:10.1002/biot.201400821.

347. Durkin, M.E.; Qian, X.; Popescu, N.C.; Lowy, D.R. Isolation of mouse embryo fibroblasts. *Bio-Protocol* **2013**, *3*, e908, doi:10.21769/bioprotoc.908.

348. Kamijo, T.; Zindy, F.; Roussel, M.F.; Quelle, D.E.; Downing, J.R.; Ashmun, R.A.; Grosveld, G.; Sherr, C.J. Tumor suppression at the mouse INK4a locus mediated by the alternative reading frame product p19(ARF). *Cell* **1997**, *91*, 649–659, doi:10.1016/S0092-8674(00)80452-3.

349. Zhang, X.; Goncalves, R.; Mosser, D.M. The isolation and characterization of murine macrophages. *Curr. Protoc. Immunol.* **2008**, *83*, 1–6, doi:10.1002/0471142735.im1401s83.

350. Longo, P.A.; Kavran, J.M.; Kim, M.-S.; Leahy, D.J. Transient mammalian cell transfection with polyethylenimine (PEI). *Methods Enzymol.* **2013**, *529*, 227–40, doi:10.1016/B978-0-12-418687-3.00018-5.

351. International Mouse Phenotyping Consortium. Immunophenotyping. Available online: www.mousephenotype.org/impress/ProcedureInfo?action=list&procID=1225&pipeID=7. Accessed on 24.04. 2021.

352. Latendresse, J.R.; Warbrittion, A.R.; Jonassen, H.; Creasy, D.M. Fixation of testes and eyes using a modified Davidson's fluid: Comparison with Bouin's fluid and conventional Davidson's fluid. *Toxicol. Pathol.* **2002**, *30*, 524–533, doi:10.1080/01926230290105721.

353. Lin, P.; Mobasher, M.E.; Hakakian, Y.; Kakarla, V.; Naseem, A.F.; Ziai, H.; Alawi, F. Differential requirements for H/ACA ribonucleoprotein components in cell proliferation and response to DNA damage. *Histochem. Cell Biol.* **2015**, *144*, 543–558, doi:10.1007/s00418-015-1359-6.

354. Wang, C.; Meier, U.T. Architecture and assembly of mammalian H/ACA small nucleolar and telomerase ribonucleoproteins. *EMBO J.* **2004**, *23*, 1857–1867, doi:10.1038/sj.emboj.7600181.

355. Wang, Y.; Wang, W.; Xu, L.; Zhou, X.; Shokrollahi, E.; Felczak, K.; van der Laan, L.J.W.; Pankiewicz, K.W.; Sprengers, D.; Raat, N.J.H.; et al. Cross talk between nucleotide synthesis pathways with cellular immunity in constraining hepatitis E virus replication. *Antimicrob. Agents Chemother.* **2016**, *60*, 2834–2848, doi:10.1128/AAC.02700-15.

356. Pujantell, M.; Riveira-Muñoz, E.; Badia, R.; Castellví, M.; Garcia-Vidal, E.; Sirera, G.; Puig, T.; Ramirez, C.; Clotet, B.; Esté, J.A.; et al. RNA editing by ADAR1 regulates innate and antiviral immune functions in primary macrophages. *Sci. Rep.* **2017**, *7*, 13339, doi:10.1038/s41598-017-13580-0.

357. Cai, L.; Liu, L.; Li, L.; Jia, L. SCFFBXO28-mediated self-ubiquitination of FBXO28 promotes its degradation. *Cell. Signal.* **2020**, *65*, 109440, doi:10.1016/j.cellsig.2019.109440.

358. Hunter, A.M.; Kottachchi, D.; Lewis, J.; Duckett, C.S.; Korneluk, R.G.; Liston, P. A novel ubiquitin fusion system bypasses the mitochondria and generates biologically active Smac/DIABLO. *J. Biol. Chem.* **2003**, *278*, 7494–7499, doi:10.1074/jbc.C200695200.

359. Scott, F.L.; Denault, J.B.; Riedl, S.J.; Shin, H.; Renatus, M.; Salvesen, G.S. XIAP inhibits caspase-3 and -7 using two binding sites: evolutionary conserved mechanism of IAPs. *EMBO J.* **2005**, *24*, 645–655, doi:10.1038/sj.emboj.7600544.

360. Deng, Y.; Lin, Y.; Wu, X. TRAIL-induced apoptosis requires Bax-dependent mitochondrial release of Smac/DIABLO. *Genes Dev.* **2002**, *16*, 33–45, doi:10.1101/gad.949602.

361. Todaro, M.; Lombardo, Y.; Francipane, M.G.; Alea, M.P.; Cammareri, P.; Iovino, F.; Di Stefano, A.B.; Di Bernardo, C.; Agrusa, A.; Condorelli, G.; et al. Apoptosis resistance in epithelial tumors is mediated by tumor-cell-derived interleukin-4. *Cell Death Differ.* **2008**, *15*, 762–72, doi:10.1038/sj.cdd.4402305.

362. Han, X.; Wang, R.; Zhou, Y.; Fei, L.; Sun, H.; Lai, S.; Saadatpour, A.; Zhou, Z.; Chen, H.; Ye, F.; et al. Mapping the mouse cell atlas by microwell-seq. *Cell* **2018**, *172*, 1091–1107.e17, doi:10.1016/j.cell.2018.02.001.

363. Hermann, B.P.; Cheng, K.; Singh, A.; Roa-De La Cruz, L.; Mutoji, K.N.; Chen, I.C.; Gildersleeve, H.; Lehle, J.D.; Mayo, M.; Westernströer, B.; et al. The mammalian spermatogenesis single-cell transcriptome, from spermatogonial stem cells to spermatids. *Cell Rep.* **2018**, *25*, 1650–1667.e8, doi:10.1016/j.celrep.2018.10.026.

364. Yukawa, M.; Jagannathan, S.; Vallabh, S.; Kartashov, A. V.; Chen, X.; Weirauch, M.T.; Barski, A. AP-1 activity induced by co-stimulation is required for chromatin opening during T cell activation. *J. Exp. Med.* **2020**, *217*, doi:10.1084/jem.20182009.

365. White, C.H.; Moesker, B.; Beliakova-Bethell, N.; Martins, L.J.; Spina, C.A.; Margolis, D.M.; Richman, D.D.; Planelles, V.; Bosque, A.; Woelk, C.H. Transcriptomic analysis implicates the p53 signaling pathway in the establishment of HIV-1 latency in central memory CD4 T cells in an in vitro Model. *PLoS Pathog.* **2016**, *12*, e1006026, doi:10.1371/journal.ppat.1006026.

366. Man, K.; Miasari, M.; Shi, W.; Xin, A.; Henstridge, D.C.; Preston, S.; Pellegrini, M.; Belz, G.T.; Smyth, G.K.; Febbraio, M.A.; et al. The transcription factor IRF4 is essential for TCR affinity-mediated metabolic programming and clonal expansion of T cells. *Nat. Immunol.* **2013**, *14*, 1155–1165, doi:10.1038/ni.2710.

367. Singh, M.; Wang, Z.; Cascio, D.; Feigon, J. Structure and interactions of the CS domain of human H/ACA RNP assembly protein Shq1. *J. Mol. Biol.* **2015**, *427*, 807–823, doi:10.1016/j.jmb.2014.12.012.

368. Hirai, Y.; Louvet, E.; Oda, T.; Kumeta, M.; Watanabe, Y.; Horigome, T.; Takeyasu, K. Nucleolar scaffold protein, WDR46, determines the granular compartmental localization of nucleolin and DDX21. *Genes to Cells* **2013**, *18*, 780–797, doi:10.1111/gtc.12077.

369. Alawi, F.; Lin, P. Dyskerin localizes to the mitotic apparatus and is required for orderly mitosis in human cells. *PLoS One* **2013**, *8*, e80805, doi:10.1371/journal.pone.0080805.

370. Rocchi, L.; Barbosa, A.J.M.; Onofrillo, C.; Del Rio, A.; Montanaro, L. Inhibition of human dyskerin as a new approach to target ribosome biogenesis. *PLoS One* **2014**, *9*, e101971, doi:10.1371/journal.pone.0101971.

371. Lin, P.; Mobasher, M.E.; Alawi, F. Acute dyskerin depletion triggers cellular senescence and renders osteosarcoma cells resistant to genotoxic stress-induced apoptosis. *Biochem. Biophys. Res. Commun.* **2014**, *446*, 1268–1275, doi:10.1016/j.bbrc.2014.03.114.

372. Alawi, F.; Lin, P. Dyskerin is required for tumor cell growth through mechanisms that are independent of its role in telomerase and only partially related to its function in precursor rRNA processing. *Mol. Carcinog.* **2011**, *50*, 334–345, doi:10.1002/mc.20715.

373. Nishimura, K.; Kumazawa, T.; Kuroda, T.; Katagiri, N.; Tsuchiya, M.; Goto, N.; Furumai, R.; Murayama, A.; Yanagisawa, J.; Kimura, K. Perturbation of ribosome biogenesis drives cells into senescence through 5S RNP-mediated p53 activation. *Cell Rep.* **2015**, *10*, 1310–1323, doi:10.1016/j.celrep.2015.01.055.

374. Carrillo, J.; González, A.; Manguán-García, C.; Pintado-Berninches, L.; Perona, R. p53 pathway activation by telomere attrition in X-DC primary fibroblasts occurs in the absence of ribosome biogenesis failure and as a consequence of DNA damage. *Clin. Transl. Oncol.* **2014**, *16*, 529–538, doi:10.1007/s12094-013-1112-3.

375. Guerrieri, A.N.; Zacchini, F.; Onofrillo, C.; Di Viggiano, S.; Penzo, M.; Ansuini, A.; Gandin, I.; Nobe, Y.; Taoka, M.; Isobe, T.; et al. Dkc1 overexpression induces a more aggressive cellular behavior and increases intrinsic ribosomal activity in immortalized mammary gland cells. *Cancers* **2020**, *12*, 3512, doi:10.3390/cancers12123512.

376. Elsharawy, K.A.; Mohammed, O.J.; Aleskandarany, M.A.; Hyder, A.; El-Gammal, H.L.; Abou-Dobara, M.I.; Green, A.R.; Dalton, L.W.; Rakha, E.A. The nucleolar-related protein dyskerin pseudouridine synthase 1 (DKC1) predicts poor prognosis in breast cancer. *Br. J. Cancer* **2020**, *123*, 1543–1552, doi:10.1038/s41416-020-01045-7.

377. Sieron, P.; Hader, C.; Hatina, J.; Engers, R.; Wlazlinski, A.; Müller, M.; Schulz, W.A. DKC1 overexpression associated with prostate cancer progression. *Br. J. Cancer* **2009**, *101*, 1410–1416, doi:10.1038/sj.bjc.6605299.

378. Liu, B.; Zhang, J.; Huang, C.; Liu, H. Dyskerin overexpression in human hepatocellular carcinoma is associated with advanced clinical stage and poor patient prognosis. *PLoS One* **2012**, *7*, 1–7, doi:10.1371/journal.pone.0043147.

379. Hou, P.; Shi, P.; Jiang, T.; Yin, H.; Chu, S.; Shi, M.; Bai, J.; Song, J. DKC1 enhances angiogenesis by promoting HIF-1α transcription and facilitates metastasis in colorectal cancer. *Br. J. Cancer* **2020**, *122*, 668–679, doi:10.1038/s41416-019-0695-z.

380. Chen, L.; Roake, C.M.; Galati, A.; Bavasso, F.; Micheli, E.; Saggio, I.; Schoeftner, S.; Cacchione, S.; Gatti, M.; Artandi, S.E.; et al. Loss of human TGS1 hypermethylase promotes increased telomerase RNA and telomere elongation. *Cell Rep.* **2020**, *30*, 1358-1372.e5, doi:10.1016/j.celrep.2020.01.004.

381. Cristofari, G.; Lingner, J. Telomere length homeostasis requires that telomerase levels are limiting. *EMBO J.* **2006**, *25*, 565–574, doi:10.1038/sj.emboj.7600952.

382. Pickett, H.A.; Cesare, A.J.; Johnston, R.L.; Neumann, A.A.; Reddel, R.R. Control of telomere length by a trimming mechanism that involves generation of t-circles. *EMBO J.* **2009**, *28*, 799–809, doi:10.1038/emboj.2009.42.

383. Xi, L.; Cech, T.R. Inventory of telomerase components in human cells reveals multiple subpopulations of hTR and hTERT. *Nucleic Acids Res.* **2014**, *42*, 8565–8577, doi:10.1093/nar/gku560.

384. Blasco, M.A.; Lee, H.W.; Hande, M.P.; Samper, E.; Lansdorp, P.M.; DePinho, R.A.; Greider, C.W. Telomere shortening and tumor formation by mouse cells lacking telomerase RNA. *Cell* **1997**, *91*, 25–34, doi:10.1016/S0092-8674(01)80006-4.

385. Lee, H.W.; Blasco, M.A.; Gottlieb, G.J.; Horner, J.W.; Greider, C.W.; DePinho, R.A. Essential role of mouse telomerase in highly proliferative organs. *Nature* **1998**, *392*, 569–574, doi:10.1038/33345.

386. Muñoz-Lorente, M.A.; Cano-Martin, A.C.; Blasco, M.A. Mice with hyper-long telomeres show less metabolic aging and longer lifespans. *Nat. Commun.* **2019**, *10*, 4723, doi:10.1038/s41467-019-12664-x.

387. Hornbeck, P. V.; Zhang, B.; Murray, B.; Kornhauser, J.M.; Latham, V.; Skrzypek, E. PhosphoSitePlus, 2014: mutations, PTMs and recalibrations. *Nucleic Acids Res.* **2015**, *43*, D512-520, doi:10.1093/nar/gku1267.

388. Mertins, P.; Qiao, J.W.; Patel, J.; Udeshi, N.D.; Clauser, K.R.; Mani, D.R.; Burgess, M.W.; Gillette, M.A.; Jaffe, J.D.; Carr, S.A. Integrated proteomic analysis of post-translational modifications by serial enrichment. *Nat. Methods* **2013**, *10*, 634–637, doi:10.1038/nmeth.2518.

389. Bouhaddou, M.; Memon, D.; Meyer, B.; White, K.M.; Rezelj, V. V.; Correa Marrero, M.; Polacco, B.J.; Melnyk, J.E.; Ulferts, S.; Kaake, R.M.; et al. The global phosphorylation landscape of SARS-CoV-2 infection. *Cell* **2020**, *182*, 685–712.e19, doi:10.1016/j.cell.2020.06.034.

390. Humphrey, S.J.; Yang, G.; Yang, P.; Fazakerley, D.J.; Stöckli, J.; Yang, J.Y.; James, D.E. Dynamic adipocyte phosphoproteome reveals that akt directly regulates mTORC2. *Cell Metab.* **2013**, *17*, 1009–1020, doi:10.1016/j.cmet.2013.04.010.

391. De Bie, P.; Ciechanover, A. Ubiquitination of E3 ligases: Self-regulation of the ubiquitin system via proteolytic and non-proteolytic mechanisms. *Cell Death Differ.* **2011**, *18*, 1393–1402, doi:10.1038/cdd.2011.16.

392. Rossi, M.; Duan, S.; Jeong, Y.T.; Horn, M.; Saraf, A.; Florens, L.; Washburn, M.P.; Antebi, A.; Pagano, M. Regulation of the $CRL4^{Cdt2}$ ubiquitin ligase and cell-cycle exit by the SCF^{Fbxo11} ubiquitin ligase. *Mol. Cell* **2013**, *49*, 1159–1166, doi:10.1016/j.molcel.2013.02.004.

393. Vince, J.E.; De Nardo, D.; Gao, W.; Vince, A.J.; Hall, C.; McArthur, K.; Simpson, D.; Vijayaraj, S.; Lindqvist, L.M.; Bouillet, P.; et al. The mitochondrial apoptotic effectors BAX/BAK activate caspase-3 and -7 to trigger NLRP3 inflammasome and caspase-8 driven IL-1β activation. *Cell Rep.* **2018**, *25*, 2339–2353.e4, doi:10.1016/j.celrep.2018.10.103.

394. Chauhan, D.; Bartok, E.; Gaidt, M.M.; Bock, F.J.; Herrmann, J.; Seeger, J.M.; Broz, P.; Beckmann, R.; Kashkar, H.; Tait, S.W.G.; et al. BAX/BAK-induced apoptosis results in caspase-8-dependent IL-1β maturation in macrophages. *Cell Rep.* **2018**, *25*, 2354–2368.e5, doi:10.1016/j.celrep. 2018.10.087.

395. Fernandez-Capetillo, O.; Mahadevaiah, S.K.; Celeste, A.; Romanienko, P.J.; Camerini-Otero, R.D.; Bonner, W.M.; Manova, K.; Burgoyne, P.; Nussenzweig, A. H2AX is required for chromatin remodeling and inactivation of sex chromosomes in male mouse meiosis. *Dev. Cell* **2003**, *4*, 497–508, doi:10.1016/S1534-5807(03)00093-5.

396. Yuan, L.; Liu, J.G.; Zhao, J.; Brundell, E.; Daneholt, B.; Höög, C. The murine SCP3 gene is required for synaptonemal complex assembly, chromosome synapsis, and male fertility. *Mol. Cell* **2000**, *5*, 73–83, doi:10.1016/S1097-2765(00)80404-9.

397. Chen, X.; Li, X.; Guo, J.; Zhang, P.; Zeng, W. The roles of microRNAs in regulation of mammalian spermatogenesis. *J. Anim. Sci. Biotechnol.* **2017**, *8*, 35, doi:10.1186/s40104-017-0166-4.

398. Zimmermann, C.; Romero, Y.; Warnefors, M.; Bilican, A.; Borel, C.; Smith, L.B.; Kotaja, N.; Kaessmann, H.; Nef, S. Germ cell-specific targeting of DICER or DGCR8 reveals a novel role for endo-siRNAs in the progression of mammalian spermatogenesis and male fertility. *PLoS One* **2014**, *9*, e107023, doi:10.1371/journal.pone.0107023.

399. Modzelewski, A.J.; Hilz, S.; Crate, E.A.; Schweidenback, C.T.H.; Fogarty, E.A.; Grenier, J.K.; Freire, R.; Cohen, P.E.; Grimson, A. Dgcr8 and Dicer are essential for sex chromosome integrity during meiosis in males. *J. Cell Sci.* **2015**, *128*, 2314–2327, doi:10.1242/jcs.167148.

400. Sakashita, A.; Maezawa, S.; Takahashi, K.; Alavattam, K.G.; Yukawa, M.; Hu, Y.C.; Kojima, S.; Parrish, N.F.; Barski, A.; Pavlicev, M.; et al. Endogenous retroviruses drive species-specific germline transcriptomes in mammals. *Nat. Struct. Mol. Biol.* **2020**, *27*, 967–977, doi:10.1038/s41594-020-0487-4.

401. Muljo, S.A.; Mark Ansel, K.; Kanellopoulou, C.; Livingston, D.M.; Rao, A.; Rajewsky, K. Aberrant T cell differentiation in the absence of Dicer. *J. Exp. Med.* **2005**, *202*, 261–269, doi:10.1084/jem.20050678.

402. Cobb, B.S.; Nesterova, T.B.; Thompson, E.; Hertweck, A.; O'Connor, E.; Godwin, J.; Wilson, C.B.; Brockdorff, N.; Fisher, A.G.; Smale, S.T.; et al. T cell lineage choice and differentiation in the absence of the RNase III enzyme Dicer. *J. Exp. Med.* **2005**, *201*, 1367–1373, doi:10.1084/jem.20050572.

403. Chong, M.M.W.; Rasmussen, J.P.; Rudensky, A.Y.; Littman, D.R. The RNAseIII enzyme Drosha is critical in T cells for preventing lethal inflammatory disease. *J. Exp. Med.* **2008**, *205*, 2005–2017, doi:10.1084/jem.20081219.

404. Podshivalova, K.; Salomon, D.R. MicroRNA regulation of T-lymphocyte immunity: Modulation of molecular networks responsible for T-cell activation, differentiation, and development. *Crit. Rev. Immunol.* **2013**, *33*, 435–476, doi:10.1615/CritRevImmunol.2013006858.

405. O'Connell, R.M.; Rao, D.S.; Chaudhuri, A.A.; Baltimore, D. Physiological and pathological roles for microRNAs in the immune system. *Nat. Rev. Immunol.* **2010**, *10*, 111–122, doi:10.1038/nri2708.

406. Bronevetsky, Y.; Villarino, A. V.; Eisley, C.J.; Barbeau, R.; Barczak, A.J.; Heinz, G.A.; Kremmer, E.; Heissmeyer, V.; McManus, M.T.; Erle, D.J.; et al. T cell activation induces proteasomal degradation of argonaute and rapid remodeling of the microRNA repertoire. *J. Exp. Med.* **2013**, *210*, 417–432, doi:10.1084/jem.20111717.

407. Grigoryev, Y.A.; Kurian, S.M.; Hart, T.; Nakorchevsky, A.A.; Chen, C.; Campbell, D.; Head, S.R.; Yates, J.R.; Salomon, D.R. MicroRNA regulation of molecular networks mapped by global microRNA, mRNA, and protein expression in activated T lymphocytes. *J. Immunol.* **2011**, *187*, 2233–2243, doi:10.4049/jimmunol.1101233.

408. Gutiérrez-Vázquez, C.; Rodríguez-Galán, A.; Fernández-Alfara, M.; Mittelbrunn, M.; Sánchez-Cabo, F.; Martínez-Herrera, D.J.; Ramírez-Huesca, M.; Pascual-Montano, A.; Sánchez-Madrid, F. MiRNA profiling during antigen-dependent T cell activation: A role for miR-132-3p. *Sci. Rep.* **2017**, *7*, 3508, doi:10.1038/s41598-017-03689-7.

409. Ye, M.; Goudot, C.; Hoyler, T.; Lemoine, B.; Amigorena, S.; Zueva, E. Specific subfamilies of transposable elements contribute to different domains of T lymphocyte enhancers. *Proc. Natl. Acad. Sci. U. S. A.* **2020**, *117*, 7905–7916, doi:10.1073/pnas.1912008117.

410. Tokuyama, M.; Kong, Y.; Song, E.; Jayewickreme, T.; Kang, I.; Iwasaki, A. ERVmap analysis reveals genome-wide transcription of human endogenous retroviruses. *Proc. Natl. Acad. Sci. U. S. A.* **2018**, *115*, 12565–12572, doi:10.1073/pnas.1814589115.

411. Young, G.R.; Eksmond, U.; Salcedo, R.; Alexopoulou, L.; Stoye, J.P.; Kassiotis, G. Resurrection of endogenous retroviruses in antibody-deficient mice. *Nature* **2012**, *491*, 774–778, doi:10.1038/nature11599.

412. Novis, C.L.; Archin, N.M.; Buzon, M.J.; Verdin, E.; Round, J.L.; Lichterfeld, M.; Margolis, D.M.; Planelles, V.; Bosque, A. Reactivation of latent HIV-1 in central memory $CD4^+$ T cells through TLR-1/2 stimulation. *Retrovirology* **2013**, *10*, 119, doi:10.1186/1742-4690-10-119.

413. Bosque, A.; Planelles, V. Induction of HIV-1 latency and reactivation in primary memory CD4+ T cells. *Blood* **2009**, *113*, 58–65, doi:10.1182/blood-2008-07-168393.

414. Volkman, H.E.; Stetson, D.B. The enemy within: endogenous retroelements and autoimmune disease. *Nat. Immunol.* **2014**, *15*, 415–422, doi:10.1038/ni.2872.

415. Mustelin, T.; Ukadike, K.C. How retroviruses and retrotransposons in our genome may contribute to autoimmunity in rheumatological conditions. *Front. Immunol.* **2020**, *11*, 593891, doi:10.3389/fimmu.2020.593891.

416. Kim, S.W.; Jung, Y.S.; Ahn, J.B.; Shin, E.S.; Jang, H.W.; Lee, H.J.; Il Kim, T.; Kim, D.Y.; Bang, D.; Kim, W.H.; et al. Identification of genetic susceptibility loci for intestinal Behçet's disease. *Sci. Rep.* **2017**, *7*, 39850, doi:10.1038/srep39850.

417. Christakoudi, S.; Runglall, M.; Mobillo, P.; Tsui, T.-L.; Duff, C.; Domingo-Vila, C.; Kamra, Y.; Delaney, F.; Montero, R.; Spiridou, A.; et al. Development of a multivariable gene-expression signature targeting T-cell-mediated rejection in peripheral blood of kidney transplant recipients validated in cross-sectional and longitudinal samples. *EBioMedicine* **2019**, *41*, 571–583, doi:10.1016/j.ebiom.2019.01.060.

418. Bakir, M.; Jackson, N.J.; Han, S.X.; Bui, A.; Chang, E.; Liem, D.A.; Ardehali, A.; Ardehali, R.; Baas, A.S.; Press, M.C.; et al. Clinical phenomapping and outcomes after heart transplantation. *J. Hear. Lung Transplant.* **2018**, *37*, 956–966, doi:10.1016/j.healun.2018.03.006.